

Pre-normative research for safety of hydrogen driven vehicles and transport through tunnels and similar confined spaces

Fuel Cells and Hydrogen Joint Undertaking (FCH JU)  
Grant Agreement Number 826193

## **Deliverable D2.3**

# **Final report on analytical, numerical and experimental studies on hydrogen dispersion in tunnels, including innovative prevention and mitigation strategies**

Lead authors: NCSRD (S.G. Giannissi, A.G. Venetsanos, N. Koutsourakis, I.C. Tolias)

Contributing authors: CEA (G. Bernard-Michel, E. Studer, D. Forero, M. Martin, F. Sauzedde)

HSE (W. Rattigan, K. Moodie, M. Pursell)

KIT (Z. Xu)

PS (J. Grune)

USN (A.V. Gaathaug)

UU (V. Shentsov, D. Cirrone, S. Kashkarov,

D. Makarov, V. Molkov)

Version: 220228

Due date: 28 February 2022

Dissemination level: Public



**FUEL CELLS AND HYDROGEN**  
JOINT UNDERTAKING

### D2.3. Final report on analytical, numerical and experimental studies on hydrogen dispersion in tunnels, including innovative prevention and mitigation strategies

Deliverable administration					
Work Package	WP2. Effect of mitigation systems on hydrogen release and dispersion in confined spaces				
N. and title	D2.3 (D7) Final report on analytical, numerical and experimental studies on hydrogen dispersion in tunnels, including innovative prevention and mitigation strategies				
Type	Report				
Status	Draft/Working/ <b>Released</b>	Due	M36	Date	28-02-2022
Means of verification	Partners upload results to website.				
Comments					
Development and revision					
Version N.	Date	Authors		Description	
220124	24-01-2022	S. Giannissi, A. Venetsanos (NCSRD)		1 <sup>st</sup> document draft, NCSRD contribution	
220210	10-02-2022	V. Shentsov, G. Bernard		UU and CEA updated contributions	
220222	22-02-2022	V. Shentsov		Review	
220227	27-02-2022	D. Makarov		Review	
220228	25-02-2022	S. Giannissi (NCSRD)		Final document	

## Disclaimer

Despite the care that was taken while preparing this document the following disclaimer applies: the information in this document is provided as is and no guarantee or warranty is given that the information is fit for any particular purpose. The user thereof employs the information at his/her sole risk and liability.

The document reflects only the authors' views. The FCH JU and the European Union are not liable for any use that may be made of the information contained therein.

## Acknowledgements

This project has received funding from the Fuel Cells and Hydrogen 2 Joint Undertaking (JU) under grant agreement No 826193. The JU receives support from the European Union's Horizon 2020 research and innovation programme and United Kingdom, Germany, Greece, Denmark, Spain, Italy, Netherlands, Belgium, France, Norway, Switzerland.



**FUEL CELLS AND HYDROGEN**  
JOINT UNDERTAKING

## D2.3. Final report on analytical, numerical and experimental studies on hydrogen dispersion in tunnels, including innovative prevention and mitigation strategies

### Summary

HyTunnel-CS project aims to conduct internationally leading pre-normative research (PNR) to close knowledge gaps and technological bottlenecks in the provision of safety and acceptable level of risk in the use of hydrogen and fuel cell cars as well as hydrogen delivery transport in underground transportation systems. Work Package 2 (WP2) of HyTunnel-CS focuses on the investigation of hydrogen releases and dispersion in underground transportation systems.

This document presents the deliverable (D2.3) on final report on analytical, numerical and experimental studies regarding unignited leaks in tunnels and underground parking.

### Keywords

Hydrogen, tunnel, release, dispersion, engineering tool, numerical simulation, experiment, confined space, unignited leak

## D2.3. Final report on analytical, numerical and experimental studies on hydrogen dispersion in tunnels, including innovative prevention and mitigation strategies

### Table of contents

Summary .....	3
Keywords .....	3
List of Figures .....	8
List of Tables .....	11
Abbreviations .....	13
1. Introduction .....	14
1.1 Work Package overview .....	14
1.1.1 Objectives .....	14
1.1.2 Structure and synergy with HyTunnel-CS work plan.....	15
2. Analytical studies and development of engineering tools (Task 2.2 / CEA).....	16
2.1 Engineering tool for the assessment of ventilation system parameters in tunnels (CEA) .....	16
2.1.1 Context.....	16
2.1.2 Approach.....	16
2.1.3 Similitude parameters .....	16
2.1.3.1 Light gas models .....	17
2.1.3.2 Smoke models – critical velocity .....	18
2.2 Choked flow and tank blowdown model with Helmholtz free-energy-based hydrogen equation of state (NCSRD) .....	19
2.3 Engineering tool for mechanical ventilation in an underground parking (UU).....	19
2.3.1 Problem formulation .....	20
2.3.2 Models for mechanical ventilation.....	20
2.3.2.1 Perfect mixing equation .....	20
2.3.2.2 Mechanical ventilation based on “HyIndoor” method.....	21
2.3.2.3 e-Laboratory of Hydrogen Safety – forced ventilation tool.....	22
2.3.3 Examples of model application to calculate the area of the parking suitable for H <sub>2</sub> vehicle .....	22
2.3.3.1 Example 1: 2 mm TPRD at 700 bar.....	22
2.3.3.2 Example 2: 0.5 mm TPRD at 700 bar.....	23
2.3.3.3 Example 3: Underground parking of known area.....	24
2.3.4 Model verification by the numerical study .....	25
2.3.4.1 CFD model details .....	25
2.3.4.2 Simulation results.....	25
2.3.5 Conclusions.....	29



## D2.3. Final report on analytical, numerical and experimental studies on hydrogen dispersion in tunnels, including innovative prevention and mitigation strategies

2.3.6 Additional work done .....	29
2.4 Non-adiabatic blowdown model for under-expanded jets from the onboard storage tank (UU) .....	31
3. Numerical studies (Task 2.3 / NCSRD).....	32
3.1 Mechanical ventilation in underground parking – pre-test simulations (Sub-task 2.3.1 / NCSRD).....	32
3.1.1 Numerical set-up.....	32
3.1.2 Computational results .....	33
3.2 Mechanical ventilation in underground parking – validation simulations (Sub-task 2.3.1 / NCSRD).....	36
3.2.1 Problem formulation .....	36
3.2.2 CFD results .....	36
3.2.3 Conclusions.....	38
3.3 Dynamics of H <sub>2</sub> release and dispersion in a tunnel – pre-test simulations (Sub-task 2.3.1 / CEA / NCSRD).....	39
3.3.1 CEA simulations .....	39
3.3.1.1 Numerical set-up.....	39
3.3.1.2 Computational results .....	41
3.3.2 NCSRD simulations.....	43
3.3.2.1 Numerical set-up.....	44
3.3.2.2 Dispersion modelling .....	45
3.3.2.3 Hydrogen sensors.....	45
3.3.2.4 Computational results .....	47
3.3.2.4.1 Car scenario – $d=2.2$ mm with vehicles .....	47
3.3.2.4.2 Train scenario – $d=5.7$ mm inside empty tunnel .....	50
3.3.2.4.3 Train scenario – $d=5.7$ mm with vehicles present .....	52
3.3.2.4.4 Recommendations for the experimental setup and general conclusions .....	53
3.4 Dynamics of H <sub>2</sub> release and dispersion in a tunnel – validation simulations (Sub-task 2.3.1 / NCSRD / UU).....	54
3.4.1 NCSRD simulations.....	54
3.4.2 UU simulations .....	54
3.4.2.1 Numerical set-up.....	56
3.4.2.2 Volumetric source approach .....	56
3.4.2.3 Results.....	58
3.4.2.4 Conclusions.....	59

## D2.3. Final report on analytical, numerical and experimental studies on hydrogen dispersion in tunnels, including innovative prevention and mitigation strategies

3.5 Efficiency of mechanical ventilation on H <sub>2</sub> dispersion – pre-test simulations (Sub-task 2.3.1 / KIT) .....	60
3.5.1 Numerical set-up.....	60
3.5.2 Computational results .....	61
3.6 Efficiency of mechanical ventilation on H <sub>2</sub> dispersion – validation simulations (Sub-task 2.3.1 / KIT / NCSRD / UU) .....	62
3.6.1 Validation simulations .....	62
3.6.2 Inter-comparison between partners' simulations .....	66
3.7 Effect of tunnel slope (Sub-task 2.3.2 / NCSRD) .....	68
3.7.1 Introduction.....	68
3.7.2 Numerical setup .....	69
3.7.3 Non-ventilated cases .....	71
3.7.4 Ventilated cases .....	75
3.7.5 A note on the release direction.....	78
3.7.6 Conclusions.....	78
4. Experiments (Task 2.4 / HSE) .....	80
4.1 Mechanical ventilation in underground parking (Sub-task 2.4.1 / USN) .....	80
4.1.1 Introduction – objectives.....	80
4.1.2 Detailed specification.....	80
4.1.2.1 Tubing installation .....	80
4.1.2.2 Hydrogen sensors.....	84
4.1.3 Experimental matrix.....	86
4.1.4 Results and discussion .....	87
4.1.4.1 . Releases with the constant mass flow rate .....	87
4.1.4.2 Releases with blowdown mass flow rates.....	95
4.1.5 Conclusions.....	99
4.2 Unignited Pressure Peaking Phenomenon (Sub-task 2.4.2 / USN) .....	99
4.2.1 Introduction and Objectives .....	99
4.2.2 Detailed specification.....	100
4.2.2.1 Set up description.....	100
4.2.2.2 Explosion chamber-geometries.....	101
4.2.2.3 Fuel supply.....	102
4.2.2.4 Air supply.....	103
4.2.2.5 Instrumentation .....	104
4.2.3 Results.....	104

## D2.3. Final report on analytical, numerical and experimental studies on hydrogen dispersion in tunnels, including innovative prevention and mitigation strategies

4.2.3.1 Experimental matrix.....	104
4.2.3.2 Mass flow.....	105
4.2.3.3 Pressure data .....	105
4.2.3.4 Hydrogen concentration.....	109
4.2.3.5 Experimental data .....	112
4.3 Dynamics of H <sub>2</sub> release and dispersion in a tunnel (Sub-task 2.4.3 / HSE) .....	112
4.3.1 Introduction and objectives.....	112
4.3.2 Detailed specification.....	112
4.3.2.1 Scaling criteria .....	113
4.3.2.2 Proposed tests.....	114
4.3.2.3 Scaling of airflow in HSE tunnel .....	118
4.3.3 Test programme .....	119
4.3.4 Expected results .....	120
4.4 Efficiency of mechanical ventilation on H <sub>2</sub> dispersion (Sub-task 2.4.4 / PS).....	120
4.4.1 Introduction – objectives.....	120
4.4.2 Detailed specification.....	120
4.4.3 Results.....	122
4.4.3.1 Ventilation efficiency analysis in terms of the length of 4 vol. % H <sub>2</sub> cloud. ....	124
4.4.3.2 Ventilation efficiency analysis in terms of the length of 10 vol. % H <sub>2</sub> cloud.....	125
4.4.3.3 Conclusive remarks.....	126
4.5 Helium dispersion test results in a full-scale tunnel (CEA).....	127
4.5.1 Introduction.....	127
4.5.2 Test geometry.....	127
4.5.3 Test sequence and test matrix .....	128
4.5.4 Test results .....	129
4.5.4.1 Reference test (200 bar, 2 mm TPRD, UP) .....	129
4.5.4.2 Effect of pressure increase for a 2 mm release .....	133
4.5.4.3 Injection under the chassis for a 2 mm release .....	136
4.5.4.4 Effect of release diameter in case of downward 45° releases.....	138
4.5.5 Conclusions and recommendations.....	139
5. Summary and interaction of work tasks.....	140
6. References.....	141
Appendix A Tables and Figures for HSE pre-tests .....	145
Appendix B Scaling criteria .....	150

## D2.3. Final report on analytical, numerical and experimental studies on hydrogen dispersion in tunnels, including innovative prevention and mitigation strategies

### List of Figures

Figure 2-1. e-Laboratory of Hydrogen Safety - forced ventilation tool, input (top), results (bottom).....	22
Figure 2-2. Underground car park layout considered in Example 3 (St. Martnes Latem, Gent, Belgium), (ArcelorMittal, case studies).....	24
Figure 2-3. General view of calculation domain and numerical grid. ....	25
Figure 2-4. Hydrogen distribution in the underground car park for different release scenarios, (hydrogen mole fraction above 4% vol. is in red colour).....	26
Figure 2-5. Flammable envelope (iso-surface 4%) in the underground car park for different release scenarios. ....	27
Figure 2-6. Fast burning mixture envelope (hydrogen mole fraction 30-42% vol.) in the underground car park for different release scenarios.....	27
Figure 2-7. Hydrogen distribution non-uniformity and maximum hydrogen fraction in the stratified layer for different release scenarios.....	28
Figure 3-1. Experimental layout. ....	32
Figure 3-2. Computational domain and grid.....	33
Figure 3-3. Predicted H <sub>2</sub> release mass flow rate. ....	33
Figure 3-4. Predicted H <sub>2</sub> mass and cloud volume time histories for 4-75 vol. % cloud.....	34
Figure 3-5. Predicted H <sub>2</sub> mass and cloud volume time histories for 10-75 vol. % cloud.....	34
Figure 3-6. Predicted H <sub>2</sub> mass and cloud volume time histories for 32-42 vol. % cloud.....	35
Figure 3-7. The mass flow rate during the blowdown (left) and the problem geometry with the grid on ground level (right). ....	36
Figure 3-8. Comparison of experimental and simulation results for the sensors near the ceiling (top) and close to the release under the car (bottom) for the case without modelling external wind. ....	37
Figure 3-9. The H <sub>2</sub> concentration contours at 1 sec using software Tecplot at a view close to the nozzle. The black point indicates the position of sensor S27. ....	38
Figure 3-10. Comparison of experimental and simulation results for the sensors near the ceiling (top) and close to the release under the car (bottom) for the case with modelling external wind. ....	38
Figure 3-11. Tunnel geometry – Left: Description of the gallery and pictures, Right: Coarse grid for the preliminary CFD computations. ....	40
Figure 3-12. Injection flowrate – Left: Comparison with NET-Tools (red) for 100 l tank of 200 bar of hydrogen through 2 mm leak, Right: Investigated helium flowrates (5 B50 bottles 200 bar). ....	41
Figure 3-13. Maximum size of the helium cloud with concentration higher than 0.5 vol. % - Top 2 mm TPRD, Bottom 3 mm TPRD.....	42
Figure 3-14. Maximum size of the helium cloud with concentration higher than 0.5 vol. % - 3 mm TPRD vertical downwards release.....	43
Figure 3-15. The blow down results using the in-house release code of NCSRD for the car case (left) and the train case (right). ....	44
Figure 3-16. The geometry of the car scenario showing the grid on the floor plane (top) and the sensors' position on yz plane (bottom).....	46
Figure 3-17. The flammable volume and the flammable to total volume ratio (top, left), Q8 (top, right), Q9 (bottom, left) and Q10 (bottom, right) criteria. ....	48
Figure 3-18. Hydrogen flammable cloud (volume fraction > 4%) at several times. The time when approximately the maximum flammable volume occurs is highlighted with red. ....	48
Figure 3-19. The concentration contours on the xz release plane and on yz bottom plane at several times. ....	49
Figure 3-20. Concentration contours (left) on the yz release plane (x=35 m) at 9 sec (almost when maximum flammable volume is achieved) and at 20 sec (right). ....	49
Figure 3-21. Top: Concentration contours above LFL on yz planes at several x distances and at 5, 9 and 20 sec (from left to right). Bottom: LFL iso-surface at 5 sec, 9 and 20 sec in close view (from left to right).....	50
Figure 3-22. Flammable volume (top, left), Q8 (top, right), Q9 (bottom, left) and Q10 (bottom, right).....	51
Figure 3-23. Hydrogen flammable cloud (volume fraction > 4%) at several times. The time when approximately the maximum flammable volume occurs is highlighted with red. ....	51
Figure 3-24. The layout of the scenario using Edes GUI of ADREA-HF code.....	52
Figure 3-25. The flammable volume (left) and the volume with concentration range 25-35% (right).....	52

### D2.3. Final report on analytical, numerical and experimental studies on hydrogen dispersion in tunnels, including innovative prevention and mitigation strategies

Figure 3-26. Nearly stoichiometric mixture (25-35% v/v) at yz release plane at 4, 5, 6 and 25 sec.....	53
Figure 3-27. Hydrogen flammable cloud (volume fraction > 4%) at several times. The time when approximately the maximum flammable volume occurs is highlighted with red. ....	53
Figure 3-28. HSE tunnel facility dimensions.....	55
Figure 3-29. Numerical grid. ....	56
Figure 3-30. Parameters of the volumetric source term imposed on the inlet: mass flow rate (top left), velocity (top right), temperature (bottom centre).....	57
Figure 3-31. Concentration decay along the tunnel at different times, iso-surface of 4% concentration and the contours across the centreline of the release in range 4-30%. ....	58
Figure 3-32. Concentration decay along the tunnel at different times, iso-surface of 1% concentration and the contours across the centreline of the release in range 1-30%. ....	59
Figure 3-33. 3D view of hydrogen jet facility, the A2 vessel at KIT hydrogen test centre. ....	60
Figure 3-34. ANSYS model for vented jet simulations. ....	61
Figure 3-35. Hydrogen concentration distribution of the jet with the co-flow ventilation. ....	61
Figure 3-36. Hydrogen concentration distribution with the adapted mesh. ....	62
Figure 3-37. Schematic of geometry model for the simulation of the vented hydrogen jet in co-flow ventilation. ....	63
Figure 3-38. Hydrogen concentration (molar fraction) contour plots in longitudinal cross section cutting through the centre of the jet: (a) experiment by ProScience; (b) simulation by COM3D. ....	64
Figure 3-39. Hydrogen concentration distribution in transverse direction along $x = 625$ mm. ....	64
Figure 3-40. Hydrogen concentration distribution in transverse direction along $x = 1000$ mm. ....	65
Figure 3-41. Hydrogen concentration distribution along axial centre line of jet. ....	65
Figure 3-42. Flow velocity at longitudinal X direction at $z = 450$ mm. ....	66
Figure 3-43. The hydrogen concentration along the jet centreline for the case with no ventilation (log-log chart). ....	67
Figure 3-44. The hydrogen concentration along the jet centreline for the case with co-flow (log-log chart).....	67
Figure 3-45. The hydrogen concentration along the jet centreline for the case with counter-flow (log-log chart). ....	68
Figure 3-46. Tunnel geometry (top), cross section (bottom left) and car geometry indicating the release position and direction (bottom right).....	70
Figure 3-47. Computational grid for the 4 mm non-ventilated case. Details of the grid around the release (red) area are shown in the last figure. ....	71
Figure 3-48. Hydrogen volume concentration iso-surface of 10% vol. and velocity contours for 2 mm at 20 sec – zero slope case. ....	72
Figure 3-49. Hydrogen volume concentration iso-surface of 10% vol. and velocity contours for 4 mm at 20 sec – zero slope (top) and 5% slope (bottom). ....	72
Figure 3-50. Hydrogen volume concentration contours for 0% slope (top) and 5% slope (bottom) for the 2 mm case. ....	73
Figure 3-51. Hydrogen volume concentration contours for 0% slope (left) and 5% slope (right) for the 4 mm case at 60 s, 80 s and 100 s. ....	73
Figure 3-52. Flow field and hydrogen contour of 4 vol. % at 260 s for the 2 mm/5% slope case. ....	74
Figure 3-53. Evolution of hydrogen cloud volumes of different concentration ranges 4-75 vol. %.....	74
Figure 3-54. Hydrogen time series for 4 mm and 2 mm case at a point above the second car (shown in the left figure). ....	74
Figure 3-55. Mid-tunnel concentration contours at 20 s, 60 s and 100 s after the start of the release for the non-ventilated (left) and 1 m/s ventilation (right) cases. For each time, the zero slope (top) and 5% inclination (bottom) results are presented. The release duration is about 400 s (2 mm PRD).....	75
Figure 3-56. Above-flammable contour slices at 20 s after the start of the release. Cases of tunnels with 0% and 5% slope are presented, for three ventilation speeds each (0 m/s, 1 m/s and 2 m/s). ....	76
Figure 3-57. Whole-tunnel flammable cloud volume evolution with time for three inclinations with the same ventilation of 1 m/s (left) and for four different ventilation cases of a tunnel with a slope of 5% (right). ....	77
Figure 3-58. Mid-plane concentration contours and stoichiometric iso-surfaces at 10 s for downwards (left), upwards (middle) and backwards (right) release directions. The ventilation is 0.5 m/s in all cases.....	78
Figure 4-1. Piping and instrumentation diagram for the experimental setup.....	81
Figure 4-2. 40 ft ISO container with installed equipment and instrumentation. ....	82

### D2.3. Final report on analytical, numerical and experimental studies on hydrogen dispersion in tunnels, including innovative prevention and mitigation strategies

Figure 4-3. Sensors' position.....	86
Figure 4-4. Hydrogen concentration during hydrogen releases through <b>1 mm</b> nozzle with ACH 6 (dash line) and ACH 10 (solid line). Maximum concentration at each sensor during ACH 10 (blue star) and ACH 6 (red circle). .....	88
Figure 4-5. Hydrogen concentration during hydrogen releases through <b>0.5 mm</b> nozzle with ACH 6 (dash line) and ACH 10 (solid line). Maximum concentration at each sensor during ACH 10 (blue star) and ACH 6 (red circle). .....	88
Figure 4-6. Location of the hydrogen sensors chosen for plot in Figure 4-7 and Figure 4-9.....	89
Figure 4-7. Constant mass flow releases with ACH BS10 and BS6, through 1 mm and 0.5 mm nozzle. Initial release pressures: 60 bar, 120 bar, and 160 bar. ....	92
Figure 4-8. Smoothing method applied for the hydrogen concentration plot in Figure 4-7 and Figure 4-9. ....	92
Figure 4-9. Constant mass flow releases with ACH BS10 (blue marker and solid line) and BS6 (red marker and dash line), through 0.5 mm nozzle. Initial release pressures: 200 bar, 350 bar and 700 bar.....	93
Figure 4-10. Hydrogen release through 1 mm nozzle from 160 bar reservoir pressure. Mass flow rate, hydrogen concentration from hydrogen (S) mounted under the car, under the ceiling and 50 cm under the ceiling. ....	94
Figure 4-11. Hydrogen concentration under the table during releases through 1 mm and 0.5 nozzles from reservoir 160 bar. ....	95
Figure 4-12. Hydrogen concentration during hydrogen releases through 0.5 mm nozzle with ACH 6 (dash line) and ACH 10 (solid line). Maximum concentration at each sensor during ACH 10 (blue star) and ACH 6 (red circle). .....	96
Figure 4-13. Constant mass flow releases with ACH BS10 (blue marker and solid line) and BS6 (red marker and dash line), through 0.5 mm nozzle. Initial release pressures: 200 bar, 350 bar and 700 bar.....	97
Figure 4-14. Hydrogen concentration under the table during blowdown releases from the reservoir with 350 bar and 700 bar. ....	99
Figure 4-15. Piping and Instrumentation Diagram (P&ID). ....	101
Figure 4-16. Explosion chamber used in PPP experiment.....	101
Figure 4-17. Ventilation pipe. Inside (left) and outside (right). ....	102
Figure 4-18. Steel pipe inside the chamber- air supply.....	102
Figure 4-19. Set up of 12 bottles of hydrogen and 2 bottles of nitrogen. ....	103
Figure 4-20. Nozzle details and location, 4mm. ....	103
Figure 4-21. Kulite pressure transducer.....	104
Figure 4-22. Hydrogen concentration sensor and its positioning. ....	104
Figure 4-23. Experimental overpressure Exp 2. ....	106
Figure 4-24. Experimental overpressure Exp 3. ....	106
Figure 4-25. Experimental overpressure Exp 4. ....	107
Figure 4-26. Experimental overpressure Exp 5. ....	107
Figure 4-27. Experimental overpressure Exp 6. ....	107
Figure 4-28. Experimental overpressure Exp 7. ....	108
Figure 4-29. Experimental overpressure Exp 8. ....	108
Figure 4-30. Experimental overpressure Exp 9. ....	108
Figure 4-31. Experimental overpressure Exp 10. ....	109
Figure 4-32. Experimental overpressure Exp 11. ....	109
Figure 4-33. Hydrogen volume concentration from experiment 2. ....	110
Figure 4-34. Hydrogen volume concentration from experiment 3. ....	110
Figure 4-35. Hydrogen volume concentration from experiment 6. ....	110
Figure 4-36. Hydrogen volume concentration from experiment 7. ....	111
Figure 4-37. Hydrogen volume concentration from experiment 8. ....	111
Figure 4-38. Hydrogen volume concentration from experiment 9. ....	111
Figure 4-39. Hydrogen volume concentration from experiment 10. ....	111
Figure 4-40. Hydrogen volume concentration from experiment 11. ....	112
Figure 4-41. A) Safety vessel V220 (A2) of HYKA, B) Technical drawing, C) Example CAD-drawing.....	120
Figure 4-42. Left, schema of the jet-facility. Right, y-positions of the sensor lines for H <sub>2</sub> concentration and airflow velocity. ....	121
Figure 4-43. Left, jet facility inside the safety vessel V220 (A2). Right, jet facility inside the safety vessel V220 (A2) with wind machine and flow measurement devices in the co-flow configuration. ....	121



### D2.3. Final report on analytical, numerical and experimental studies on hydrogen dispersion in tunnels, including innovative prevention and mitigation strategies

Figure 4-44. Example of measured airflow velocity for the co-flow configuration with a wind speed of 3.5 m/s.	122
Figure 4-45. Example of H <sub>2</sub> -concentration contour plots for 1 mm nozzle and 5 g/s H <sub>2</sub> -jet mass flow rate.	123
Figure 4-46. Length of 4 vol. % H <sub>2</sub> cloud as a function of ventilation velocity in different cases: (a) nozzle $\Phi$ 1 mm and 1 g/s H <sub>2</sub> ; (b) $\Phi$ 1 mm and 5 g/s H <sub>2</sub> ; (c) $\Phi$ 1 mm and 1.5 g/s H <sub>2</sub> ; (d) $\Phi$ 4 mm and 1 g/s H <sub>2</sub> ; (e) $\Phi$ 4 mm and 5 g/s H <sub>2</sub> ; (f) $\Phi$ 4 mm and 2.5 g/s H <sub>2</sub> .	125
Figure 4-47. Length of 10 vol. % H <sub>2</sub> cloud as a function of ventilation velocity in different cases: (a) nozzle $\Phi$ 1 mm and 1 g/s H <sub>2</sub> ; (b) $\Phi$ 1 mm and 5 g/s H <sub>2</sub> ; (c) $\Phi$ 1 mm and 1.5 g/s H <sub>2</sub> ; (d) $\Phi$ 4 mm and 1 g/s H <sub>2</sub> ; (e) $\Phi$ 4 mm and 5 g/s H <sub>2</sub> ; (f) $\Phi$ 4 mm and 2.5 g/s H <sub>2</sub> .	126
Figure 4-48. General sketch of the 2021 dispersion tests.	128
Figure 4-49. Results of 2020 test 4 : a) Experiment setup, b) Helium concentration at M3 and M6, c) Helium concentration at M2 and M7, d) Helium concentration at M1 and M8, e) Wind velocity inside the tunnel (+ refers from Montaud side to Autrans side).	130
Figure 4-50. 2021 Test 01: Helium concentration close to the ceiling of the tunnel.	131
Figure 4-51. 2021 Test 01: Ventilation flow in the tunnel a) Orientation measured by the 2D ultrasonic anemometer, b) Velocities.	131
Figure 4-52. 2021 Test 01: Top - Helium concentration, Bottom - Position of sensors close to the injection (He3 is located on the vertical axis of the injection) b) M5 and c) M6.	132
Figure 4-53. 2021 Test 02: Helium concentration close to the ceiling of the tunnel.	133
Figure 4-54. 2021 Test 02: Ventilation flow in the tunnel a) Orientation measured by the 2D ultrasonic anemometer, b) Velocities.	134
Figure 4-55. 2021 test 02: Helium layer at +24 m a) Helium concentration, b) Sensors location.	134
Figure 4-56. 2021 Test 02: Helium concentration near the injection (He3 is located on the vertical axis of the injection).	135
Figure 4-57. 2021 Test 02: Additional results, Top – gas temperature along the tunnel ceiling, Bottom – left Oxygen concentration and right Helium concentration at the same location (Mast 4).	136
Figure 4-58. 2021 Test 05: Helium concentration close to the ceiling of the tunnel.	136
Figure 4-59. 2021 Test 05: Ventilation flow in the tunnel a) Orientation measured by the 2D ultrasonic anemometer, b) Velocity.	137
Figure 4-60. 2021 Test 05: Helium concentration close to the chassis.	137
Figure 4-61. 2020 versus 2021 Test results: Helium accumulation in case of 2 mm release downward a) 2020 vertical 200 bar 50 liters type II tank, b) 2021 45° to the rear 700 bar 78 liters type IV tank.	138
Figure 4-62. Effect of orifice diameter 45° downward: concentration close to the tunnel ceiling a) 2 mm and b) 1 mm, concentration at the rear of the chassis c) 2 mm and d) 1mm.	139

## List of Tables

Table 2-1. Example 1 calculation results.	23
Table 2-2. Example 2 calculation results.	24
Table 2-3. Example 3 calculation results.	24
Table 2-4. Hydrogen mole fraction: two reduced models versus averaged CFD simulation results.	28
Table 2-5. Hydrogen mole fraction: two reduced models versus maximum CFD simulation results (excluding jet zone).	29
Table 3-1. Conditions for the pre-tests of hydrogen dispersion inside scaled tunnel.	43
Table 3-2. The conditions at the notional nozzle for the two cases.	45
Table 3-3. HSE tunnel facility dimensions.	54
Table 3-4. Input parameters.	55
Table 4-1. Pipe, valves description for blowdown and constant type of mass flow releases.	83
Table 4-2. Hydrogen sensor positions	84
Table 4-3. Experimental parameters.	86
Table 4-4. Maximum concentrations for hydrogen releases from 350 bar and 700 bar.	98
Table 4-5. Experimental matrix-hydrogen.	105
Table 4-6. Scaled hydrogen inventories for cars. Buses and trains (Double bore only values in bold are those to be used for the actual modelling exercise).	115

### D2.3. Final report on analytical, numerical and experimental studies on hydrogen dispersion in tunnels, including innovative prevention and mitigation strategies

Table 4-7. Proposed hydrogen to actual tank inventories. ....	116
Table 4-8. Equivalent orifice sizes for full-sized releases. ....	117
Table 4-9. Initial mass flow rates and discharge times for full size and for scaled inventories. ....	117
Table 4-10, Scaled orifice size for experimental releases. ....	118
Table 4-11. Scaled ventilation velocities in HSE tunnel .....	118
Table 4-12. Proposed matrix of tests .....	119
Table 4-13. Test matrix of unignited H <sub>2</sub> jets. ....	122
Table 4-14. Helium dispersion test matrix. ....	128



### D2.3. Final report on analytical, numerical and experimental studies on hydrogen dispersion in tunnels, including innovative prevention and mitigation strategies

## Abbreviations

ACH	Air Changes per Hour
BC	Boundary Condition
BOS	Background Oriented Schlieren
CFD	Computational Fluid Dynamics
CGH <sub>2</sub>	Compressed Gaseous Hydrogen
EoS	Equation of State
HFC EV	Hydrogen Fuel Cell Electrical Vehicle
HRR	Heat Release Rate
LFL	Lower Flammability Limit
LH <sub>2</sub>	Liquid hydrogen
MFR	Mass Flow Rate
MTR	Mid-Term Review
NDA	Non-Disclosure Agreement
P&ID	Piping & Instrumentation Diagram
PPP	Pressure Peaking Phenomenon
PRD	Pressure Relief Device
RCS	Regulations, Codes and Standards
SAB	Stakeholders Advisory Board
SOA	State of the Art
TPRD	Thermally activated Pressure Relief Device

## D2.3. Final report on analytical, numerical and experimental studies on hydrogen dispersion in tunnels, including innovative prevention and mitigation strategies

### 1. Introduction

The research programme on releases and dispersion of hydrogen in underground transportation systems was built on the complementarities and synergies of theoretical (analytical), numerical and experimental studies. The effect of ventilation and its interaction with other mitigation systems, e.g. water spray and mist, bulkheads, is investigated. The selection of release scenarios accounts for different hydrogen release rates, hydrogen release inventories, release direction, ventilation rate, facility geometry, etc. Effects of structures, ventilation in tunnels in both positive and negative directions and its potential effect to disperse hydrogen are addressed. The goals include but are not limited to: clarification of the effectiveness of regulated ventilation systems in case of hydrogen release accident; evaluation of hazard distances, i.e. location of the flammable hydrogen-air mixture, under different scenario conditions.

For this scope experimental series, pre-test simulations and validation simulations have been conducted. Engineering tools/models are also employed and their capabilities are presented. The next Sections show the results and the main conclusions of the studies that have been carried out within HyTunnel-CS project.

The activities reported here follow the detailed programme and plan defined in deliverable D2.1 “Detailed research programme on unignited leaks in tunnels and confined space” (HyTunnel-CS D2.1, 2019). Plan for few activities have been updated during the project course according to new developments, findings and strategic advice from the Stakeholders Advisory Board (SAB). A first step to the preparation of this document was given by Milestone MS4 “M2.3. Results of experimental, analytical and numerical studies for final report”, which presents a first version on the research outcomes and final results. The milestone was achieved in November 2021 (M33).

#### 1.1 Work Package overview

##### 1.1.1 Objectives

Work Package 2 focuses on the investigation of hydrogen releases and dispersion in underground transportation systems, such as tunnels and underground parking. The research activities focus on the main knowledge gaps that were defined through the critical review of the state of the art conducted in HyTunnel-CS D1.2 “Report on hydrogen hazards and risks in tunnels and similar confined spaces” (HyTunnel-CS D1.2, 2019). The analytical, numerical and experimental work is aimed at improving the current understanding of unignited hydrogen dispersion in underground transportation systems, including the effect of ventilation and its interaction with other mitigation systems, e.g. water spray and mist. The experimental campaigns generate unique experimental data to support the validation of engineering and numerical models to be used in hydrogen safety engineering. The final scope is the identification of innovative safety strategies and solutions for the prevention and mitigation of hydrogen accumulation in flammable concentrations, providing recommendations for RCS and for an inherently safer use of hydrogen vehicles in underground transportation systems. A detailed list of the work-package objectives can be found in (HyTunnel-CS D2.1, 2019).

## D2.3. Final report on analytical, numerical and experimental studies on hydrogen dispersion in tunnels, including innovative prevention and mitigation strategies

### 1.1.2 Structure and synergy with HyTunnel-CS work plan

Work Package 2 is structured in 5 tasks closely interconnected between each other and with HyTunnel-CS work plan. Task 2.1 aimed at the design of the research programme of WP2. The detailed programme is available in (HyTunnel-CS D2.1, 2019) and it defines the activities being performed in Tasks 2.2, 2.3 and 2.4. Task 2.2 aims at the development of analytical studies and engineering tools to be used in hydrogen safety engineering. Experiments available in literature or performed within HyTunnel-CS experimental campaign in Task 2.4 are being used for validation. Task 2.3 aims at the development and validation of computational fluid dynamics (CFD) models against experiments conducted in Task 2.4. This task includes pre-test simulations aiding the design of the experimental tests conducted in Task 2.4. The latter focuses on carrying out the experimental programme, which aims at enhancing the current understanding of hydrogen release and dispersion, and its interaction with mitigation systems in tunnels and underground parking. The generated experimental data are used to validate the engineering tools and CFD models developed in tasks 2.2 and 2.3, respectively. For this reason, a close collaboration between modellers and experimentalists was being ensured to optimise and refine the design of experiments. Finally, Task 2.5 consolidates the knowledge and outcomes achieved in tasks 2.2, 2.3 and 2.4, and the intermediate and final reports, D2.2 and D2.3, respectively, were prepared.

WP2 activities are closely connected with WP4 research investigating the consequences from ignition of hydrogen jets and clouds following a release. Finally, the outcomes developed within tasks 2.2-2.4 will be translated into a suitable language and format to be integrated into the guidelines and recommendations for RCSs developed within WP6.

D2.3. Final report on analytical, numerical and experimental studies on hydrogen dispersion in tunnels, including innovative prevention and mitigation strategies

## 2. Analytical studies and development of engineering tools (Task 2.2/CEA)

### 2.1 Engineering tool for the assessment of ventilation system parameters in tunnels (CEA)

#### 2.1.1 Context

This work concerns models and validation of ventilation systems in the case of an unignited release of hydrogen in a tunnel. Ideally, the goal would be to address two main problems, which have been extensively studied for smoke dispersion in a tunnel fire:

- The backlayering effect is characterized by the length of smoke going backwards the ventilation direction from the emitting source (Weng, Lu, Liu, Shi, & Yu, 2015).
- The temperature distribution along the tunnel is in connection with the smoke propagation (Ingason & Li, 2010).

The backlayer effect has been extensively studied and many models have been proposed and validated in more and more complex situations: the presence of a slope (Ji, et al., 2019), obstacles in the tunnel, bifurcation in the tunnel, external pressure influence, the position of the source along the tunnel and so on. The second point has been numerically studied but no “universal” models are available yet.

Our idea is to try to derive similar models with similitude arguments that would apply to light gas dispersion (hydrogen, helium).

#### 2.1.2 Approach

Ideas about reusing the smoke models by writing an analogy between the thermal buoyancy effect and the density buoyancy effect were presented at Grenoble meeting in Feb. 2020. This is actually straightforward. The second idea was to write an analogy with the thermal buoyancy source term and the density buoyancy source term. This analogy has already been developed and also been experimentally validated by (Vauquelin, 2008) (Le Clanche, et al., 2014).

Actually, it is to be noted that models for helium have been developed in the past to validate smoke models due to the easiness of setting up experiments with helium. The approach was then the opposite of the present one: using helium models to validate or improve fire models. We, therefore, have access directly to models on light gas dispersion but also on methods to jump between thermal models and density models.

#### 2.1.3 Similitude parameters

Two kinds of similitude approaches are discussed:

- The similitude approach for a given phenomenon (fire or light inert gas release) which led to determining the number of parameters describing the phenomenon, exhibiting some dimensionless numbers such as Richardson numbers, Reynolds numbers, length ratios etc.
- The similitude between smoke dispersion and light gas dispersion which leads to identifying how some of the common parameters in both situations (the source term, the Richardson number) are expressed.

### D2.3. Final report on analytical, numerical and experimental studies on hydrogen dispersion in tunnels, including innovative prevention and mitigation strategies

In this section, we will only use models from the literature and won't do any similitude analysis to build up models. We will only present the way we express parameters allowing to swap from fire to light gas.

For any approach, most of the parameters are common and unchanged:

- Geometrical properties (tunnel's height, length, width, source geometry etc.)

The two parameters that are changing are:

- The gas density  $\rho$
- The heat flux  $\dot{Q}$  (fires) or momentum flux  $B_i$  (light gas).

It has been established (Le Clanche, et al., 2014), (Vauquelin, 2008), the following relationship:

$$B_i = \dot{Q} \frac{g}{\rho_0 T_0 C_p}, \quad (2-1)$$

where,  $\dot{Q}$  is the heat release rate (W),  $\rho_0$  the density of air at the ambient temperature  $T_0$  and the specific heat  $C_p$  is considered constant in the first approximation. This equation gives a connection between the fire models and the light gas release models. Practically, for a fire source, the convective heat release rate will be defined as:

$$\dot{Q} = \rho_s C_p q_s (T_s - T_0), \quad (2-2)$$

where the index  $s$  designs the values at the source,  $q_s$  is the smoke flow rate at the source. For the bouoyant release of light inert gas, we have the buoyant flux:

$$B_i = g q_s \frac{\rho_0 - \rho_s}{\rho_0}, \quad (2-3)$$

where  $q_s$  is the inert gas flow rate at the injection. In this case, the density of the air/gas mixture is given by:

$$\rho = Y \rho_s + (1 - Y) \rho_0, \quad (2-4)$$

where  $Y$  is the volume fraction of the inert gas in the binary mixture. The volume fraction plays a similar role as the temperature in a fire, where density is proportional to the temperature.

#### 2.1.3.1 Light gas models

We first present models designed from the beginning to describe backlayering for light gas.

The first general model according to (Le Clanche, et al., 2014) is characterizing the critical tunnel ventilation velocity  $U_c$  above which backlayering is suppressed:

$$\frac{U_c}{W_s} = a R_i^{\frac{1}{3}}, \quad (2-5)$$

where  $W_s$  is the velocity at the injection and  $a$  is supposed to be constant (with  $a = 0.32$ ), which has been validated on experiments for a plume Richardson number  $R_i = \frac{5}{16 \alpha} \frac{g (\rho_0 - \rho_s) D_i}{\rho_0 W_s^2}$  varying from 0.1 up to 70,  $D_i$  is the diameter of the injection nozzle and  $\alpha$  is the entrainment coefficient defined in Morton (Morton, 1959).

### D2.3. Final report on analytical, numerical and experimental studies on hydrogen dispersion in tunnels, including innovative prevention and mitigation strategies

It has been proven that the parameter  $\alpha$  remains constant when the Richardson number tends to infinity. It means that the relation holds for pure plumes. The relation is therefore independent of the density ratio at the injection, nor on the source diameter to the tunnel height ratio.

On the other hand, in a more recent publication (Jiang, M., R., & Salizzoni, 2019), a dependence on the density ratio  $\sqrt{\frac{\rho_s}{\rho_0}}$  as well as the source width over the tunnel height ratio  $\frac{D_i}{H}$  has been established for plume Richardson number lower than 0.01, that is for pure jets. This has to be taken into account, for example for TPRD releases where the jet has high momentum.

Although the model reproduces correctly the order of magnitude for the dependency against those two parameters, it is not very accurate due to the limitation of the analytical model, derived with very simplified assumptions about the jet. In the case of very low plume Richardson numbers, it is advised either to derive the one-dimensional system of the differential equation (Van den Bremer & Hunt, 2010) or CFD calculation. Nevertheless, in the particular case of a small diameter release against the tunnel height (a ratio lower than 0.02), it is shown that an asymptotic behaviour is reached, and therefore:

$$\frac{U_c}{W_s} = \alpha 0.01^{\frac{1}{3}}, \quad (2-6)$$

which leads to  $U_c \approx 0.1 W_s$ . This relationship has no practical use since it won't be possible to ventilate the tunnel in order to prevent backlayering in this particular case of an upward TPRD release toward the ceiling. In this particular case, i.e. for high momentum jets, the 1D equations proposed in Jiang and Salizzoni 2019 have to be solved numerically. Therefore we can't produce an analytical model in that case.

**First conclusion:** The relationship connecting the tunnel critical velocity, the injection velocity and the plume Richardson number can be used for plume Richardson number above 0.1. Practically, it will be useful for moderate flow rate release or for fountains or release under a chassis. This first step of modelling will then be used in order to determine the backlayer length in case of subcritical tunnel ventilation.

#### 2.1.3.2 Smoke models – critical velocity

Since we have introduced equivalence between light inert gas and thermal gas (smoke), we want first to compare up to date backlayering models for smoke and the model exposed in the previous section.

A recent article by (Haddad, Maluk, Reda, & Harun, 2019) does an SOA review for critical velocities and backlayering covering extensively the most used correlations until now. On a first approach, we are interested in the critical velocity for a horizontal tunnel and with no heat exchange on the wall, which corresponds to a no-diffusion flux on the walls with a light non thermal gas (hydrogen for example). For a moderate HRR, the following relation applies:

$$U_c^* = 0.35 (0.124)^{-1/3} (Q^*)^{1/3}, \quad (2-7)$$

where  $U_c^*$  is the dimensionless critical velocity and  $\dot{Q}$  the dimensionless convective flux. Using the previously defined equivalence between  $B_i$  and  $\dot{Q}$  and the definitions of the dimensionless velocity and flux, we can derive the following relation:

### D2.3. Final report on analytical, numerical and experimental studies on hydrogen dispersion in tunnels, including innovative prevention and mitigation strategies

$$U_c = 0.35 \left( \frac{B_i}{0.124H} \right)^{1/3}, \quad (2-8)$$

whereas the previous relation (Le Clanche, et al., 2014) can be expressed as:

$$U_c = 0.35 \left( \frac{B_i}{D_i} \right)^{1/3}. \quad (2-9)$$

#### Remarks:

If the source diameter is 0.124 times the tunnel height, the two relations are the same. Practically, for a 10 meters high tunnel, the source diameter has to be of 1.24 meters. It is quite realistic in the case of a car fire (order of magnitude).

Nevertheless, Le Clanche has shown an independency of his relation when the ratio  $D_i/H$  is varying. Therefore, Le Clanche claims independence of the critical velocity from the tunnel height, but a dependence on the source diameter. Both relations agree on the other hand on dependence on the source heat (or buoyancy) flux with a  $1/3$  power law.

This first result is interesting since all those smoke models have been established with similitude arguments AND experiments. Since the diameter of the heat source seems to remain unstudied in the articles published so far, it might explain why articles introduce various corrections as  $0.124^{1/3}$  or  $0.2^{1/3}$  and so on. It has to be investigated further, but it seems those correcting parameters correspond to aspect ratios between the tunnel height and the source diameter.

#### Conclusion:

We advise to use Le Clanche model to evaluate the critical velocity for non-ignited hydrogen release in a tunnel.

Nevertheless, it is probable that models established for smoke will give also good results with the following correction:

$$U_c^* = 0.35 \left( \frac{D_i}{H} \right)^{-1/3} (Q^*)^{1/3}. \quad (2-10)$$

This assertion has to be validated experimentally.

## 2.2 Choked flow and tank blowdown model with Helmholtz free-energy-based hydrogen equation of state (NCSRD)

This research activity will be reported in (HyTunnel-CS D4.4, 2022).

## 2.3 Engineering tool for mechanical ventilation in an underground parking (UU)

UU identified two approaches for calculation of hydrogen concentration in semi-confined space like underground parking, as reported in (HyTunnel-CS D1.2, 2019) and (HyTunnel-CS D2.1, 2019):

- solution based on the perfect mixing equation,
- model for passive ventilation (Molkov et al., 2014).



## D2.3. Final report on analytical, numerical and experimental studies on hydrogen dispersion in tunnels, including innovative prevention and mitigation strategies

Description, comparison and verification of both approaches against highly-accurate CFD simulations are briefly described below.

### 2.3.1 Problem formulation

Realistic hydrogen release from compressed gaseous hydrogen (CGH<sub>2</sub>) onboard storage is likely to form a non-uniform hydrogen-air mixture, especially in big volumes and areas. The passive ventilation model was developed within FCH JU project “HyIndoor” and described in (Molkov et al., 2014). The calculation procedure also includes the process to find the volumetric flow rate of air not to exceed a targeted maximum hydrogen concentration (in a stratified layer or in a uniform mixture) for a given hydrogen release rate. The approach was validated against the series of 48 experiments on helium release in a small-scale enclosure. The perfect mixing equation allows to calculate the forced ventilation airflow rate (for a given hydrogen release rate) required to keep the hydrogen concentration below a safe level at steady-state conditions and in the assumption of a uniform mixture of hydrogen and air.

In absence of the experimental data up to now, both models are verified against numerical simulations performed here for mechanical ventilation in the real underground parking. The model verification is based on current regulations for ventilation in the underground parking (BS 7346-7:2013).

**General scenario:** Hydrogen release through the TPRD of a hydrogen-powered vehicle in underground parking with TPRD diameters of 0.5 mm, 1 mm, 2 mm and 5 mm. Different floor areas could be considered for underground parking with a height of 3 m. Theoretical considerations and previous experience suggest that “Perfect mixing” model gives averaged concentration prediction within the enclosure, while “HyIndoor” model calculates maximum concentration in a layered mixture. CFD simulations, used here for verification, provide a more realistic distribution of hydrogen taking into account the complexity of the building, presence of obstacles congestion zones and ventilation ducts.

#### Aims of the study:

- Compare two reduced ventilation models results;
- Verify the models against CFD simulations;
- Define the model to design mechanical ventilation;
- Define maximum TPRD diameter to satisfy current ventilation requirements (without their change).

### 2.3.2 Models for mechanical ventilation

Two reduced models of mechanical ventilation were proposed in the Deliverable D1.2 (HyTunnel-CS D1.2, 2019): “HyIndoor method” applicable for the non-uniform layered mixtures (Molkov et al., 2014) and “Perfect mixing” equation for uniform mixtures. It is worth mentioning that both models are applicable to steady-state releases only.

#### 2.3.2.1 Perfect mixing equation

The perfect mixing equation is the simplest that can be used to calculate airflow by forced ventilation depending on hydrogen release rate to keep hydrogen concentration below a required level at steady-state conditions (constant flow rates of hydrogen from a leak and air by forced ventilation):



### D2.3. Final report on analytical, numerical and experimental studies on hydrogen dispersion in tunnels, including innovative prevention and mitigation strategies

$$C\% = \frac{100 \cdot Q_g}{Q_a + Q_g}, \quad (2-11)$$

where  $C\%$  is the steady-state gas concentration (% by volume),  $Q_a$  is the airflow rate ( $\text{m}^3/\text{min}$ ), and  $Q_g$  is the gas leakage rate ( $\text{m}^3/\text{min}$ ).

#### 2.3.2.2 Mechanical ventilation based on “HyIndoor” method

The theory for mechanical ventilation is based on the equation for passive ventilation (Molkov et al., 2014) to calculate the hydrogen gas mole fraction,  $X$ , following a release in the ventilated enclosure:

$$X = f(X) \cdot \left[ \frac{Q_0}{C_D A (g'H)^{1/2}} \right]^{2/3}, \quad (2-12)$$

where  $Q_0$  is the volumetric flow rate of release,  $C_D$  is a discharge coefficient,  $A$  is vent area,  $g' = g(\rho_{air} - \rho_{H_2})/\rho_{air}$  is the reduced gravity, and  $g$  is the gravity acceleration,  $\rho$  is the density of *air* and  $H_2$  respectively,  $H$  is the vent height. Function  $f(X)$  defines the difference between the approximate solution for a volumetric fraction of hydrogen by the natural ventilation theory and the exact solution of the problem using the passive ventilation theory. Function  $f(X)$  is calculated as:

$$f(X) = \left(\frac{9}{8}\right)^{1/3} \cdot \left\{ \left[ 1 - X \left( 1 - \frac{\rho_{H_2}}{\rho_{air}} \right) \right]^{1/3} + (1 - X)^{2/3} \right\}. \quad (2-13)$$

A “forced ventilation” model has been built on the principles of the passive ventilation model that calculates ventilation flow rate to provide maximum hydrogen concentration in an enclosure below the required level.

Eq. (2-12) is rewritten in terms of the height as follows:

$$H = \left( \left[ \frac{Q_0}{C_D \left[ \frac{X}{f(X)} \right]^{3/2}} \right]^2 / g' \right)^{1/3}. \quad (2-14)$$

If we know the height of the vent, then location of the neutral plane separating the flow across the vent can be calculated as:

$$h_{NP} = \frac{H \cdot \left( 1 - \frac{X \rho_{H_2}}{\rho_{mix}} \right)^{2/3} \left( \frac{\rho_{mix}}{\rho_{air}} \right)^{1/3}}{1 + \left( 1 - \frac{X \rho_{H_2}}{\rho_{mix}} \right)^{2/3} \left( \frac{\rho_{mix}}{\rho_{air}} \right)^{1/3}}. \quad (2-15)$$

Then the mass and volumetric flow rates of air stream are:

$$\dot{m}_{air} = (h_{NP})^{3/2} \frac{2}{3} \sqrt{2 \rho_{air} g (\rho_{air} - \rho_{mix})}, \quad (2-16)$$

$$Q_{air} = \dot{m}_{air} / \rho_{air}. \quad (2-17)$$

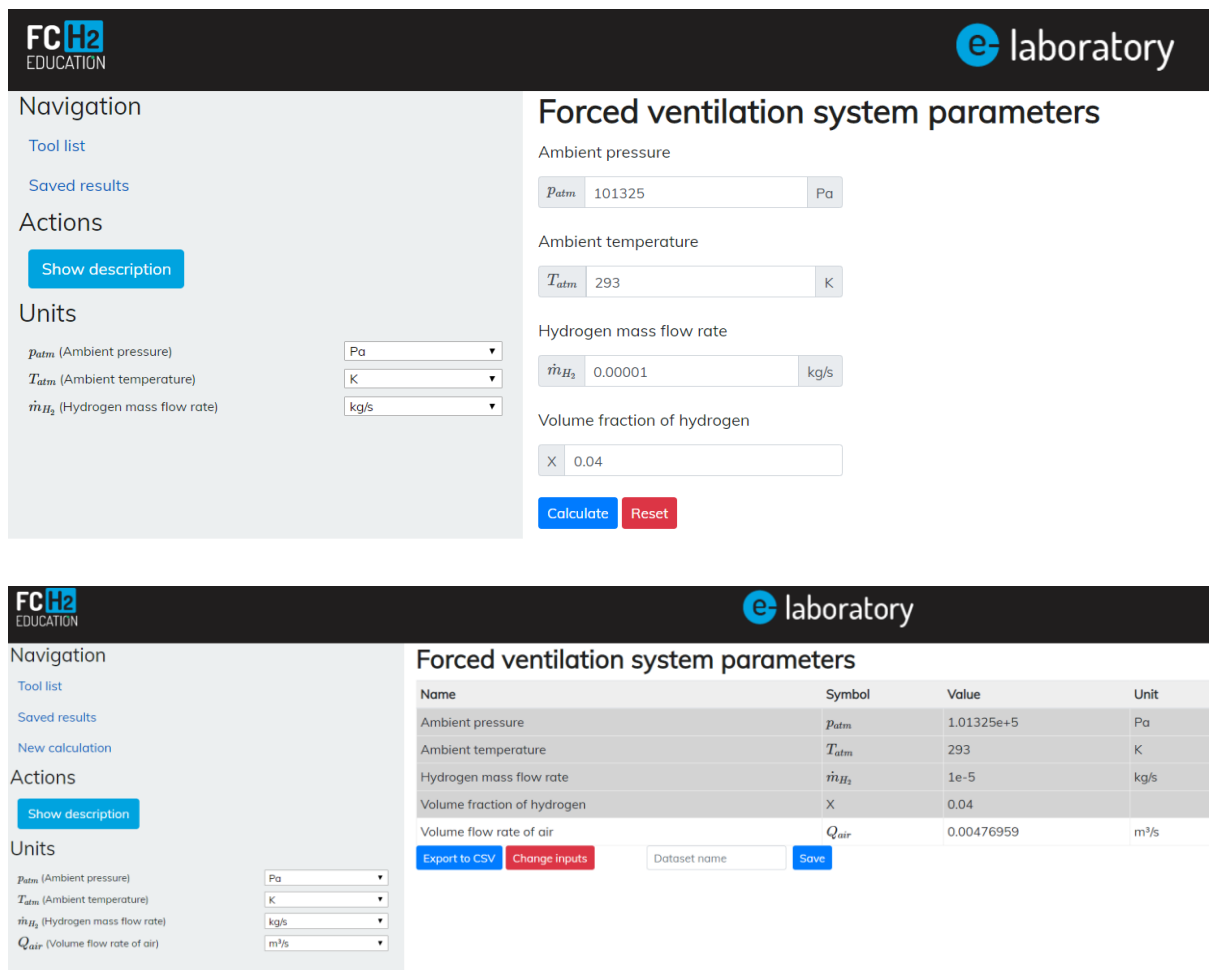
The perfect mixing equation (2-11) gives an average concentration of hydrogen in the volume while mechanical ventilation based on the equation for passive ventilation gives maximum concentration, therefore a difference in calculated hydrogen concentration by passive theory and perfect mixing is expected.

## D2.3. Final report on analytical, numerical and experimental studies on hydrogen dispersion in tunnels, including innovative prevention and mitigation strategies

In most of the realistic releases hydrogen concentration in an enclosure will be rather non-uniform. Thus, averaged concentration calculated by perfect mixing equation could be below the maximum concentration under the enclosure ceiling and hence both theories have to be tested.

### 2.3.2.3 e-Laboratory of Hydrogen Safety – forced ventilation tool

The “forced ventilation” tool, implementing the theory described above, is available at [https://elab-prod.iket.kit.edu/integrated/forced\\_ventilation/input](https://elab-prod.iket.kit.edu/integrated/forced_ventilation/input) (login: **HyTunnel**, password: **Safety2019**). As shown in Figure 2-1 below the user has to provide the desired hydrogen mole fraction and the mass flow rate of the release to get the volume flow rate of air required.



**FC<sub>H2</sub> EDUCATION** **e laboratory**

**Navigation**

- Tool list
- Saved results

**Actions**

Show description

**Units**

$p_{atm}$  (Ambient pressure) Pa

$T_{atm}$  (Ambient temperature) K

$\dot{m}_{H_2}$  (Hydrogen mass flow rate) kg/s

**Forced ventilation system parameters**

Ambient pressure

$p_{atm}$  101325 Pa

Ambient temperature

$T_{atm}$  293 K

Hydrogen mass flow rate

$\dot{m}_{H_2}$  0.00001 kg/s

Volume fraction of hydrogen

X 0.04

Calculate Reset

**Forced ventilation system parameters**

Name	Symbol	Value	Unit
Ambient pressure	$p_{atm}$	1.01325e+5	Pa
Ambient temperature	$T_{atm}$	293	K
Hydrogen mass flow rate	$\dot{m}_{H_2}$	1e-5	kg/s
Volume fraction of hydrogen	X	0.04	
Volume flow rate of air	$Q_{air}$	0.00476959	m³/s

Export to CSV Change inputs Dataset name Save

**Units**

$p_{atm}$  (Ambient pressure) Pa

$T_{atm}$  (Ambient temperature) K

$\dot{m}_{H_2}$  (Hydrogen mass flow rate) kg/s

$Q_{air}$  (Volume flow rate of air) m³/s

Figure 2-1. e-Laboratory of Hydrogen Safety - forced ventilation tool, input (top), results (bottom).

### 2.3.3 Examples of model application to calculate the area of the parking suitable for H<sub>2</sub> vehicle

According to (BS 7346-7:2013) existing requirement to air change per hour (ACH)=10 in underground parking is kept. The height of the underground parking in the examples below was taken as 3 m according to (ArcelorMittal, case studies).

#### 2.3.3.1 Example 1: 2 mm TPRD at 700 bar

Here we consider the scenario of a hydrogen-powered vehicle in an underground park. The height of the underground park is 3 m, hydrogen is stored onboard the vehicle at pressure

### D2.3. Final report on analytical, numerical and experimental studies on hydrogen dispersion in tunnels, including innovative prevention and mitigation strategies

700 bar and the orifice diameter of the thermally activated pressure relief device (TPRD) is 2 mm. Let us calculate using the “Forced ventilation” tool of the [e-Laboratory](#), which realises “HyIndoor method”, at what area of the underground park the required ventilation rate ACH=10 will be sufficient to maintain hydrogen volume fraction within 4% vol. (i.e. LFL) assuming the steady-state release.

According to [Jet Parameters model of e-Laboratory](#) the release from such TPRD gives a mass flow rate of 107 g/s as shown in the table below and the forced ventilation tool “HyIndoor method” of the [e-Laboratory](#) gives the volumetric flow rate of 50.2 m<sup>3</sup>/s or 3010 m<sup>3</sup>/min. According to the “Perfect mixing” equation (2-11) this ventilation rate results in 2.46% vol. hydrogen:

$$C\% = \frac{100 \cdot Qg}{Qa + Qg} = \frac{100 \cdot 76}{3010 + 76} = 2.46\%. \quad (2-18)$$

In the considered example the “Perfect mixing” equation provides hydrogen volume fraction 38% lower compared to the “forced ventilation” tool (i.e. “HyIndoor method”) which presumes stratified hydrogen-air mixture formation. Results summary for this scenario are presented in Table 2-1.

*Table 2-1. Example 1 calculation results.*

<b>H<sub>2</sub> mass flow rate (g/s)</b>	<b>107</b>
<b>H<sub>2</sub> volumetric flow rate, (m<sup>3</sup>/min)</b>	<b>76</b>
<b>Air volumetric flow rate, (m<sup>3</sup>/min)</b>	<b>3010</b>
<b>Hydrogen concentration: (“HyIndoor” method), %</b>	<b>4.00</b>
<b>Hydrogen concentration: (“Perfect mixing” equation), %</b>	<b>2.46</b>

Taking into account that the calculated ventilation rate should correspond to the required ACH=10 and parking area height is 3 m, we can calculate the parking area that cannot be less than:

$$3010 \left( \frac{\text{m}^3}{\text{min}} \right) \times \frac{60(\text{min})}{10(\text{ACH})} / 3(\text{m}) = 6020 \text{m}^2 \approx \mathbf{78\text{m} \times 78\text{m}}. \quad (2-19)$$

#### 2.3.3.2 Example 2: 0.5 mm TPRD at 700 bar

Now let’s decrease the TPRD diameter from 2 mm to 0.5 mm for the same storage pressure of 700 bar and follow the same calculation logic as in Example 1 above. Here mass flow rate of hydrogen through TPRD is 6.73 g/s, and the airflow rate that required to maintain 4% vol. hydrogen fraction in a stratified layer under the parking area ceiling is 189 m<sup>3</sup>/min. Such air flow rate corresponds to the required ACH=10 in an underground park with area:

$$189 \left( \frac{\text{m}^3}{\text{min}} \right) \times \frac{60(\text{min})}{10(\text{ACH})} / 3(\text{m}) = 378 \text{m}^2 \approx \mathbf{19.5\text{m} \times 19.5\text{m}}. \quad (2-20)$$

From the practical point of view it is less than the area of any residential parking (e.g. under an apartment block) or in a commercial building (e.g. shopping mall). Results summary for this scenario is presented in Table 2-2.

## D2.3. Final report on analytical, numerical and experimental studies on hydrogen dispersion in tunnels, including innovative prevention and mitigation strategies

Table 2-2. Example 2 calculation results.

<b>H<sub>2</sub> mass flow rate (g/s)</b>	<b>6.73</b>
<b>H<sub>2</sub> volumetric flow rate, (m<sup>3</sup>/min)</b>	4.8
<b>Air volumetric flow rate, (m<sup>3</sup>/min)</b>	<b>189</b>
<b>Hydrogen concentration: (“HyIndoor” method), %</b>	4.00
<b>Hydrogen concentration: (perfect mixing equation), %</b>	2.47

### 2.3.3.3 Example 3: Underground parking of known area

In this example we look into the real underground car park in St. Martnes Latem (Gent, Belgium) (ArcelorMittal, case studies). The total parking area is known and equal to 1115 m<sup>2</sup>, underground park height is 3m, see Figure 2-2. The same onboard hydrogen storage with storage pressure 700 bar and TPRD orifice diameter 0.5 mm was presumed. Now we know the volume of the enclosure which is  $1115 \times 3 = 3345$  m<sup>3</sup>. In order to satisfy the standard requirement of ACH=10 the air volumetric flow rate should be  $3345 \times 10 = 33450$  m<sup>3</sup>/h, i.e. 557 m<sup>3</sup>/min. In the forced ventilation tool of the [e-Laboratory](#) the hydrogen concentration (as a sought parameter) corresponding to volumetric flow rate 33450 m<sup>3</sup>/h (557 m<sup>3</sup>/min) is 1.4% vol. For the same volume flow rate the perfect mixing equation results in hydrogen vol. fraction as low as 0.85%. Calculation results for Example 3 are summarised in Table 2-3.

Table 2-3. Example 3 calculation results.

<b>H<sub>2</sub> mass flow rate (g/s)</b>	<b>6.73</b>
<b>H<sub>2</sub> volumetric flow rate, (m<sup>3</sup>/min)</b>	4.8
<b>Air volumetric flow rate, (m<sup>3</sup>/min)</b>	557
<b>Hydrogen concentration: (“HyIndoor” method), %</b>	<b>1.4</b>
<b>Hydrogen concentration: (perfect mixing equation), %</b>	<b>0.85</b>

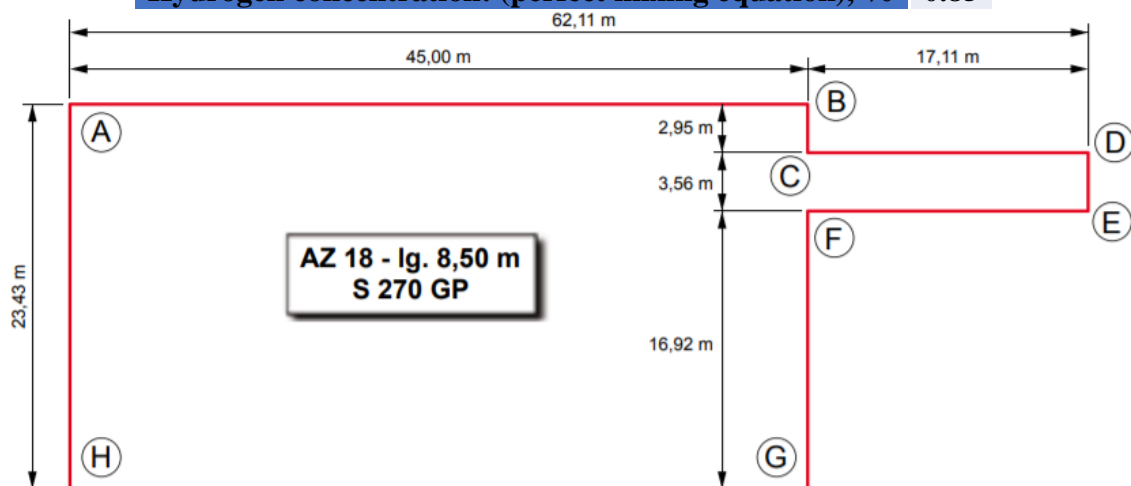


Figure 2-2. Underground car park layout considered in Example 3 (St. Martnes Latem, Gent, Belgium), (ArcelorMittal, case studies).

## D2.3. Final report on analytical, numerical and experimental studies on hydrogen dispersion in tunnels, including innovative prevention and mitigation strategies

### 2.3.4 Model verification by the numerical study

Now calculation results of the perfect mixing model and “HyIndoor” model in Example 3 are compared against steady-state CFD simulations to conclude which of the two models is more realistic and applicable for the calculation of ventilation parameters in the underground parking.

#### 2.3.4.1 CFD model details

The steady-state problem formulation has been selected to verify the equations since both are derived in the assumption of steady-state release and ventilation. The pressure-based implicit solver with the realizable  $k-\varepsilon$  turbulence model and the second order upwind scheme selected for the momentum, species and energy equations were employed. The calculation domain and numerical mesh are given in Figure 2-3. The calculation domain included the underground parking itself and part of the entrance tunnel (section E-D in Figure 2-2). The numerical grid consisted of 183,047 polyhedral control volumes uniformly distributed inside the calculation domain. The numerical grid was refined closer to the walls and ventilation openings to better resolve velocity and hydrogen concentration gradients. Inflow boundary is shown in Figure 2-3 by green colour and outflow boundary (ventilation openings) are designated by blue colour.

Ventilation according to the requirements of (BS 7346-7:2013) has been provided through 18 extraction vents of 1x1 m each evenly distributed over the ceiling with outflow velocity calculated based on 10 ACH as:

$$33450(\text{m}^3/\text{h})/60(\text{min})=557(\text{m}^3/\text{min})/60(\text{s})=9.28(\text{m}^3/\text{min})/18(\text{m}^2)=0.516(\text{m/s}).$$

CFD simulations of four scenarios were performed - hydrogen release from TPRD diameters 0.5 mm, 1 mm, 2 mm and 5 mm.

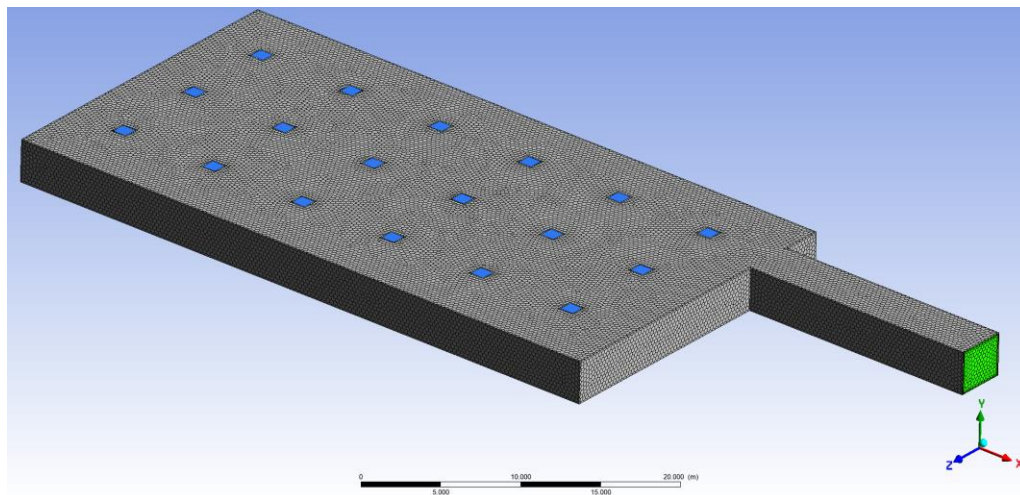


Figure 2-3. General view of calculation domain and numerical grid.

#### 2.3.4.2 Simulation results

Figure 2-4 shows the volume rendering of the hydrogen mole fraction in the range 0-4% at the steady-state condition for all four cases. Front, back, side and top views of the parking is given to better observe the difference between simulation results. It can be clearly seen that only in the case of release from 0.5 mm TPRD diameter orifice the flammable concentration is less pronounced compared to the other three.

### D2.3. Final report on analytical, numerical and experimental studies on hydrogen dispersion in tunnels, including innovative prevention and mitigation strategies

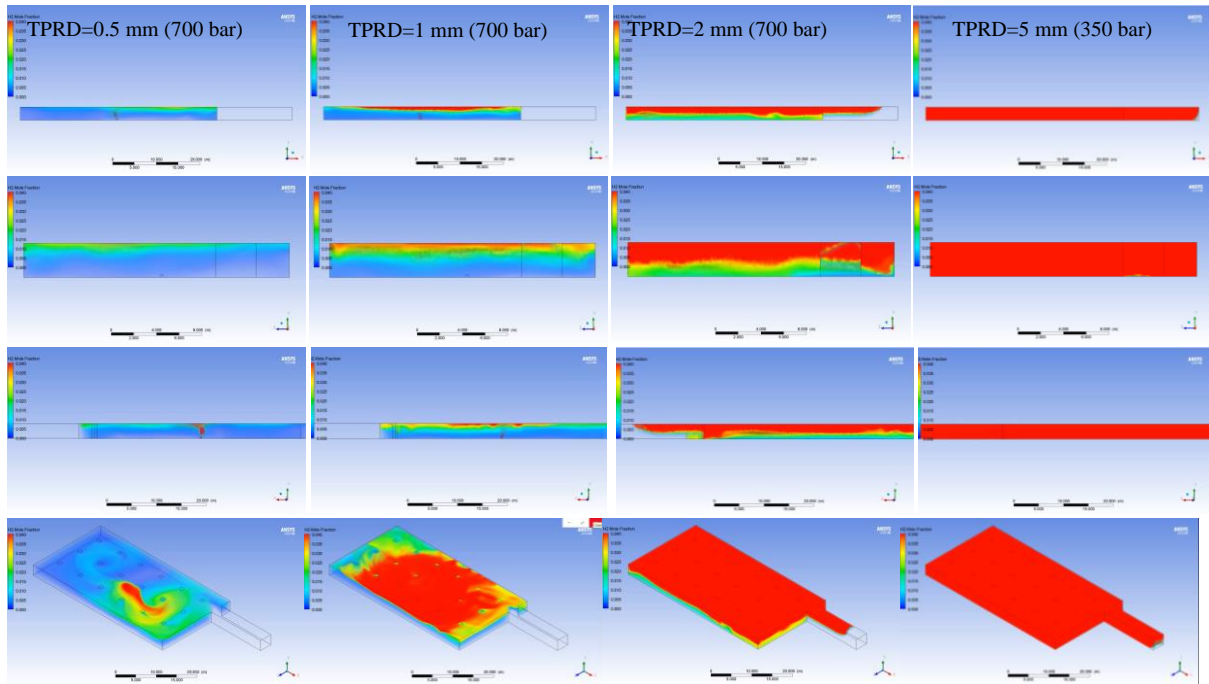


Figure 2-4. Hydrogen distribution in the underground car park for different release scenarios, (hydrogen mole fraction above 4% vol. is in red colour).

Figure 2-5 shows the iso-surface of hydrogen mole fraction 4% vol. for all four scenarios. Only in the case of release from 0.5mm TPRD orifice diameter the iso-surface envelope containing flammable composition is isolated close to the release point, while with an increase of release diameter in the other cases the 4% boundary progressively propagates further towards the car park periphery and for the 5 mm orifice it reaches the car park entrance occupying the whole enclosure with combustion mixture (in line with what is shown in Figure 2-4).

Figure 2-6 shows the volume rendering of the fastest burning hydrogen-air mixture – in the range of mole fraction 30-42%, according to the preliminary results from the study on delayed ignition of hydrogen jets performed within HyTunnel-CS. Again, for the 0.5 mm TPRD diameter this area is a tiny spot close to the release and unlikely to create overpressure hazards in case of deflagration (simulation of deflagration is out of the scope of this study).



### D2.3. Final report on analytical, numerical and experimental studies on hydrogen dispersion in tunnels, including innovative prevention and mitigation strategies

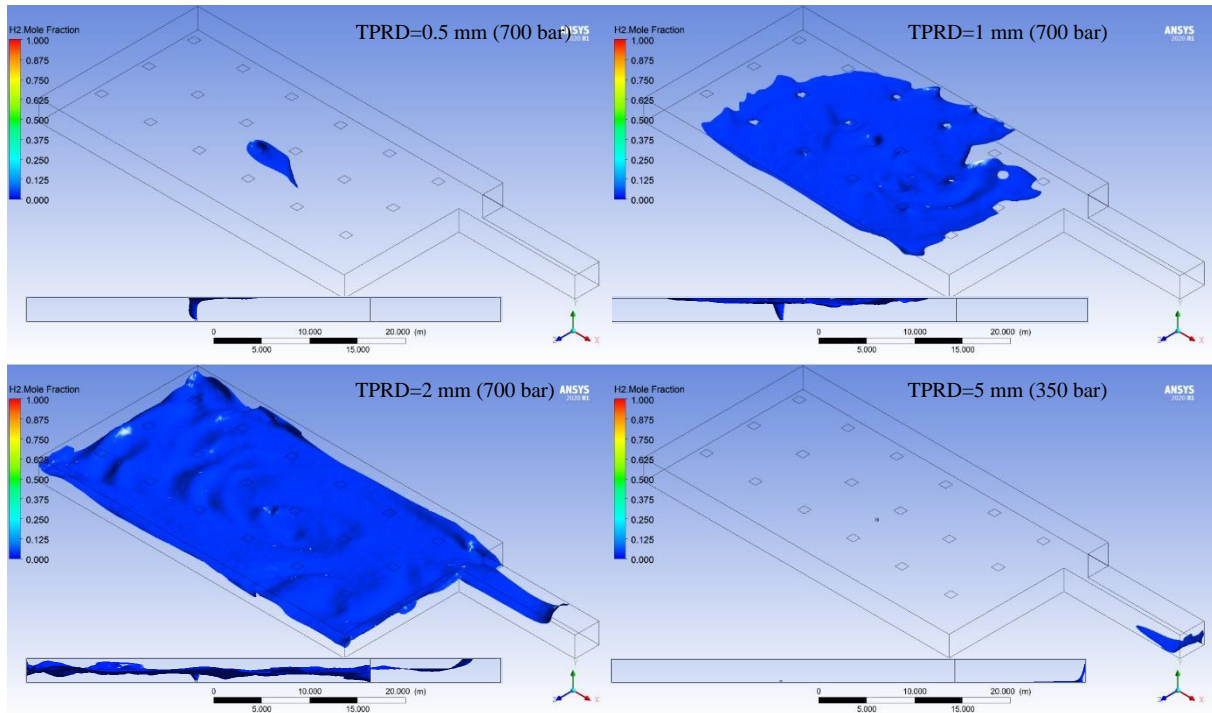


Figure 2-5. Flammable envelope (iso-surface 4%) in the underground car park for different release scenarios.

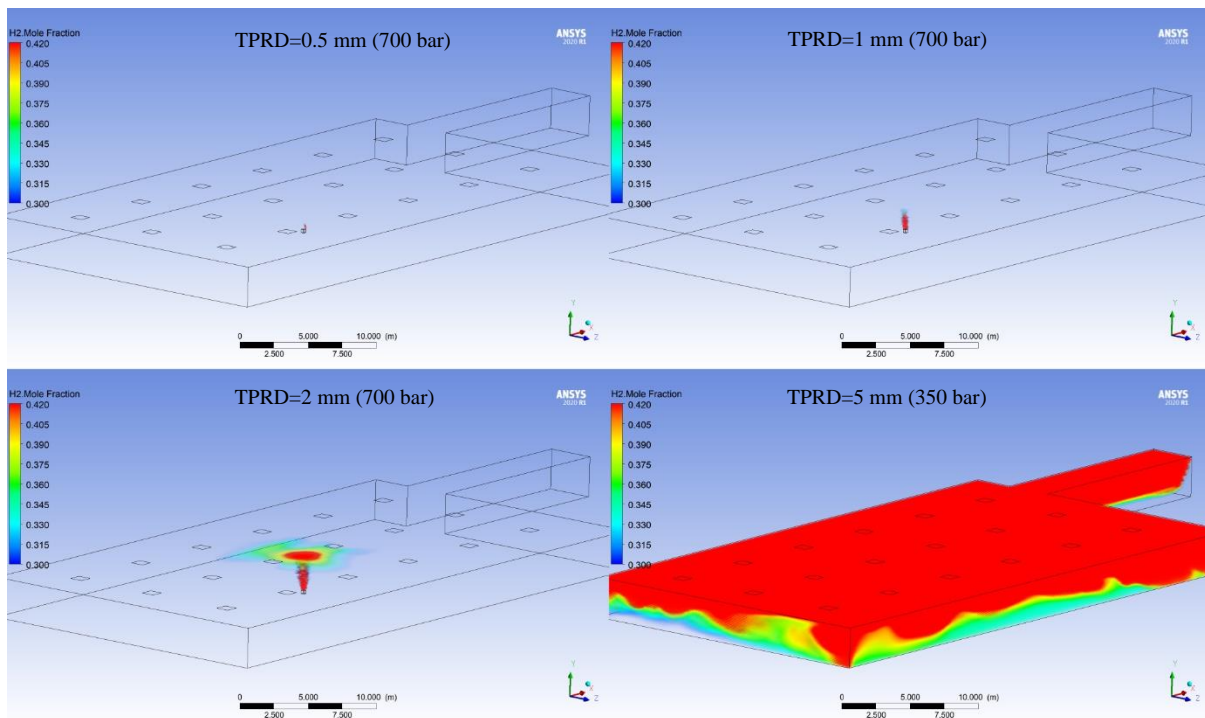


Figure 2-6. Fast burning mixture envelope (hydrogen mole fraction 30-42% vol.) in the underground car park for different release scenarios.

Figure 2-7 provides information about the uniformity of the hydrogen concentration in the vertical and horizontal directions and also the presence of spots with high concentrations. It can be seen that for all considered cases the concentration pattern is highly non-uniform both in the

### D2.3. Final report on analytical, numerical and experimental studies on hydrogen dispersion in tunnels, including innovative prevention and mitigation strategies

vertical and horizontal directions and the maximum simulated hydrogen concentration in the layer is larger than those calculated by the analytical models

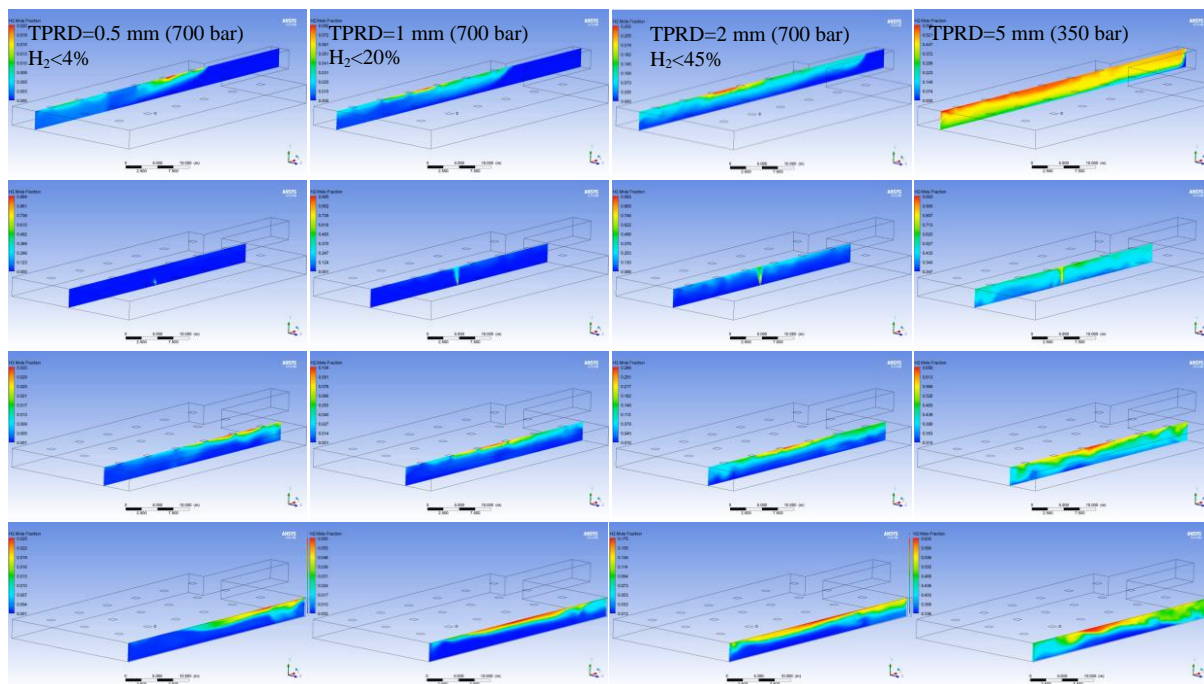


Figure 2-7. Hydrogen distribution non-uniformity and maximum hydrogen fraction in the stratified layer for different release scenarios.

Table 2-4 gives the average hydrogen mole fraction predicted by CFD simulations and by the analytical models. One may see that averaging CFD simulation results give the lowest values of hydrogen mole fraction obtained when compared to the analytical models and does not convey useful information for hydrogen safety engineering. Hazards and associated risk analysis should include simulation of deflagration of the flammable cloud calculated by this study using the deflagration CFD model.

Table 2-4. Hydrogen mole fraction: two reduced models versus averaged CFD simulation results.

TPRD, mm	P <sub>s</sub> , bar	$\dot{m}$ , g/s	“Perfect”, % <sub>av</sub>	“HyIndoor”, % <sub>max</sub>	CFD averaged, % <sub>av</sub>
0.5	700	6.73	0.85	1.4	<b>0.4</b>
1	700	26.9	4.02	6.56	<b>1.3</b>
2	700	107	14.29	21.8	<b>6.2</b>
5	350	378	37.07	49.1	<b>43</b>

Table 2-5 shows the comparison of two reduced models versus maximum concentration predicted by CFD in the layer for all considered scenarios. It can be seen that only the scenario with TPRD orifice diameter 0.5 mm excludes flammable layer formation (this also could be obtained by the similarity law calculation using the e-Laboratory). According to the similarity law, the distance to 4% vol. hydrogen fraction from 0.5 mm orifice at 700 bar is 4.2 m which



### D2.3. Final report on analytical, numerical and experimental studies on hydrogen dispersion in tunnels, including innovative prevention and mitigation strategies

is in line with CFD calculations and can be confirmed by Figure 2-5 where the iso-surface of 4% vol. hydrogen spreads at the distance close to that value.

*Table 2-5. Hydrogen mole fraction: two reduced models versus maximum CFD simulation results (excluding jet zone).*

TPRD, mm	Pressure, bar	Hydrogen mole fraction @10 ACH, %		
		“Perfect mixing”	“HyIndoor” method	CFD <sub>max</sub>
0.5	700	0.85	1.4	4
1	700	4.02	6.56	20
2	700	14.29	21.8	45
5	350	37.07	49.1	70

#### 2.3.5 Conclusions

Calculation of parameters of mechanical ventilation in underground parking was performed using two reduced models and a CFD model. Both proposed analytical reduced models underestimated hydrogen concentration in a layer under the ceiling. The “Perfect mixing” model underprediction is due to averaging throughout the parking volume, and the “HyIndoor” model underprediction is due to horizontal concentration uniformity assumption. It has been shown that the “Perfect mixing” equation has the lowest predictive capability and cannot be applied due to drastic underprediction of maximum hydrogen fraction in a realistic hydrogen release from onboard hydrogen storage. The only model that could be considered as a reliable tool for the design of mechanical ventilation in the underground parking is CFD, especially taking into account highly dynamic release character (i.e. blowdown of the storage tank), a large volume of parking, presence of obstacles, losses in the ventilation ducts etc.

“HyIndoor” modelling method can only be applied when the designer proves that the distribution is uniform across the layer and there are no spots with high hydrogen concentration and the geometry of the parking is simple. That is not applicable when there is layering in the horizontal direction.

CFD simulations provided the most realistic and useful for engineering analysis solution for hydrogen distribution, and as such should be targeted as the preferable tool for hydrogen safety engineering. Among simulated release scenarios only release from TPRD with orifice diameter 0.5 mm does not create a flammable layer and is a safe solution for practically any parking space where the regulation requirement 10 ACH is met. Simulation of the formed flammable mixture deflagration and analysis of pressure hazards was out of the scope of this study and not included in the analysis of ventilation design acceptability.

#### 2.3.6 Additional work done

Following the steady-state simulation conclusions presented above there was a number of questions that have been answered in a later study:

- The previous study assumed the steady-state release but in reality, the release in unsteady and therefore transient simulations to account for the blowdown of the storage tank were performed with the presence of the vehicle to give a true picture of the

### D2.3. Final report on analytical, numerical and experimental studies on hydrogen dispersion in tunnels, including innovative prevention and mitigation strategies

concentration distribution and also the timing and location of the hazardous concentrations.

- Most TPRDs installed on vehicles located in downward direction under the car and these scenarios were also simulated to account for the correct direction and concentration decay of hydrogen before it will start to form hazardous concentration and layer.

Comprehensive CFD study on hydrogen release in an underground car parking has been done and described in the publication presented at the International Conference on Hydrogen Safety (Shentsov et al., 2021).

The overall set of conclusions resulting from the conducted research is:

- The originality of the performed research is in conducting analysis of hydrogen release and dispersion from a high-pressure hydrogen tank in underground parking taking into account the effect of release direction, angle, ceiling height and ventilation. Safety strategy based on similarity law for concentration decay along hydrogen jet axis and allowing to exclude flammable mixture formation under car parking ceiling by limiting TPRD diameter is demonstrated for vertical release direction. The series of 15 simulations of unignited blowdown releases taking into account realistic vehicle and car parking geometry with and without account of mechanical ventilation in underground parking is performed providing detailed information on hydrogen-air mixture dynamics.
- The rigour of this work is in the consistent and detailed analysis across the whole range of potential TPRD design parameters (diameter, release direction), realistic car park geometries (heights, space), ventilation rates (from no ventilation, ACH=0, up to the regulated 10 ACH).
- The significance of this study is in demonstration that the proper design of TPRD deem to satisfy safety requirements in case of accidental hydrogen release in underground car parking which mechanical ventilation is compliant with currently existing RCS. The fact enables the use of currently existing parking and underground infrastructure with the new generation of HFC EV.

To underpin the safe introduction of HFC EV into underground infrastructure the following conclusions were drawn:

- The general strategy for underground parking is to eliminate the formation of flammable cloud under the ceiling.
- For the upward releases, the similarity law can be used to calculate at what TPRD size the hydrogen jet will decay below 4% before reaching the ceiling.
- The ventilation does not affect hydrogen flammable clouds formed by releases from TPRD with diameter 0.5-0.75 mm.
- TPRD release direction downward at the angle  $A=45^\circ$  to vertical deem to be the overall best safety solution in the range of studied TPRD diameters 0.5-2.0 mm. Releases directly downward (at the angle to vertical  $A=0^\circ$ ) generate buoyant hydrogen-air plume and form flammable layer under the ceiling. Releases at the angle  $A=0^\circ$  and  $30^\circ$  provide mixture propagation toward the front and rear wheels, which, if ignited, will contradict to RCS requirements for HFC EV.

### D2.3. Final report on analytical, numerical and experimental studies on hydrogen dispersion in tunnels, including innovative prevention and mitigation strategies

- Releases from TPRD with diameter 0.5 and 0.75 mm don't result in a flammable layer formation under the car park ceiling for the considered range of ceiling heights (2.1-3.0 m) and ventilation rates – ACH=0 (no ventilation) and ACH=10 (required mechanical ventilation rate in case of fire).
- Releases from TPRDs with a diameter above 0.75 mm have the potential to create a flammable layer, especially in the absence of mechanical ventilation.
- Releases from TPRD towards obstacles tend to prohibit hydrogen mixing with air and promote the accumulation of a flammable cloud; it should be recommended not to park HFC EV with TPRD directed towards obstruction.
- The use of analytical models for the analysis of mechanical ventilation effect on hydrogen propagation from onboard storage releases seems to suffer a loss of accuracy due to transient and highly non-uniform hydrogen distribution. This is particularly pronounced for enclosures with large volumes and complex geometries. The use of more accurate methods capable to resolve spatial and temporal hydrogen dynamics like CFD should be considered for these problems.

The above discussion has provided a valuable contribution to the recommendations to regulations, codes and standards (RCS) related to dealing with unignited hydrogen releases in confined spaces.

#### **2.4 Non-adiabatic blowdown model for under-expanded jets from the onboard storage tank (UU)**

The developed non-adiabatic blowdown model for under-expanded jets from the onboard storage tank as well as the application of the model for the design of the inherently safer tank-TPRD system with reduced TPRD diameter, were described in the publication presented at the International Conference on Hydrogen Safety (Dadashzadeh et al., 2019) and in the journal publication (Molkov et al., 2021).

### 3. Numerical studies (Task 2.3/NCSR D)

#### 3.1 Mechanical ventilation in underground parking – pre-test simulations (Sub-task 2.3.1/NCSR D)

The aim was to use pre-test simulations to primarily assess the safety of the planned experiments in Sub-task 2.4.1 at USN.

##### 3.1.1 Numerical set-up

Assumed experimental layout (see Figure 3-1):

- 40 feet iso-container with internal dimensions  $12.022 \times 2.352 \times 2.395$  m and  $V = 67.72 \text{ m}^3$  vol.
- Ventilation inlet at one side, fully open at the opposite side
- Mockup car with dimensions  $3.5 \times 1.176 \times 0.5$  m, located 4.5 m from ventilation wall, 0.2 m from the floor, 0 m from the lateral wall of the container

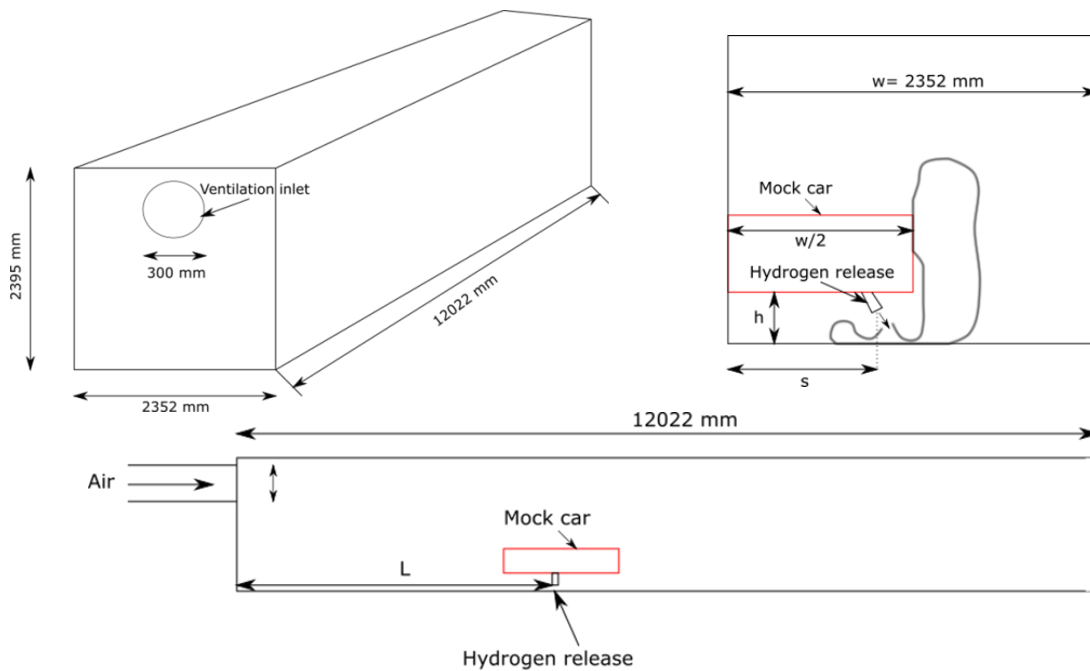


Figure 3-1. Experimental layout.

Release characteristics:

- Release nozzle laterally centered below car pointing vertically downwards, 5 m from ventilation wall
- Blow-down of 1kg of H<sub>2</sub> from stagnation conditions 100 bar, 15 C
- Two nozzle diameters 1.0 and 2.0 mm

Ventilation characteristics:

- 300 mm diameter, top of inlet 10 cm below the ceiling
- Two ventilation rates of 11.25 (as per regulation (Krarti and Ayari, 2001)) and 22.5 ACH (i.e. double).

## D2.3. Final report on analytical, numerical and experimental studies on hydrogen dispersion in tunnels, including innovative prevention and mitigation strategies

Computational characteristics:

- ADREA-HF CFD to simulate 3D steady state pre-existing flow before release
- NCSRD release tool for blow-down, with Helmholtz Free Energy (HFE) formulation hydrogen equations of state (EoS)
- ADREA-HF CFD code for H<sub>2</sub> dispersion
- MUSCL (2<sup>nd</sup> order) scheme for convective discretization
- Computational domain extended 2m beyond open side
- Notional nozzle scheme: (Birch et al., 1984)
- Number of grid cells: 84k (see Figure 3-2)

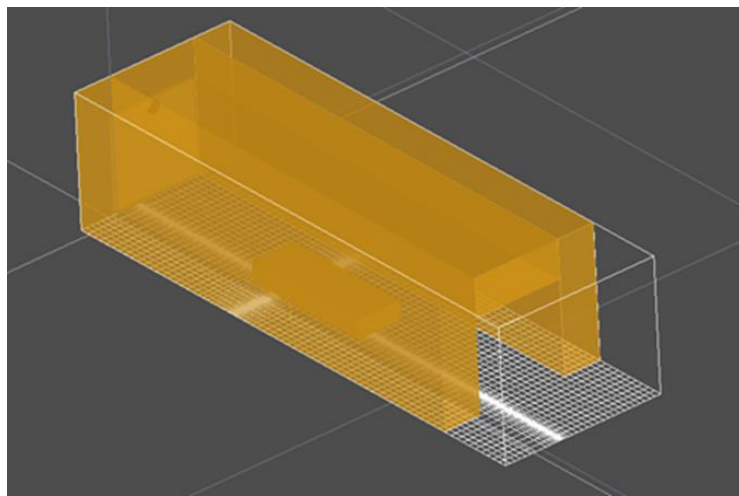


Figure 3-2. Computational domain and grid.

### 3.1.2 Computational results

Release tool predicted mass flow rates are shown in Figure 3-3.

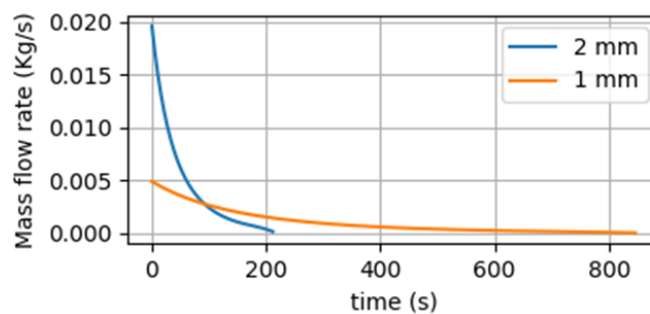


Figure 3-3. Predicted H<sub>2</sub> release mass flow rate.

Predicted flammable (4-75 vol. %) H<sub>2</sub> mass and cloud volume time histories are shown in Figure 3-4. The effect of nozzle size on the maximum flammable volume is significant. For the 2 mm nozzle, maximum flammable volume reaches approximately 70% of the garage volume, while for the 1 mm nozzle approximately 25%. The effect of doubling the ventilation on the maximum flammable volume is found not very important. More precisely, for 1 mm nozzle,

### D2.3. Final report on analytical, numerical and experimental studies on hydrogen dispersion in tunnels, including innovative prevention and mitigation strategies

max. flammable mass and volume decrease with ventilation, while for 2 mm nozzle both increase.

Hydrogen clouds of 10-75 vol. % are more significant in terms of the overpressure that will be produced in case of ignition. It is also experimentally known that the flame can propagate downwards (i.e. against gravity) only if hydrogen concentration is above 10 vol. %. Predicted 10-75 vol. % clouds are shown in Figure 3-5.

It can be observed that the maximum volume is reduced by at least factor of 10 compared to the maximum flammable cloud volume, and is 7% of the garage volume for the 2mm nozzle and 1.5% for 1mm. Again, as with the flammable cloud the effect of nozzle size is much more significant than the effect of ventilation. Increasing the ventilation, results in the decrease of the 10-75% hydrogen cloud volume, for both nozzle diameters.

Hydrogen clouds of 32-42 vol. % are considered as the most dangerous one in the case of an explosion due to the high flame speed, following the preliminary results obtained from the study on delayed ignition of hydrogen jets in HyTunnel-CS. In Figure 3-6 we observe that the maximum corresponding cloud volume reaches 0.4 m<sup>3</sup> for 2 mm nozzle and 0.05 m<sup>3</sup> for 1 mm nozzle. These volumes are located close to the release.

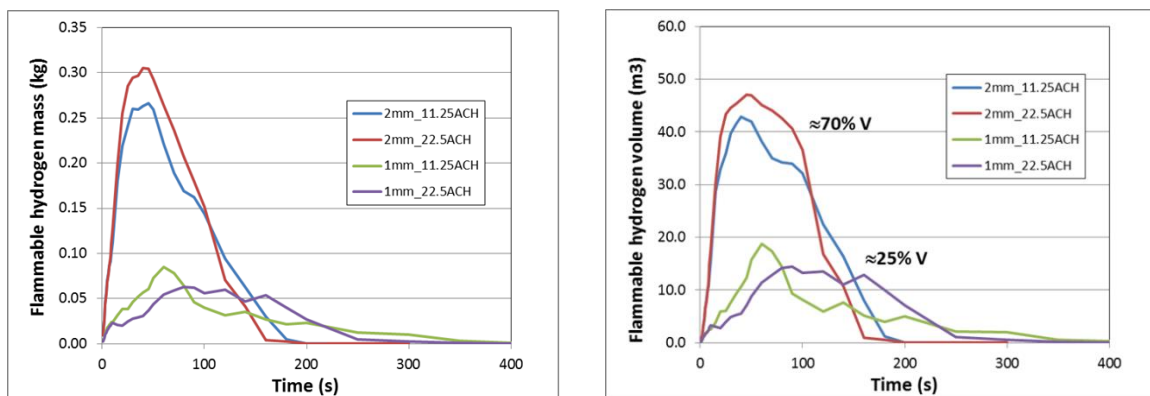


Figure 3-4. Predicted H<sub>2</sub> mass and cloud volume time histories for 4-75 vol. % cloud.

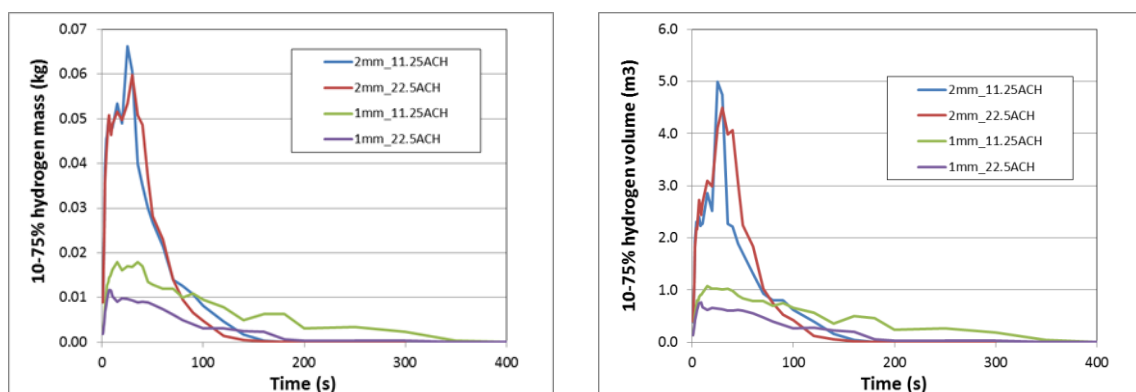


Figure 3-5. Predicted H<sub>2</sub> mass and cloud volume time histories for 10-75 vol. % cloud.

### D2.3. Final report on analytical, numerical and experimental studies on hydrogen dispersion in tunnels, including innovative prevention and mitigation strategies

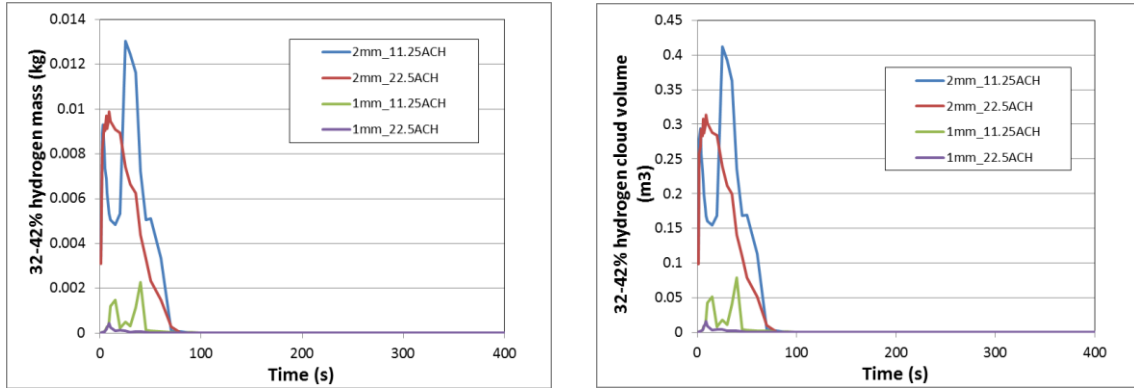


Figure 3-6. Predicted H<sub>2</sub> mass and cloud volume time histories for 32-42 vol. % cloud.



## 3.2 Mechanical ventilation in underground parking – validation simulations (Sub-task 2.3.1/NCSRd)

### 3.2.1 Problem formulation

NCSRd performed validation simulations based on test-19 of the USN experiments in underground parking (see Section 4.1). In test-19, hydrogen blowdown release inside a semi-confined garage with forced ventilation took place. Hydrogen was released under a table- to model the car- with direction vertically downwards. The tank pressure was approximately 700 bar, the nozzle was 0.5 mm and the ventilation rate through the fan was 10 ACH. More details can be also found in (Lach and Gaathaug 2021).

Figure 3-7 (left) shows the experimental mass flow rate, which was also used as input data in the simulations. Figure 3-7 (right) shows the problem geometry, the grid on ground level and the sensor positioning of the simulation. Symmetry along the y-axis was assumed. The simulation was performed with the in-house CFD code, ADREA-HF, which solves the 3D time-dependent conservation equations. To model the under-expanded jet that is formed due to the high released pressure the Birch 84 notional nozzle approach was employed.

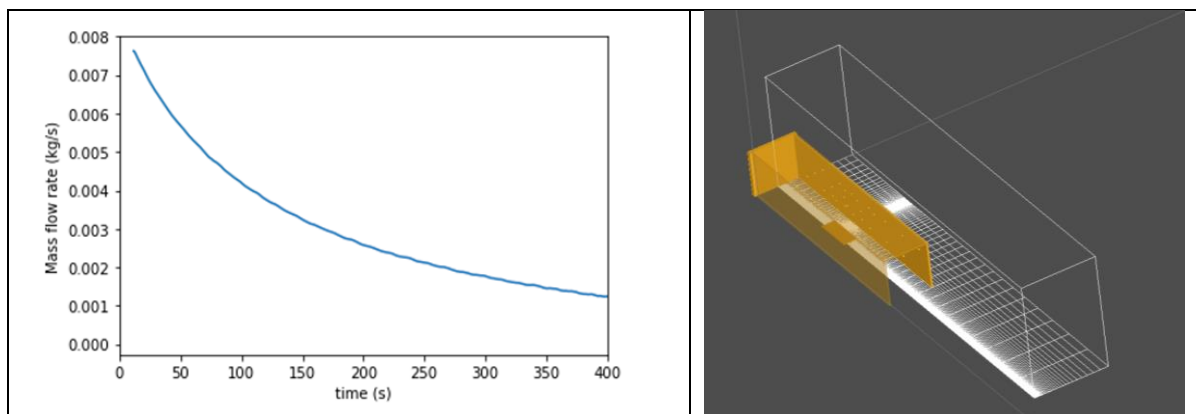


Figure 3-7. The mass flow rate during the blowdown (left) and the problem geometry with the grid on ground level (right).

During the experiment the facility was exposed to the external wind of 1 m/s by average with direction towards the one side of the facility. Wind effect on the hydrogen distribution inside the parking can be significant (Giannissi et al., 2016). Therefore, an additional simulation that models the external wind was also performed.

To account for the external wind, a 3D steady state simulation was initially carried out to obtain the velocity field generated by the external wind and the fan. The steady state results were used as initial and inflow boundary conditions in the 3D dispersion simulation. No symmetry assumption was used in this case.

### 3.2.2 CFD results

Figure 3-8 displays the computational versus the experimental time series at several sensors for the case without modelling the external wind. Fairly good agreement is found for all sensors near the ceiling. The concentration at the sensors close to the nozzle and under the car (S25 and S27) is over predicted, especially at the first half of the blowdown (until about 500 and 300 sec for S25 and S27, respectively).



### D2.3. Final report on analytical, numerical and experimental studies on hydrogen dispersion in tunnels, including innovative prevention and mitigation strategies

For S27, which is located below the nozzle few millimetres offset the release centreline, the over prediction can be partially explained by the fact that at distances so close to the nozzle high concentration gradients occur (thus, also, the high peak at the first few seconds of the release). As shown in Figure 3-9 sensor S27 is located exactly at the jet boundary. Tecplot gives a value of H<sub>2</sub> volume fraction approximately equal to 0.2 exactly in that point at 1 sec, while 5 mm offset, i.e. at  $x=5.015$  m, it gives a volume fraction equal to 0.088. This brings two things under consideration: a) the interpolation method that is performed to compute the concentration at an exact point, which is not the cell centre (where scalar variables are computed), will affect significantly the predicted value if this point lies within a region with high gradients, i.e. at jet boundary, b) in such regions the exact position that the experimental sensor takes the sampling is a significant factor, because even 5 mm offset of the sensor might lead to different measurement. As blowdown progresses this phenomenon (the high gradients) is less pronounced and thus the differences between experiment and simulation are reduced. Based on the above it is recommended to pay special attention when one compares simulation results with experimental results at jet boundaries where high gradients are expected. The use of a very fine grid and/or a mesh design such that the sensor's exact position to fall at the cell centre avoiding any interpolation might be a possible solution to that issue.

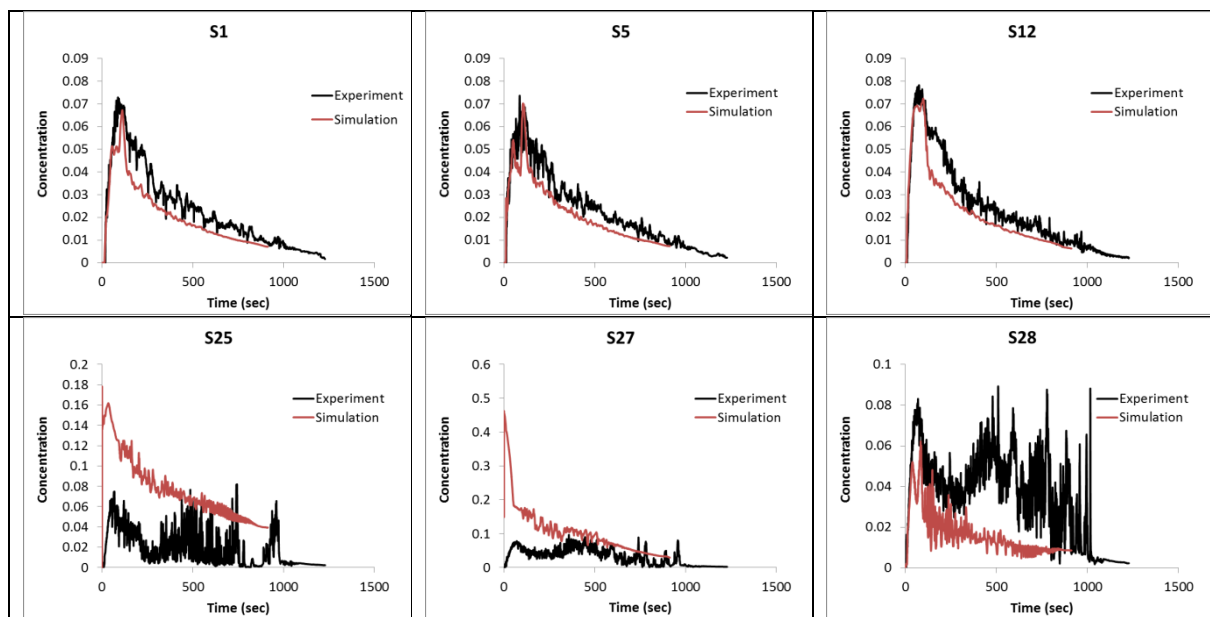


Figure 3-8. Comparison of experimental and simulation results for the sensors near the ceiling (top) and close to the release under the car (bottom) for the case without modelling external wind.

Another possible reason for the discrepancies between experiment and simulation at S27 could be the fact that simulation produces a higher level of diffusion.

As far as S25 is concerned, which is located at floor level and 370 mm offset the release point along the garage width, the over prediction at the first half of the blowdown, implies that in the simulation there is a higher level of spreading along the lateral direction. Several factors can influence the diffusion of the jet, e.g. numerical issues like discretization schemes, turbulence, imposed release momentum etc. A different notional nozzle approach (Ewan and Moodie approach) with lower notional velocity and temperature was examined to investigate its effect on the lateral spreading of the mixture. The results showed a negligible effect on the prediction.

### D2.3. Final report on analytical, numerical and experimental studies on hydrogen dispersion in tunnels, including innovative prevention and mitigation strategies

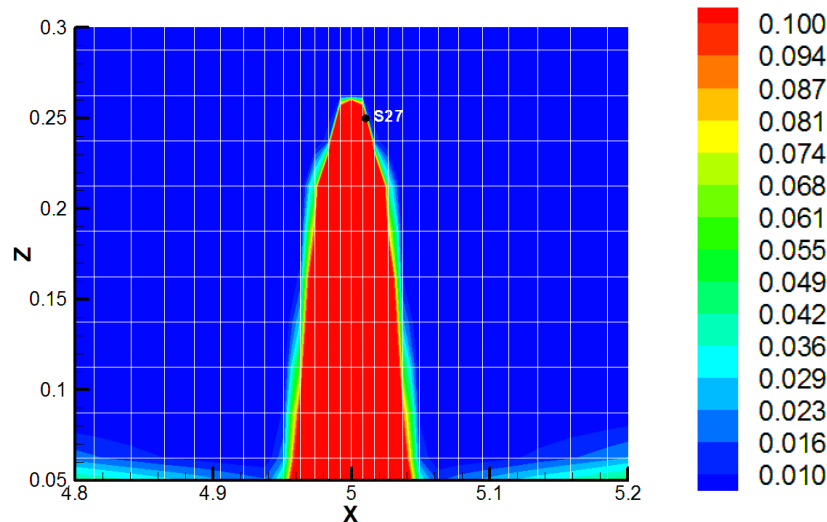


Figure 3-9. The H<sub>2</sub> concentration contours at 1 sec using software Tecplot at a view close to the nozzle. The black point indicates the position of sensor S27.

Figure 3-10 displays the computational versus the experimental time series at several sensors for the case with modelling the external wind. Very good agreement is found between experiment and simulation. Direct comparison between the simulation results with wind and without wind is not applicable, because different mesh resolution was used. In the future, simulations with exactly the same mesh for the two cases can be performed for consistent comparison.

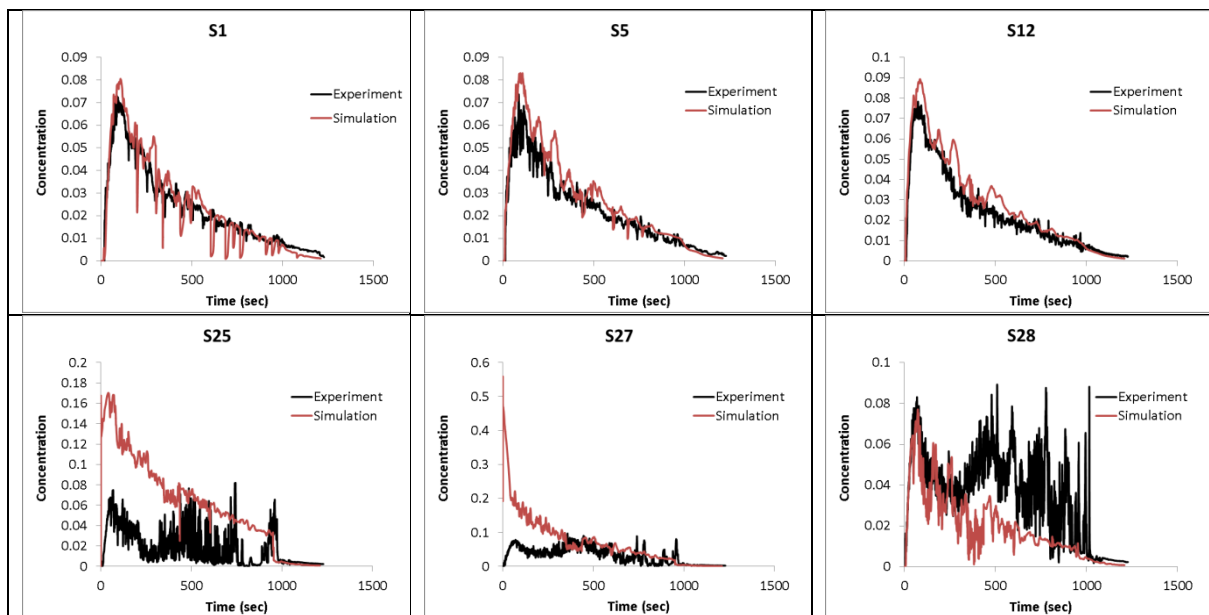


Figure 3-10. Comparison of experimental and simulation results for the sensors near the ceiling (top) and close to the release under the car (bottom) for the case with modelling external wind.

### 3.2.3 Conclusions

Validation simulations were carried out based on the USN underground parking experiments. Test 19 was simulated with blowdown release through 0.5 mm nozzle at 700 barg. A notional nozzle approach that assumes sonic velocity at ambient conditions on notional nozzle (Birch et al., 1984) was applied to model the high-pressure release. Generally good agreement was found

## D2.3. Final report on analytical, numerical and experimental studies on hydrogen dispersion in tunnels, including innovative prevention and mitigation strategies

between simulation and experiment. Additional simulation, which models the external measured wind, was also tested and it was shown that the predictions were affected.

In both cases, overprediction was found at the sensor very close to the nozzle. The reason for that can be partially attributed to the fact that this sensor is placed at the jet boundary, where high gradients occur and the interpolation of the neighbouring concentration values to compute the concentration at one exact single point can lead to overestimation. Another possible reason for the overestimation close to the nozzle could be that simulation predicts higher level of diffusion.

Higher levels of lateral spreading were also found in the simulation. Several factors can contribute to that effect, such as turbulence, numerical schemes, mesh design, etc. To examine if a reason for the over prediction of the lateral spreading is the high introduced momentum at the effective nozzle, another notional nozzle approach was examined. In this approach the notional nozzle velocity is lower and the notional nozzle temperature is lower than ambient (Ewan and Moodie, 1986). Nonetheless, no impact was found on the results.

### 3.3 Dynamics of H<sub>2</sub> release and dispersion in a tunnel – pre-test simulations (Sub-task 2.3.1/CEA/NCSR)

#### 3.3.1 CEA simulations

CEA aims at performing simulation of H<sub>2</sub> (or helium) release in a tunnel for multiple reasons:

- First, it will be used as an input of combustion calculation on an initially unignited dispersed cloud in a tunnel;
- Second, as a validation support to simple models and to experimental measurement of a dispersed helium cloud (then a hydrogen dispersed cloud if non ignited which is not guaranteed);
- Third, as pre calculation for the above-mentioned experiments.

Therefore, we perform realistic calculations on geometries as close as possible to reality. Nevertheless, they suffer two inconveniences: they are simple calculations on helium only as pre-calculation of the chosen tunnel configuration; the real configuration had to be given up the day the experimental campaign started due to COVID-19 confinement at CEA (and in France). The team who were on site were called back and the right to access the tunnel are effectively lost for unknown time. A back-up tunnel has been found, but the presented results are of less interest since they don't match the geometry of the newly selected tunnel.

##### 3.3.1.1 Numerical set-up

As part of the HyTunnel project's dispersion and combustion experiments, CEA carried out preliminary CFD calculations to characterize the evolution of helium clouds and overpressures on the tunnel walls in the case of tank rupture. In this document, we report only selected dispersion calculations.

NEPTUNE CFD is a three-dimensional multi-fluid code developed especially for nuclear reactor applications by EDF, CEA, AREVA, and IRSN (Guelfi et al., 2017), (Mimouni et al., 2017). This CFD code is dedicated to the simulation of incompressible and compressible multicomponent/multiphase flows (Mimouni et al., 2011). The solver is based on a finite volume discretization, together with a collocated arrangement for all variables. Different

### D2.3. Final report on analytical, numerical and experimental studies on hydrogen dispersion in tunnels, including innovative prevention and mitigation strategies

turbulence models are available and we used the standard k-epsilon model in the simulations together with standard wall functions.

Concerning validation, NEPTUNE-CFD was used to simulate the GARAGE experiments carried out at CEA Saclay for helium dispersion in a confined volume. It also successfully simulated a helium transport transient by molecular diffusion in the CEA MISTRA enclosure. Finally, it is currently being used to simulate the erosion of a helium stratification by a diffused buoyant jet (Studer et al., 2018), (Abe et al., 2018).

#### Tunnel geometry

The tunnel envisaged for the tests corresponds to a technical gallery of the Villarodin-Bourget-Modane descenderie (Figure 3-11 – left). It is 110 meters long, approximately 7.5 meters high and 11.2 meters wide. It is blind on one side and connected to another access gallery at its other end. Ventilation can reach 138,000 m<sup>3</sup>/h, which corresponds to a speed of flow of 0.5 m/s in the gallery.

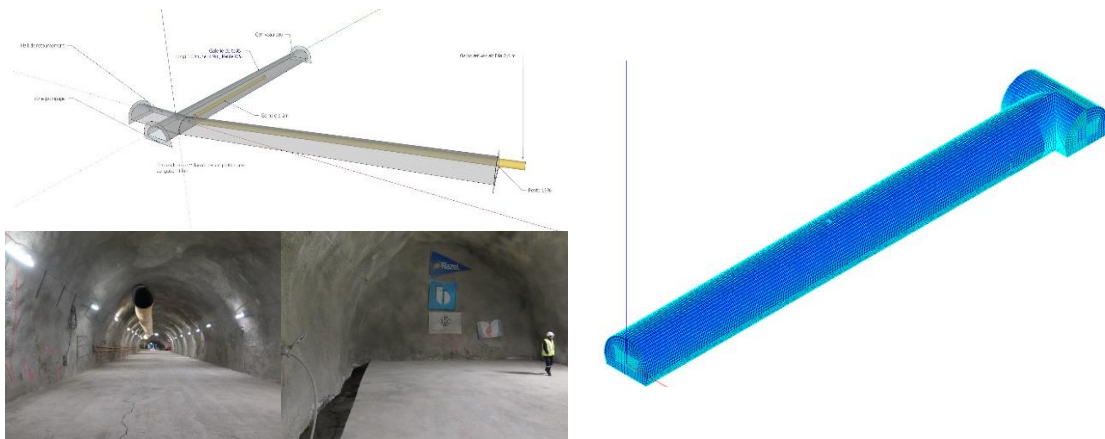


Figure 3-11. Tunnel geometry – Left: Description of the gallery and pictures, Right: Coarse grid for the preliminary CFD computations.

The coarse mesh was made with hexahedrons as regular as possible and contains about 140,000 cells (Figure 3-11 – right). Only a small part of the access gallery has been meshed. The reference mesh size is 40 cm. The helium injection takes place in the middle of the main gallery.

#### Simulated scenarios

As the planned hydrogen tests will be carried out with a 70-litre tank at 700 bar, we have simulated a helium release of the same volume, i.e. approximately 5 B50 cylinders at 200 bar. Helium discharge tests are planned in the qualification phase of the experimental device and we are simulating them in order to help the positioning of the concentration measurement sensors. The diameter of the discharge corresponds to TPRDs of 2 and 3 mm. The releases are oriented upwards or towards the ground. They are carried out at a height of 80 cm above the ground (2 coarse grid meshes).

The release transient was calculated with a simple depressurization model developed by CEA with an adiabatic discharge assumption and a perfect gas model (suitable for this pressure level). The results were successfully compared with those produced by the corresponding

## D2.3. Final report on analytical, numerical and experimental studies on hydrogen dispersion in tunnels, including innovative prevention and mitigation strategies

NETTOOLS modules (Figure 3-12- left). The values were then fitted with a polynomial to be implemented in the boundary conditions of the numerical model (Figure 3-12 – right).

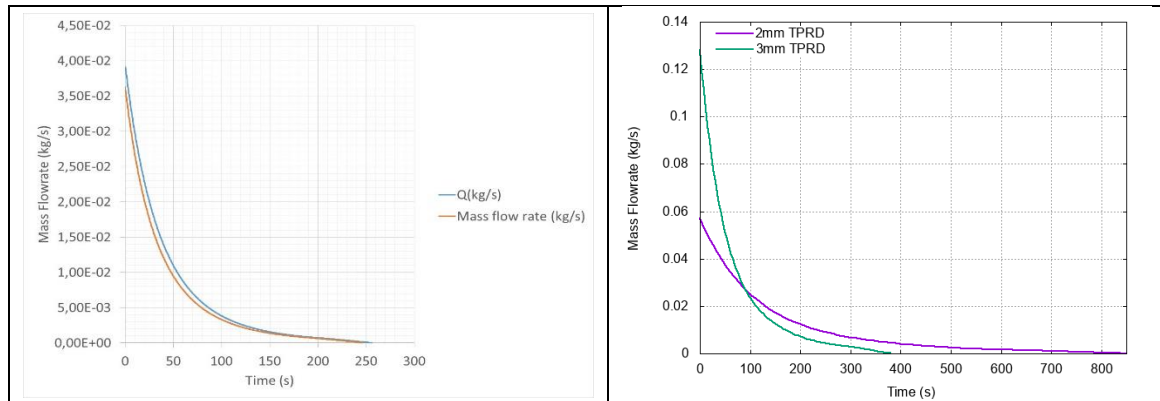


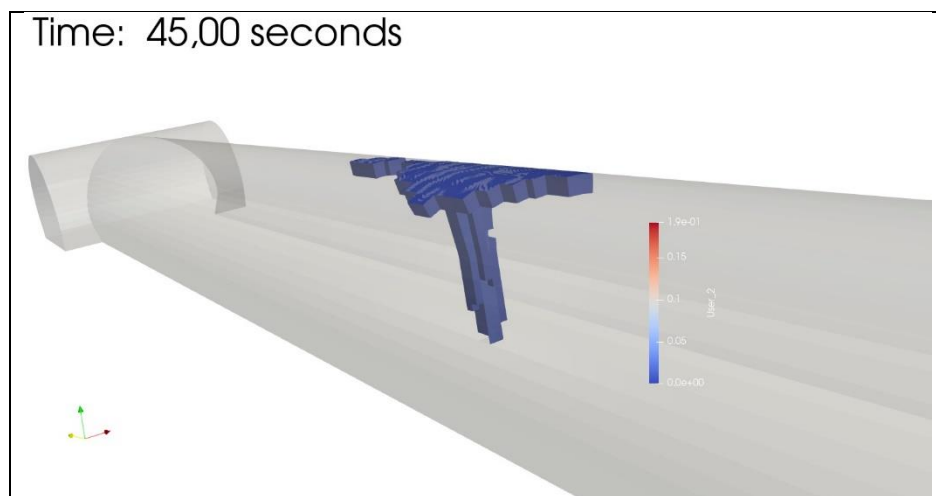
Figure 3-12 . Injection flowrate – Left: Comparison with NET-Tools (red) for 100 l tank of 200 bar of hydrogen through 2 mm leak, Right: Investigated helium flowrates (5 B50 bottles 200 bar).

In all the computations, the effect of the ventilation was neglected.

### 3.3.1.2 Computational results

The objective of these preliminary calculations was to obtain an estimate of the size of the helium cloud that could be quantified with catharometers. For these calculations, we present the cloud's volume size for which the helium concentration is higher than 0.5 vol. %. The sensor catharometers are given for an accuracy of 0.1 vol. %.

For vertical upward injection, the maximum cloud extension ( $>0.5$  vol. %) is shown in Figure 3-13 for two sizes of TPRD. The maximum extension is obtained in both cases after a few tens of seconds. As expected, the cloud generated by the opening of a 2 mm TPRD is much smaller than that for a 3 mm TPRD. The shape of the cloud is basically composed of two zones: the rising pattern and a layer along the tunnel ceiling. The axial extension is a few meters for 2 mm and reaches more than ten meters for 3 mm. In all cases, the gradient is limited to a mesh thickness of less than 40 cm. Finer grid simulations are needed to accurately quantify this layer.



### D2.3. Final report on analytical, numerical and experimental studies on hydrogen dispersion in tunnels, including innovative prevention and mitigation strategies

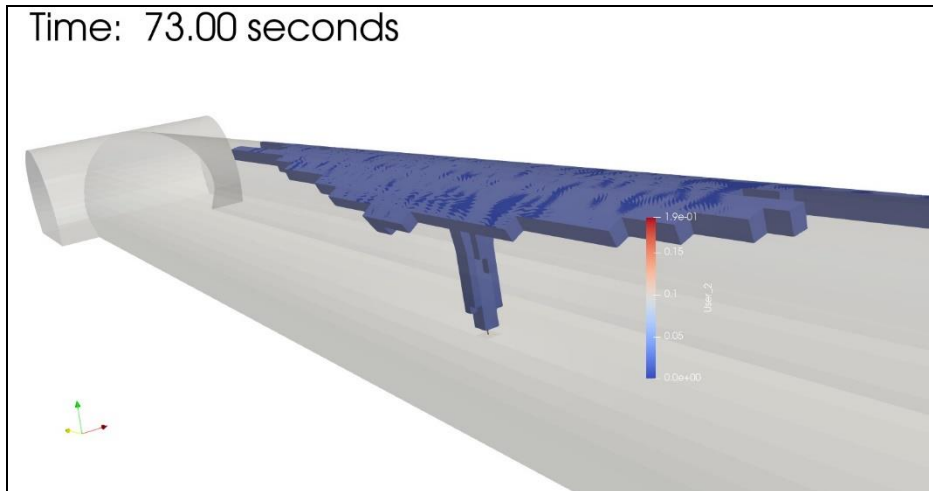
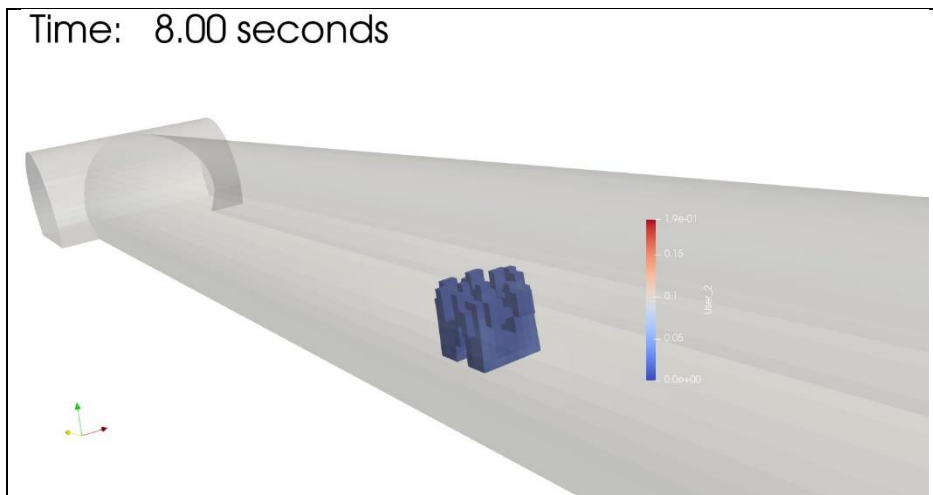


Figure 3-13. Maximum size of the helium cloud with concentration higher than 0.5 vol. % - Top 2 mm TPRD, Bottom 3 mm TPRD.

In the case of a vertical downward discharge, the flow structure is much more complex (Figure 3-14). First, in the first few seconds the extension is symmetrical with the flow rising a few meters from the injection point. This result is probably highly dependent on the modeling method used (turbulence model and mesh refinement). Then, the flow is structured in two rising plumes located axially in the tunnel. Again, the exact position is probably highly dependent on the modeling approach used. Nevertheless, these rough calculations show us that the location of the sensors for this type of discharge is much more difficult to predict. It will therefore be necessary to strongly densify the measurements in this case.





## D2.3. Final report on analytical, numerical and experimental studies on hydrogen dispersion in tunnels, including innovative prevention and mitigation strategies

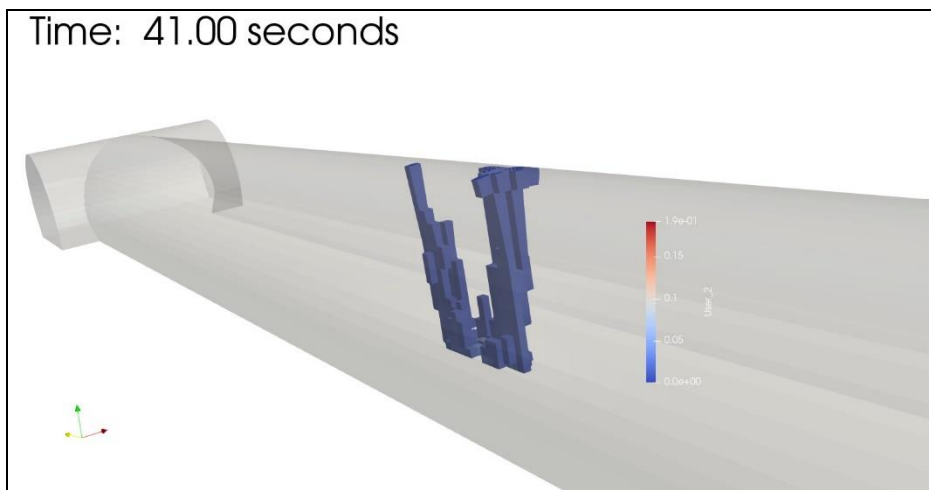


Figure 3-14. Maximum size of the helium cloud with concentration higher than 0.5 vol. % - 3 mm TPRD vertical downwards release.

These preliminary simulations showed us where to locate our concentration measurement sensors during helium discharges. A BOS system is also foreseen to visualize the spatial extension especially for vertical downwards releases. The Covid-19 pandemic did not allow these tests to be carried out in the above-mentioned tunnel. The experiments were therefore conducted in a different geometry.

### 3.3.2 NCSRD simulations

The aim of this task is to perform pre-test simulations of hydrogen release and dispersion inside scaled tunnel, in order to provide directions to the experimental setup, e.g., positioning the sensors, requirement on the measuring ranges of the sensor etc. The measured data after the completion of the experiments will be used to validate the simulation results.

For this task three tests from the HSE experimental campaign were simulated: 1) a simulation with release from a car inside a tunnel filled with vehicles, 2) a simulation with release from a train inside an empty tunnel and 3) a simulation with release from train inside a tunnel filled with train carriages. The last scenario was selected as it can be characterized as the worst case scenario with high congestion that could lead to high overpressures in case of deflagration. This scenario and the scenario with release from train inside an empty tunnel were also selected for pre-test simulations of deflagration of non-uniform hydrogen-air cloud (HyTunnel-CS D4.3, 2022), in order to assess the level of risk and provide valuable information to the experimentalist regarding the overpressure that is likely to be developed during the specific test cases.

In this Section, the computational results of the three pre-test simulations are shown. Table 3-1 presents the pre-tests' conditions. In the car scenario the release was vertically downwards (D), while for the train scenarios the release was vertically upwards (U).

Table 3-1. Conditions for the pre-tests of hydrogen dispersion inside scaled tunnel.

	Car	Train	Train
<b>Tank Mass (kg)</b>	0.46	5.07	5.07
<b>Scaled nozzle (mm)</b>	2.2	5.7	5.7
<b>Scaled ventilation velocity (m/s)</b>	1.25	1.25	1.25



### D2.3. Final report on analytical, numerical and experimental studies on hydrogen dispersion in tunnels, including innovative prevention and mitigation strategies

Release direction	D	U	U
Car models	8 mock-up vehicles	no vehicles	8 carriages

#### 3.3.2.1 Numerical set-up

All pre-test simulations were performed using the ADREA-HF CFD code. The release conditions during the blowdown were calculated using an in-house release code of NCSRD (Venetsanos et al., 2021a), (Venetsanos et al., 2021b). The release code performs isentropic expansion from tank conditions to nozzle conditions using the NIST EoS. The Birch 84 notional approach was employed to model the under-expanded jet and to estimate the conditions after the jet has expanded to ambient pressure. The results of the blowdown for both the car case and the train case are shown in Figure 3-15.

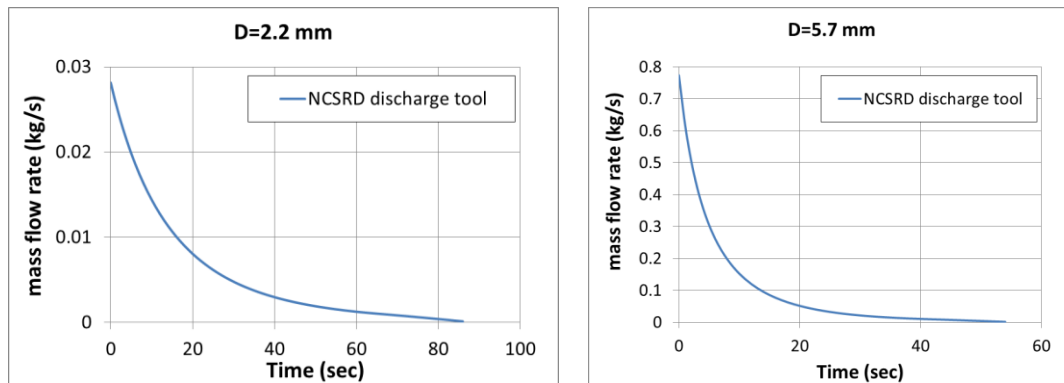


Figure 3-15. The blow down results using the in-house release code of NCSRD for the car case (left) and the train case (right).

The notional conditions are set as hydrogen release conditions in the CFD simulation. Table 3-2 presents the notional nozzle conditions at the initial time ( $t=10^{-3}$  s) for the two different cases. As time progresses temperature and velocity remain constant, while the notional diameter and the mass flow rate decrease.

## D2.3. Final report on analytical, numerical and experimental studies on hydrogen dispersion in tunnels, including innovative prevention and mitigation strategies

*Table 3-2. The conditions at the notional nozzle for the two cases.*

	Temperature (K)	Velocity (m/s)	Diameter (m)	Flow rate (kg/s)
Car, $d=2.2$ mm	288	1289.92	0.018	0.028
Train, $d=5.7$ mm	288	1289.92	0.095	0.77

### 3.3.2.2 Dispersion modelling

In general, the modelling set-up followed the Best Practice Guidelines developed within the SUSANA project (2013-2016). The modeling strategy consists of the two following steps:

- 3D simulation without release to obtain the steady state of the ventilation. The ventilation velocity is imposed uniformly along the one opening of the tunnel and the established steady state velocity field is set as initial and inflow boundary condition in the CFD dispersion simulation (next step). Approximate values for  $k$  and epsilon on the inlet boundary were imposed based on the values that the CFD code predicts at the beginning of the simulation according to the applied inlet velocity. Given non-zero values at the inlet boundary are necessary, because if no turbulence is imposed the initially generated turbulence is dampened down. This leads to extremely low turbulence kinetic energy (almost zero) at steady state, which is unphysical. Furthermore, if the initial and inlet boundary conditions in the dispersion simulation (next step) have very small  $k$  and epsilon values the results exhibit instabilities and are highly susceptible to solvers' numerical errors (even if they are initially very small), which are "accumulated" as simulation progresses and result in taking different predictions if different number of CPUs is used.
- 3D dispersion simulation with time-dependent hydrogen release (based on the blowdown results).

Domain extension at all directions was imposed at the opening of the tunnel where there is no ventilation and constant pressure boundary condition was applied at open boundaries. The hydrogen release is discretized using 4 cells and low expansion ratios smaller than 1.12 were applied close to the release point. ADREA-HF uses the porosity method for the definition of the active (fluid) domain. To reduce the active cells and consequently the run time of the simulation, fully blocked cells were used around the tunnel in  $y$ - and  $z$ - direction. The number of the active cells is 415,767, 212,016 and 411,089 for the car case, the train case inside empty tunnel and the train case with vehicles present, respectively. At this point it should be mentioned that for the train case with vehicles present the grid was extended more outside the tunnel to use a similar grid as in deflagration simulation. This is mainly the reason for the almost double number of cells in this case compared to the train case inside empty tunnel.

For time integration the 1<sup>st</sup> order implicit scheme is used, while for the convective terms the MUSCL numerical scheme is used. The central differences are used to discretize the diffusive terms. A very small initial time step ( $=10^{-10}$  s) is applied, but soon it is increased with maximum CFL restriction equal to 10.

### 3.3.2.3 Hydrogen sensors

To monitor the  $H_2$  concentration (volume fraction) we set 400 sensors inside the tunnel. The sensors are located at 1.0 m, 2.5 m, 5.0 m, 7.5 m, 10.0 m, 15.0 m, 20.0 m and 25.0 m from the

### D2.3. Final report on analytical, numerical and experimental studies on hydrogen dispersion in tunnels, including innovative prevention and mitigation strategies

center-point of the tunnel in the downwind direction along x-axis and at 1.0 m, 2.5 m, 5.0 m, 7.5 m, 10.0 m, 15.0 m in the downwind direction, similar to the instruments ports of the experimental set-up. Due to the circular geometry of the tunnel, proper transformation from cylindrical coordinates was performed to calculate the sensors' exact position (y,z). More precisely, they were placed according to the following scheme: for each x-coordinate, sensor positions were set by subdividing the radius of the tunnel in 4 equally spaced segments and by subdividing the azimuthal angle range in 5 equal angles (see Figure 3-16). Next, the duplicate sensors at  $r = 0$  as well as the sensors that were either on or under the ballast of the tunnel were removed. In Appendix A, Table A-1 displays the exact coordinates of the sensors along with their numbering.

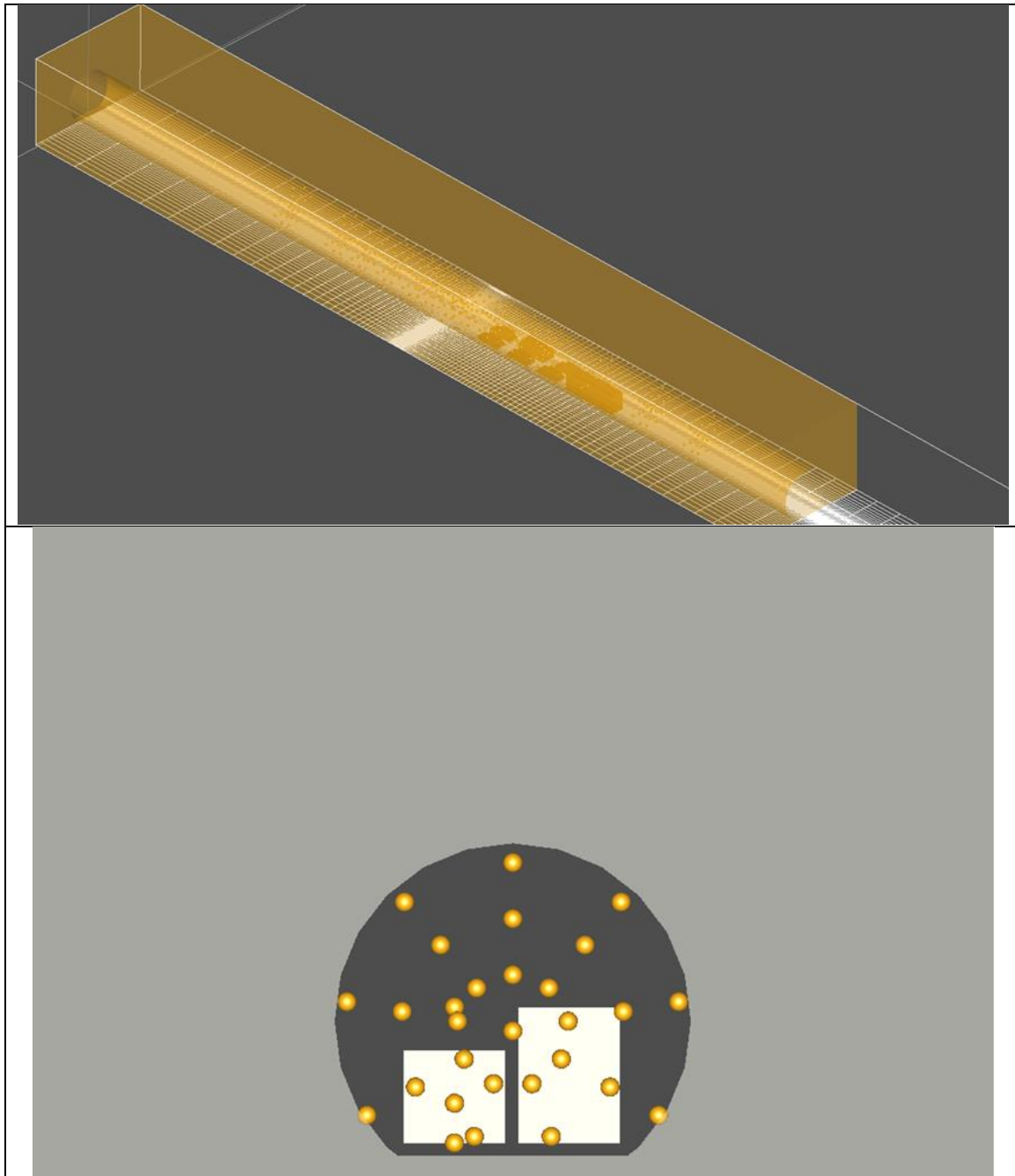


Figure 3-16. The geometry of the car scenario showing the grid on the floor plane (top) and the sensors' position on yz plane (bottom).

## D2.3. Final report on analytical, numerical and experimental studies on hydrogen dispersion in tunnels, including innovative prevention and mitigation strategies

### 3.3.2.4 Computational results

For the evaluation of each scenario in terms of safety, there are several parameters. Here, we present the flammable volume, percentage of flammable volume to total confined volume, flammable volume between 25-35% (if applicable), and criteria Q8, Q9 and Q10. The Q8, Q9 and Q10 are defined as,

$$Q8 = \sum V \times E / E_{\text{stoich}} , \quad (3-1)$$

$$Q9 = \sum V \times BV \times E / (BV \times E)_{\text{stoich}} , \quad (3-2)$$

$$Q10 = \sum V \times BV \times \chi \times E / (BV \times \chi \times E)_{\text{stoich}} , \quad (3-3)$$

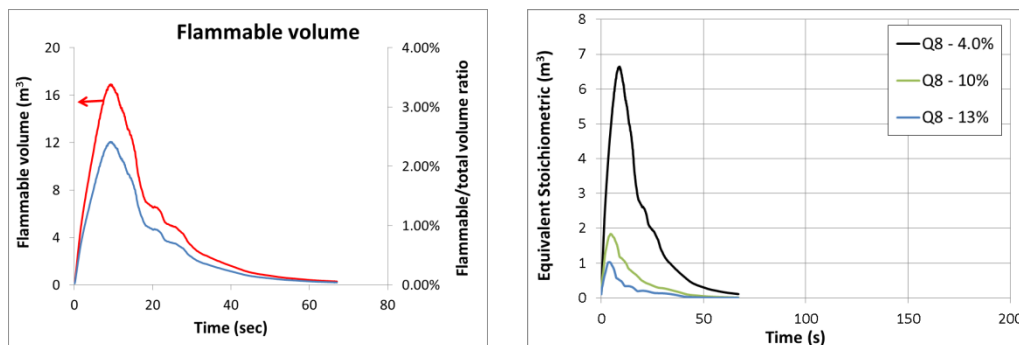
where  $V$  is the flammable volume,  $BV$  is the laminar burning velocity (corrected for flame wrinkling/Lewis number effects),  $E$  is volume expansion caused by burning at constant pressure in air,  $\chi$  is the thermodiffusivity and the summation is over all control volumes.

Q8 evaluates the hazard of the gas cloud by estimating an equivalent stoichiometric gas cloud with comparable explosion consequence. Q9 cloud is a scaling of the non-homogeneous gas cloud to a smaller stoichiometric gas cloud that is expected to give similar explosion loads as the original cloud (provided conservative shape and position of cloud, and conservative ignition point), while Q10 is similar to Q9 but it takes into account the thermodiffusive instability.

Contour and iso-surface plots are produced and presented to provide more insight on the dispersion behavior. Selective sensor time series for the car scenario and the train scenario with vehicles are also presented in Appendix A for space economy.

#### 3.3.2.4.1 Car scenario – $d=2.2$ mm with vehicles

Figure 3-17 shows the hydrogen flammable volume ( $\alpha_{H_2} > 4\%$ ) and the flammable to total tunnel volume ratio, and the Q8, Q9 and Q10 criteria for the equivalent flammable volume above 4%, 10% and 13% concentration. The maximum flammable volume in the entire tunnel is about 17 m<sup>3</sup> and it occurs 9 s after the release. This volume corresponds to approximately 2.5% of the total tunnel volume. The equivalent flammable volume based on all criteria is lower than the original flammable volume (almost 2.5 times lower for Q8 with Q9 and Q10 to give flammable volume lower than 0.6 m<sup>3</sup> regardless the concentration limits).



### D2.3. Final report on analytical, numerical and experimental studies on hydrogen dispersion in tunnels, including innovative prevention and mitigation strategies

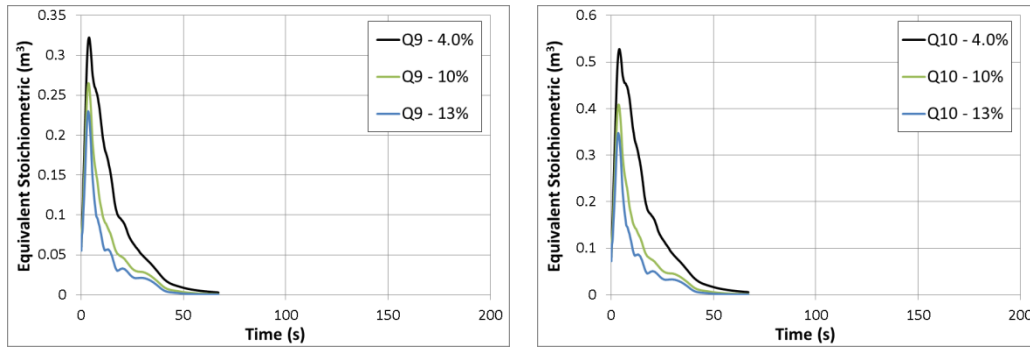


Figure 3-17. The flammable volume and the flammable to total volume ratio (top, left), Q8 (top, right), Q9 (bottom, left) and Q10 (bottom, right) criteria.

Figure 3-18 illustrates the hydrogen flammable cloud evolution at several times. It can be observed that the upwind distance of the flammable cloud is limited due to the ventilation and flammable volume is spotted mainly downwind the release point surrounding the first row of the vehicles. Flammable cloud does not escape from the exit tunnel due to low release rate combined with the ventilation.

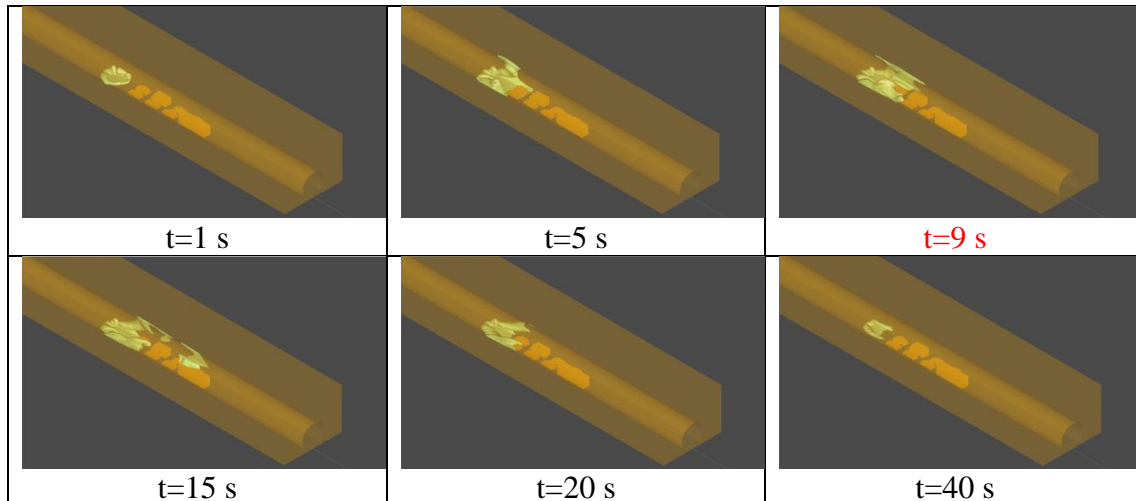


Figure 3-18. Hydrogen flammable cloud (volume fraction > 4%) at several times. The time when approximately the maximum flammable volume occurs is highlighted with red.

Based on the post-processing of the results after approximately 87 s (~ 1.5 min), i.e. after the stop of the release, the tunnel has no flammable volume inside as the concentration levels fall below the LFL (4 vol. %). The majority of deployed sensors detected concentrations above the LFL for small duration less than 30 sec (a couple of sensors very close to the release point reached the maximum of around 1 min). After the stop of the release (at 88 sec) the tunnel has emptied from ½ LFL concentrations as well. This means that even with the conservative ½ LFL no flammable cloud is predicted as soon as the release is stopped. No flammable cloud escapes the tunnel.

Figure 3-19 shows the concentration contours, on xz release plane ( $y = 0.605$ ) and on xy bottom plane, while Figure 3-21 shows contour plots on several yz planes and a close view of LFL iso-surface in the 3D geometry and at several times. We observe that as the jet impinges with high momentum on the ground, it spreads laterally along the tunnel floor and starts to rise near the tunnel wall (see also Figure 3-20). Due to the blowdown release at low rate combined with the high ventilation rate the mixture dilutes fast and even at the top of the tunnel very small concentration (way smaller than LFL) are predicted. As release progresses, the cloud with

### D2.3. Final report on analytical, numerical and experimental studies on hydrogen dispersion in tunnels, including innovative prevention and mitigation strategies

concentrations above LFL extends in the x-direction only to reach close to the first row of vehicles at 4 m distance.

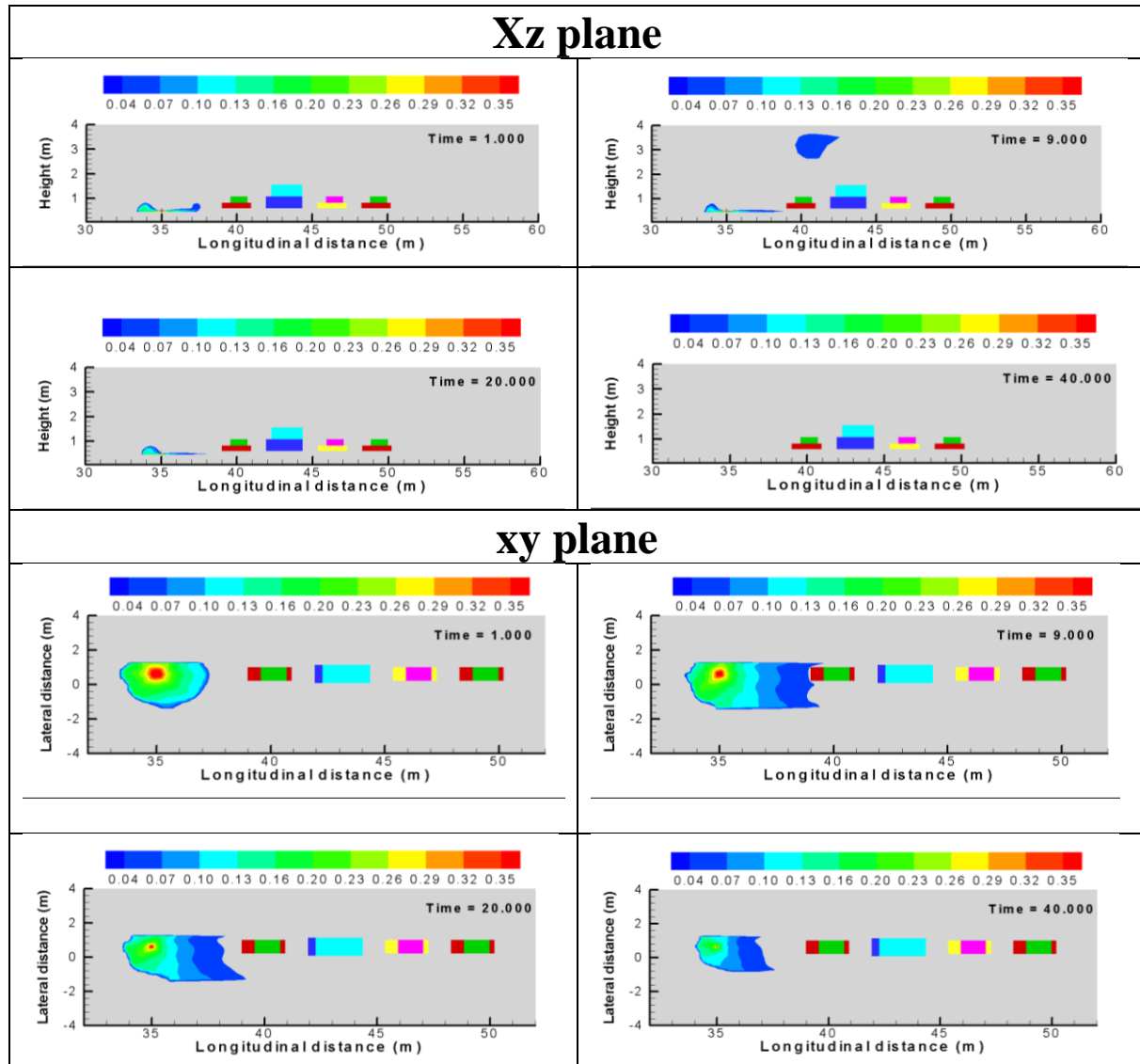


Figure 3-19. The concentration contours on the xz release plane and on yz bottom plane at several times.

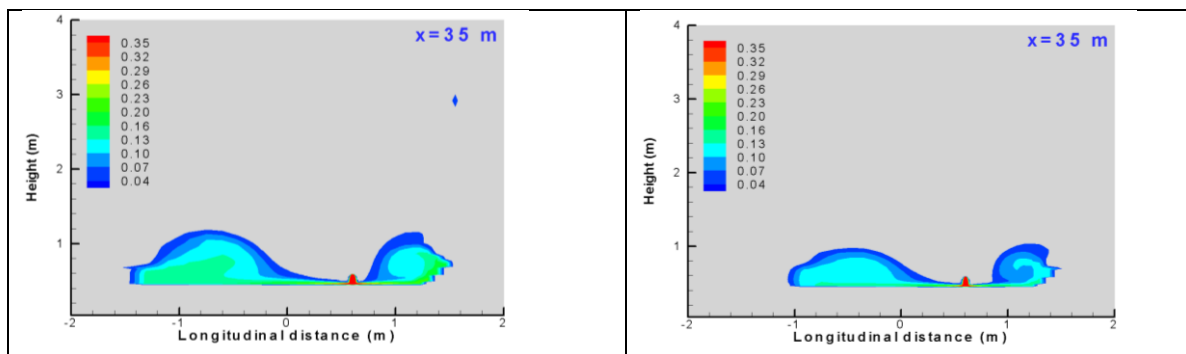


Figure 3-20. Concentration contours (left) on the yz release plane (x=35 m) at 9 sec (almost when maximum flammable volume is achieved) and at 20 sec (right).



## D2.3. Final report on analytical, numerical and experimental studies on hydrogen dispersion in tunnels, including innovative prevention and mitigation strategies

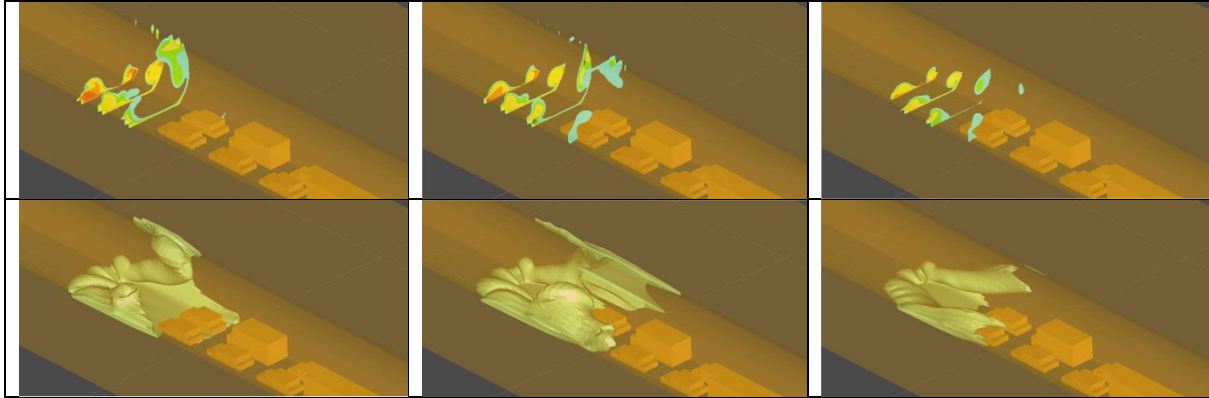


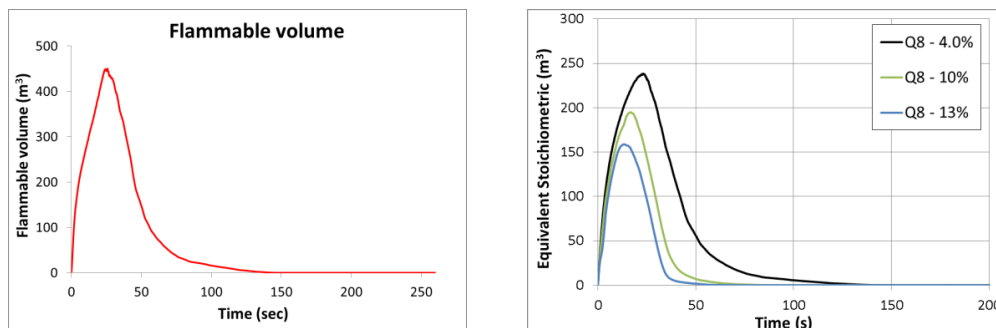
Figure 3-21. Top: Concentration contours above LFL on yz planes at several x distances and at 5, 9 and 20 sec (from left to right). Bottom: LFL iso-surface at 5 sec, 9 and 20 sec in close view (from left to right).

Apart from the lower flammability limit, which gives information about whether the mixture can burn if an ignition source is present the concentration mixture ranged from 25 to 35 vol. % H<sub>2</sub> is also of interest. At such concentration range the mixture can develop the fastest burning velocities resulting in high overpressures, which can lead to severe consequences. Based on the pre-test, concentrations between these limits (25-35 vol. % H<sub>2</sub>) are detected in a limited area (see Figure 3-20). A very small volume of the mixture was predicted with such concentrations. This volume is located not exactly beneath the release point (below the TPRD) but in the near vicinity around the release.

In Appendix A, Table A-2 indicates which sensors detect concentrations above the LFL. Selective time series of sensors are also presented.

### 3.3.2.4.2 Train scenario – $d=5.7$ mm inside empty tunnel

Figure 3-22 shows the hydrogen flammable volume and the Q8, Q9 and Q10 criteria for the equivalent flammable volume above 4%, 10% and 13% concentration. The maximum flammable volume in the entire domain is about 450 m<sup>3</sup> and it occurs 25 sec after the release. The equivalent flammable volume based on all criteria is lower than the original flammable volume predicting volumes (lower than 240 m<sup>3</sup> for Q8 and lower than 40 and 60 m<sup>3</sup> for Q9 and Q10, respectively) regardless the concentration limit.





### D2.3. Final report on analytical, numerical and experimental studies on hydrogen dispersion in tunnels, including innovative prevention and mitigation strategies

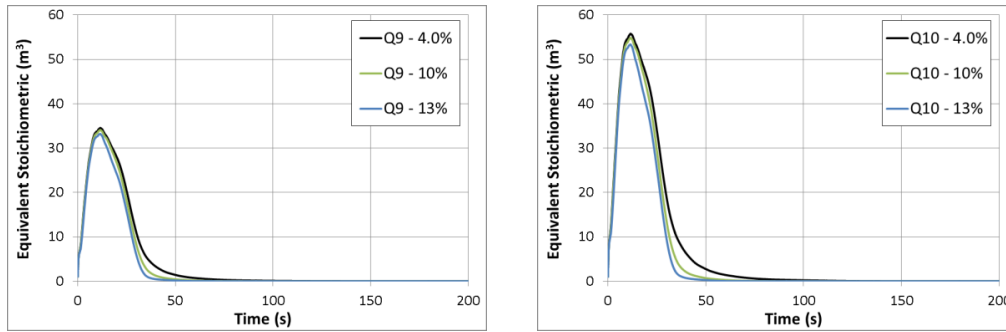


Figure 3-22. Flammable volume (top, left), Q8 (top, right), Q9 (bottom, left) and Q10 (bottom, right)

Figure 3-23 illustrates the iso-surface of 4% v/v H<sub>2</sub>. The flammable cloud fills almost the entire tunnel downwind the release and some amount manages to exit the tunnel (10 sec after the release initiation). Furthermore, despite the ventilation, flammable concentrations are extended almost towards the upwind tunnel opening (the opening with ventilation), but mainly on the top of the tunnel. After the end of the release (at 54 sec) the flammable mixture starts to decrease and is limited only to the top part of the tunnel. 260 sec after the stop of the release there is still small amount of flammable cloud predicted on the top and close to the downwind tunnel opening. The simulation was set to stop at that time. It is estimated that after few seconds the tunnel will be totally emptied from flammable concentrations. This means that flammable concentrations remain inside the tunnel for a little more than 4 min.

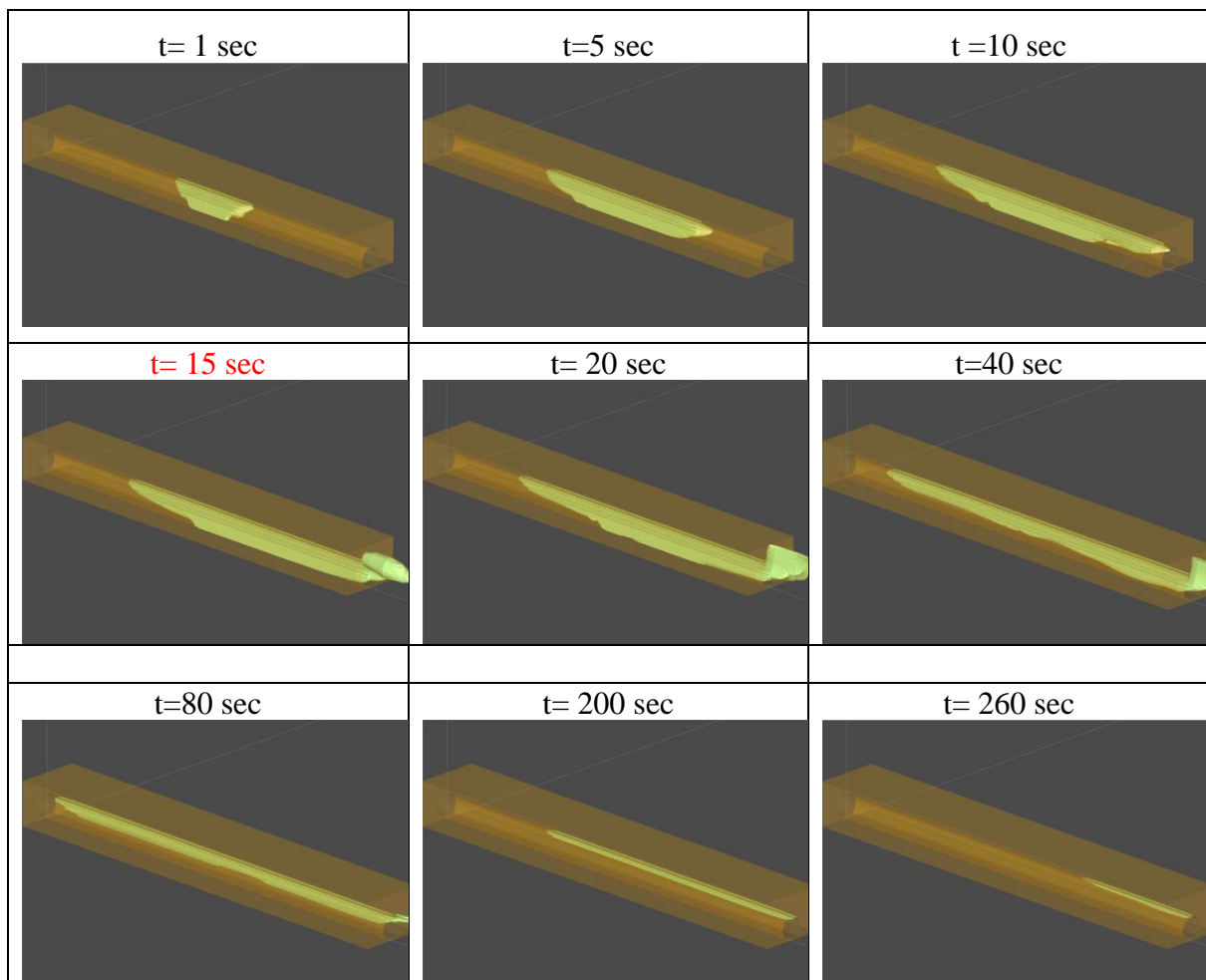


Figure 3-23. Hydrogen flammable cloud (volume fraction > 4%) at several times. The time when approximately the maximum flammable volume occurs is highlighted with red.

## D2.3. Final report on analytical, numerical and experimental studies on hydrogen dispersion in tunnels, including innovative prevention and mitigation strategies

### 3.3.2.4.3 Train scenario – $d=5.7$ mm with vehicles present

Figure 3-24 shows the layout of this scenario. Two rows of mock-up vehicles were placed to model the train carriages. Figure 3-25 shows the time history of the flammable volume and the mixture within the concentration range of 25-35 %. Large flammable volume (max.  $423 \text{ m}^3$  at  $\sim 21$  sec) is predicted inside the tunnel, which extends mainly in the downstream direction towards the tunnel free opening, from where it flows out at about 10 sec (see Figure 3-27). Comparing with the case without vehicles (Section 3.3.2.4.2) small differences are detected in terms of both the total flammable mixture and the nearly stoichiometric mixture (25-35 % v/v).

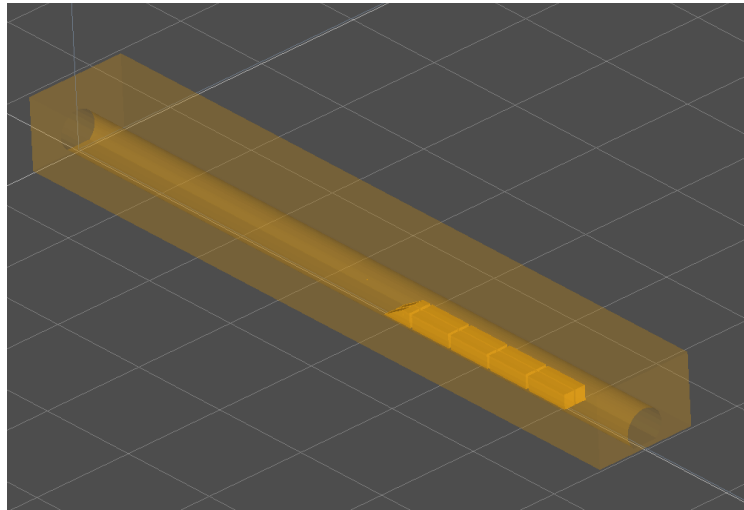


Figure 3-24. The layout of the scenario using Edes GUI of ADREA-HF code.

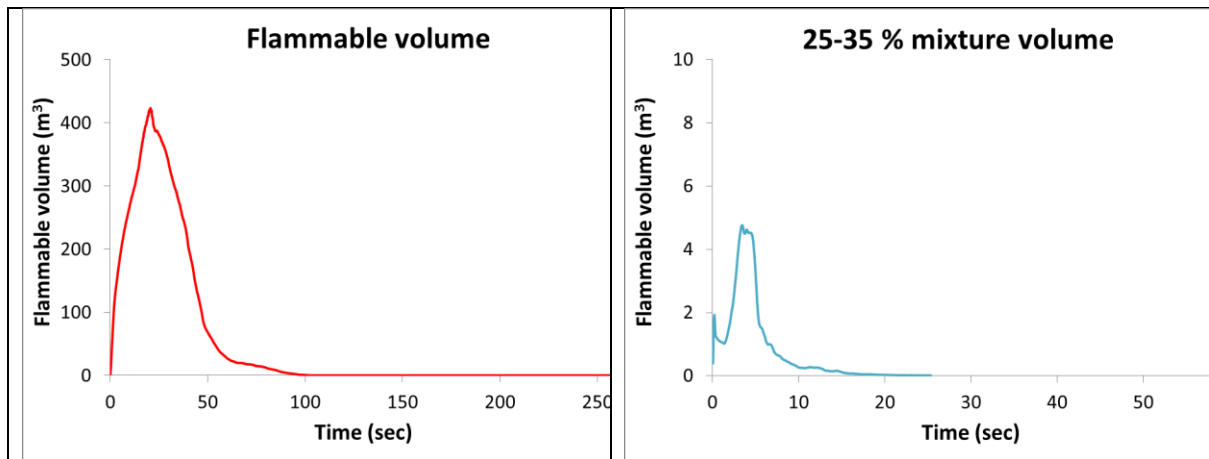


Figure 3-25. The flammable volume (left) and the volume with concentration range 25-35% (right).

The volume of the mixture at nearly stoichiometric concentrations (25-35 % v/v) is relatively low ( $< 5 \text{ m}^3$ ) and the maximum value is achieved at around 4 sec. Figure 3-26 displays the nearly stoichiometric mixture (25-35% v/v) at yz release plane ( $x=35$  m). It is observed that the mixture spreads along the tunnel ceiling and the wall and reaches approximately the middle of the tunnel height. Exactly above the release point higher concentrations are predicted.

### D2.3. Final report on analytical, numerical and experimental studies on hydrogen dispersion in tunnels, including innovative prevention and mitigation strategies

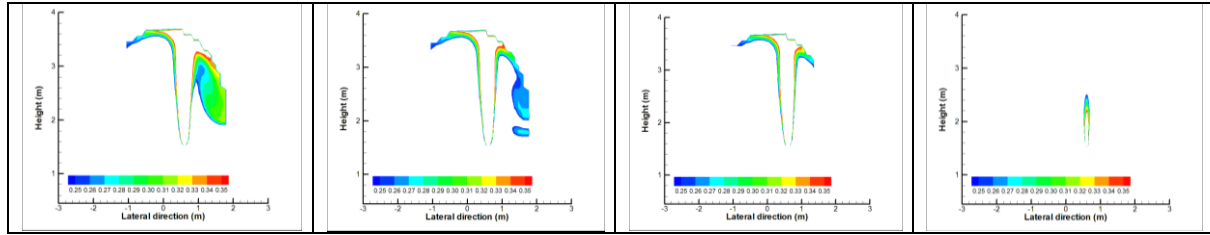


Figure 3-26. Nearly stoichiometric mixture (25-35% v/v) at yz release plane at 4, 5, 6 and 25 sec.

Figure 3-27 illustrates the hydrogen flammable cloud evolution. It can be observed that the upwind distance of the flammable cloud is limited due to the ventilation and flammable volume is spotted mainly downwind the release point. The cloud hits the ceiling and starts to spread along the tunnel walls. Great levels of mixing occur and the flammable cloud progressively surrounds all train carriages along tunnel. Flammable cloud escapes the downwind tunnel opening at around 10 sec. As the end of the release approaches (~ 50 sec) flammable cloud is detected only on the top of the tunnel.

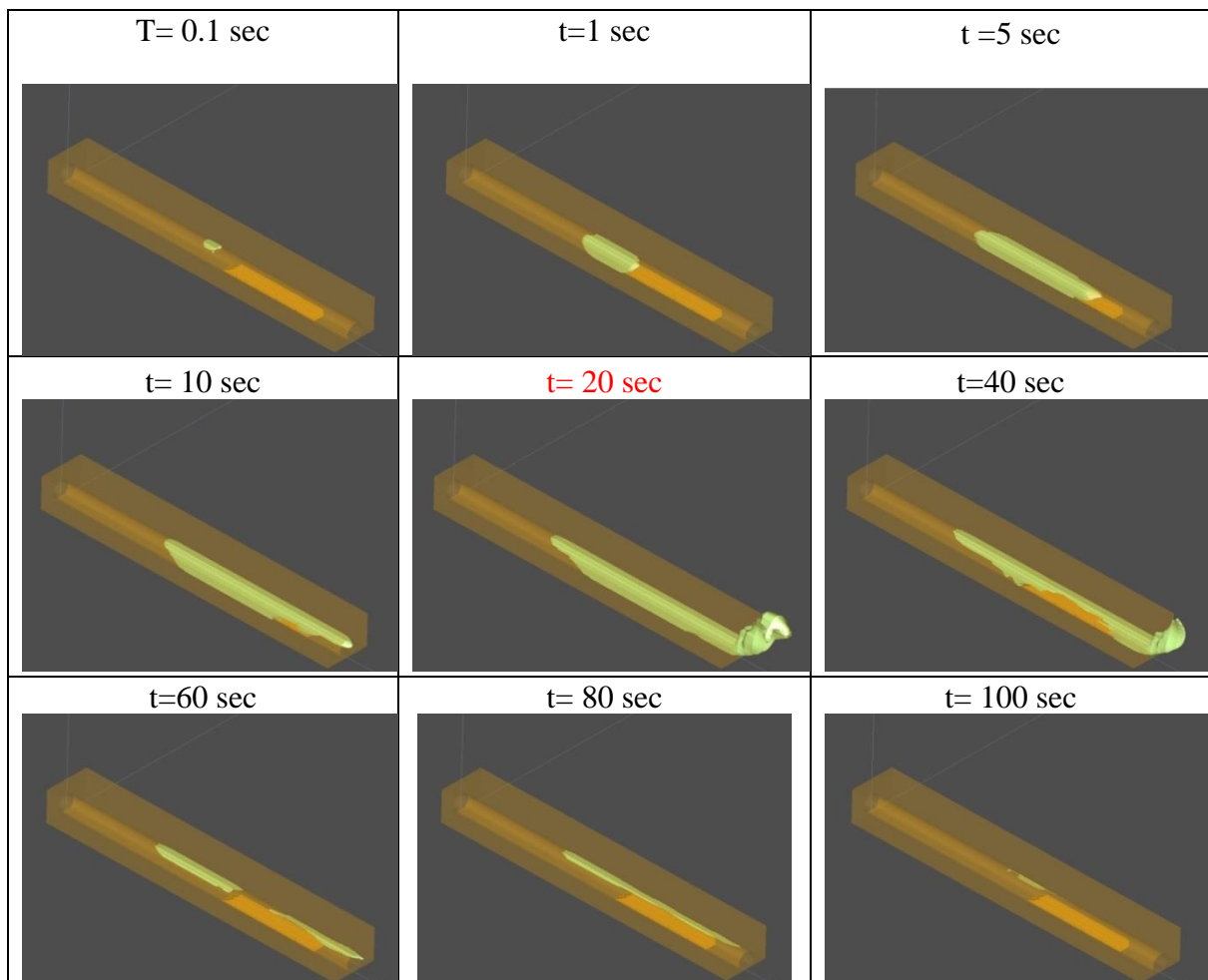


Figure 3-27. Hydrogen flammable cloud (volume fraction > 4%) at several times. The time when approximately the maximum flammable volume occurs is highlighted with red.

#### 3.3.2.4.4 Recommendations for the experimental setup and general conclusions

Based on all pre-test simulations we recommend the following for the experimental setup:

## D2.3. Final report on analytical, numerical and experimental studies on hydrogen dispersion in tunnels, including innovative prevention and mitigation strategies

1. Concentration sensors upwind the release point and very close to the ventilation opening are not essential in small releases (car scenario). In case of large releases flammable cloud travels more towards the upwind direction, but mainly on the top of the tunnel.
2. Sensors on the top of the tunnel are necessary, as flammable hydrogen-air cloud is expected in close proximity to the ceiling due to the buoyant nature of hydrogen. The sensors must be placed not only along the release centerline but also near the side walls of the tunnel. A ring-like structure (bifurcation) with considerable concentration levels is generated, especially close to the release.
3. The car scenario is of less risk. The volumes of flammable cloud and the mixture at near stoichiometric concentration (25-35% v/v) are small. On the contrary, the train scenario is of higher risk with a large flammable volume that extends until the downwind tunnel opening from which it escapes outside. However, even in the train scenario the volume of the mixture with nearly stoichiometric concentrations (25-35%) is relatively small.

### 3.4 Dynamics of H<sub>2</sub> release and dispersion in a tunnel – validation simulations (Sub-task 2.3.1/NCSR/ UU)

#### 3.4.1 NCSR simulations

The CFD simulations have been performed and the comparison will be conducted once the experimental results are available. The results will be reported in the (HyTunnel-CS D4.4, 2022).

#### 3.4.2 UU simulations

Work in this section is going to be expanded based on the experiments on the hydrogen release and dispersion inside the HSE tunnel. The experimental programme formulated in Section 4.3 was used to start pre-test simulations. The CFD model validation simulations will be performed when experiments will be available and reported in (HyTunnel-CS D4.4, 2022).

UU performed a pre-test “blind” simulation for the reference case selected by HSE. All parameters of the experiment have been described in the document prepared by HSE.

The objectives of this study include:

- examination of hydrogen release scenarios that are designed to simulate current and future fuel cell vehicles;
- investigating experimentally the dynamics of hydrogen dispersion in tunnels;
- measuring the characteristics of downstream flow developed by normal tunnel ventilation with a view to determining whether the resultant hydrogen layer (i) is flammable and (ii) depending on the degree of mixing may extend a substantial distance from the source;
- study the effects of obstructions in the tunnel on near field dispersion;
- provision of unique experimental data for the development and validation of models for unignited hydrogen behaviour in tunnels (for their use as predictive engineering tools).

The parameters of the tunnel facility dimensions are given in Table 3-3 and Figure 3-28 below.

*Table 3-3. HSE tunnel facility dimensions.*

### D2.3. Final report on analytical, numerical and experimental studies on hydrogen dispersion in tunnels, including innovative prevention and mitigation strategies

Radius	1.85 m
Depth of roadway	0.45 m
Cross-section area of roadway	0.75 m <sup>2</sup>
Circular cross-section area (excluding roadway)	10.75 m <sup>2</sup>
Open area, through which vehicles travel	10.00 m <sup>2</sup>
Equivalent diameter, $D_{HSE}$	3.57 m

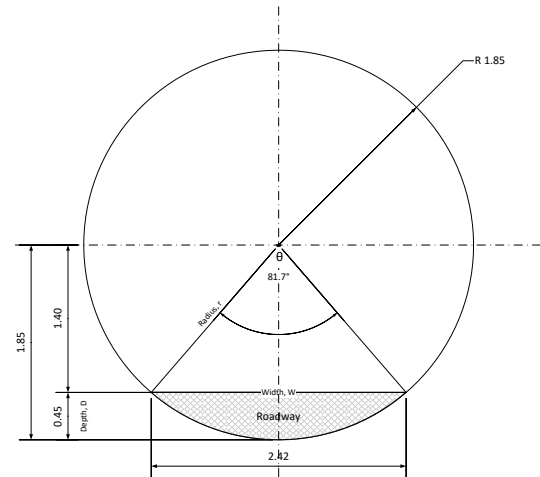


Figure 3-28. HSE tunnel facility dimensions.

The obstacles were represented by three types of vehicles i.e. bus, van and a car scaled for the tunnel size as per experimental description document.

The input parameters of the experimental release are given in Table 3-4.

Table 3-4. Input parameters.

<b>Nozzle Size</b>	<b>2.2 mm</b>
Nozzle orientation	vertically downward
Cylinder Pressure (Gauge)	11.8 Mpa ( <b>much lower NWP=70Mpa!</b> )
Volume	53 L
Mass of Hydrogen	0.45 kg
Tunnel Ventilation Velocity	1.25 m/s
Jet orientation and angle	Downward (0 deg)
Jet orientation to Ventilation	Cross-flow
Nozzle distance from the ground	137 mm
Release location from the tunnel entrance	35 m

### 3.4.2.1 Numerical set-up

The CFD model and methodology that is planned to be applied is based on physical and numerical requirements for simulation of light gas release as described in (Molkov, Shentsov, 2014). The validation of the model has been performed on the small-scale set of tests and full details are available from (Giannissi et al., 2015). CFD model details include the use of incompressible ideal gas with a pressure-based solver and RANS k- $\epsilon$  realizable for turbulence. The constant time step 0.005 s was employed for the poly-hex-core mosaic mesh with the total number of control volumes 258k. To model release and blowdown the volumetric source was employed. The Pressure-Velocity-Coupling was SIMPLE. The spatial discretisation of pressure – standard and 2<sup>nd</sup> order upwind for all variables. Figure 3-29 shows the numerical grid for the simulations.

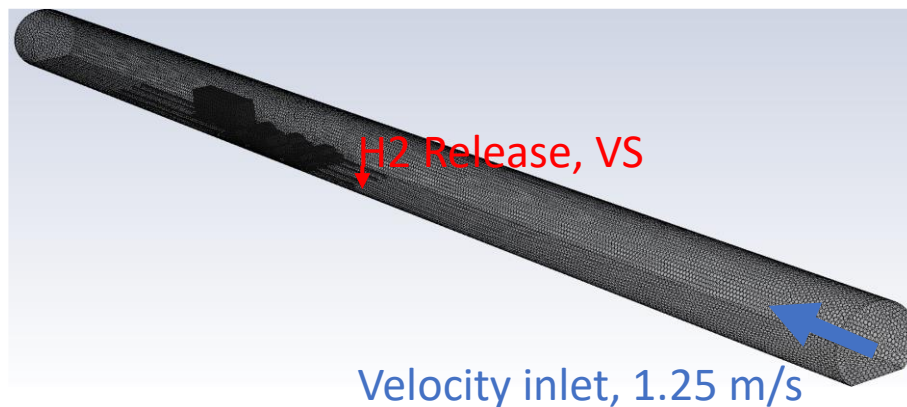


Figure 3-29. Numerical grid.

### 3.4.2.2 Volumetric source approach

The user-defined functions we used to impose the mass flow rate, velocity and temperature at the real nozzle. The volumetric source term was approximated top the cube of 1.492 cm size and the parameters of mass flow rate, rate velocity and temperature were calculated and shown in Figure 3-30 below.



## D2.3. Final report on analytical, numerical and experimental studies on hydrogen dispersion in tunnels, including innovative prevention and mitigation strategies

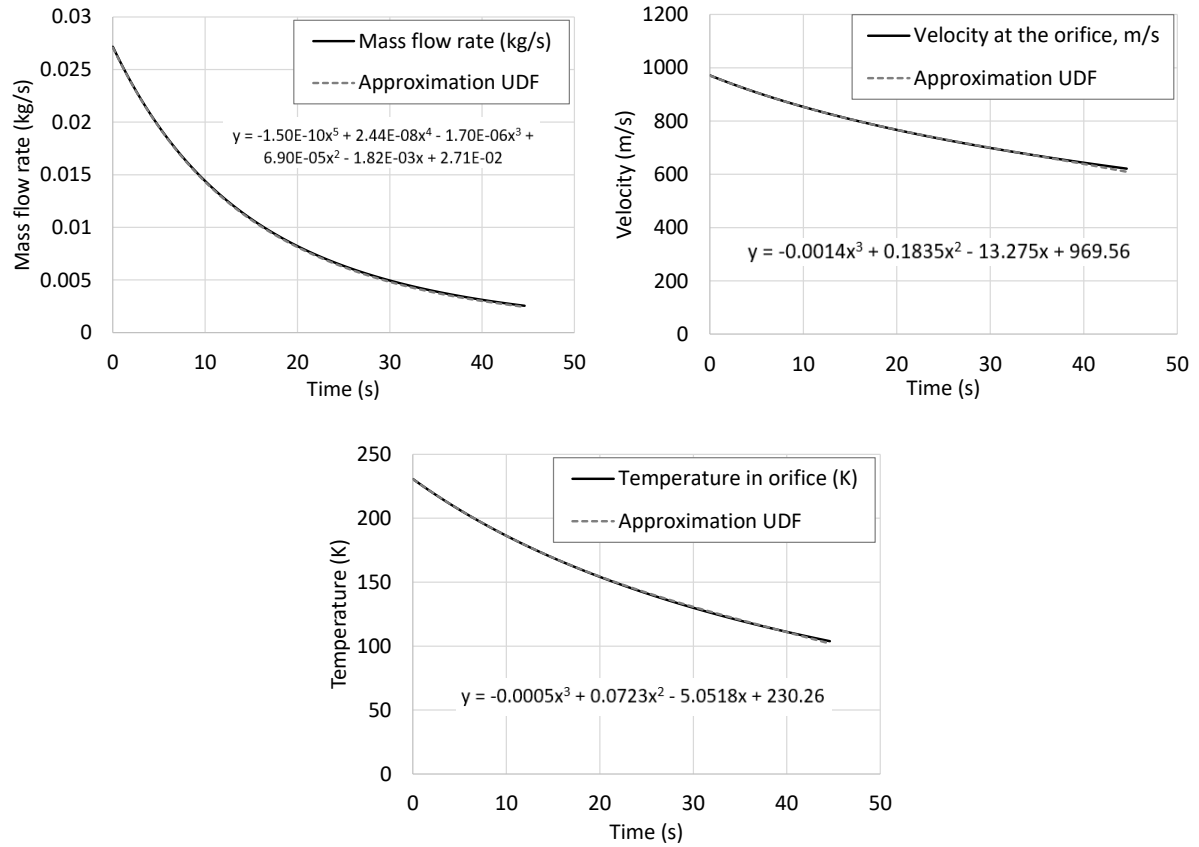


Figure 3-30. Parameters of the volumetric source term imposed on the inlet: mass flow rate (top left), velocity (top right), temperature (bottom centre).

Parameters of turbulence were specified following the equations below:

- Mass:  $S_{mass} = \frac{\dot{m}_{H_2}}{V_{vs}}$ ,
- Momentum:  $S_{mom} = \frac{u_{H_2} \cdot \dot{m}_{H_2}}{V_{vs}}$ ,
- Kinetic energy:  $S_{\kappa} = \frac{\kappa \cdot \dot{m}_{H_2}}{V_{vs}}$ ,
- Dissipation energy:  $S_{\varepsilon} = \frac{\varepsilon \cdot \dot{m}_{H_2}}{V_{vs}}$ ,
- Energy:  $S_E = \frac{c_{p,H_2} \cdot (T_{H_2} - T_0) \cdot \dot{m}_{H_2}}{V_{vs}}$ .

Additional equations:

$$\kappa = \frac{3}{2} (u_{H_2} \cdot TI)^2, \text{ where } TI=25\% ,$$

$$\varepsilon = 0.0845^{0.75} \frac{\kappa^{1.5}}{TLS}, \text{ where } TLS = 0.07 d_{not} .$$



## D2.3. Final report on analytical, numerical and experimental studies on hydrogen dispersion in tunnels, including innovative prevention and mitigation strategies

### 3.4.2.3 Results

Preliminary results on concentration decay along the tunnel are shown in Figure 3-31 and Figure 3-32 below. As can be seen the decay of concentration 4% start to reach the car after 5 s of release and propagate towards the congestion zone driven by the wind. After losing momentum hitting the ground concentration decays quickly to the safe level.

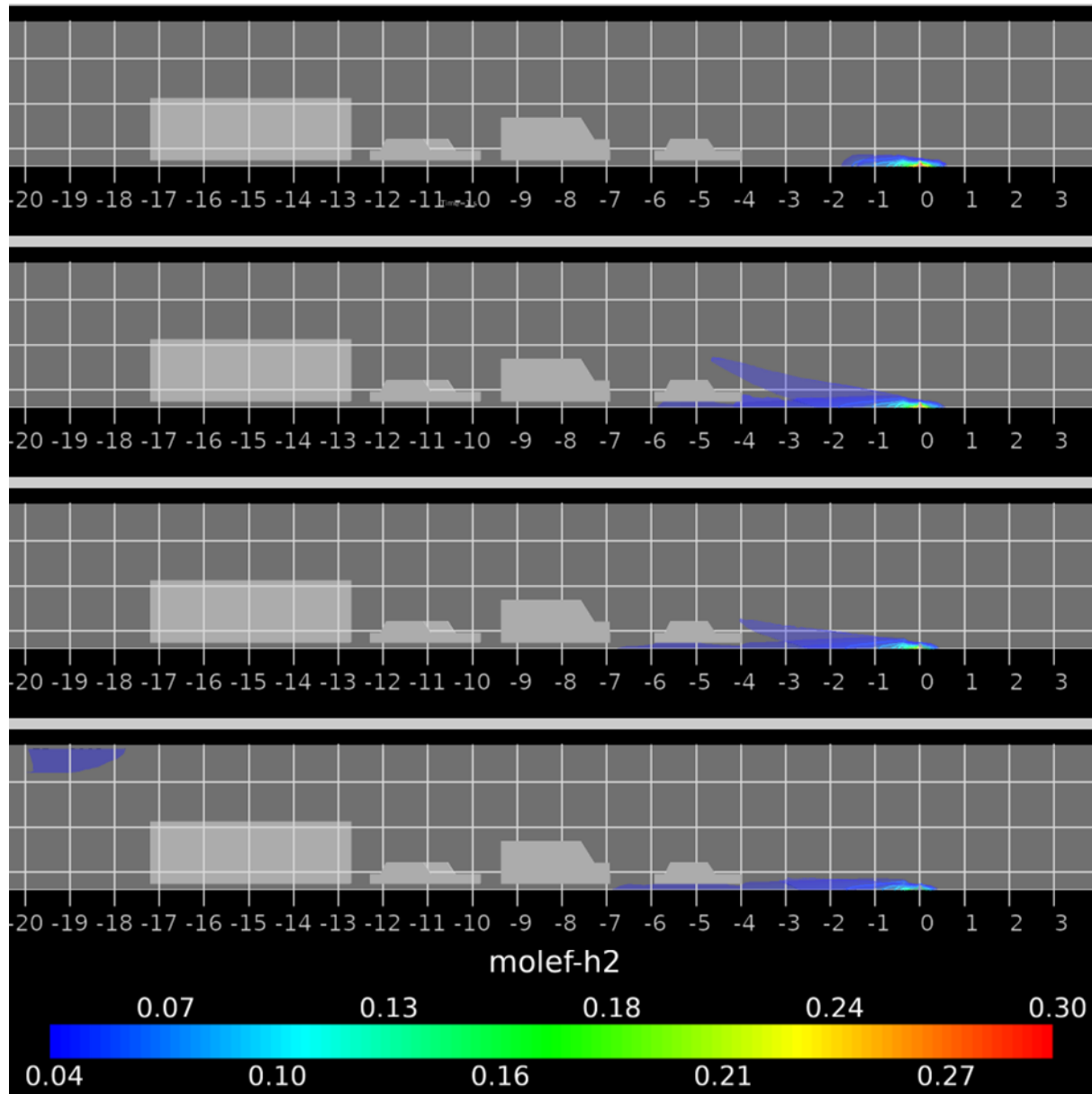


Figure 3-31. Concentration decay along the tunnel at different times, iso-surface of 4% concentration and the contours across the centreline of the release in range 4-30%.

Figure 3-32 shows the way concentration of 1% is driven by the velocity inside the tunnel and the buoyancy of the hydrogen.

### D2.3. Final report on analytical, numerical and experimental studies on hydrogen dispersion in tunnels, including innovative prevention and mitigation strategies

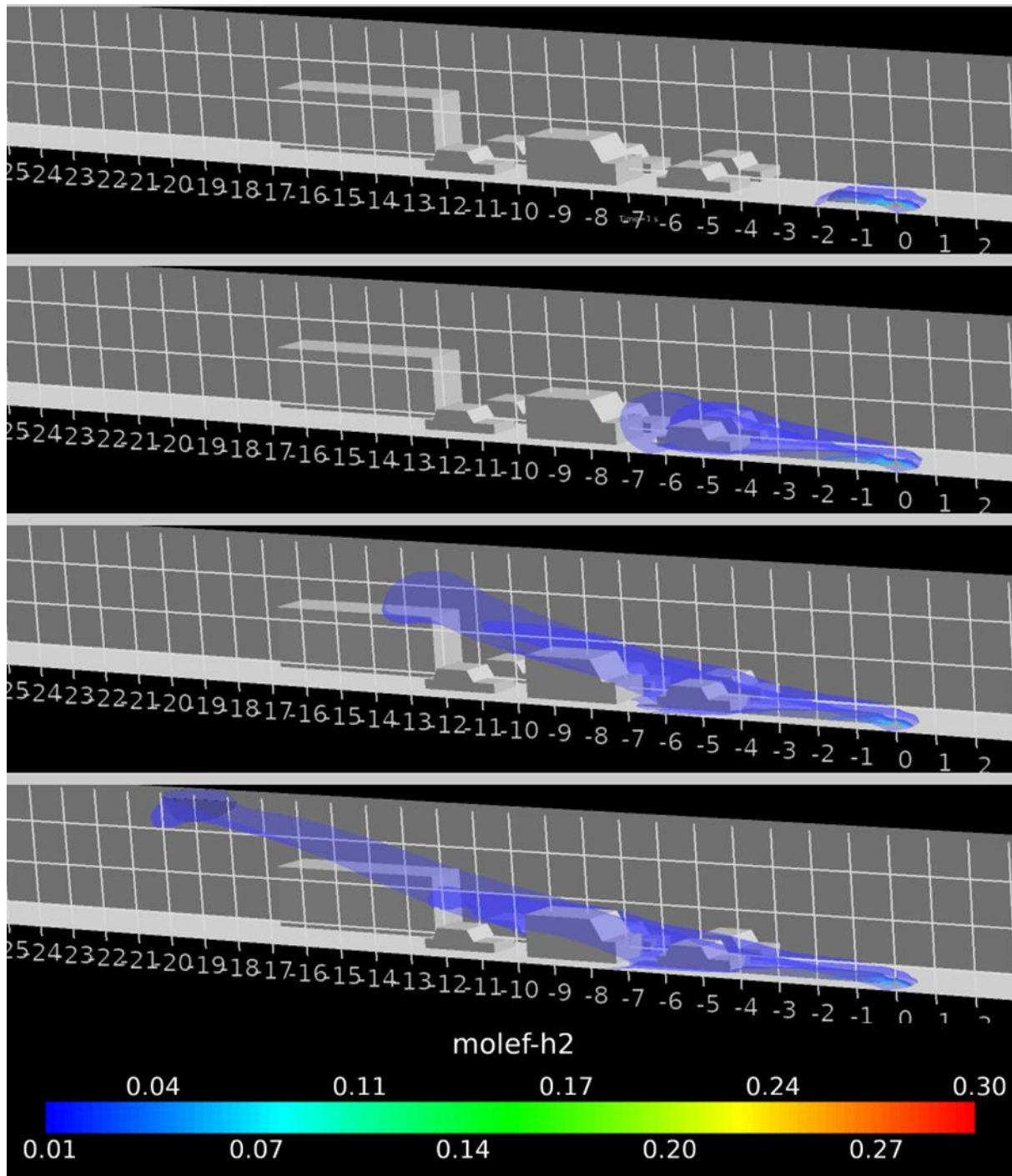


Figure 3-32. Concentration decay along the tunnel at different times, iso-surface of 1% concentration and the contours across the centreline of the release in range 1-30%.

#### 3.4.2.4 Conclusions

The reference case selected for the pre-test simulation was at a much lower NWP which gives a significant safety margin compared to a realistic release from 700 bar. Following the preliminary results the current case is not considered to be dangerous in terms of high concentration collated near the vehicles. It can be concluded that in case of downward release there will be no accumulation of flammable mixture inside the tunnel for the given parameters. New release scenarios required to be performed by HSE to simulate realistic release are

### D2.3. Final report on analytical, numerical and experimental studies on hydrogen dispersion in tunnels, including innovative prevention and mitigation strategies

required. The dynamics of hydrogen dispersion in the tunnel has been assessed, however further studies will be performed following the completion of the experimental programme. Measurements of downstream flow developed inside the scaled tunnel with ventilation concluded that there is no flammable hydrogen layer formation from the selected source. The model will be further validated versus unique experimental data of hydrogen release in the tunnel.

## 3.5 Efficiency of mechanical ventilation on H<sub>2</sub> dispersion – pre-test simulations (Sub-task 2.3.1/KIT)

### 3.5.1 Numerical set-up

The vented hydrogen jet experiments are carried out in the A2 vessel at the KIT hydrogen test centre. Figure 3-33(a) presents a cut-through 3D view of the concerned part of the vessel. The big holes in the vessel wall act as the ventilation inlet and outlet. The jet nozzle with auxiliary systems is positioned on the rail frame at the centre of the vessel. A view of the hydrogen jet device from one ventilation hole is shown in Figure 3-33(b).

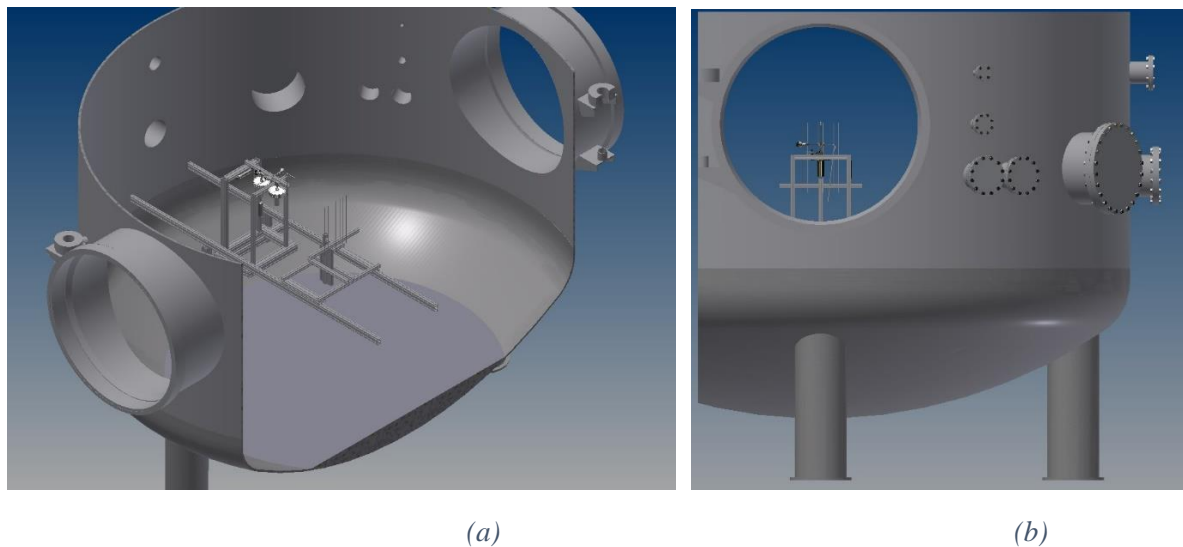


Figure 3-33. 3D view of hydrogen jet facility, the A2 vessel at KIT hydrogen test centre.

ANSYS Fluent software is adopted to make the 3D numerical model of the facility, including the jet nozzle itself and the ventilation holes, as shown in Figure 3-34. According to the figure, the adapted mesh is generated with refined cells in the jet region and coarse cells in the ambient region for computational resource savings.

## D2.3. Final report on analytical, numerical and experimental studies on hydrogen dispersion in tunnels, including innovative prevention and mitigation strategies

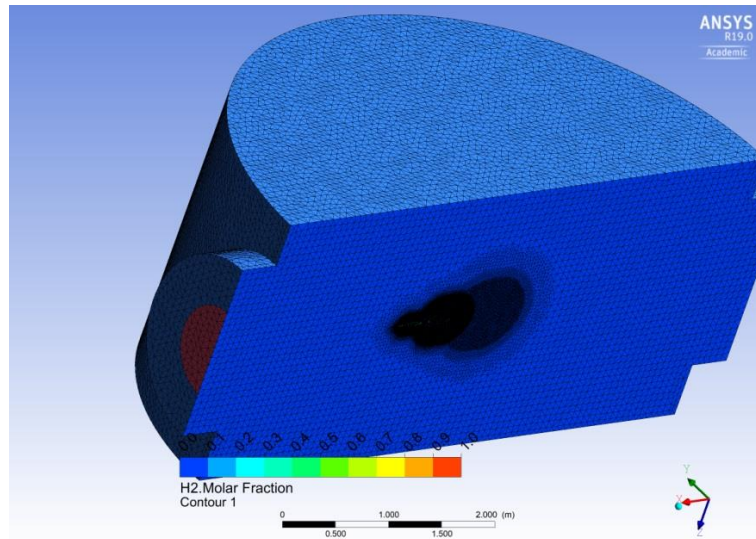


Figure 3-34. ANSYS model for vented jet simulations.

### 3.5.2 Computational results

Preliminary simulation results are presented in Figure 3-35 and Figure 3-36, showing the hydrogen concentration distributions in a co-flow ventilation, i.e., the ventilation air flow and hydrogen jet flow share the same direction. The jet plume region with greater than 10 vol. % H<sub>2</sub> can be clearly distinguished in the figure. Hopefully the simulated hydrogen concentration contour plot could provide hints to the experimentalists about the dimensions of the jet plume and further ideas of positioning the sensors properly.

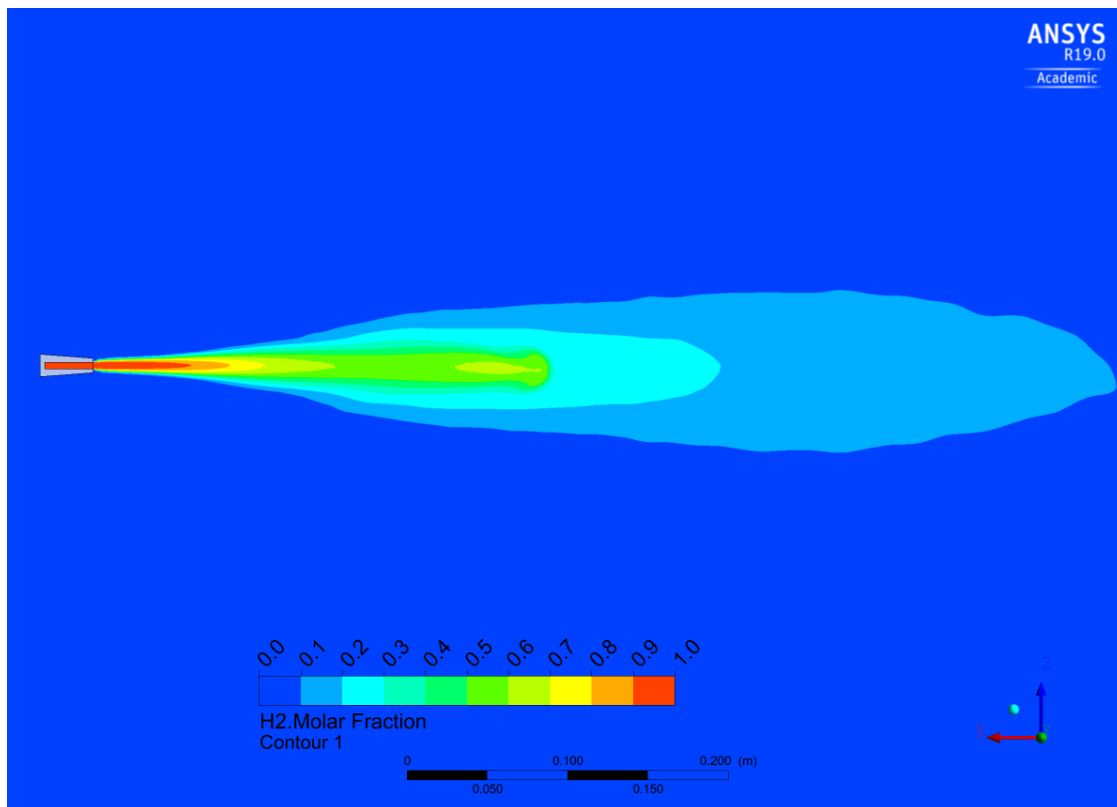


Figure 3-35. Hydrogen concentration distribution of the jet with the co-flow ventilation.



## D2.3. Final report on analytical, numerical and experimental studies on hydrogen dispersion in tunnels, including innovative prevention and mitigation strategies

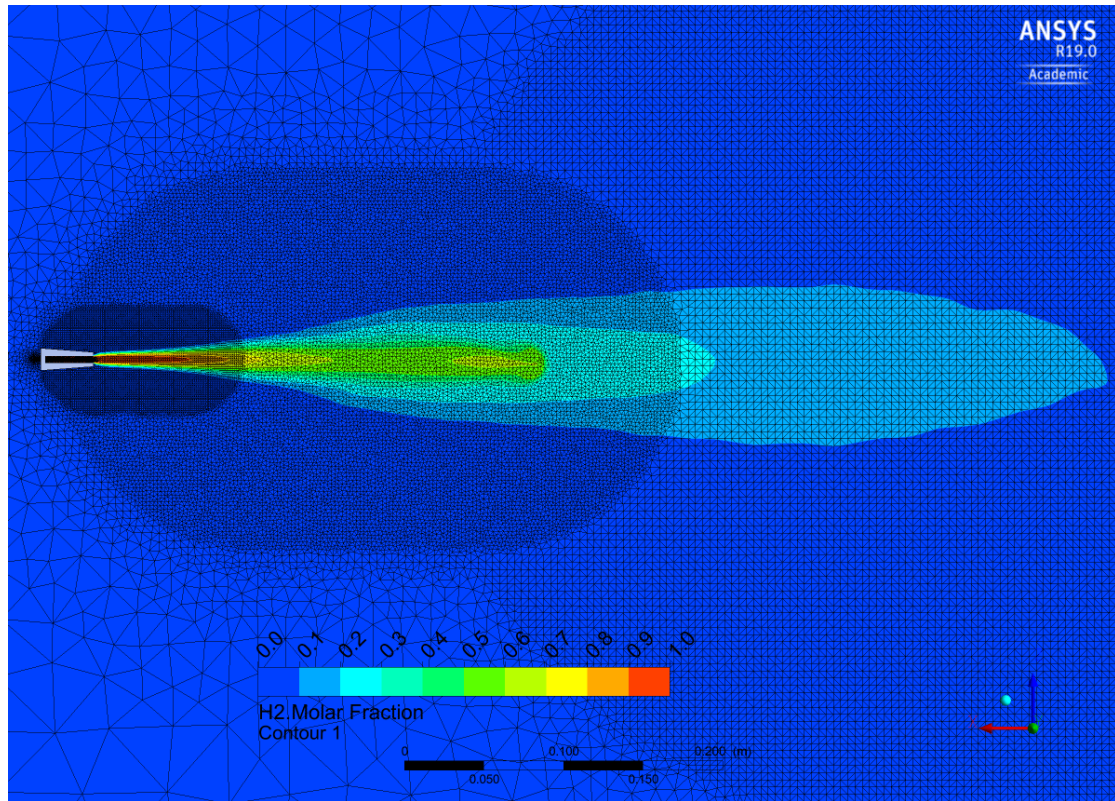


Figure 3-36. Hydrogen concentration distribution with the adapted mesh.

In the next stage, model validation simulation was performed by using the KIT in-house code instead of the ANSYS code (see Section 3.6.1).

### 3.6 Efficiency of mechanical ventilation on H<sub>2</sub> dispersion – validation simulations (Sub-task 2.3.1 / KIT / NCSR / UU)

#### 3.6.1 Validation simulations

KIT performed validation simulations based on the PS experiments (Section 4.4). More precisely, the numerical simulation of a hydrogen jet into a uniform co-flow ventilation field was carried out with the in-house COM3D code developed in the Karlsruhe Institute of Technology. The term “co-flow” means the hydrogen jet flow and the air ventilation flow share the same direction.

The geometry model for the vented hydrogen jet simulation was developed according to the experiment, as shown in Figure 3-37. The hydrogen was injected from a nozzle with a 1 mm diameter into the ventilation co-flow of air. The stationary hydrogen mass flow rate was 5 g/s. The nominal velocity of the air ventilation was 3.5 m/s.

### D2.3. Final report on analytical, numerical and experimental studies on hydrogen dispersion in tunnels, including innovative prevention and mitigation strategies

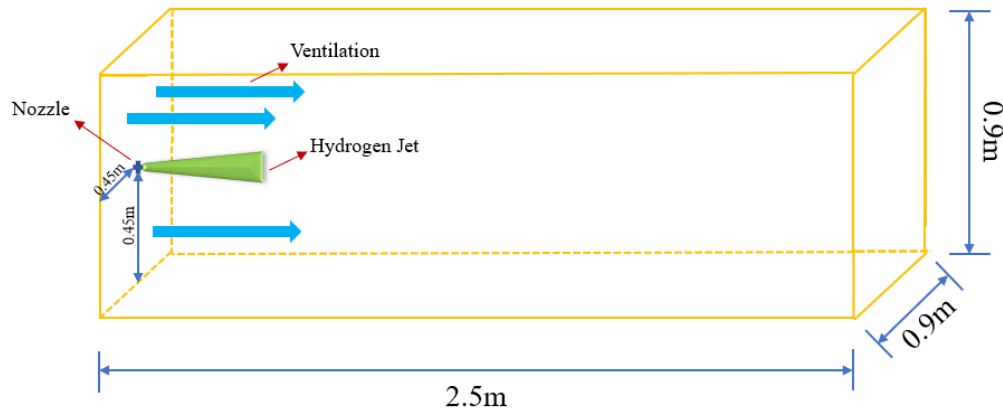


Figure 3-37. Schematic of geometry model for the simulation of the vented hydrogen jet in co-flow ventilation.

The computational domain was a rectangular zone with  $2500 \times 900 \times 900 \text{ mm}^3$ , as shown in Figure 3-37, discretized into 7,644,000 numerical cells with a cell size of 6.4 mm. The boundary condition at  $x = 0$  was set as the velocity inflow with 3.5 m/s ventilation of air. The nozzle was located at the centre of the ventilation boundary. The open non-reflection boundary conditions were utilized at the remaining five surface boundaries of the rectangular domain to reproduce gas dispersion and mixing. The notional nozzle diameter for hydrogen blowdown is 7.25 mm that was calculated by an adiabatic blowdown model of hydrogen in high pressure (Molkov, 2012). The flow turbulence was modelled by the RNG k- $\epsilon$  model, and the TVD 2<sup>nd</sup> order solver was utilized in the present simulations.

Figure 3-38 shows the contour plots of hydrogen volume fraction at a converged steady state (0.707 s). The length of the 4 vol. % hydrogen concentration is about 2.25 m in Figure 3-38 (b), which is longer than that of the experiment result, which is about 1.65 m. Accordingly, the length of 10 vol. % hydrogen cloud is approximately 0.5 m in simulation and 0.6 m in experiment, respectively. The hydrogen concentration distributions in transverse direction at  $x = 625 \text{ mm}$  and  $1000 \text{ mm}$  are shown in Figure 3-39 and Figure 3-40, respectively. It can be seen that the transverse concentration distribution of hydrogen jet is very close to a Gaussian distribution, with a fitting degree ( $R^2$ ) of 0.9964. However, a discrepancy exists between the simulation and the measured data. It seems that the modelled diffusion in transverse direction is greater than that based on the measured data. Figure 3-41 shows the hydrogen concentration distribution along the centre axial line ( $z = 450 \text{ mm}$  and  $y = 450 \text{ mm}$ ). The figure shows that the hydrogen concentration decreases rapidly near the nozzle and then slows down along the centre line of the jet. The axial distribution of the hydrogen concentration is close to the analytical solution by Gebhart et al. (1988). However, the concentration is slightly higher than the solution when  $x > 250 \text{ mm}$ , as shown in Figure 3-41. Due to the faster diffusion in the transverse direction in the simulation, the predicted hydrogen concentration at the axial line is a little lower than the data, especially at the earlier stage of the jet, e.g., when  $x < 1000 \text{ mm}$ .

### D2.3. Final report on analytical, numerical and experimental studies on hydrogen dispersion in tunnels, including innovative prevention and mitigation strategies

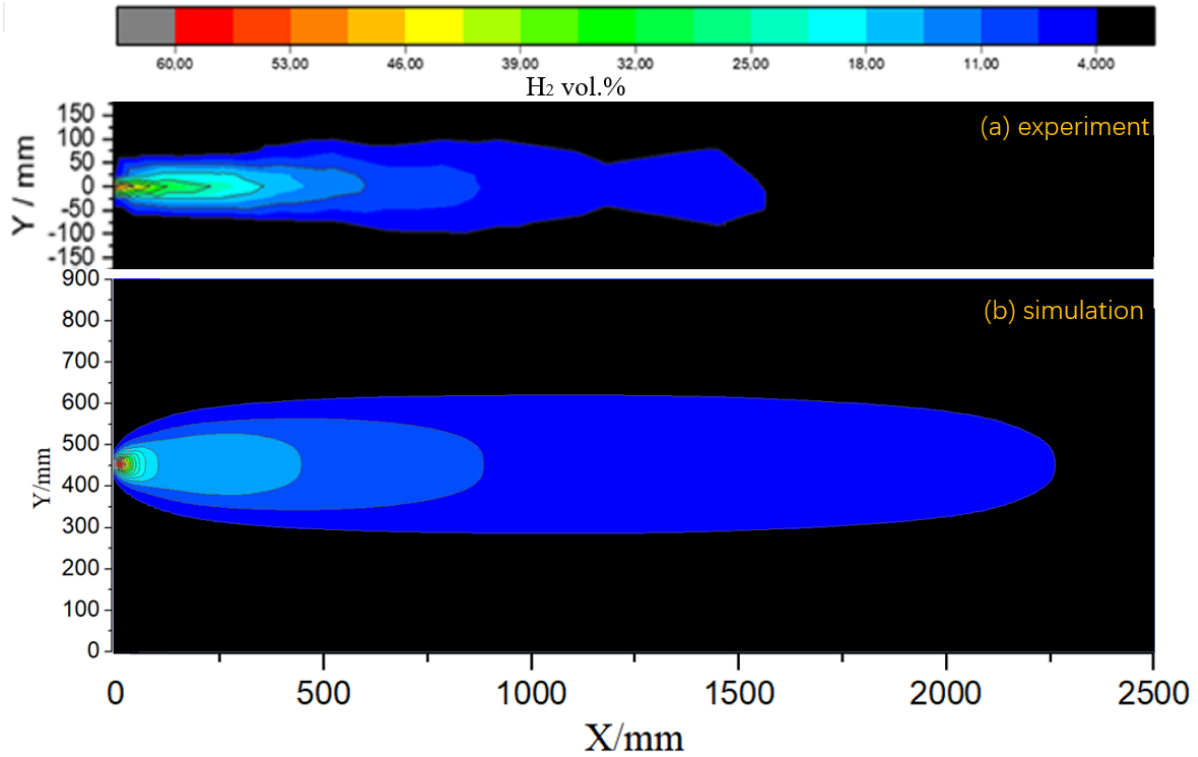


Figure 3-38. Hydrogen concentration (molar fraction) contour plots in longitudinal cross section cutting through the centre of the jet: (a) experiment by ProScience; (b) simulation by COM3D.

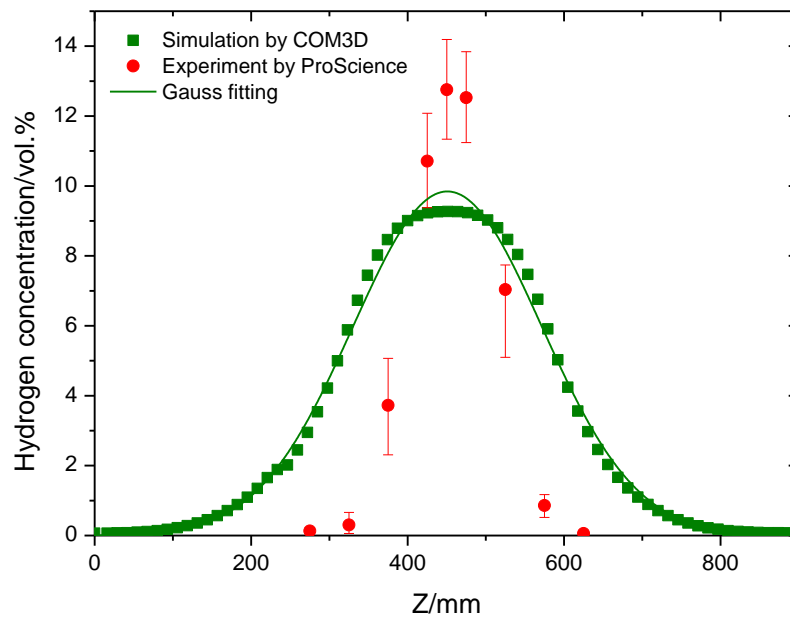


Figure 3-39. Hydrogen concentration distribution in transverse direction along  $x = 625$  mm.



### D2.3. Final report on analytical, numerical and experimental studies on hydrogen dispersion in tunnels, including innovative prevention and mitigation strategies

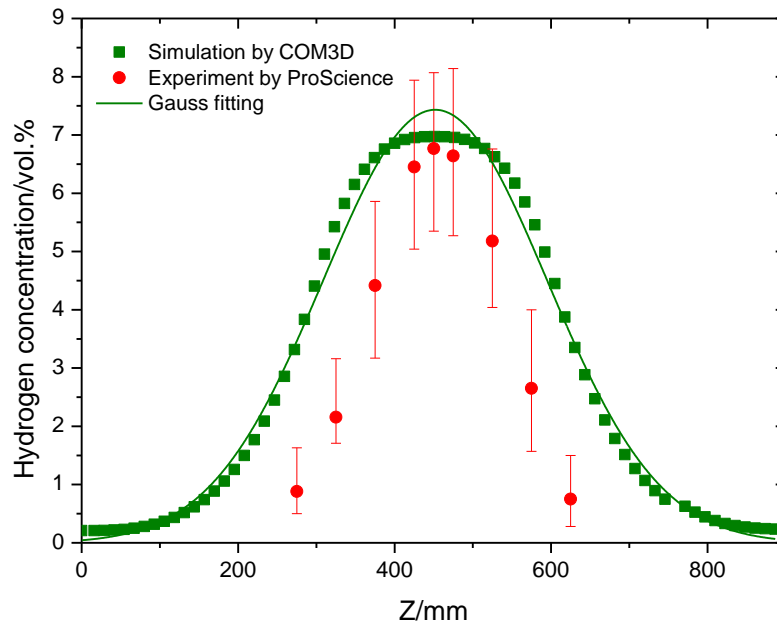


Figure 3-40. Hydrogen concentration distribution in transverse direction along  $x = 1000$  mm.

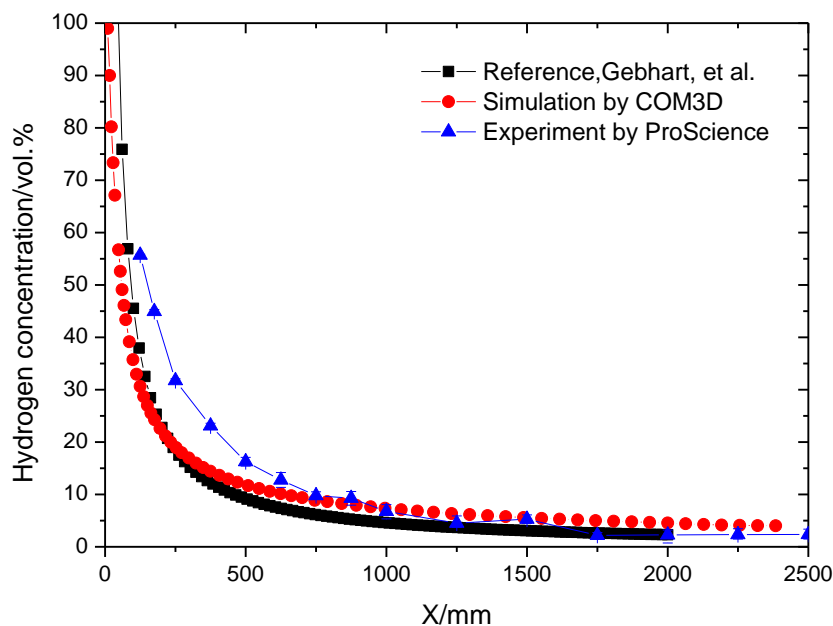


Figure 3-41. Hydrogen concentration distribution along axial centre line of jet.

The flow velocity in longitudinal direction (X) at steady state is shown in Figure 3-42. The maximum X velocity is 535.06 m/s at the nozzle exit, which is certainly subsonic due to the application of notional nozzle approximation. The X velocity downstream is greater than 3.5 m/s due to the hydrogen injection. The X velocity along the centre line also decreases rapidly

### D2.3. Final report on analytical, numerical and experimental studies on hydrogen dispersion in tunnels, including innovative prevention and mitigation strategies

near the nozzle. The flow velocity drops to 6 m/s at  $x=262$  mm and to 4.5 m/s at  $x=1153$  mm, respectively.

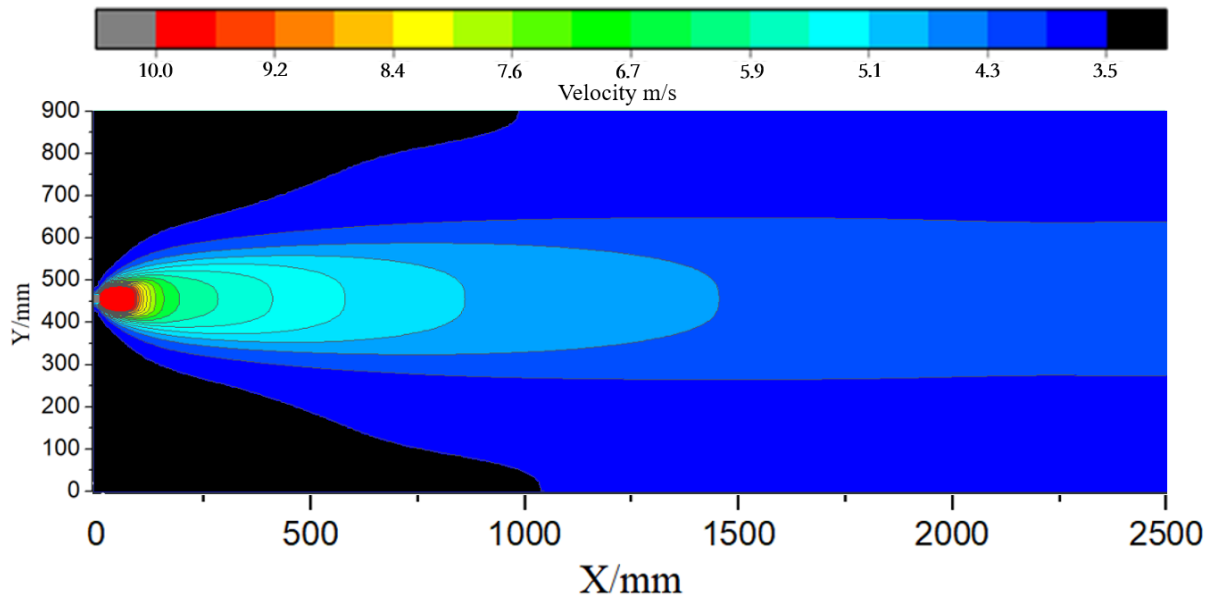


Figure 3-42. Flow velocity at longitudinal X direction at  $z = 450$  mm.

#### 3.6.2 Inter-comparison between partners' simulations

An inter-comparison between partners' simulations was carried out within the HyTunnel-CS project. For this activity three PS unignited release experiments were simulated testing different ventilation configurations. The full description and the results of the inter-comparison among partners' CFD simulations are presented in (Giannissi et al, 2021). Next, a summary of the study is provided.

NCSR and UU simulated the PS experiments (Section 4.4) that involve hydrogen release inside a safety vessel with different ventilation configurations. The co-flow and counter-flow tests along with the no ventilation test ( $\dot{m} = 5$  g/s,  $d = 4$  mm) as reference were simulated with the aim to validate available and well-known CFD codes against such applications and to provide recommendations on modeling strategies.

Special focus was given to the modelling of the airflow generated by the fan. Different approaches were followed and evaluated. UU modelled the fan airflow by 1) imposing uniform velocity profile and  $TI=50\%$  in an open atmosphere and 2) imposing linear source term with zero velocities at the fan centre and include the entire vessel geometry. NCSR modelled the fan airflow by 1) imposing uniform velocity profile with  $TI=50\%$ , and 2) imposing gaussian velocity profile. The vessel was not modelled in both NCSR approaches. In the NCSR approach with uniform profile, a larger length scale (consequently a smaller dissipation rate) and smaller  $TI$  ( $=10\%$ ) were also examined.

In the no ventilation configuration, the predictions were in good agreement with the experiment with UU simulations to over-predict the LFL distance, as shown in Figure 3-43. Comparing the two UU simulations is shown that the volume of the vessel is large enough to not affect hydrogen dispersion. Thus, its modelling can be neglected for simplicity. Nonetheless, the position of the ventilation boundary in the co-flow and counter-flow configuration had an

### D2.3. Final report on analytical, numerical and experimental studies on hydrogen dispersion in tunnels, including innovative prevention and mitigation strategies

impact on the results and thus it is recommended to be placed at a distance from the nozzle similar to the experiment/application of interest.

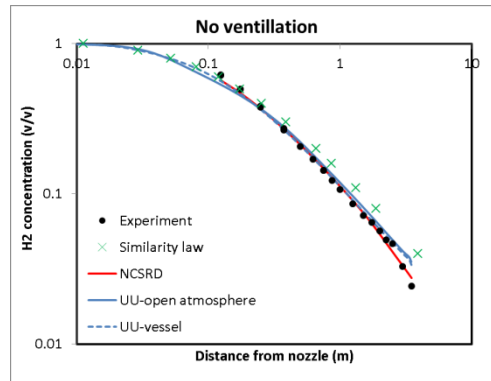


Figure 3-43. The hydrogen concentration along the jet centreline for the case with no ventilation (log-log chart).

In the co-flow configuration, the approach that best mimics the actual fan flow and is in better agreement with the experiment was the one with the linear source term. The rest approaches over-predicted the concentration at distances further downwind the nozzle. Large values of turbulence intensity (50%) and small values of dissipation rate at the fan boundary were found necessary in uniform flow field approaches for better predictions.

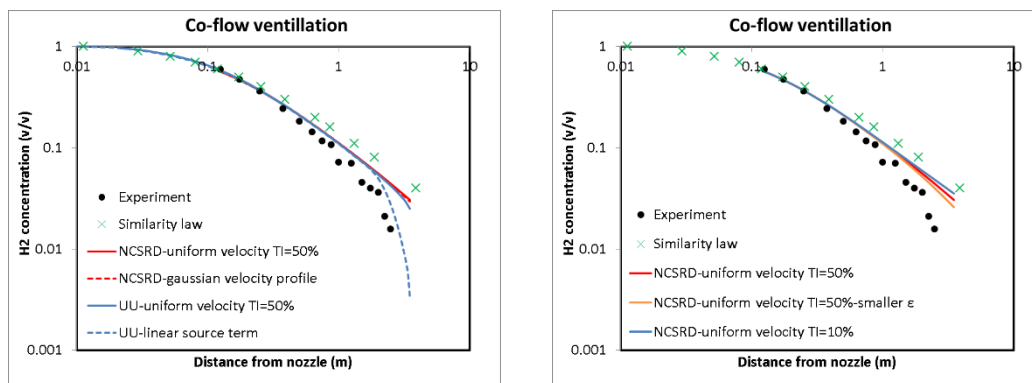


Figure 3-44. The hydrogen concentration along the jet centreline for the case with co-flow (log-log chart).

In counter-flow configuration, the approaches UU-uniform profile with TI=50% and NCSRD-uniform profile with TI=10% reproduce better the interaction of airflow with the jet. However, the linear source term approach and the gaussian velocity profile approach predict more accurately the LFL distance (over-prediction and under-prediction by about 5%, respectively). Close follows the UU-uniform profile, while the NCSRD-uniform profile with TI=50% underestimated the LFL distance. The reason for the better prediction with the lower TI in the counter-flow configuration in contrast to the co-flow is not clear yet.

## D2.3. Final report on analytical, numerical and experimental studies on hydrogen dispersion in tunnels, including innovative prevention and mitigation strategies

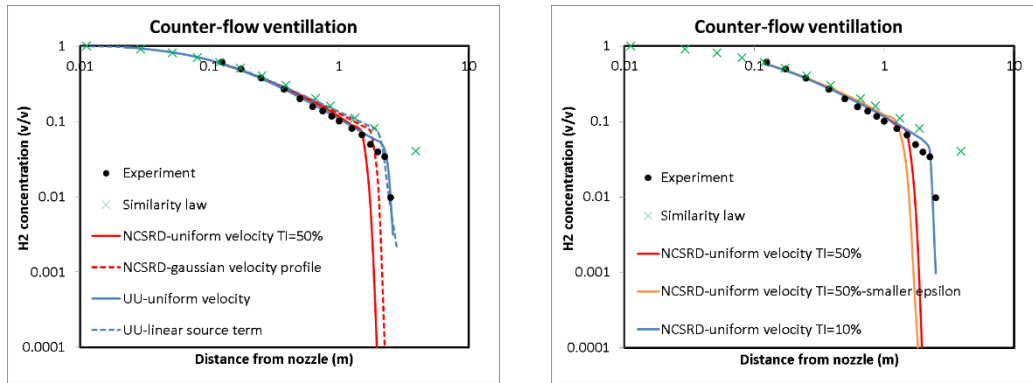


Figure 3-45. The hydrogen concentration along the jet centreline for the case with counter-flow (log-log chart).

Similarity law results for concentration decay rate are also shown in Figure 3-43-Figure 3-45. Comparison with the experiments shows that similarity law gives satisfactory predictions in the case with no ventilation, while it is over-conservative for the co-flow configuration and it cannot reproduce the jet behaviour in the counter-flow configuration.

In terms of safety, experiments and simulations showed that both co-flow and counter-flow configuration lead to the reduction of the LFL distance compared to no ventilation. This is attributed to the better mixing and dilution of the cloud. However, to reproduce this behaviour in simulations, either high turbulence should be imposed or approaches with non-uniform velocity field across inflow boundary should be applied to mimic the fan flow and to better calculate the flow field generated by the fan.

### 3.7 Effect of tunnel slope (Sub-task 2.3.2/NCSR)

#### 3.7.1 Introduction

The vast majority of tunnels are actually inclined (Zhao et al., 2019). The most obvious reasons for inclination are physical restrictions, like for example in undersea tunnels. Other reasons include construction or drainage needs.

The slope is usually a few per cent. According to the current EU Directive 2004/54/EC, new tunnels are not allowed to have a slope higher than 5% (2.86°), unless no other solution is geographically possible. Slopes under 2% (1.15°) are considered to be small. An inclined tunnel can have a longitudinal “V”, a “Lambda” (inverted “V”) or a straight-line shape. For one-directional circulation, the straight-line tunnel is mentioned as “ascending”, when the vehicles move towards the higher end of the tunnel and “descending” otherwise.

The most important physical consequence of the slope of a tunnel in the dispersion of hydrogen or smoke is the “stack effect”, or “chimney effect” due to buoyancy: for straight-line shaped tunnels, lower density gases have the tendency to be transferred upwards, towards the higher end of the tunnel.

In general, hydrogen dispersion studies in sloped tunnels are rare. Tunnel inclination has attracted the scientific interest especially concerning its effects on fire and smoke propagation. Due to the fact that both smoke and hydrogen are buoyant though, their dispersion is expected to present several similarities. Smoke propagation studies at naturally-ventilated inclined tunnels have revealed that the smoke reaching the ceiling initially expands towards (more or

### D2.3. Final report on analytical, numerical and experimental studies on hydrogen dispersion in tunnels, including innovative prevention and mitigation strategies

less) both directions, like in the horizontal tunnel case (Tuovinen et al., 1996). Then the ‘stack effect’, due to buoyancy, increases the propagation speed towards the upper end of the tunnel (Woodburn, Britter, 1996), affecting both the flow and the dispersion field (Ji et al, 2015), especially at high inclinations and long tunnels (Fan et al., 2017). At mechanically-ventilated tunnels, as the slope increases, the critical velocity (in order to avoid back-layering) also increases, but slightly (Musto, Rotondo, 2014). Several times higher pressure increase should be provided from the ventilation system though, in order to achieve the required critical speed at descending tunnels, due to the significant flow resistance that the stack effect imposes (Du et al., 2018). In general, the case of descending tunnels is one of the most unfavourable concerning safety (Ballesteros-Tajadura et al. 2006) and should be carefully examined for several positions of the source, especially due to the fact that in some cases confusion may be created about how to act in emergency (Zhao et al., 2019).

The work of Mukai et al. 2005 deserves special attention, since it examines hydrogen dispersion in inclined tunnels. Analysis was performed for three cases: 1) “Lambda” type horseshoe-shaped tunnel with inclination of 2%, 2) V-type rectangular tunnel with inclination of 5%, and 3) “Lambda” type horseshoe-shaped tunnel with inclination of 2%. In all cases the tunnels are uni-directional with 2 lanes, non-ventilated, having 5 cars simulated as boxes. The leakage is horizontal, from the rear of the front-most car, which stops mid-way. The leak rate is set at 133 L/min (20°C), based on U.S. federal automobile safety standard FMVSS301, for a period of 30 minutes and the leak hole is square with sides of 0.05 m. The STAR-CD RANS CFD code is employed, with the k- $\epsilon$  turbulence model. The results revealed that in all cases the potential risk due to a hydrogen-air mixture above the lower flammability limit is minimal, since only the core of the upward jet close to the car has volume concentrations above 4%.

Seike et al. 2019, in their recent study, examine the thermal fume behaviour of a hydrogen fuel cell vehicle on fire in a non-ventilated tunnel. The CFD simulations do not include hydrogen dispersion, but are mentioned here since three different tunnel inclinations are studied (0%, 2% and 4%). As expected, as the slope increases, at the downwind side the fume propagates faster, while at the upwind side the fume propagation distance decreases.

The effect of tunnel slope on hydrogen dispersion has been studied within HyTunnel-CS using the CFD methodology. For the CFD analysis three descending tunnels 200 m long each were tested, with slopes equal to 0.0%, 2.5% and 5.0% and two nozzle sizes, 2 and 4 mm. The release was downwards below a car and there was also a second car present inside the tunnel. In addition, simulations with ventilation in sloped and non-sloped tunnels and simulations to examine the effect of release orientation on hydrogen distribution in zero-sloped tunnel were performed.

The CFD analysis and the detailed results are shown in (Koutsourakis et al., 2021) and are summarized in the next Subsections.

#### 3.7.2 Numerical setup

Figure 3-46 presents the geometry of the examined problem. A typical horseshoe-shaped tunnel was selected with a length of 200 m, maximum height of 7.1 m and width (at the road level) of 9.2 m. Two simple car models with dimensions 4.2 x 1.8 x 1.3 m<sup>3</sup> were placed at the centre-line of the tunnel. Hydrogen is released from the bottom of the first car. The source is located at the centre of the tunnel and at a distance of 0.5 m from the back of the car and 0.2 m from

### D2.3. Final report on analytical, numerical and experimental studies on hydrogen dispersion in tunnels, including innovative prevention and mitigation strategies

the ground. Three descending tunnels were studied, with slopes equal to 0.0%, 2.5% and 5.0%, respectively. Descending tunnels are considered as the worst case because buoyancy pushes smoke or hydrogen towards the area where the trapped people are and also because in case of ventilation, confusion might be created about how to react.

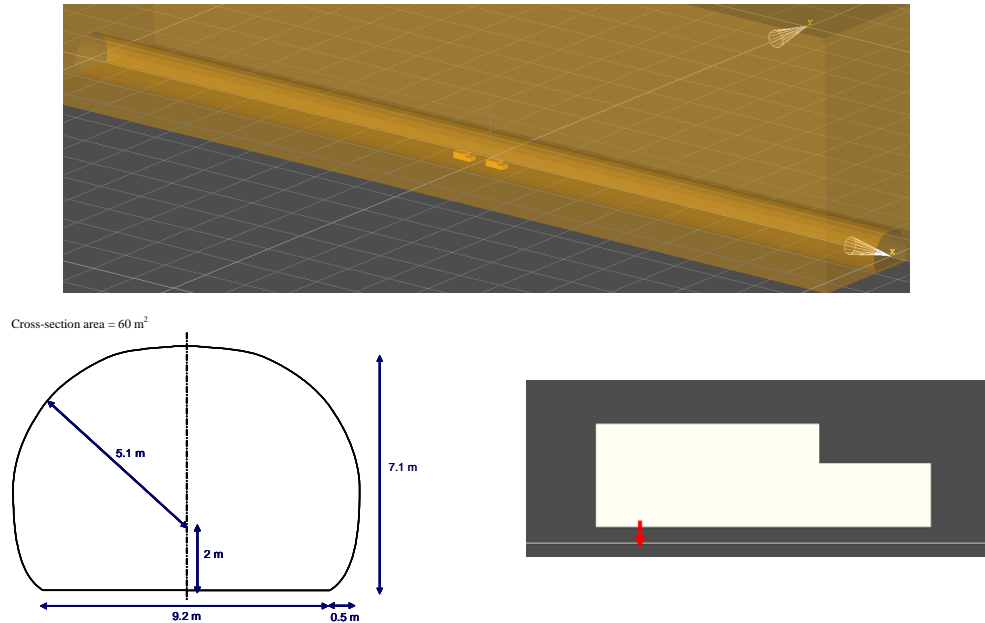
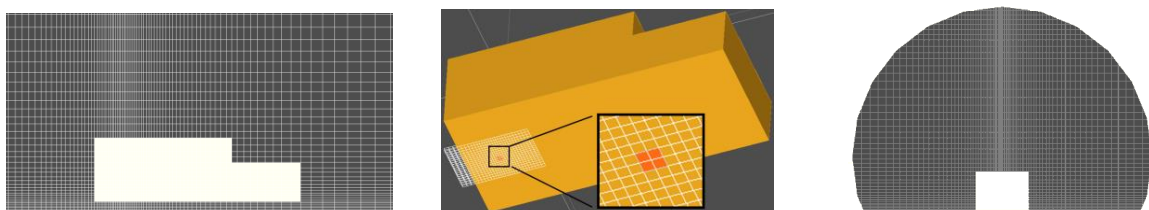


Figure 3-46. Tunnel geometry (top), cross section (bottom left) and car geometry indicating the release position and direction (bottom right).

Computational Fluid Dynamics (CFD) simulations were conducted using the ADREA-HF code which has been extensively validated against hydrogen dispersion cases (Venetsanos et al., 2010; Giannissi et al., 2015).

A notional nozzle approach was used, as Best Practise Guidelines suggest (Tolias et al., 2019), in order to avoid the simulation of the complex shock structure near the release point due to the under-expanded jet that is formed. The Birch approach (Birch et al., 1984) combined with the NIST equation of state was followed. A constant sonic velocity (equal to about ~1305 m/s) and a variable notional nozzle area were considered in order to account for the blowdown. The release duration is approximately 100 s and 400 s for the 4 mm and 2 mm cases, respectively.

Computational grid was extended outside the tunnel in all directions in order to minimize the effect of boundary conditions. The dimensions of the domain are  $260 \times 40 \times 42 \text{ m}^3$ . Figure 3-47 displays some views of the computational grid. Four cells were used to discretize the release area. The grid around the release is uniform. Away from the release cells, the size increases with an expansion factor around 1.04 to 1.1. In the 2 mm case, symmetry was assumed in the simulations in order to reduce the total number of cells in half. The total number of active cells is equal to 1.1 million for the 4 mm case and 0.85 million (for half of the tunnel) for the 2 mm case.





## D2.3. Final report on analytical, numerical and experimental studies on hydrogen dispersion in tunnels, including innovative prevention and mitigation strategies

*Figure 3-47. Computational grid for the 4 mm non-ventilated case. Details of the grid around the release (red) area are shown in the last figure.*

The continuity equation along with the Navier-Stokes equations and the equation for the hydrogen mass fraction are solved on a Cartesian grid. Complex geometries are handled with the use of porosities method (Bartzis, 1991). The  $k$ - $\varepsilon$  turbulence model is used in this study with small initial values of  $k$  ( $0.0025 \text{ m}^2/\text{s}^2$ ) and  $\varepsilon$  (approximately  $4.0\text{e-}004 \text{ m}^2/\text{s}^3$  near walls and  $1.0\text{e-}005 \text{ m}^2/\text{s}^3$  at the centerline). Tunnel slope was modelled by changing the gravitational direction in the momentum equations and by setting the appropriate initial hydrostatic pressure. The MUSCL numerical scheme, which exhibits very good results in impinging jets simulations (Tolias et al., 2015), was chosen for the discretization of the convective terms of all equations.

Most simulation parameters in general, were the same as both ventilated and non-ventilated cases. The main difference was the computational domain, which in the ventilated cases was restricted to the tunnel itself, with no extension outside. This way the flow is more easily controlled and the bulk velocity can be defined with accuracy. An additional advantage is that the number of cells and thus the calculation time are smaller.

To model ventilation, a uniform velocity parallel to the ground is considered at the inlet, while at the other end of the tunnel, pressure outlet is applied. All cases tested were initialized from converged, ventilation-only runs, with no hydrogen. Such runs were performed for both with and without domain extensions and in-tunnel flow results did not differ. Symmetry is considered and the number of active cells of half-tunnel is about 800,000. The maximum CFL number in whole domain was assured to be less than 8. In general the results are presented as comparisons between the various cases/ inclinations and thus any modelling inaccuracies are generally not expected to affect the conclusions.

### 3.7.3 Non-ventilated cases

Figure 3-48 and Figure 3-49 (top figures) display the hydrogen isosurfaces of 10 vol. % and the velocity contours for the 2 mm and 4 mm release diameters, respectively, at 20 s for 0% slope case. As hydrogen accumulates and climbs towards the top of the tunnel, an impinging-like flow is formed at the ceiling for both 2 mm and 4 mm cases. We observe that high velocities of about 2-3 m/s are noticed above the car for the 2 mm and 4 mm case, respectively. The impinging-like jet hits the roof and spreads in both lateral directions, again with high velocities. The velocities in the 2 mm case are lower due to the lower mass flow rate at the release at the first 20 s.

In Figure 3-49 (bottom figures) the hydrogen isosurfaces (of 10 vol. %) and velocity contours are presented for the 4 mm and 5% slope case. We observe that the impinging-like flow is also formed in the sloped case. Both hydrogen isosurfaces and the velocity field are similar to the 0% case (Figure 3-49 – top). The only noticeable difference in hydrogen isosurface is that it is inclined towards the entrance of the tunnel due to buoyancy. In the velocity field, the main difference is that the impinging jet has been moved to the back of the car.

### D2.3. Final report on analytical, numerical and experimental studies on hydrogen dispersion in tunnels, including innovative prevention and mitigation strategies

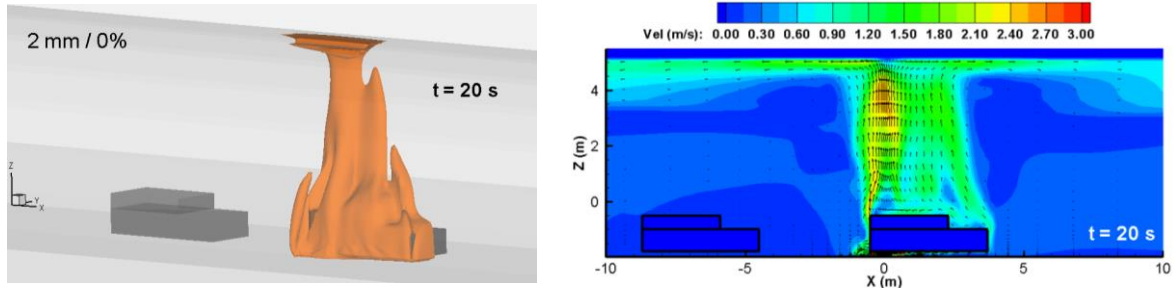


Figure 3-48. Hydrogen volume concentration iso-surface of 10% vol. and velocity contours for 2 mm at 20 sec – zero slope case.

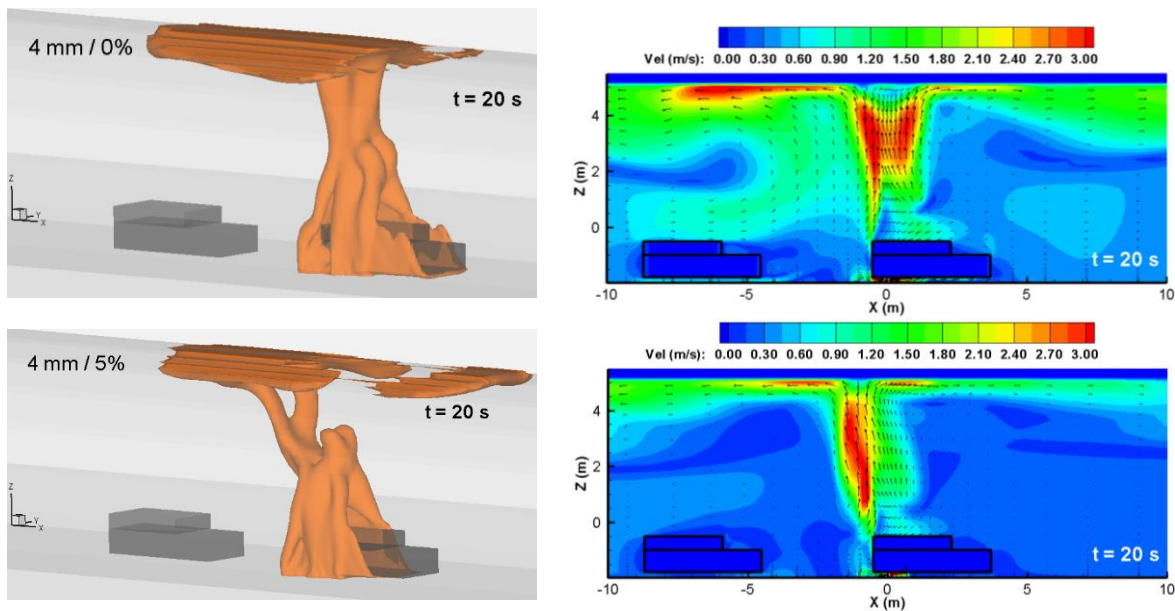


Figure 3-49. Hydrogen volume concentration iso-surface of 10% vol. and velocity contours for 4 mm at 20 sec – zero slope (top) and 5% slope (bottom).

In Figure 3-50 the concentration contours are shown for 0% (top) and 5% (bottom) slope for the 2 mm release diameter at 20 s, 40 s and 60 s, respectively. Concentrations below the Lower Flammability Limit (LFL) of 4 vol. % are not shown. We observe that the effect of the slope is small. At 20 s, hydrogen of 10-15 vol. % occupies the most of the space above the car, reaching the roof of the tunnel. Higher concentrations of around 20 vol. % also exist above the car occupying a lower volume. The yellow area corresponds to concentration of 32-42 vol. % and occupies little volume below the car. The red area beneath the car corresponds to hydrogen volume concentration above the Higher Flammability Limit of 75 vol. %. At 40 s and 60 s, we observe that concentrations, in general, decrease due to the decreased mass flow rate from the tank (blowdown).

The only noticeable difference between 0 and 5% slope is at the right part of the roof above the car at 60 s. We observe that in 0% slope case a gap is formed in that area. This gap is formed due to the decreased mass flow rate with time and due to the fact that the hydrogen that was there has moved towards the right exit of the tunnel. On the other hand, in 5% case this gap does not exist because buoyancy hinders hydrogen movement towards the exit.

### D2.3. Final report on analytical, numerical and experimental studies on hydrogen dispersion in tunnels, including innovative prevention and mitigation strategies

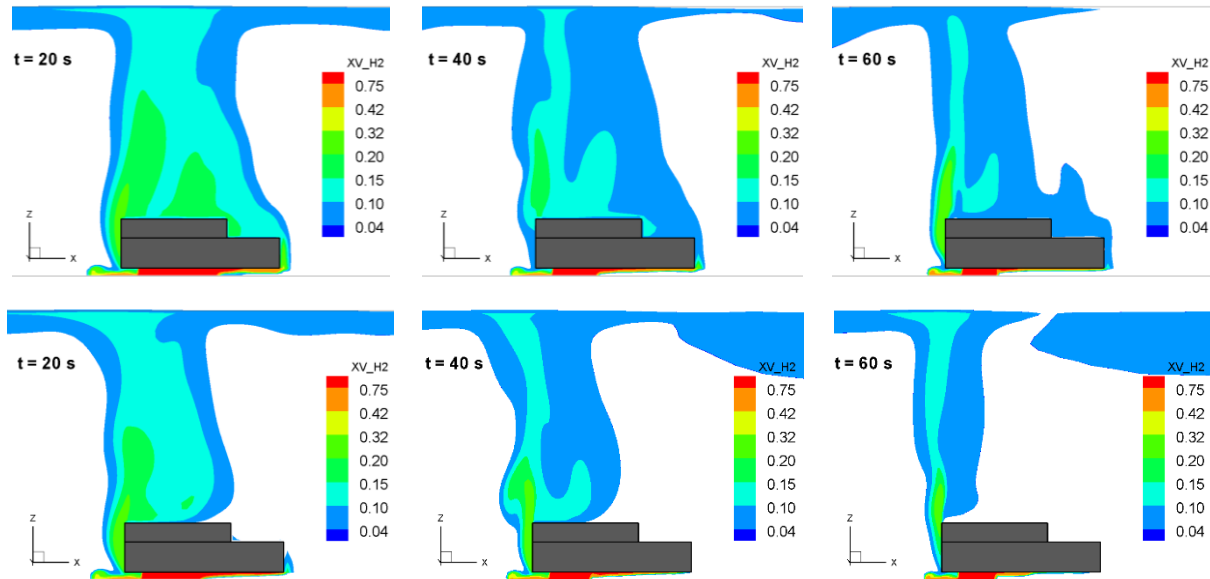


Figure 3-50. Hydrogen volume concentration contours for 0% slope (top) and 5% slope (bottom) for the 2 mm case.

In Figure 3-51 the propagation of hydrogen with time for the 4 mm case is shown for the 0 and the 5% case, respectively. Red area is the area above the LFL. We observe that hydrogen spreads in both directions of the tunnel in both slope cases. In 0% case, a gap is formed upon the release area due to the impingement-like flow and to the decrease of the flow rate. On the other hand, in 5% case and mainly at the right, this gap does not exist because of buoyant effects. When it comes to flammable cloud spread length, we observe that in 0% case hydrogen reaches the exit of the tunnel and escapes through it, whereas in the case of 5% slope, hydrogen cannot reach the exit due to buoyancy, so it is trapped inside the tunnel and it is pushed back towards the release area. Simialr bervation were made for the 2 mm case.

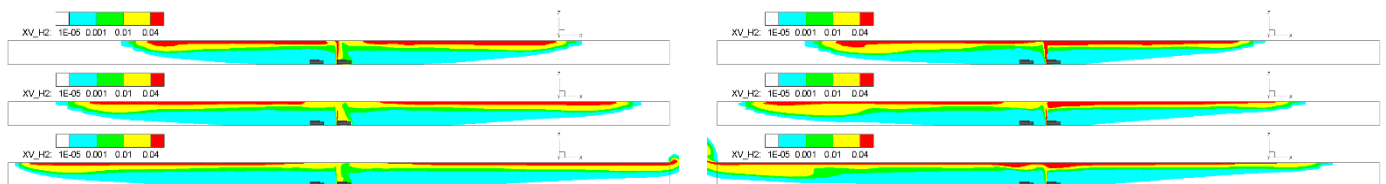


Figure 3-51. Hydrogen volume concentration contours for 0% slope (left) and 5% slope (right) for the 4 mm case at 60 s, 80 s and 100 s.

In Figure 3-52 the battle between the impinging jet flow and the flammable cloud that is pushed towards the entrance of the tunnel due to buoyancy (5% slope) is presented for the 2 mm case at 260 s. We observe that the generated flow field forms a ‘curtain’ that hinders H<sub>2</sub> move to the left (air curtain effect). That effect is not noticed at the 4 mm case, because the release has stopped before the main mass of hydrogen of the lower end of the tunnel has started moving towards the upper end.

### D2.3. Final report on analytical, numerical and experimental studies on hydrogen dispersion in tunnels, including innovative prevention and mitigation strategies

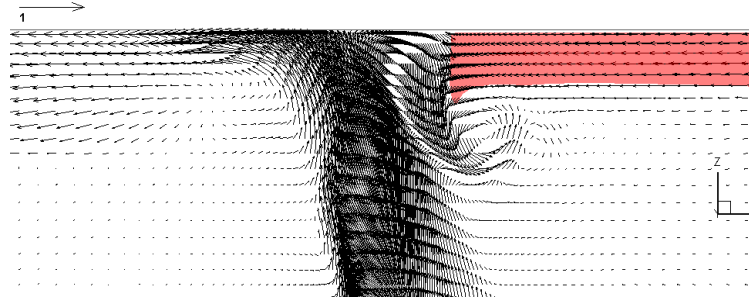


Figure 3-52. Flow field and hydrogen contour of 4 vol. % at 260 s for the 2 mm/5% slope case.

In Figure 3-53 the flammable clouds (4 – 75% volume concentration) are presented as functions of time for both release diameters and for all slope cases. We observe that differences exist among the different slopes only after the end of the release. At times greater than 150 s, the 2.5% slope has higher values than the 0% case. However, flammable cloud vanishes earlier as slope increases, which is positive in terms of safety. In the 2 mm case, the flammable cloud for the sloped tunnels achieves higher maximums compared to the zero-slope case. The lingering trapping of hydrogen at the right part of the tunnel plays a critical role on this. Comparing the clouds between 4 mm and 2 mm cases, we observe that the reduction of flammable cloud in 2 mm case is less than expected (given the fact that the release area is 4 times smaller), especially for the sloped cases.

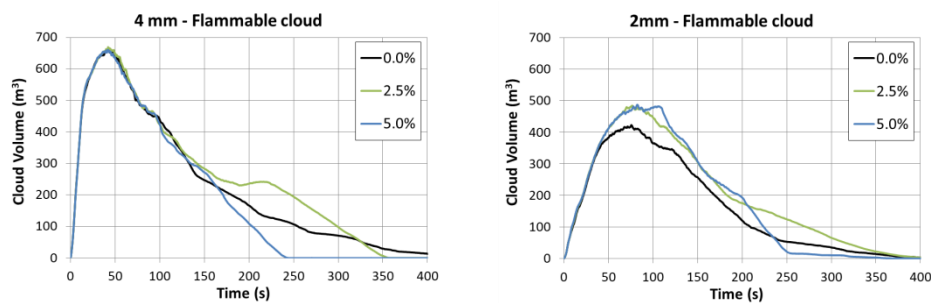


Figure 3-53. Evolution of hydrogen cloud volumes of different concentration ranges 4-75 vol. %.

Figure 3-54 presents the concentration time series at a single point above the second car, for the 4 and 2 mm cases. Strong oscillations exist during the first half of the release phase (until 50 s for the 4 mm case and 200 s for the 2 mm case, respectively) due to the unsteadiness of the flow. An interesting observation is the fact that near the end of the release (at 100 s and 400 s respectively) concentration suddenly increases in all cases. The reason for this is the end of the impinging like flow at the ceiling when emission stops, which allows hydrogen to fill the ‘gap’ due to diffusion from the neighbour regions.

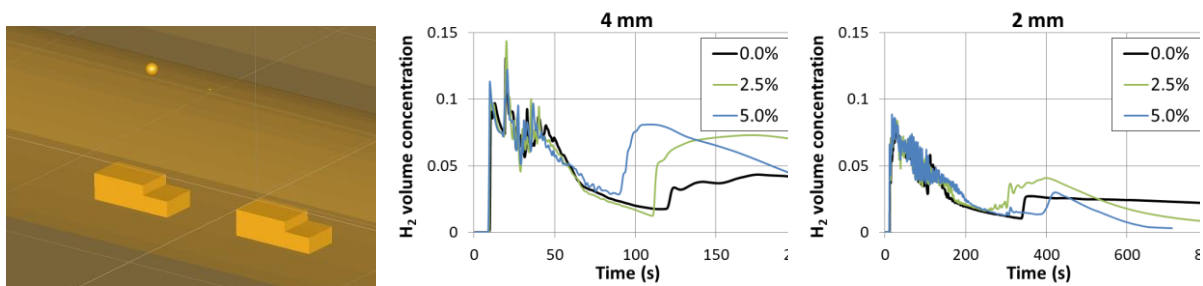


Figure 3-54. Hydrogen time series for 4 mm and 2 mm case at a point above the second car (shown in the left figure).

## D2.3. Final report on analytical, numerical and experimental studies on hydrogen dispersion in tunnels, including innovative prevention and mitigation strategies

### 3.7.4 Ventilated cases

Ventilated case is of interest, because in reality all tunnels are expected to have at least small ventilation. Even in the cases where there is no mechanical ventilation, the pressure differences between the edges of the tunnel, or the moving vehicles (that can cause the “piston effect”), may generate a small ventilation inside the tunnel.

For the ventilated scenarios only the PRD of 2 mm was used, since the no-ventilation results showed that the 2 mm PRD should be preferred against the 4 mm PRD for safety reasons. The geometry of the problem and the numerical parameters are the same as in the non-ventilated cases. Only the grid design differs as described in Section 3.7.2.

Ventilation velocities of 0.5 m/s, 1 m/s and 2 m/s for slopes of 0%, 2.5% and 5% were examined. A simulation where the ventilation stops five seconds after the start of the release was also performed, in order to study the case in which the ventilation is caused by the piston effect and the cars stop moving due to an accident. This can also happen in case of failure of the mechanical ventilation system, due to a fire, for example. Descending tunnels were studied since they were expected to represent the most unfavourable scenario, due to the fact that the stack effect in that case acts against the ventilation and this might trap hydrogen inside the tunnel, especially if the ventilation stops.

Figure 3-55 shows the mid-tunnel concentration contours for various times. It is obvious that the concentration field is completely different in case of ventilation. In general the average concentrations are lower and the flammable part is almost absent at the symmetry plane of the tunnel, even with a small ventilation of 1 m/s. On the other hand, after the time of 60 s, the cloud spreads across the whole tunnel height downwind. The effect of slope is minor at the 1 m/s case and results in a small tendency for backlayering at the roof of the tunnel. It should be noted though that at ventilation cases, hydrogen spreads mainly from the sides of the car – it does not surround the whole car as in no-ventilation cases.

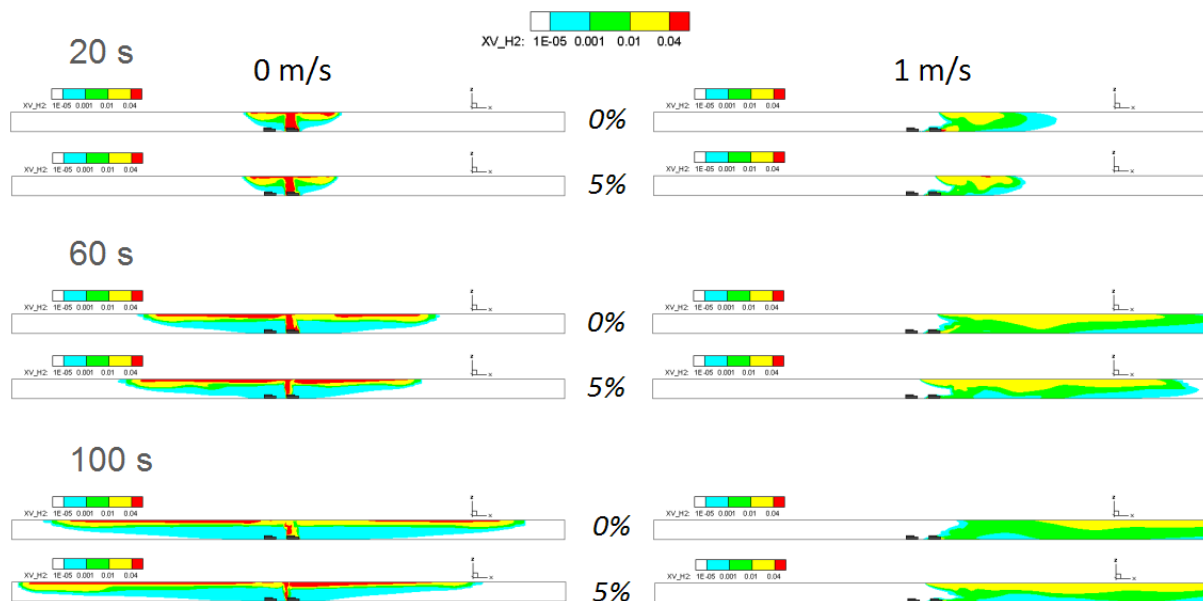


Figure 3-55. Mid-tunnel concentration contours at 20 s, 60 s and 100 s after the start of the release for the non-ventilated (left) and 1 m/s ventilation (right) cases. For each time, the zero slope (top) and 5% inclination (bottom) results are presented. The release duration is about 400 s (2 mm PRD).



### D2.3. Final report on analytical, numerical and experimental studies on hydrogen dispersion in tunnels, including innovative prevention and mitigation strategies

After examining the general characteristics of the concentration field throughout the tunnel, we will now focus around the car, which is an area of high interest. At each subfigure of the Figure 3-56, four contour slices are plotted. The one is at a XZ plane, just after the right side of the car, and the other three are at three YZ planes: 1) at the point of the PRD, 2) in front of the windscreen and 3) one meter in front of the car. Only the concentrations above the flammable are shown. At the same time the 0.04% vol. iso-surface is shown, with high translucency, in order to have an idea of the whole volume occupied from the flammable cloud. The color of the most dangerous concentration of 25-35% vol. (due to high burning velocity) is stressed with an arrow at the first subfigure.

At the no-ventilation cases, the hydrogen, after impinging to the ground and spreading horizontally, surrounds the car. The buoyancy is the driving mechanism for the flow and as a result hydrogen reaches the ceiling of the tunnel on top of the car very rapidly and with high velocity and spreads again along the roof of the tunnel. The concentrations at the sides of the car are very high during the initial stages.

In case of ventilation, the hydrogen that comes out from the bottom of the car towards its sides interacts with the wind. This results in recirculating flow at the YZ planes at the sides of the car, which, along with the wind and the buoyancy, results in the inclined elongated vortices, one at each side of the car (Figure 3-56). The hydrogen spreads mainly through those vortices and it is transferred downwind. Counter-rotating vortices on top of the main vortices may also be formed and this, along with the effect of buoyancy, results in very complicated flow patterns. Depending on the wind strength, the cloud reaches the walls of the tunnel far downwind at an oblique angle and then spreads towards the ceiling of the tunnel and across the symmetry plane, having much lower concentrations there than in the no-ventilation cases. The flow and concentration fields are thus very different.

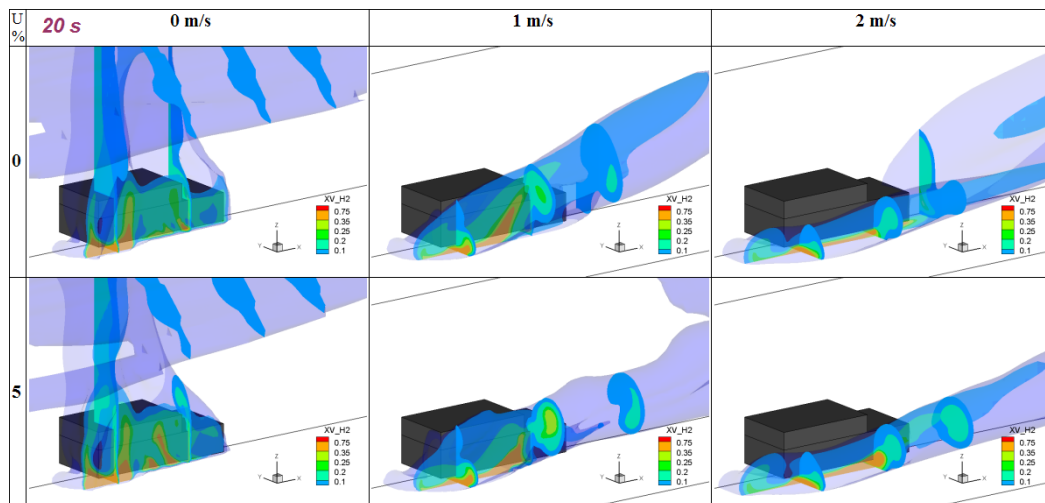


Figure 3-56. Above-flammable contour slices at 20 s after the start of the release. Cases of tunnels with 0% and 5% slope are presented, for three ventilation speeds each (0 m/s, 1 m/s and 2 m/s).

Concerning the most dangerous concentration range of 25%-35% v/v, we notice that in the no-ventilation cases, the relevant cloud stays in touch with the car sides, while in the ventilation cases it can be transferred alongside at distances up to one meter. This increases the possibility of ignition from sources in the neighbourhood of the car.



### D2.3. Final report on analytical, numerical and experimental studies on hydrogen dispersion in tunnels, including innovative prevention and mitigation strategies

As the ventilation speeds get higher, the elongated side-vortices get longer and more parallel to the ground. If we would look at similar contour slices as those of Figure 3-56 around the car at longer times, we would notice that the high-concentration clouds shrink. From that point of view, we could say that the most dangerous area is the area around the car for the first 20 s after the start of the release, regardless of the ventilation and of the inclination.

In order to see clearly the effect of inclination at ventilated tunnels, at Figure 3-57 (left) the evolution of flammable cloud for various slopes in the case of a ventilation speed of 1 m/s is presented. As expected, the maximum cloud volume increases as the inclination increases, but the differences are very small. Moreover, the 0% and 2.5% slope cases have almost the same evolution throughout the release. The 5% inclination case presents up to two times higher cloud volumes at times between 10 s and 40 s after the start of the release. If we compare Figure 3-57 with the flammable volume of the respective cases without ventilation (Figure 3-53), we can notice that the ventilation cases present about 4 times lower maximum flammable cloud volumes.

If we focus on the 5% slope tunnels, at Figure 3-57 (right) we can notice that in general the higher the speed, the lower the maximum flammable cloud. If we ignore the too low ventilation case of 0.5 m/s, we notice that the differences at cloud evolution are small. This is valid even in the case we turn off the ventilation at 5 s after the start of the release. In conclusion, concerning the flammable cloud of the examined cases, the big difference is whether there is ventilation or not – the absolute value of ventilation (as long as it is above 0.5 m/s) and the possible inclination of the tunnel, are of secondary importance.

It should be noted that even if the total nearly-stoichiometric hydrogen cloud volumes are comparable for all examined cases (not shown here), the distribution of the cloud around the car may be very different, especially between the ventilated and the no-ventilated cases. The inclination on the other hand has in general a minor role on the specific high-concentration cloud. The results at the particular concentration range depend very much on the flow details below the car, which are very difficult to predict.

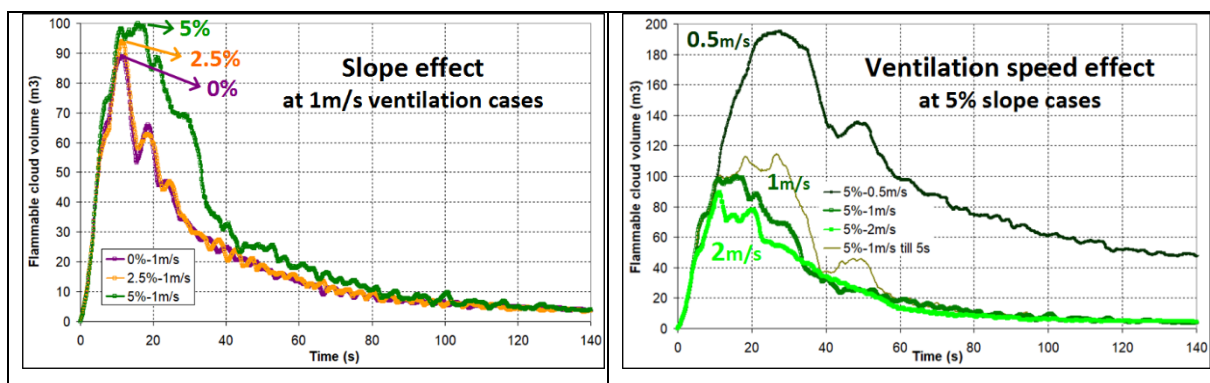


Figure 3-57. Whole-tunnel flammable cloud volume evolution with time for three inclinations with the same ventilation of 1 m/s (left) and for four different ventilation cases of a tunnel with a slope of 5% (right).

Interestingly, it was observed that ventilation might also have negative effects for some spaces/times. For instance, the case with no adverse inclination (0% slope) and with the 2 m/s ventilation, predicted two to three times bigger volumes with 25-35 % concentration between 100 s and 250 s, than the other cases. This can be explained by the fact that at 2 m/s the

### D2.3. Final report on analytical, numerical and experimental studies on hydrogen dispersion in tunnels, including innovative prevention and mitigation strategies

dispersion is more intense and a significant nearly-stoichiometric region below the car is formed. If hydrogen is released from the bottom of the car, there might be cases where the concentrations can be close to the stoichiometric for relatively long periods of time. This raises a question about whether it is a good practice to have the PRD pointing towards the street.

#### 3.7.5 A note on the release direction

Due to the fact that the downwards release direction appeared to present some disadvantages, two more release directions were roughly examined: upwards and backwards. The zero inclination and 0.5 m/s ventilation case was considered as a reference case. It was found that the orientation of the release has significant effect. In both alternative release direction cases the maximum total nearly-stoichiometric cloud volume (25% - 35% v/v) was about 70 times smaller. The reason is that the nearly-stoichiometric cloud is confined at a small region around the core of the jet (see Figure 3-58), while at the downward case it spreads all around the car. Thus, alternative PRD release directions should be seriously considered when designing hydrogen cars.

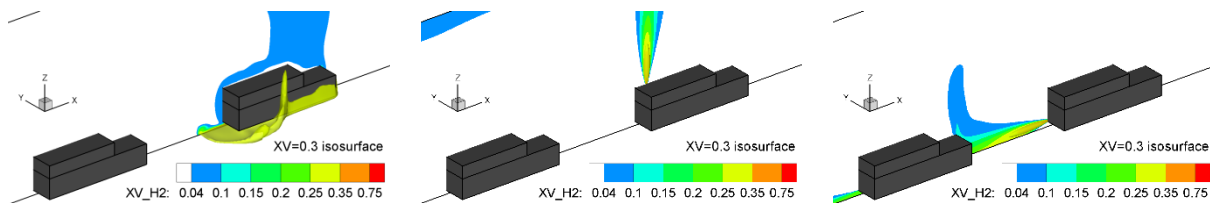


Figure 3-58. Mid-plane concentration contours and stoichiometric iso-surfaces at 10 s for downwards (left), upwards (middle) and backwards (right) release directions. The ventilation is 0.5 m/s in all cases.

Concerning the total flammable cloud, in upwards case it was slightly bigger compared to the downwards case (maximum of 142 m<sup>3</sup> instead of 126 m<sup>3</sup>) and it lasts much longer, having a maximum at 71 s instead of 13 s. In backwards release case, the maximum flammable cloud was about three times smaller compared to the downwards case.

#### 3.7.6 Conclusions

The main conclusions (see also (Koutsourakis et al., 2021), for the particular 200 m long tunnel examined, are summarized in the following bullets:

- Inclination, at both ventilated and non-ventilated tunnels, has small effect on the velocity and concentration field around the car. It affects hydrogen dispersion at larger time and spatial scales where interesting phenomena occur.
- The long-term influence of the inclination is positive: that is, in case of straight sloped tunnels, the higher the inclination, the sooner hydrogen will reach near-zero concentrations.
- There are though cases/places/times where adverse effects may exist at inclined tunnels. For example, volume of flammable cloud can be bigger in case of inclination.
- Hydrogen clouds of concentrations above 10 vol. %, which matter more in case of an ignition, are only very slightly affected by the slope.
- The reduction of the release diameter from 4 mm to 2 mm leads to the reduction of the maximum flammable cloud of about 38% and of the 10-75 vol. % cloud of about 75%. However, after a certain time the 2 mm case exhibits higher hydrogen cloud volumes

D2.3. Final report on analytical, numerical and experimental studies on hydrogen dispersion in tunnels, including innovative prevention and mitigation strategies

of 10-75 vol. % and 32-42 vol. % compared to the 4 mm case due to the longer release duration.

- The ventilation has strong effect on the flow and concentration field of the tunnel and it usually overwhelms any stack effects due to inclination. However, at the most flammable cloud volumes (25%-35% v/v), even if the cloud shape heavily depends on the wind speed, no systematic effect on the maximums of the total cloud volumes could be identified.
- Even if the ventilation has in general a positive effect in hydrogen safety, there may be cases with adverse effects.
- Vertically downwards release direction through TPRD should be avoided. In general, oblique direction should be preferred.

## 4. Experiments (Task 2.4/HSE)

### 4.1 Mechanical ventilation in underground parking (Sub-task 2.4.1/USN)

#### 4.1.1 Introduction – objectives

The release of hydrogen inside buildings may pose a hazard to people and structures. It is given in (IEC 60079-10-1, 2015), (NFPA 2, 2011), and (ISO/DIS 19880-1, 2018) that the hydrogen volume concentration should not exceed 1% in air.

A real release of hydrogen inside a confined space, such as an underground parking garage, will give a time and space dependent hydrogen concentration. This inhomogeneous nature of hydrogen requires a set condition of the distance from the release to the position of desired 1 vol. % hydrogen. The ceiling is directly above the release in one such position, while real systems may require a position offset by a distance.

The physical geometry is assumed to influence the concentration largely. Both the actual concentration value and the dynamics of the buildup will still be important to find the release rates at which the mass flow of hydrogen does not create a cloud of concentration above 1 vol. % (or 4 vol. %, or other criteria). The influence of mechanical ventilation in such a setup is also an important factor in the investigation.

The direction of the release inside the enclosure is also important, as a downwards impinging jet will give a different concentration compared to a straight upwards jet. In confined spaces and semi confined spaces, hydrogen will accumulate under the ceiling creating a hydrogen cloud. The hydrogen-air mixture is highly explosive and keeping hydrogen concentration under flammability limit is crucial. The forced ventilation systems used today operate according to the standards. In parking houses or the storage hall, the recommended air change per hour (ACH) is 6 or 10 depending on the area size, according to British Standards (BS 6, BS 10) (BS7346-7, 2013).

In this report, the work of series of experiments and data analysis of hydrogen releases in semi-confined enclosures is presented. This work is also published in (Lach and Gaathaug, 2021). The enclosure used for experiments imitates parking houses. The influence of the existing standards of mechanical ventilation on created hydrogen cloud will be tested. Two British standards will be investigated against releases through 1 mm and 0.5 mm nozzle from different reservoir pressures. The purpose of this report is to generate data for further model validation and to recommend a safety diameter of Thermal and Pressure Relief Device which may secure low concentration (< 4%) with existing ventilation systems. The hydrogen dispersion results will be used for the planning campaign where the hydrogen will be ignited at the nozzle (no premix).

#### 4.1.2 Detailed specification

##### 4.1.2.1 Tubing installation

All experiments were carried out in 40 ft ISO container. The container was placed at the Norward AS in Bamble.

## D2.3. Final report on analytical, numerical and experimental studies on hydrogen dispersion in tunnels, including innovative prevention and mitigation strategies

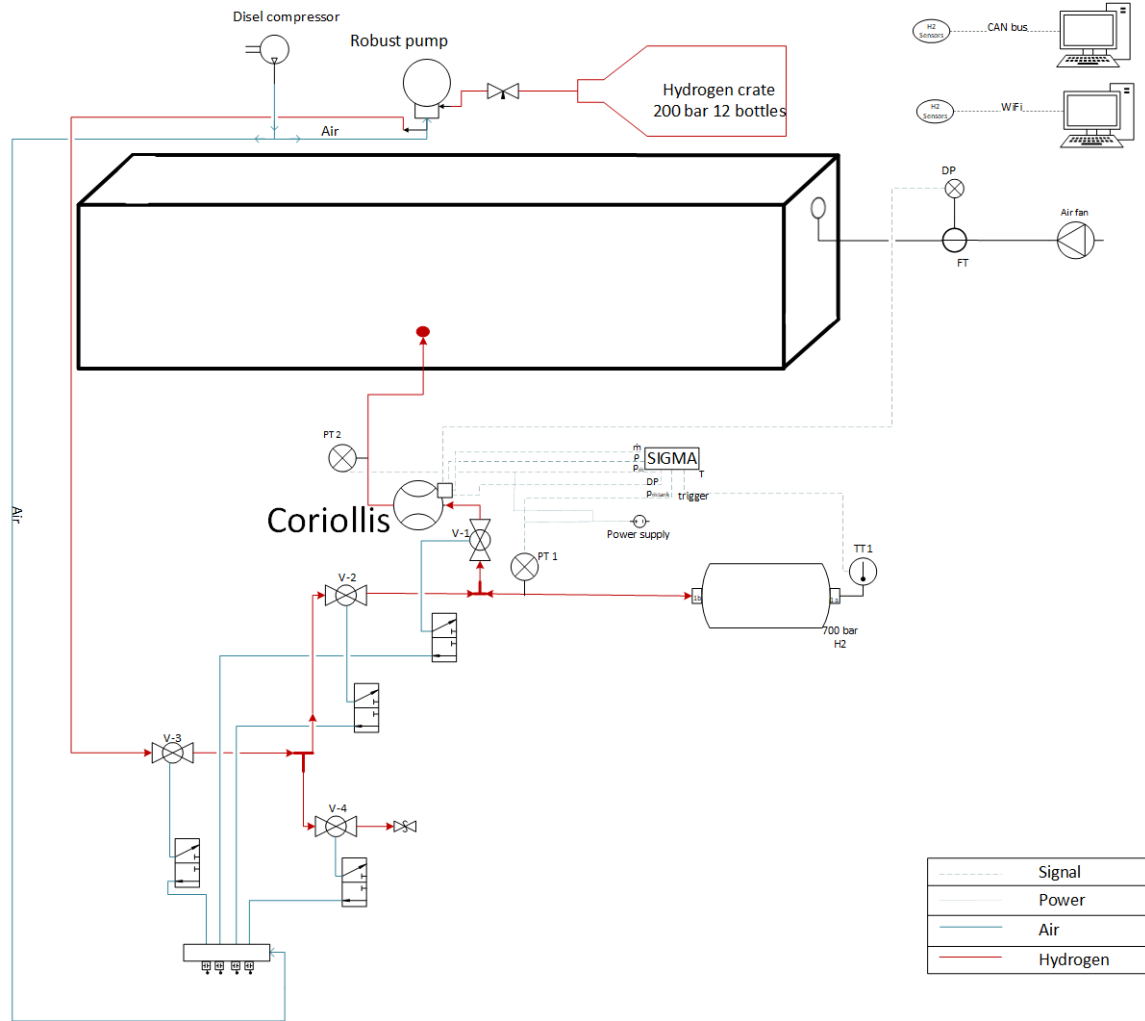


Figure 4-1. Piping and instrumentation diagram for the experimental setup.

The 40 ft ISO container (see Figure 4-1, Figure 4-2) with isolated walls was used for all experiments with both open exit doors. Its inner dimension LxWxH: 11885 x 2240 x 2285 mm gives a total volume of 60.8 m<sup>3</sup>. The isolation thickness was approximately 0.07 m. The real-scale parking house/underground parking has the standard 2.25 m minimum free height (source:[https://www.vegvesen.no/s/bransjekontakt/Hb/hb017-1992/DelC\\_Detaljkapitler/20.Parkering/20\\_Parkeringshus.htm](https://www.vegvesen.no/s/bransjekontakt/Hb/hb017-1992/DelC_Detaljkapitler/20.Parkering/20_Parkeringshus.htm))



### D2.3. Final report on analytical, numerical and experimental studies on hydrogen dispersion in tunnels, including innovative prevention and mitigation strategies

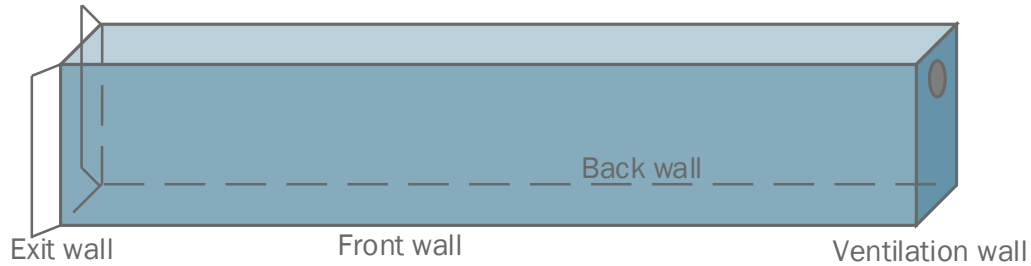

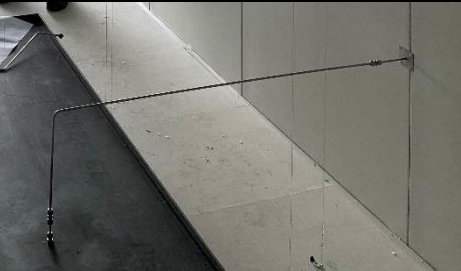






Figure 4-2. 40 ft ISO container with installed equipment and instrumentation.

The container was equipped with:

<p>1. The ventilation system consists of ~4 m long pipes with an outlet of 0.315 m located 0.05 m from the ceiling at the ventilation wall (0.2075 to the outlet center), the air fan and duct damp IRIS 200 with mounted differential pressure transmitter.</p>	
<p>2. Hydrogen pipe mounted at the back wall was located 5 m from the ventilation wall and 0.6 m above the floor. The H<sub>2</sub> outlet was mounted vertically through the steel table 0.25 m above the floor. The nozzle (1 mm or 0.5 mm) was installed over the table. The unit with 0.003 m ID was connected to the nozzle unit to discharge H<sub>2</sub> under the table.</p>	
<p>3. Steel table with dimensions LxWxH: 1965 x 730 x 250. The table was scaled against the hydrogen car (Toyota Mirai) with a 0.4 scaling factor.</p> <div data-bbox="576 1467 874 1697">  <p>Toyota Mirai</p> <p>1535 mm</p> <p>4890 mm</p> <p>1815 mm</p> <p>L x W x H: 4890 x 1815 x 1535 mm</p> <p>Boot capacity: 361 dm<sup>3</sup></p> </div>	



### D2.3. Final report on analytical, numerical and experimental studies on hydrogen dispersion in tunnels, including innovative prevention and mitigation strategies

<p>4. Wire threads for 30 Canbus hydrogen sensors.</p> <p>5. Eight Velcro fasteners mounted on the walls, ceiling and table.</p> <p>6. Fire plates on the floor placed under the table with 6.5 m total length.</p>	
<p>7. Fastening clamps mounted on the wall outside to attach a 6 mm 'hydrogen' pipe.</p>	

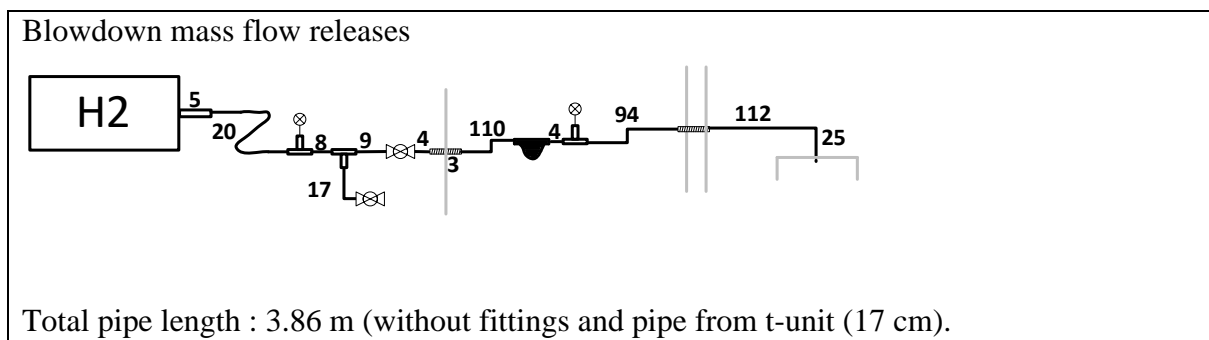
The experiments were performed in the ISO container with two setups:

One for constant mass flow releases. The hydrogen was flowed from the hydrogen crate (12 bottles with 200 bar) through Coriolis mass flow meter and releases through a 1 mm or 0.5 mm nozzle in the container.

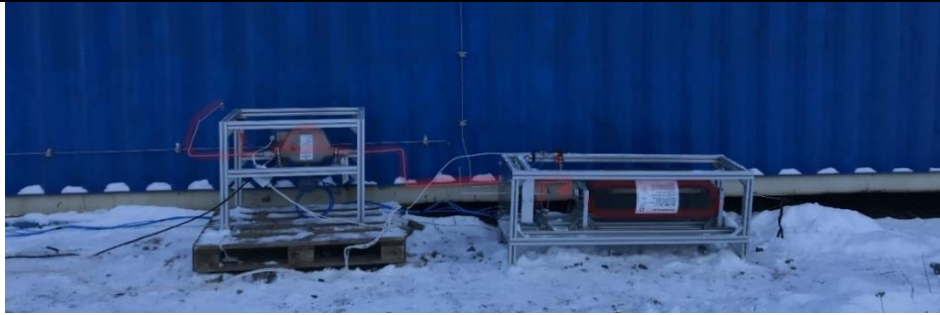
Second for blowdown type mass flow releases. The hydrogen was pumped from the hydrogen crate by a gas booster pump (Haskel-Proserv operating pressure 1600 bar) through pipes attached around the container to the hydrogen tank (Hexagon, 700 bar). During experiments, hydrogen flow started from the tank through Coriolis mass flow meter and released through a 0.5 mm nozzle.

The hydrogen pipe length and design in the setup for constant mass flow releases were different than for blowdown releases. The length presented in the Table 4-1 below is only between hydrogen source (tank for blowdown and hydrogen crate for constant mass flow releases) and release end in the container. All the pipes for blowdown type releases has 6 mm OD and 3 mm ID. During the experiments, the hydrogen flow started from the tank through Coriolis mass flow meter and was released through a 0.5 mm nozzle.

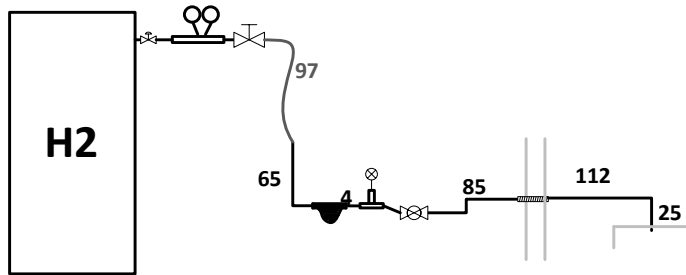
*Table 4-1. Pipe, valves description for blowdown and constant type of mass flow releases.*



### D2.3. Final report on analytical, numerical and experimental studies on hydrogen dispersion in tunnels, including innovative prevention and mitigation strategies



#### Constant mass flow releases



Total pipe length: 3.84 m (without units). Between the pressure valve from the crate and



Coriolis mass flow meter, the flexible hose (97 cm) and pipe with 4 mm ID (65 cm) were used.

The experiments were performed with constant and blowdown type of flow. All experiments were performed with hydrogen flow through Coriolis mass flowmeter for high-pressure flows.

Constant releases were performed directly from the hydrogen crate, through Coriolis where mass flow, hydrogen pressure (measured 'after' Coriolis) and density were constantly measured. The same pressure transmitter was installed at the outlet of the tank during blowdown releases. During blowdown releases the pressure transmitter was installed at the tank.

During all experiments, the same ventilation system was used. The air volumetric flow was controlled by IRIS 200 damper and duct fan model CK 200 controlled with volatage speed controller. In order to obtain ACH British Standard (BS) 10 and 6 the need airflow was calculated, and the ventilation fan was adjusted accordingly.

#### 4.1.2.2 Hydrogen sensors

Along the container, the 30 CANbus hydrogen sensors (04D) were installed and 8 Wifi sensors (DC). The positions of the sensors are listed in Table 4-2 and Figure 4-3.

Table 4-2. Hydrogen sensor positions

D2.3. Final report on analytical, numerical and experimental studies on hydrogen dispersion in tunnels, including innovative prevention and mitigation strategies

<i>ID</i>	<i>H2 sensor No</i>	<i>x</i>	<i>y</i>	<i>z</i>
04D139	1	-11600	2170	0
04D140	2	-11600	1670	0
04D141	3	-10100	2170	0
04D142	4	-10100	1670	0
04D143	5	-8600	2170	0
04D144	6	-8600	1670	0
04D145	7	-7100	2170	0
04D146	8	-7100	1670	0
04D147	9	-5600	2170	0
04D148	10	-5600	1670	0
04D149	11	-4500	2170	0
04D150	12	-4500	1670	0
04D151	13	-3000	2170	0
04D152	14	-3000	2170	430
04D153	15	-4500	2170	863
04D154	16	-4500	2170	430
04D155	17	-5600	2170	863
04D156	18	-5600	2170	430
04D157	19	-7100	2170	863
04D158	20	-7100	2170	430
04D159	21	-7100	1670	430
04D160	22	-5600	1670	430
04D161	23	-4500	1670	430
04D162	24	-5000	1170	863
04D163	25	-5000	0	370
04D164	26	-5000	250	370
04D165	27	-5010	250	0
04D166	28	-4760	250	0
04D167	29	-6465	250	0
04D168	30	-6465	0	0
DC13	31	-11600	2170	863
DC09	32	-10100	2170	863
DC06	33	-8600	2170	863
DC12	34	-7100	1670	1100
DC11	35	-5600	1670	1100
DC08	36	-4500	1670	1100
DC10	37	-3000	2170	863
DC14	38	-4500	250	0

## D2.3. Final report on analytical, numerical and experimental studies on hydrogen dispersion in tunnels, including innovative prevention and mitigation strategies

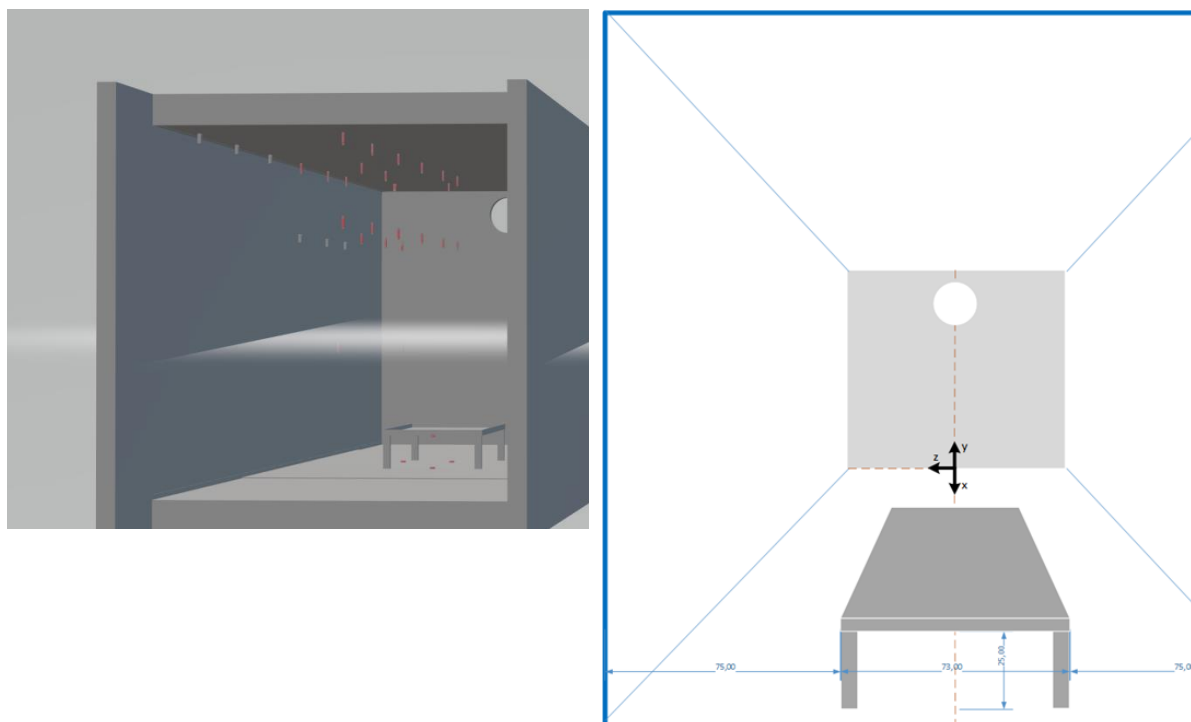


Figure 4-3. Sensors' position.

### 4.1.3 Experimental matrix

The experiments were designed for two volumetric air flows, according to BS10 and BS6. Nozzles with 0.5 mm and 1 mm diameter were used. The experimental campaign was started with constant mass flow releases due to safety precautions. Both ACH were tested for 3 mass flow rates (Table 4-3). The pressure at the hydrogen crate was the decisive (controlling) method of the mass flow rate. The ventilation system was tested for high mass flow rates obtained with a bigger nozzle diameter (with the same initial pressures). After completing constant mass flow releases, the setup was rebuilt (enriched with) for blowdown mass flow releases. The same ACHs were tested against hydrogen releases from the three reservoir pressures (Table 4-3).

Table 4-3. Experimental parameters.

Exp	Nozzle	H2 release time	p0 wanted [bar]	p0 sensor [bar]	MFR [g/s]	Max H2 conc under the ceiling [%]	Max H2 conc 50 cm below the ceiling [%]	Max H2 conc under the table [%]	Out temp [C]	Wind [m/s]	ACH
1	0.5	30	60	—	—	—	—	—	-1	3N	10
2	0.5	30	60	—	—	—	—	—	-1	3N	10
3	0.5	30	120	-251	1.1	0.028	—	—	-1	3N	10
4	0.5	60	120	-251	0.8	2.3	2.1	14	-1	3N	10
5	0.5	60	160	-251	1.1	2.9	3.2	14.7	-1	3N	10
6	0.5	60	160	166	1	2.6	2.5	14.9	-3	2N	6
7	0.5	60	120	121	0.7	2.2	2.5	11.4	-3	2N	6
8	0.5	60	60	60	0.4	1.7	1.7	8.1	-3	2N	6
9	1	60	160	157	6	8.3	8	17	-3	2N	6

### D2.3. Final report on analytical, numerical and experimental studies on hydrogen dispersion in tunnels, including innovative prevention and mitigation strategies

10	1	60	160	165	6	7.2	7.7	16.9	-3	2N	10
11	1	60	120	140	5.2	7.2	7	15.7	-3	2N	10
12	1	60	120	120	4.2	6.1	5.8	15.3	-3	2N	10
13	1	60	120	121	4.2	6.2	6.2	15.4	-1	3N	6
14	1	60	60	59	2.2	3.6	4.1	12.3	-1	3N	6
15	1	60	60	55	2.2	3.7	4	11.2	-1	3N	10
16	1	1000	140	144	5.3*	8.7	8.3	15.9	-1	3N	10
17	0.5	1000	532	532	6*	2.7	2.7	13.7	-5	2NW	10
18	0.5	1000	200	203	3.2*	6.8	6.5	14.5	-3	2N	10
19	0.5	1000	700	721	7.9*	8.1	7.8	16.1	-4	1W	10
20	0.5	1000	700	713	7.8*	8.2	8.1	16	-2	6N	6
21	0.5	1000	360	362	4.2*	5.7	5.7	14.5	-3	5N	6
22	0.5	1000	207	209	2.5*	3.8	3.7	15.7	-3	5N	6
23	0.5	1000	360	359	4.2*	4.6	5.2	15	-8	3NW	10

\*mass flow rate at  $t_0$

#### 4.1.4 Results and discussion

The experiments performed at Norward were carried out regardless of weather conditions. The direction and speed of wind and temperature are listed in the table below together with the result (Table 4-4, column 10-11). The container was aligned north-south with the open doors directly southwards.

During constant releases (exp 1 – exp 15) the hydrogen mass flow was controller by the pressure:

- During constant releases (exp1 1- exp 15) by the control pressure valve at the hydrogen crate. Three mass flow rates were designed from 60 bar, 120 bar, and 160 bar for 0.5 mm and 1 mm inner diameter.
- The blowdown type hydrogen releases (exp 17- exp 23) were designed for tank filled with hydrogen up to 700 bar, 350 bar, and 200 bar.
- Exp 16 is the blowdown type mass flow release from 140 bar with set up from constant mass flow releases.

The initial pressure was read by the pressure transmitter (Table 4-4, column 5) and mass flow rate by the Coriolis mass flow meter (Figure 4-4, column 6). The highest measured concentrations from the sensors are listed in columns 7 and 8. Six hydrogen sensors were installed under the table (sensors 25-30) and one Wi-Fi sensor on the backside of the table (DC14). The concentration results from hydrogen sensors are presented in (Lach, Gaathaug, 2020), (Lach, Gaathaug, 2021), and the max value during the release time is listed in the table below (column 9).

The hydrogen concentrations results from all the experiments are shown in (Lach, Gaathaug, 2020).

##### 4.1.4.1 . Releases with the constant mass flow rate

From Table 4-3 is clear that the hydrogen mass flow rate increases with increasing the nozzle diameter (at the same initial pressure release) and with increasing the release pressure. The consequence of a higher mass flow rate is a higher concentration in accumulated hydrogen

### D2.3. Final report on analytical, numerical and experimental studies on hydrogen dispersion in tunnels, including innovative prevention and mitigation strategies

cloud (Table 4-3 and plot in Figure 4-7). The effect of the mechanical ventilation system for releases with 1 mm and 0.5 mm nozzle is shown in Figure 4-4 and Figure 4-5. The mean value of the 200 maximum concentration measurements of each sensor is presented. Experiments with releases through 1 mm and ACH 10 showed in Figure 4-4 are Exp 15, Exp 12, and Exp 10 from 60 bar, 120 bar, and 160 bar pressure releases respectively. With ACH 6 with the same pressure order: Exp 14, Exp 9, and Exp 13. The influence of the higher ACH increases with increasing pressure release hence hydrogen mass flow rate. This can be observed also in Figure 4-5 where three experiments with ACH 6 (Exp 8, Exp 4, and Exp 5 with 60 bar, 120 bar, and 160 bar respectively) and two experiments with ACH 10 are presented (Exp 7 and exp 6 from 120 bar and 160 bar pressure release respectively). The maximum concentration is 3 times higher when comparing releases with 0.5 mm and 1 mm nozzle. The influence of higher ACH for releases through 0.5 mm nozzle is lower but with increasing the reservoir pressure the influence increases. Due to failure with the concentration measurements from the reservoir with 60 bar through 0.5 mm the comparison between ACH 10 and ACH 6 with that parameter is not presented.

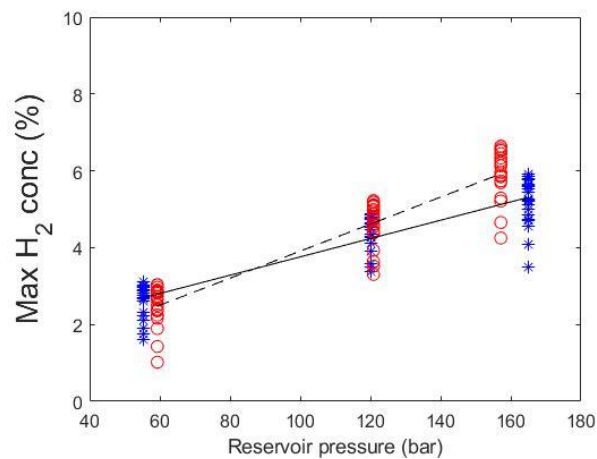


Figure 4-4. Hydrogen concentration during hydrogen releases through **1 mm** nozzle with ACH 6 (dash line) and ACH 10 (solid line). Maximum concentration at each sensor during ACH 10 (blue star) and ACH 6 (red circle).

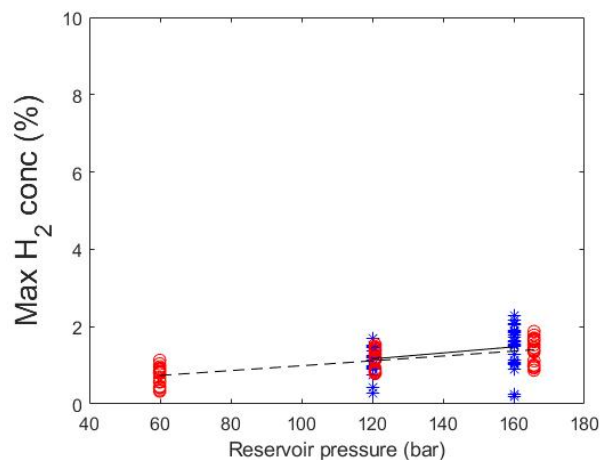


Figure 4-5. Hydrogen concentration during hydrogen releases through **0.5 mm** nozzle with ACH 6 (dash line) and ACH 10 (solid line). Maximum concentration at each sensor during ACH 10 (blue star) and ACH 6 (red circle).



### D2.3. Final report on analytical, numerical and experimental studies on hydrogen dispersion in tunnels, including innovative prevention and mitigation strategies

The hydrogen concentrations from the sensors mounted 50 cm under the ceiling and under the ceiling show similar values to the sensor mounted under the ceiling. The hydrogen concentration results from the measurements indicate the hydrogen cloud in the container has a minimum of 50 cm in height (Table 4-3).

The concentration results from sensors presented on plots in Figure 4-4 and Figure 4-5 were chosen to observe the hydrogen dispersion in the hydrogen cloud. Sensors' locations are illustrated in Figure 4-6 where colours correspond to those used on the plots. The red lines (solid for ACH 10 and dash line for ACH 6) presents hydrogen concentration at the exit of the container (open door) – sensor 1 located 6.6 m from the nozzle. The black lines show concentration located between sensor 1 and the nozzle (2.6 m from the nozzle). Blue lines show the hydrogen concentration from sensor 13 located 1.5 m behind the nozzle (3 m from the ventilation pipe exit). From the plots, in Figure 4-7 the ‘progress’ of the hydrogen cloud can be observed by looking at the time when the hydrogen concentration starts to increase. The hydrogen dispersion can be clearly observed between the sensors. Starts close to the hydrogen release source (blue line) and propagates towards container doors/exit (red line). While comparing the hydrogen concentration and its dispersion among the container, the hydrogen releases with ACH 6 show faster dispersion than those with ACH 10. Nevertheless, the hydrogen cloud with ACH 10 shows a tendency to decrease its concentration faster than with ACH 6 with the same mass flow rates (reservoir pressures). The difference reaches 2 min for some experiments. This effect needs further investigation and will be presented in near future.

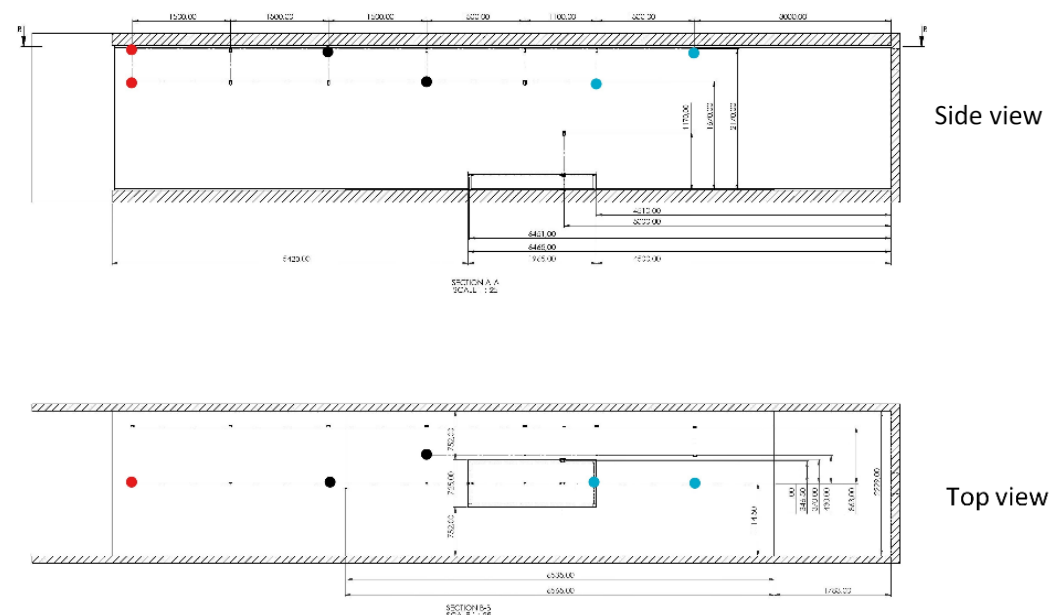
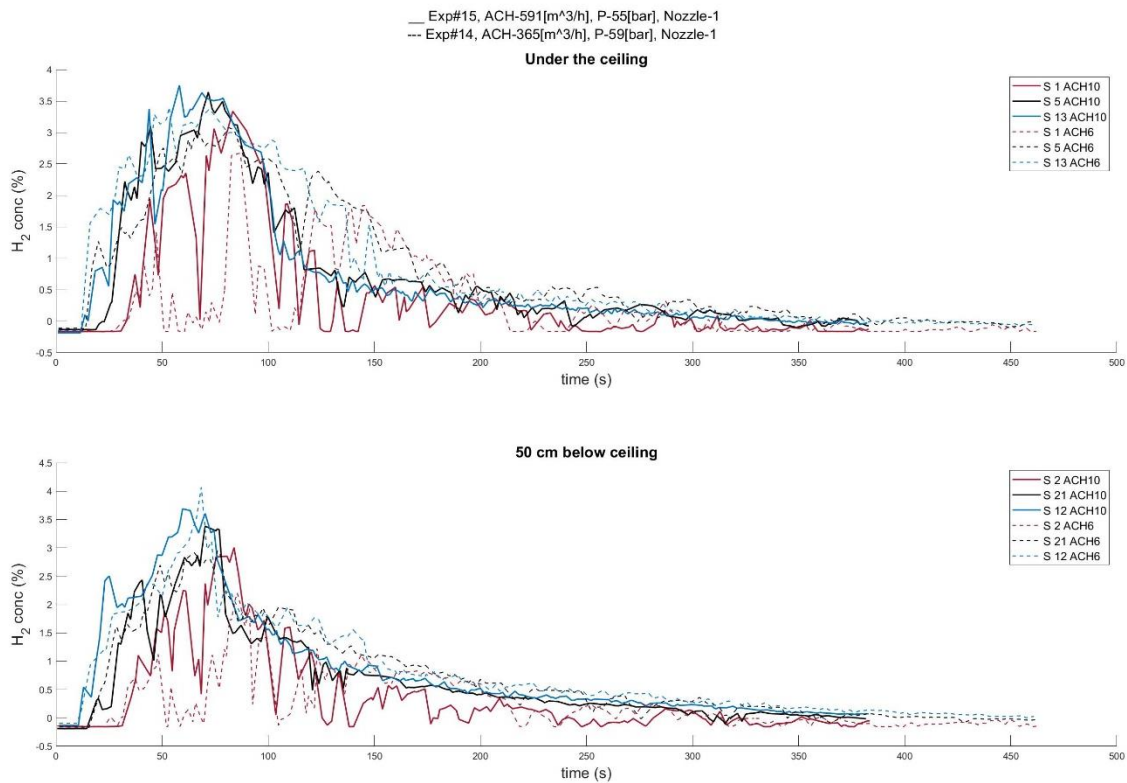


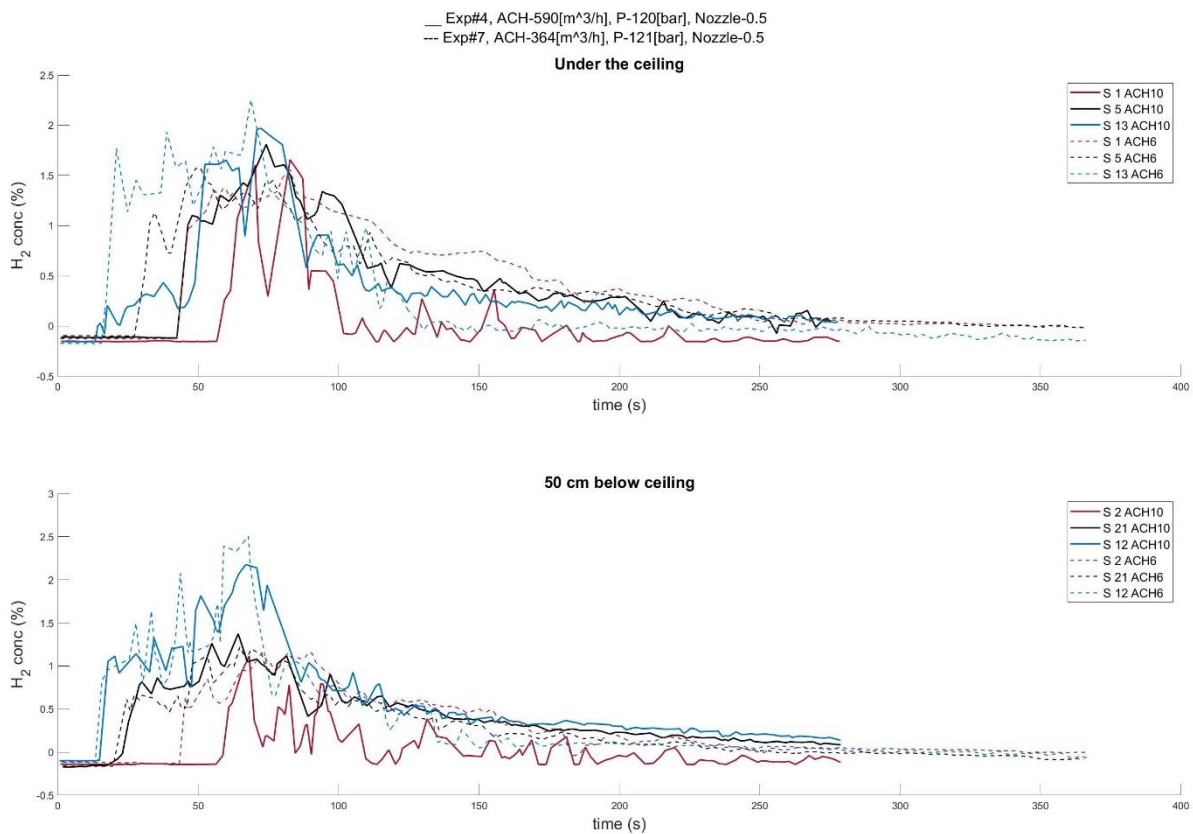
Figure 4-6. Location of the hydrogen sensors chosen for plot in Figure 4-7 and Figure 4-9.

## D2.3. Final report on analytical, numerical and experimental studies on hydrogen dispersion in tunnels, including innovative prevention and mitigation strategies

### Exp 15 and 14

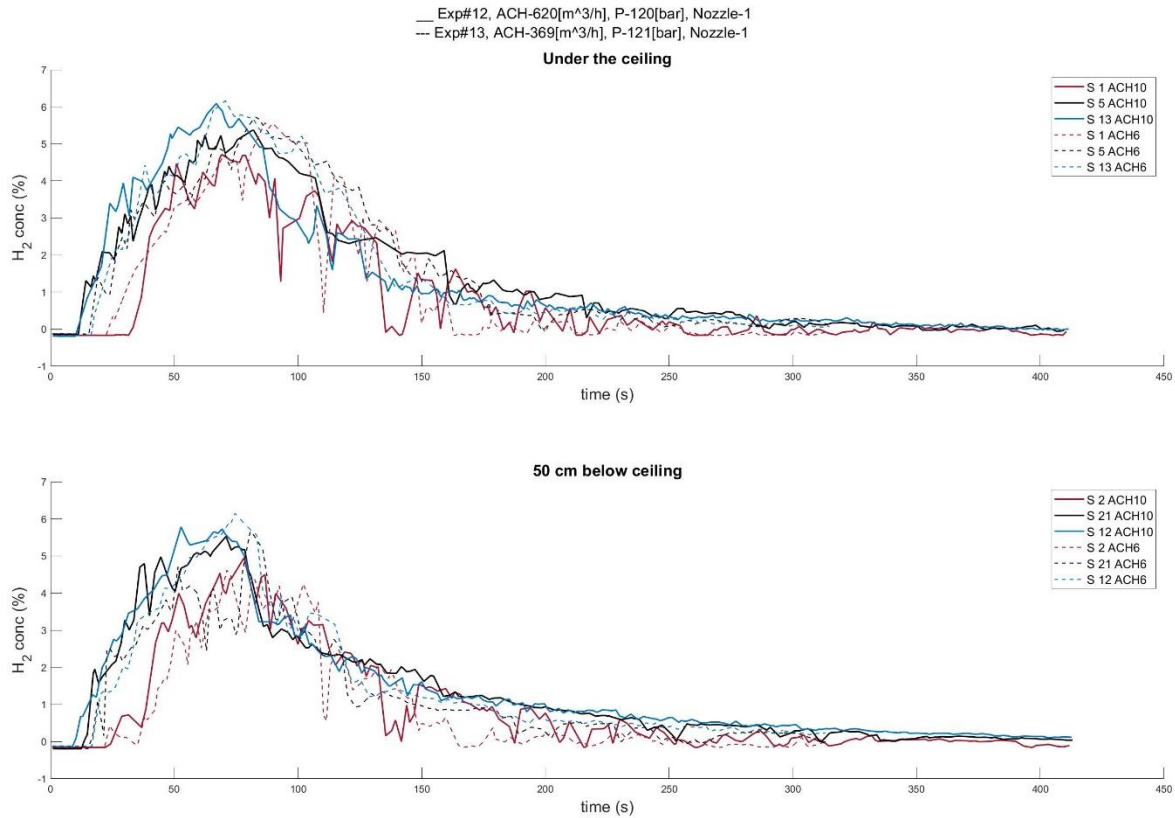


### Exp 4 and 7

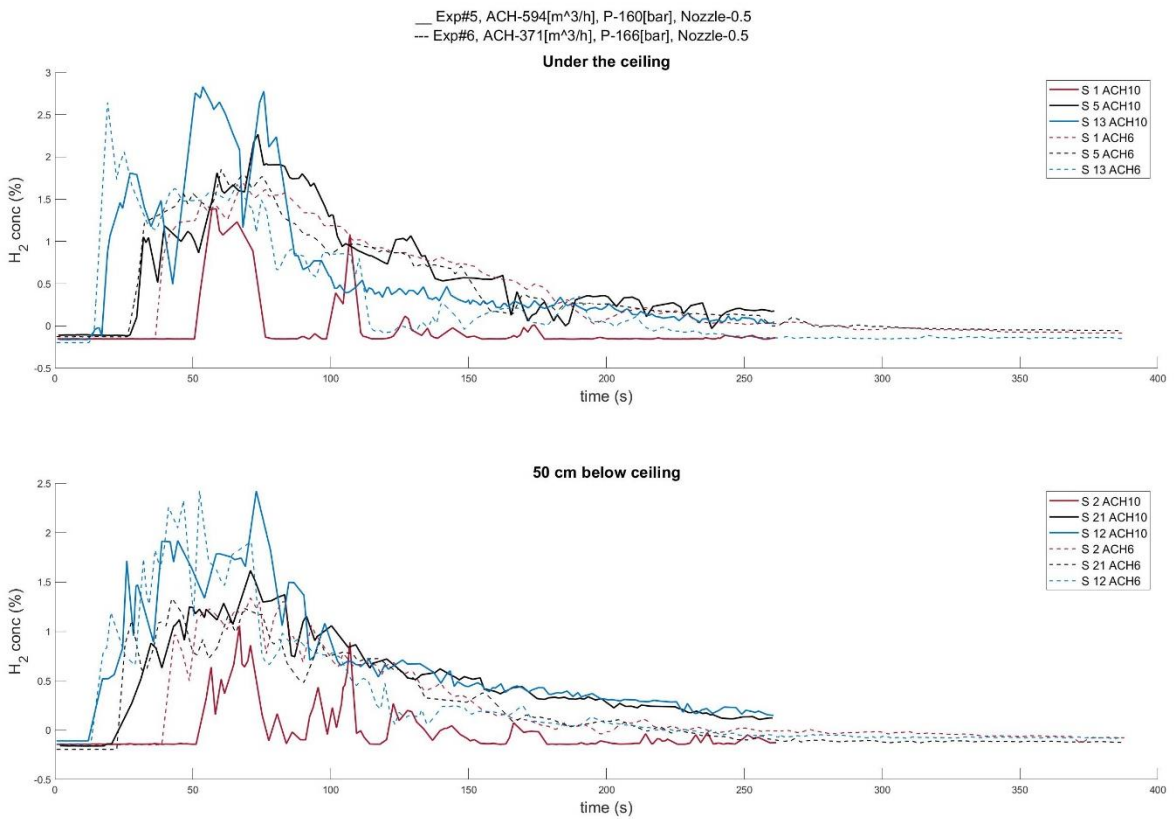


## D2.3. Final report on analytical, numerical and experimental studies on hydrogen dispersion in tunnels, including innovative prevention and mitigation strategies

### Exp 12 and 13



### Exp 5 and 6



## D2.3. Final report on analytical, numerical and experimental studies on hydrogen dispersion in tunnels, including innovative prevention and mitigation strategies

### Exp 10 and 9

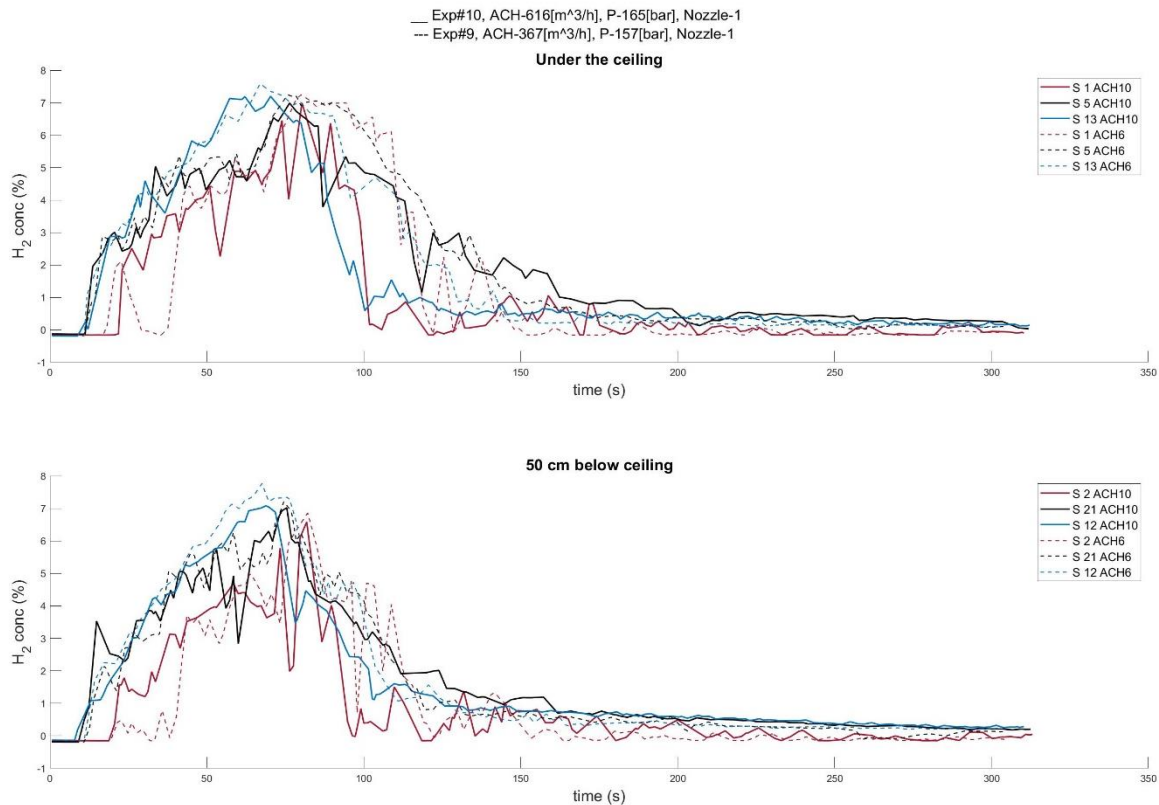


Figure 4-7. Constant mass flow releases with ACH BS10 and BS6, through 1 mm and 0.5 mm nozzle. Initial release pressures: 60 bar, 120 bar, and 160 bar.

Due to the big amount of data the results presented in Figure 4-7 and Figure 4-9 are smooth data. The method of finding local maxima (findpeaks, Matlab) was used. The resulted hydrogen concentrations are plots with data samples that were larger than the two adjoining samples. The example is presented in Figure 4-8.

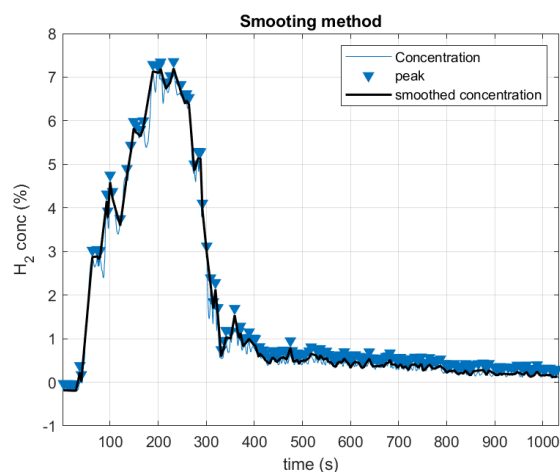
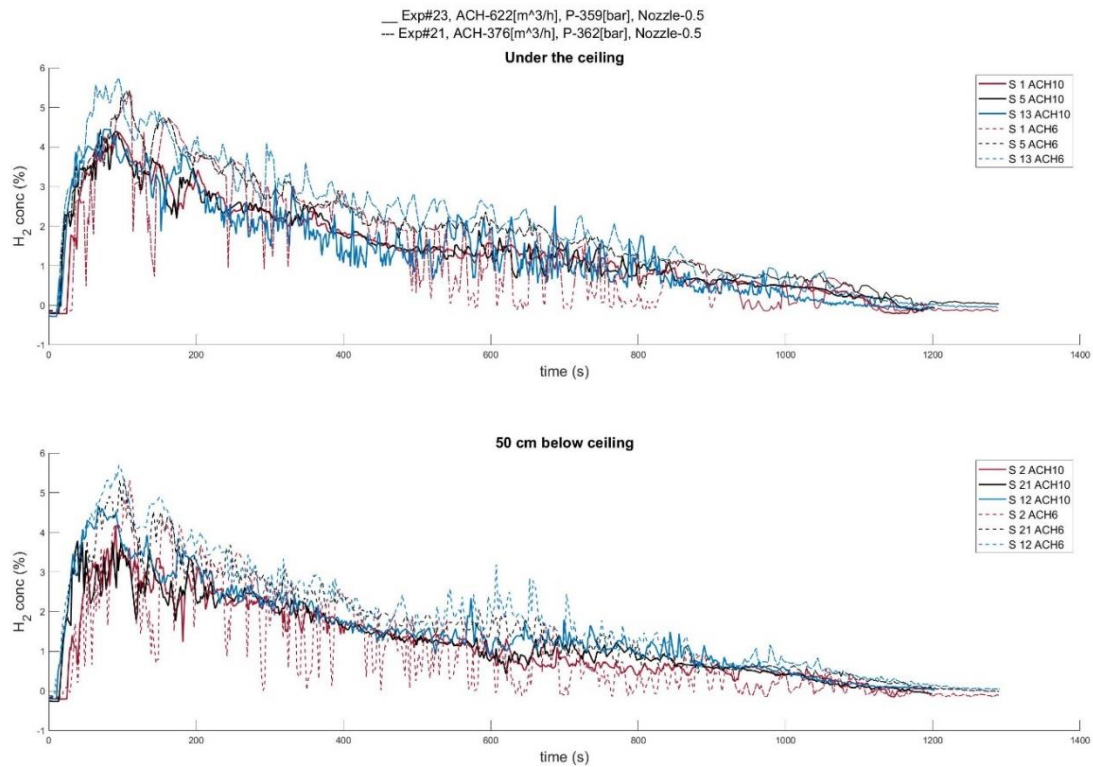


Figure 4-8. Smoothing method applied for the hydrogen concentration plot in Figure 4-7 and Figure 4-9.

## D2.3. Final report on analytical, numerical and experimental studies on hydrogen dispersion in tunnels, including innovative prevention and mitigation strategies

### Exp 21 and Exp 23



### Exp 19 and Exp 20

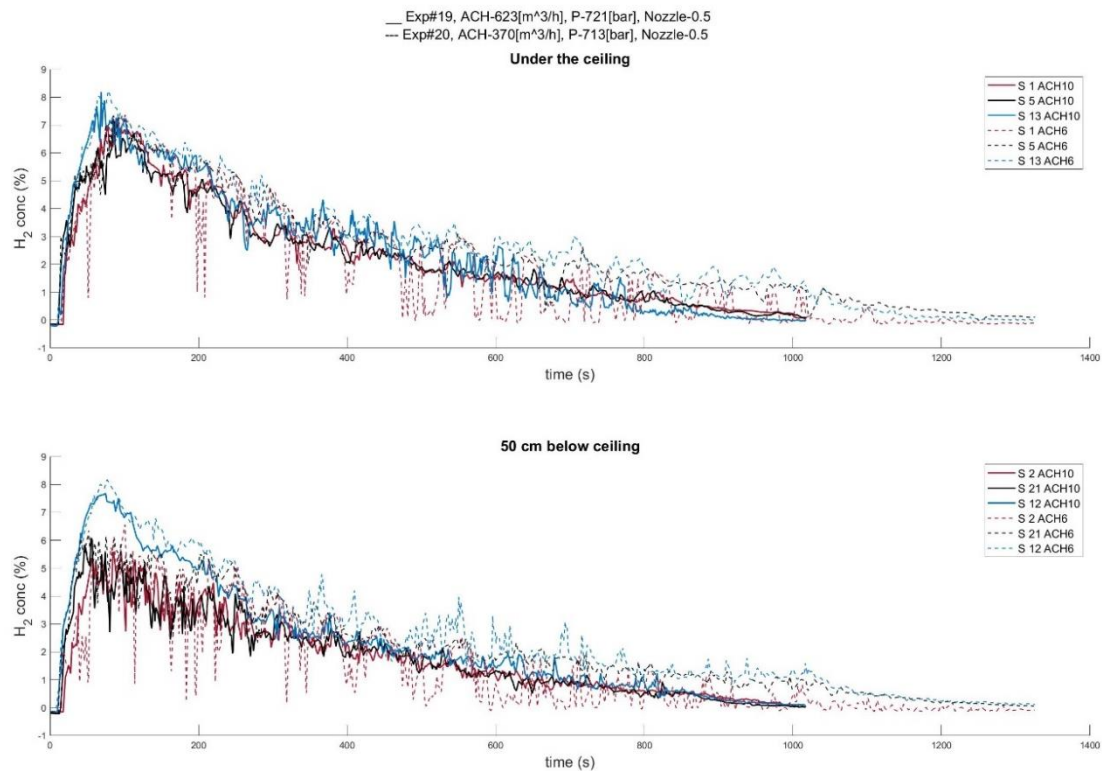


Figure 4-9. Constant mass flow releases with ACH BS10 (blue marker and solid line) and BS6 (red marker and dash line), through 0.5 mm nozzle. Initial release pressures: 200 bar, 350 bar and 700 bar.



### D2.3. Final report on analytical, numerical and experimental studies on hydrogen dispersion in tunnels, including innovative prevention and mitigation strategies

The hydrogen leak was not dispersed under the ceiling immediately after the releases during constant releases, where the highest mass flow rates were from the reservoir pressure 160 bar and 1 mm nozzle (6 g/s). During the first seconds, the hydrogen was accumulating under the table (Figure 4-10). The momentum jet during constant mass flow releases was not strong enough to create separate plums escaping from under the table. The buoyancy, the main driving force under the table, shows the effects of the rising concentration around the table after few seconds from the release, depending on the reservoir pressure and the nozzle diameter. The concentration under the table during releases with 1 mm results in higher mass flow rates than through 0.5 mm from the same reservoir pressure. As the consequence, the hydrogen escapes from under the table resulting in rising concentration under the table (Figure 4-11). While the hydrogen releases through 0.5 mm nozzle result in semi constant (steady-state) concentration under the table. The main factor on the concentration under the table is the mass flow rate, hence nozzle diameter, and reservoir pressure.

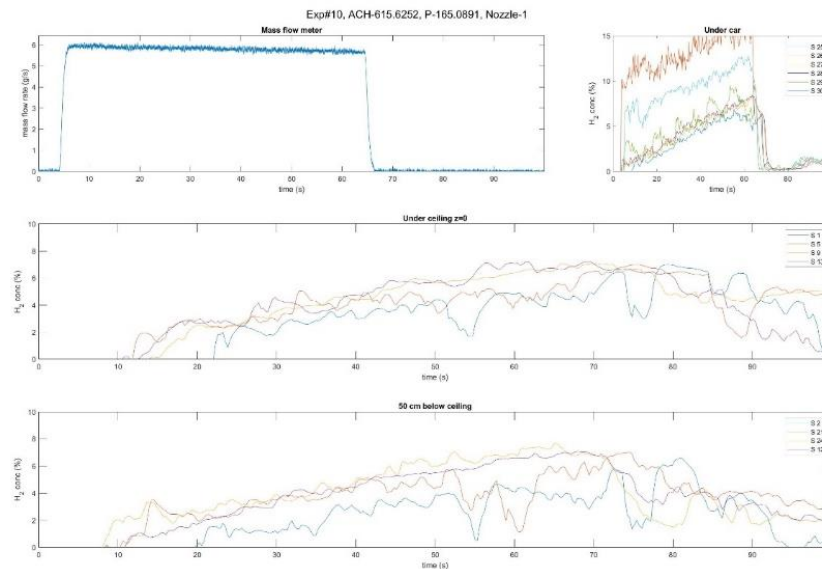


Figure 4-10. Hydrogen release through 1 mm nozzle from 160 bar reservoir pressure. Mass flow rate, hydrogen concentration from hydrogen (S) mounted under the car, under the ceiling and 50 cm under the ceiling.



## D2.3. Final report on analytical, numerical and experimental studies on hydrogen dispersion in tunnels, including innovative prevention and mitigation strategies

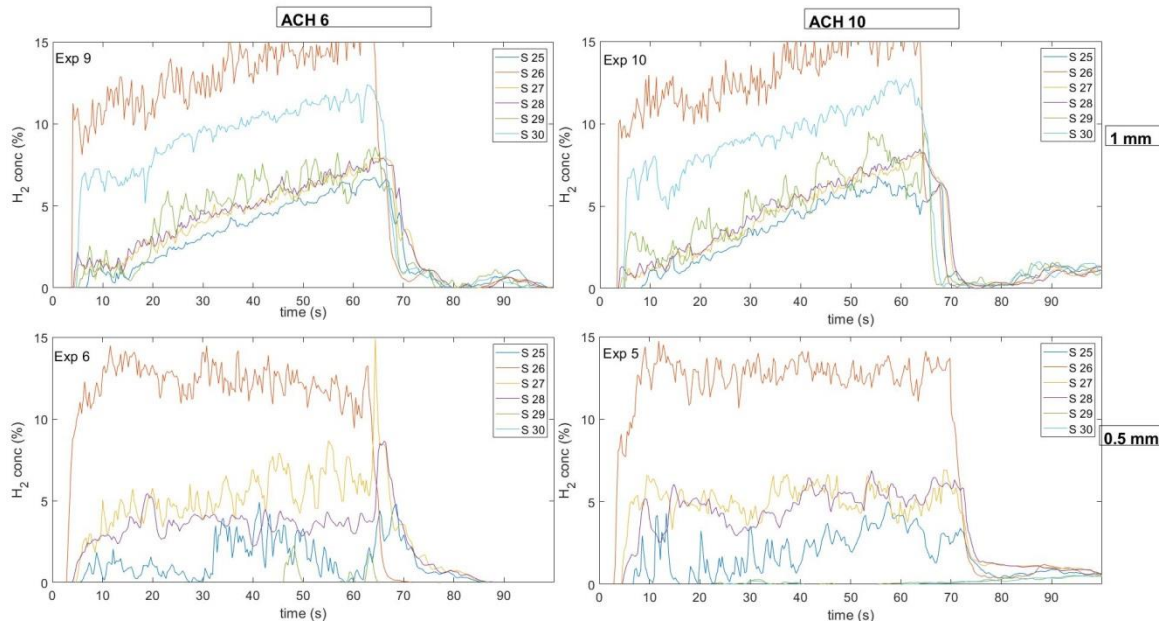


Figure 4-11. Hydrogen concentration under the table during releases through 1 mm and 0.5 nozzles from reservoir 160 bar.

The ventilation system mounted close to the ceiling does not show the influence on the hydrogen dispersion under the table.

### 4.1.4.2 Releases with blowdown mass flow rates

After conducting experiments with constant mass flow rate releases, the experimental setup was modified and adjusted to blowdown type mass flow rate releases. The results from the releases through 0.5 mm nozzle with ACH BS 10 and ACH BS 6 are presented in Table 4-3. Due to unnoticed problems during the experiments, the results from experiment 18 from 200 bar with ACH 10 are not included in Figure 4-12 (the mass flow rate results suggest the conclusions of the ice blockage during the experiment, look at [(Lach and Gaathaug, 2020), Appendix 1]). In Figure 4-12 the influence of the ACH on the hydrogen concentration is presented. The same method as for the constant mass flow releases was used and the same sensor was chosen to show hydrogen dispersion in the container. The mechanical ventilation with ACH 6 resulted in higher hydrogen concentration than with ACH 10. For releases from 350 bar ventilation system with ACH 10 was able to ‘keep’ concentration in hydrogen cloud under 4 % (Figure 4-12). Nevertheless, the values in Figure 4-12 are the mean values. In Figure 4-13 the concentration from the sensors mounted under the ceiling and 50 cm under the ceiling are shown. The plot in the first row (hydrogen concentration from 350 bar) shows that concentration was slightly over 4% for sensor number 12 which was located above the table (50 cm under the ceiling).

### D2.3. Final report on analytical, numerical and experimental studies on hydrogen dispersion in tunnels, including innovative prevention and mitigation strategies

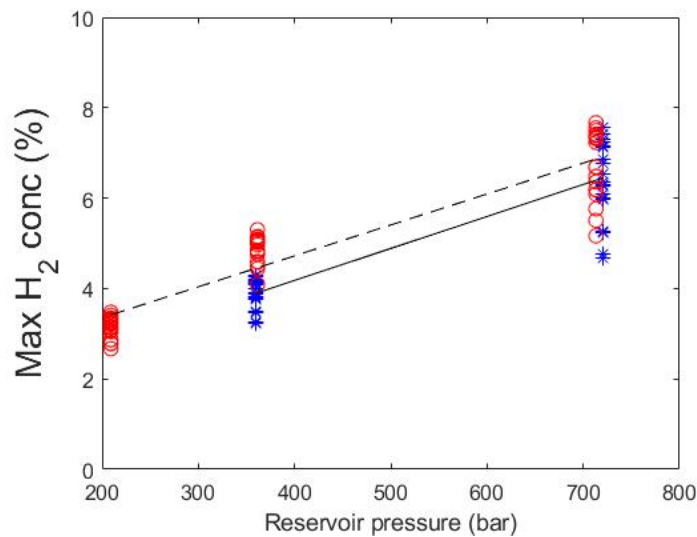


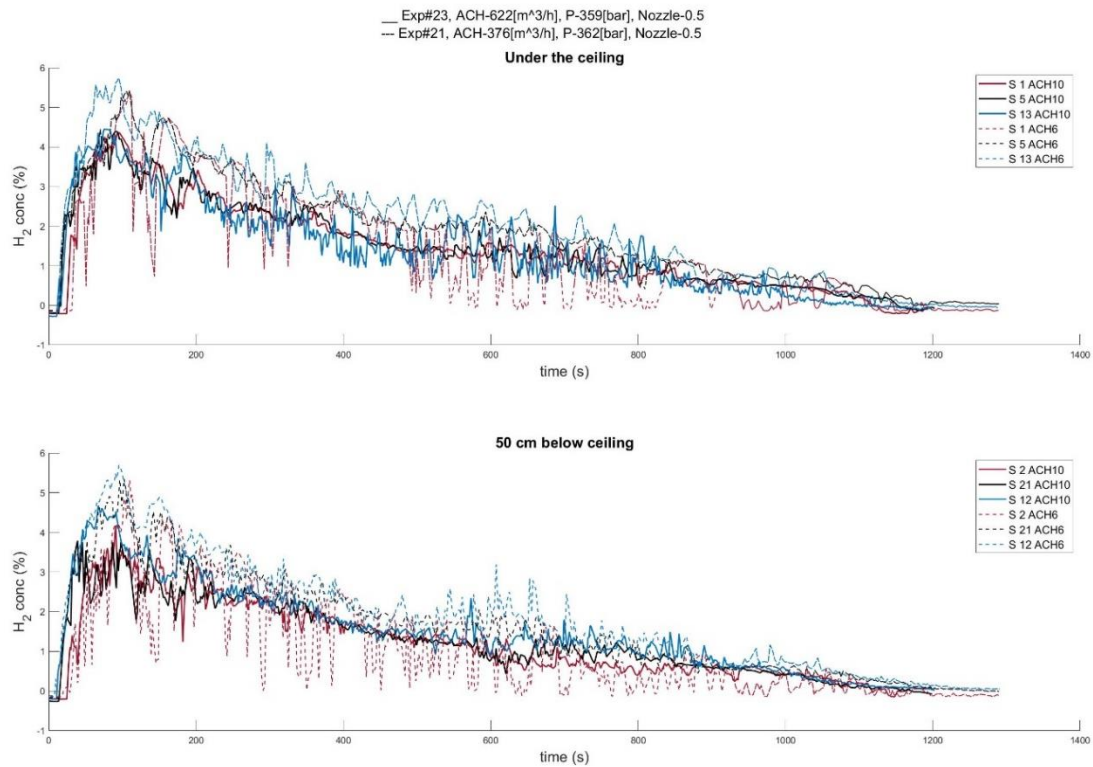
Figure 4-12. Hydrogen concentration during hydrogen releases through 0.5 mm nozzle with ACH 6 (dash line) and ACH 10 (solid line). Maximum concentration at each sensor during ACH 10 (blue star) and ACH 6 (red circle).

The hydrogen concentration results (Figure 4-13) were plotted with the smoothing method as was done for constant mass flow releases (in (Lach, Gaathaug, 2020) the results are presented without the smoothing method). The location of the sensor (concentration results) is identical to those used to present concentration results during constant mass flow releases.

The same 'behaviour' of hydrogen dispersion as for constant mass flow releases (where the low release pressures were applied) was observed. The concentration increase in the container was observed 4 s after the releases 0.92 m above the nozzle and 9 s under the ceiling for releases from 350 bar with ACH 10. Slightly faster hydrogen dispersion was observed for the experiment with ACH 6 where hydrogen concentration started to increase after 3 seconds (0.92 m above the nozzle) and 8 s under the ceiling. For the hydrogen releases from 700 bar reservoir with ACH 6 the increase of hydrogen concentration was observed after 2 s (0.92 m above the nozzle) and after 5 s under the ceiling. The observed hydrogen dispersion with ACH 6 was slightly faster than with ACH 10 (the same as it was for releases from 350 bar). The increase of hydrogen concentration with ACH 10 was observed after 5 s – under the ceiling, and after 3 s – 0.92 m above the nozzle.

### D2.3. Final report on analytical, numerical and experimental studies on hydrogen dispersion in tunnels, including innovative prevention and mitigation strategies

#### Exp 21 and Exp 23



#### Exp 19 and Exp 20

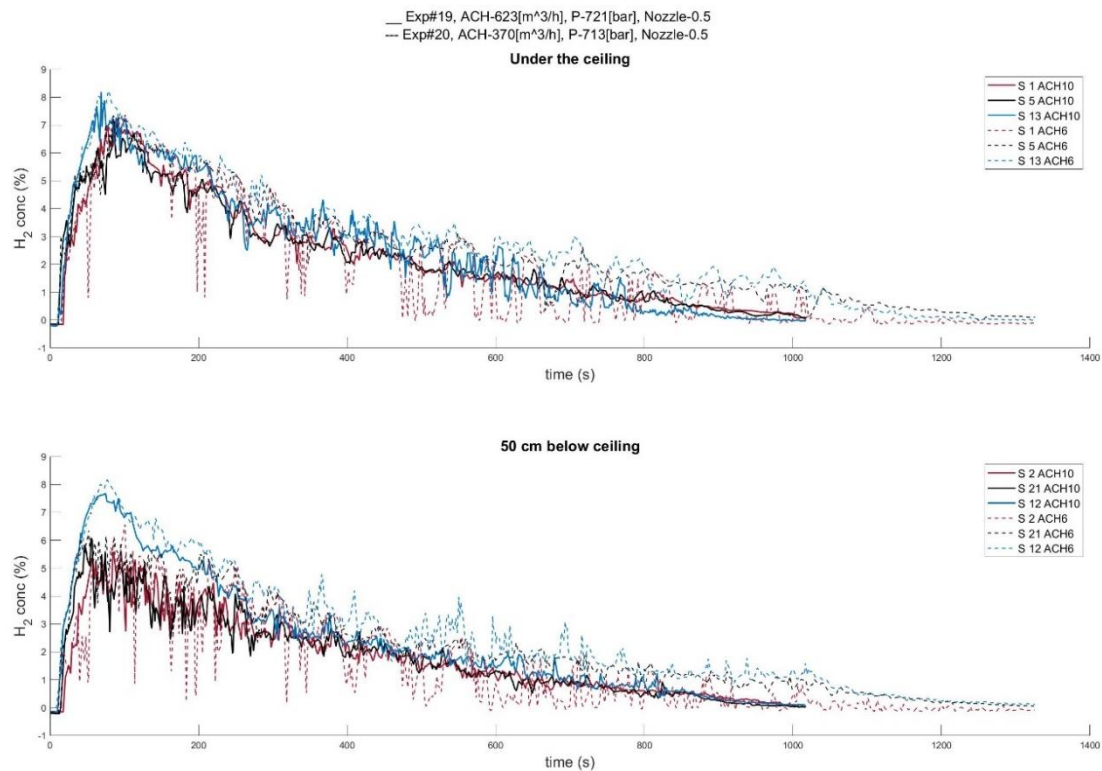


Figure 4-13. Constant mass flow releases with ACH BS10 (blue marker and solid line) and BS6 (red marker and dash line), through 0.5 mm nozzle. Initial release pressures: 200 bar, 350 bar and 700 bar.

### D2.3. Final report on analytical, numerical and experimental studies on hydrogen dispersion in tunnels, including innovative prevention and mitigation strategies

In Table 4-4 the influence of mechanical ventilation is presented by maximum concentrations (column 2 and column 6) and dispersion time, where the observed increase of hydrogen concentration at the container door was noted with time after the hydrogen release (column 3 and column 6). The time when hydrogen concentration reached (decreased) below 4 % is presented in column 4 and column 7. The results with mechanical ventilation with BS 10 showed faster decreases in concentration in the hydrogen cloud with 80 s for both 350 and 700 bar (under the ceiling). The results indicate that mechanical ventilation systems may reduce concentration under the flammable limit, or reduce the time of concentration in the cloud when hydrogen ignition is possible. Higher mass flow releases caused by higher reservoir pressure resulted in higher maximum concentration and as well as shorter dispersion time. Shorter dispersion can be observed by comparing the time after the hydrogen releases when the hydrogen concentration starts increasing at the container's door (exit). The explanation of dispersion differences can be turbulences caused by the airflow.

*Table 4-4. Maximum concentrations for hydrogen releases from 350 bar and 700 bar.*

	6 ACH			10 ACH		
	Max conc [%]	% time at the door [s]	Time when % < 4% [s]	Max conc [%]	% time at the door[s]	Time when % < 4% [s]
<b>350 bar</b>						
Under the ceiling	5.7	29	<b>185</b>	4.6	25	<b>105</b>
50 cm below the ceiling	5.8	16	<b>180</b>	5.2	25	<b>90</b>
<b>700 bar</b>						
Under the ceiling	8.2	16	<b>385</b>	7.9	18	<b>305</b>
50 cm below the ceiling	8.1	15	<b>370</b>	7.8	19	<b>270</b>

During the releases, the main hydrogen plums were on the long sides of the table at the top of the table Figure 4-14, S 26). At the first 3-4 min of the release, the strong hydrogen plume was observed at the front of the table and with decreasing mass flow the hydrogen was eluding on the sites of the table. It can be observed in Figure 4-14 looking at the orange curve (S 26), which is increasing after the green (S 29) and light blue (S 30) curves decreased. The accumulation of the hydrogen under the table was observed at the end purple curve (S 28) and the yellow curve (S 27) increased.

## D2.3. Final report on analytical, numerical and experimental studies on hydrogen dispersion in tunnels, including innovative prevention and mitigation strategies

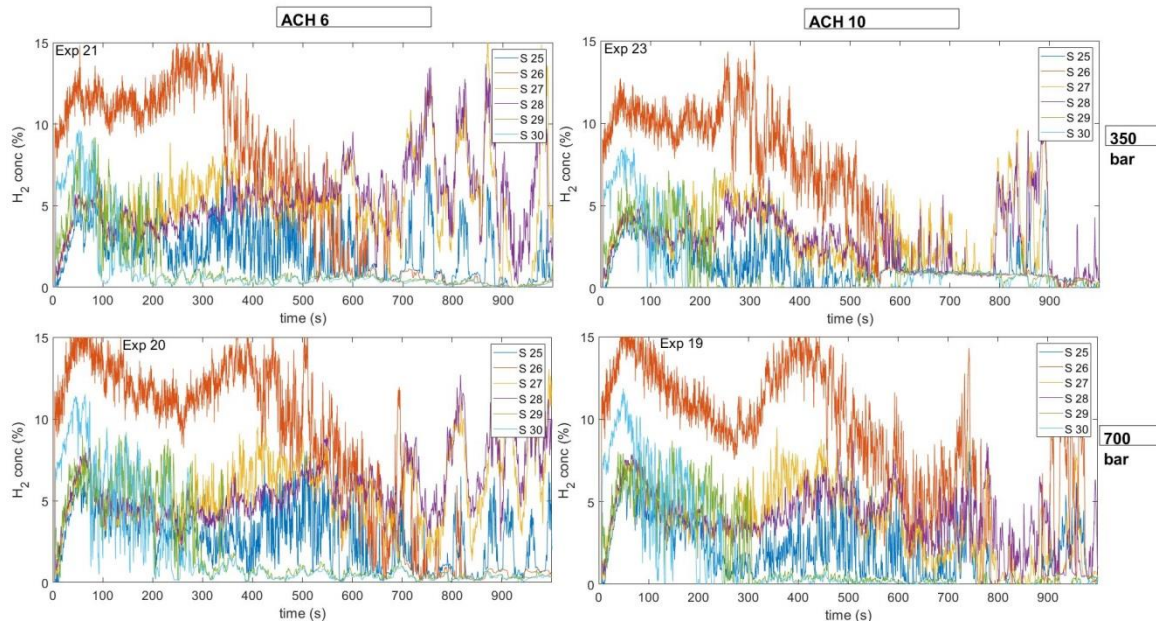


Figure 4-14. Hydrogen concentration under the table during blowdown releases from the reservoir with 350 bar and 700 bar.

### 4.1.5 Conclusions

Performed experiments showed the influence of mechanical ventilation on hydrogen dispersion in the container. Two standards used today were investigated against hydrogen releases. The hydrogen concentration in the cloud accumulated under the ceiling was lower for ACH 10 than for ACH 6. The higher ventilation restrains high concentration (<4%) in the accumulated cloud for releases from 350 bar. Nevertheless, ACH 10 was not sufficient to decrease hydrogen concentration under the flammability limit for releases from 700 bar. The dispersion of hydrogen in the container was investigated. The results showed with higher ventilation the concentration 50 cm under the ceiling has a constant decreasing trend, while for the lower ventilation rate the concentration in the cloud is more unstable. The carried experiments can be used for model validation for the mechanical ventilation system to develop engineering tool for safety engineers.

The experimental data is open and available at: <https://doi.org/10.23642/usn.14405903>

## 4.2 Unignited Pressure Peaking Phenomenon (Sub-task 2.4.2/USN)

### 4.2.1 Introduction and Objectives

The rapid hydrogen discharge from the tank in confined spaces leads to high overpressure, that may cause personal and property damages. The phenomenon (pressure peaking phenomenon (PPP)) is characterized as transient overpressure with a characteristic peak in vented enclosure. PPP occurs while introducing gas with a lower density than the gas inside the enclosure. The phenomenon is distinct for hydrogen and occurs when released hydrogen mass flow rate is relatively high and the vent area is relatively small (Makarov et al. 2018). With these conditions the mole fraction at the vent area will consist of hydrogen and air from the enclosure. At the nozzle the mole fraction will consist only of hydrogen. The overpressure in the enclosure will grow until the mole fraction at both openings will be equal to 1. Then pressure peak will be reached and the air mole fraction at the vent area starts to decrease and so does the overpressure.



### D2.3. Final report on analytical, numerical and experimental studies on hydrogen dispersion in tunnels, including innovative prevention and mitigation strategies

Previous work of numerical validation (Hussein et al. 2018) showed and confirmed that the two major parameters to determine the overpressure in an enclosure are the vent size and hydrogen mass flow rate into enclosure. These parameters have the most significant role on producing high overpressures. Brennan and Molkov (2018) have investigated ‘safety’ PRD (Pressure Relief Device) parameters with the correlation of natural ventilation variables in enclosure for blowdown scenario. Their work provides a model description used during the experiments described in this report. The study showed that with decreasing the PRD diameter, the overpressure will drop accordingly. Their study presented a correlation between hydrogen concentration and the vent area. With increasing the vent area, the maximum overpressure will be lower but the hydrogen concentration will increase more rapidly. This will lead to higher hydrogen concentration at the maximum overpressure, with the assumption of no air ingress into enclosure. High level of hydrogen concentration creates hazards of asphyxiation and ignition. The hydrogen tanks designed for cars, currently in use, are type 4 (Stephenson R. 2005) and will not stand the longer exposure to high temperatures which will happen with decreasing the PRD diameter. This issue has to be solved in order to avoid pressure threshold from too rapidly hydrogen releases in confined spaces. The PPP validation study was made for the first time (Makarov et al. 2018) with A comparison of air, helium and hydrogen. The 40 experiments were performed in order to confirm that PPP is appearing only for the gases lighter than air. In the study the model for ignited releases from TPRD (Thermal activated Pressure Relief Devices) has been developed and revealed the risk of much higher overpressure.

The work presented in this report is demonstrating pressure peaking phenomenon in large scale scenario. The quality of experiments was ensured by joint decision-making together with HyTunnel-CS project members. The results will be a base for further ignited PPP experiments.

#### 4.2.2 Detailed specification

In this chapter the details of set up, calculation and model description are presented.

##### 4.2.2.1 Set up description

All the experiments were performed at the military area in Horten. The explosion chamber located there was lent by Forsvarets forskningsinstitutt for experiments. The P&ID of set up and instrumentation is shown in Figure 4-15.



### D2.3. Final report on analytical, numerical and experimental studies on hydrogen dispersion in tunnels, including innovative prevention and mitigation strategies

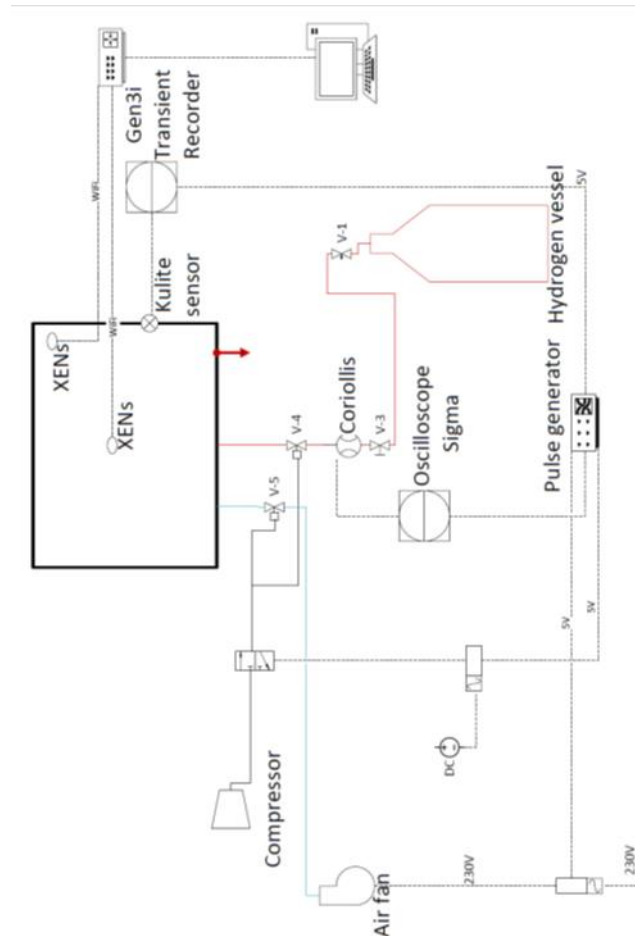


Figure 4-15. Piping and Instrumentation Diagram (P&ID).

#### 4.2.2.2 Explosion chamber-geometries

The hydrogen experiments were performed in an explosion chamber shown in Figure 4-16, placed approximately 15m from the controlling set up. The explosion chamber has the inner dimensions: 2000x2980x2500 mm, which gives a total volume of 14.9 m<sup>3</sup>. The explosion chamber has two plates installed with 50 screws each around the plate. The back plate has assembled a door. The explosion chamber's walls in total have five vents of 80 mm diameter each. Four of them are located in the down corners (two vents at the wall), whereas the 5<sup>th</sup> is located in the middle of the front wall coming out inside of the chamber floor.



Figure 4-16. Explosion chamber used in PPP experiment.

### D2.3. Final report on analytical, numerical and experimental studies on hydrogen dispersion in tunnels, including innovative prevention and mitigation strategies

The vent in the middle of the front wall was used for the fuel supply (and the ignition supply for the following tests on ignited releases). The other four vents give total vent area equal to  $A_v=0.0201\text{m}^2$  which is too large to be able to investigate the PPP. Even for only one vent open with  $A_v=0.005024\text{m}^2$  the ventilation area provides a too large outlet and pressure peak cannot be obtained based pre-calculation through the available engineering tool for PPP from unignited hydrogen releases. The detailed description of the explosion chamber is presented in the experimental report (Lach et al., 2020). Two of the four vents were closed with flanges (central image, Figure 4-16). The other two were used for air input and for ventilation.

The explosion chamber's vents are located at the bottom (15 cm above the floor). In order to place passive ventilation at the top of the chamber a PVC pipe of diameter 75 mm was installed (Figure 4-17, left). The vent area was adjusted to the desired ventilation diameter by placing a cover at the end of the pipe, outside the explosion chamber (Figure 4-17, right).



*Figure 4-17. Ventilation pipe. Inside (left) and outside (right).*



*Figure 4-18. Steel pipe inside the chamber- air supply.*

#### 4.2.2.3 Fuel supply

The fuel supply consisted of 2 bottles (2x50 litre) of nitrogen and set up of 12 bottles (12x50 litre) of hydrogen as shown in Figure 4-19.

### D2.3. Final report on analytical, numerical and experimental studies on hydrogen dispersion in tunnels, including innovative prevention and mitigation strategies



Figure 4-19. Set up of 12 bottles of hydrogen and 2 bottles of nitrogen.

The fuel mass flow rate was measured by a Coriolis mass flow meter with maximum pressure of 110 bar. A 6x1 mm steel pipe was used for all tubing, and a valve was installed between the Coriolis mass flow meter and the explosion chamber.

The nozzle was mounted at the 6mm pipe outlet at the designed construction, with place for ignition source for the next stage of the experiments. The nozzle was installed on the floor in the center of the explosion chamber, as shown in Figure 4-20.



Figure 4-20. Nozzle details and location, 4mm.

#### 4.2.2.4 Air supply

The doors of the explosion chamber were leak secured before starting the experiments. Due to 25-65 vol. % of hydrogen concentration inside the chamber (depending on the test) after performing an experiment, the explosion chamber was ventilated/flushed with air. In order to prepare the explosion chamber for the following experiments without opening the doors, mechanical ventilation was implemented, see Figure 4-18. To avoid a rise of the inlet air temperature by the fan, a cold water cooling system was installed.

## D2.3. Final report on analytical, numerical and experimental studies on hydrogen dispersion in tunnels, including innovative prevention and mitigation strategies

### 4.2.2.5 Instrumentation

To measure overpressure inside the explosion chamber the Kulite pressure transducer XTM - 190-50A was used. The transducer was mounted into the 18M screw and installed in the middle of the back plate (Figure 4-21). Detailed specification of the Kulite transducer can be found in the experimental report (Lach et al. 2020). The complete overpressure development (with 25 ks/s) was recorded and stored by an oscilloscope.

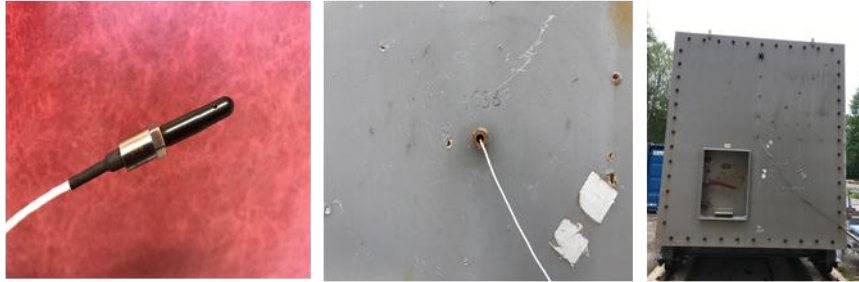


Figure 4-21. Kulite pressure transducer.

To measure hydrogen concentration inside the chamber, two XEN-3520 wireless sensors were used. Due to technical problems, an USB cable was used instead of wireless connection. Sensors were connected to the laptop computer to read the data.

One sensor was mounted at the center of the side wall between the air supply and ventilation area, over the fuel supply. The second sensor was mounted on the back plate at the middle-top as shown in Figure 4-22.



Figure 4-22. Hydrogen concentration sensor and its positioning.

The sensors were calibrated every morning before the experiment took place. Data restored from the sensor gave hydrogen concentration data measurements each 300ms.

### 4.2.3 Results

Experiments were performed during one week from the 17/06/2019 to the 21/06/2019.

#### 4.2.3.1 Experimental matrix

Table 4-5 presents the experimental matrix along with the obtained results.

## D2.3. Final report on analytical, numerical and experimental studies on hydrogen dispersion in tunnels, including innovative prevention and mitigation strategies

Table 4-5. Experimental matrix-hydrogen.

Exp nr	Nozzle diameter [m]	Enclosure volume [m <sup>3</sup> ]	Vent area [m <sup>2</sup> ]	Vent size [mm]	Mass flow rate [g/s]	Static pressure - reservoir [bar]	Experimental overpressure [kPa]	Exp time for pressure peak [s]	Duration time [s]
2	0,004	14,9	0,0012	9x $\varnothing$ 13	1,9	26,8	<b>0,42</b>	10	90
3	0,004	14,9	0,002	1x $\varnothing$ 51,6	3,5	40	<b>0,51</b>	10	120
4	0,004	14,9	0,002	1x $\varnothing$ 51,6	9,05	104	<b>2,86</b>	17	120
5	0,004	14,9	0,0014	1x $\varnothing$ 42	9,9	110	<b>6,45</b>	37	120
6	0,004	14,9	0,0014	1x $\varnothing$ 42	10,1	117,5	<b>6,74</b>	37	120
7	0,004	14,9	0,0006*	4x $\varnothing$ 13	3,05	36	<b>4,07</b>	80	180
8	0,004	14,9	0,0006*	4x $\varnothing$ 13	3,05	39,7	<b>3,96</b>	77	180
9	0,004	14,9	0,0006*	4x $\varnothing$ 13	4,75	58,5	<b>8,05</b>	89	200
10	0,004	14,9	0,0006*	4x $\varnothing$ 13	4,2	52,6	<b>6,70</b>	89	200
11	0,004	14,9	0,0006*	4x $\varnothing$ 13	blowdown	49,6	<b>7,00</b>	64	1000

### 4.2.3.2 Mass flow

Experiments 2-10 were performed in a near to constant mass flow rate. The last experiment, Exp. 11, was performed with blowdown from maximum mass flow of 4.85 g/s. The measured mass flow data is available on the HyTunnel-CS website as CSV format.

### 4.2.3.3 Pressure data

The experimental overpressures obtained in the tests are presented above in Table 4-5. Every experimental test was performed successfully, allowing to observe the pressure peaking phenomenon. The maximum overpressure was observed for Exp 9:  $p=8.05\text{kPa}$  with  $\dot{m}_{in}=4.75\text{ g/s}$  and vent area  $A_v=0.0006\text{ m}^2$ . The first two experiments, Exp 2 and 3, were performed with small hydrogen mass flow rates together for relatively large vent area. Therefore, the obtained overpressures are the smallest among the experimental results. The measured overpressure dynamics are shown in Figure 4-23 to Figure 4-32.



### D2.3. Final report on analytical, numerical and experimental studies on hydrogen dispersion in tunnels, including innovative prevention and mitigation strategies

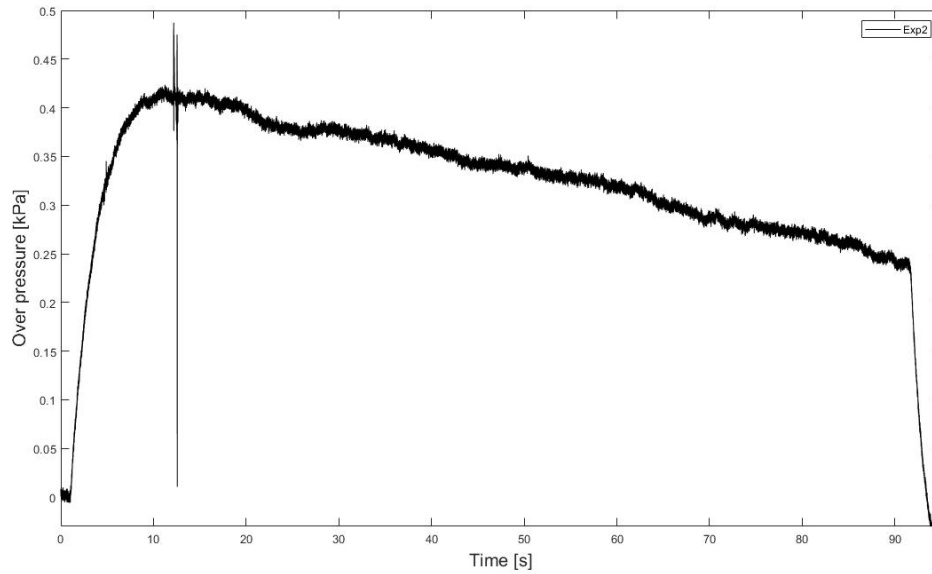


Figure 4-23. Experimental overpressure Exp 2.

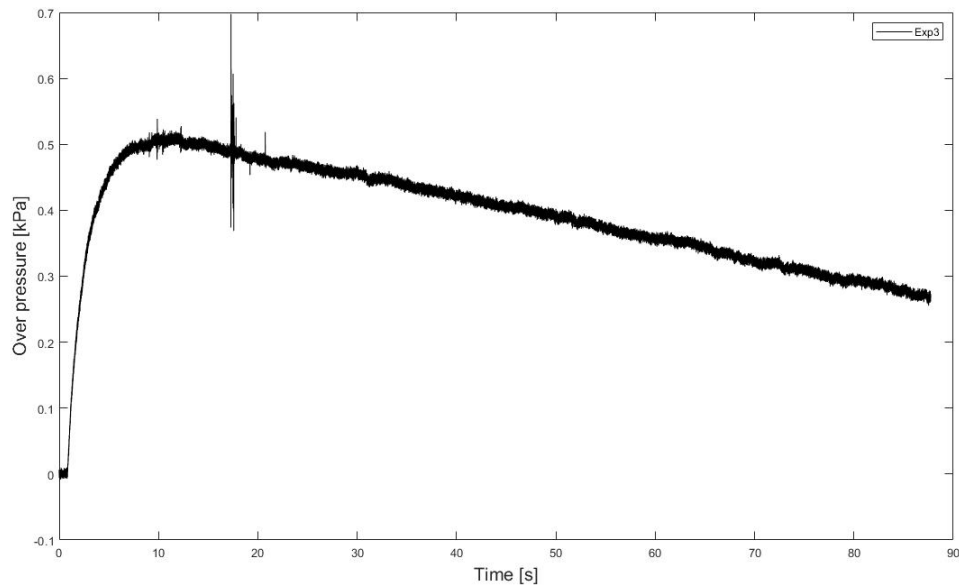


Figure 4-24. Experimental overpressure Exp 3.



### D2.3. Final report on analytical, numerical and experimental studies on hydrogen dispersion in tunnels, including innovative prevention and mitigation strategies

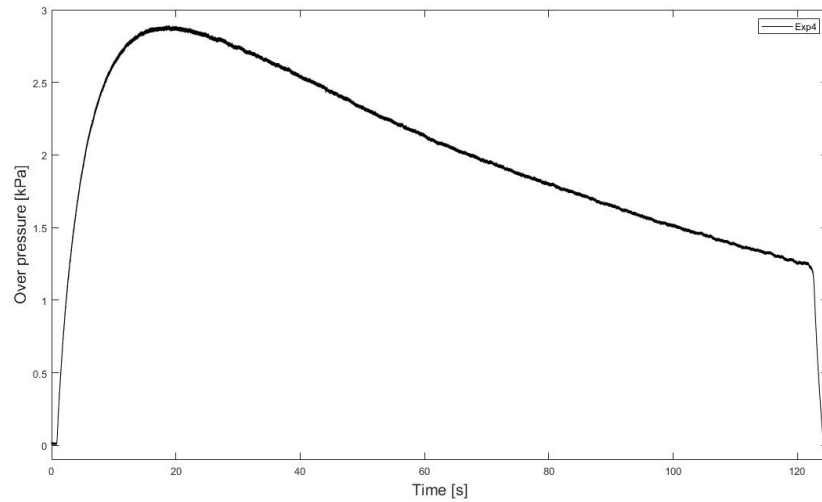


Figure 4-25. Experimental overpressure Exp 4.

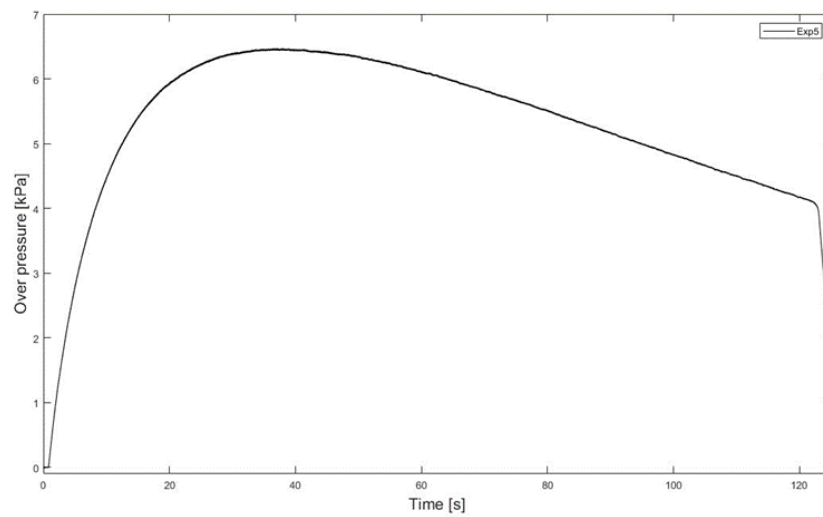


Figure 4-26. Experimental overpressure Exp 5.

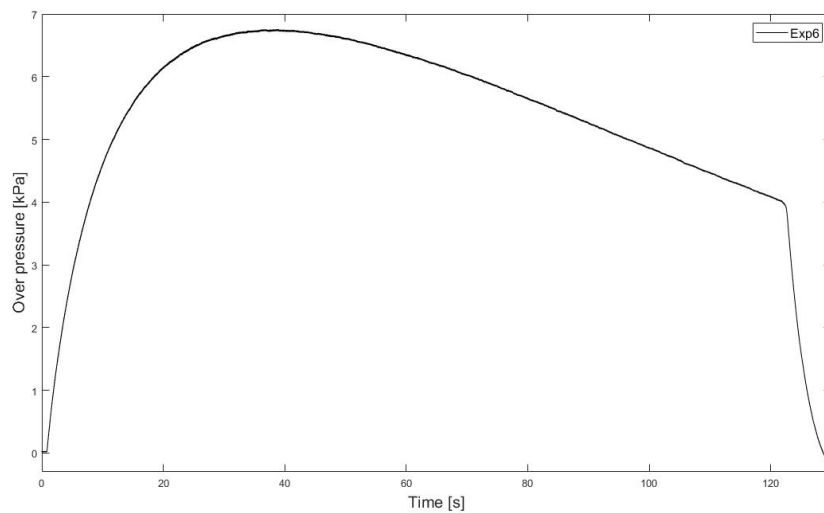


Figure 4-27. Experimental overpressure Exp 6.

## D2.3. Final report on analytical, numerical and experimental studies on hydrogen dispersion in tunnels, including innovative prevention and mitigation strategies

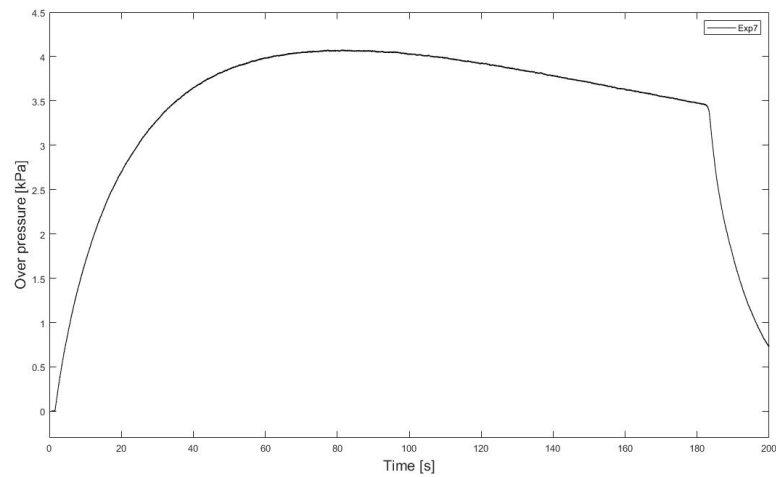


Figure 4-28. Experimental overpressure Exp 7.

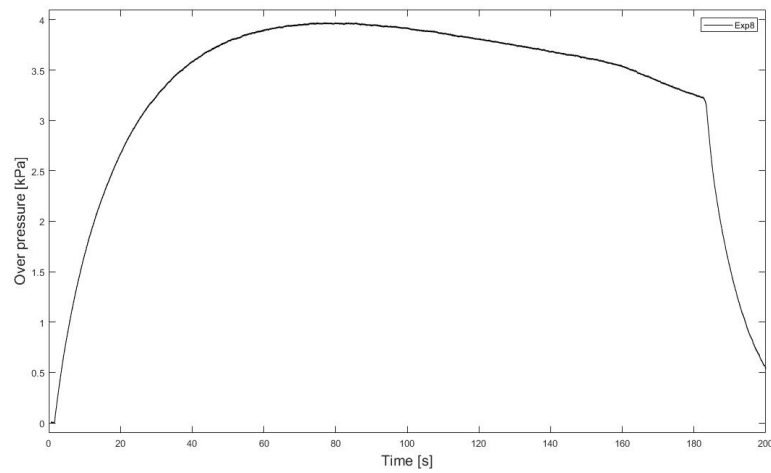


Figure 4-29. Experimental overpressure Exp 8.

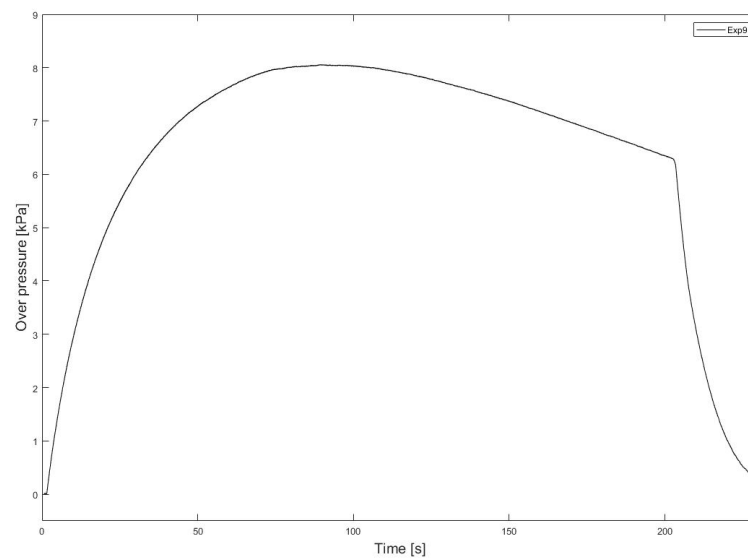


Figure 4-30. Experimental overpressure Exp 9.

### D2.3. Final report on analytical, numerical and experimental studies on hydrogen dispersion in tunnels, including innovative prevention and mitigation strategies

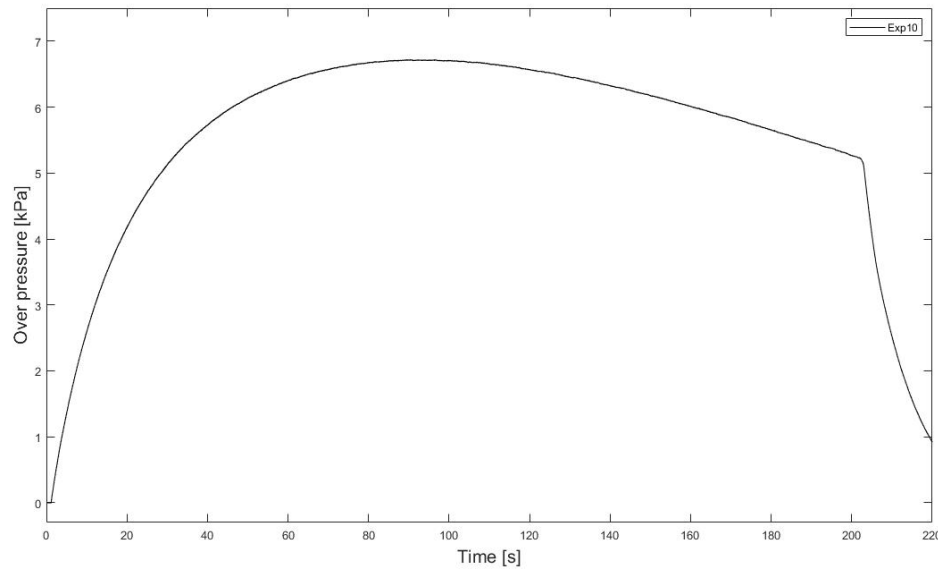


Figure 4-31. Experimental overpressure Exp 10.

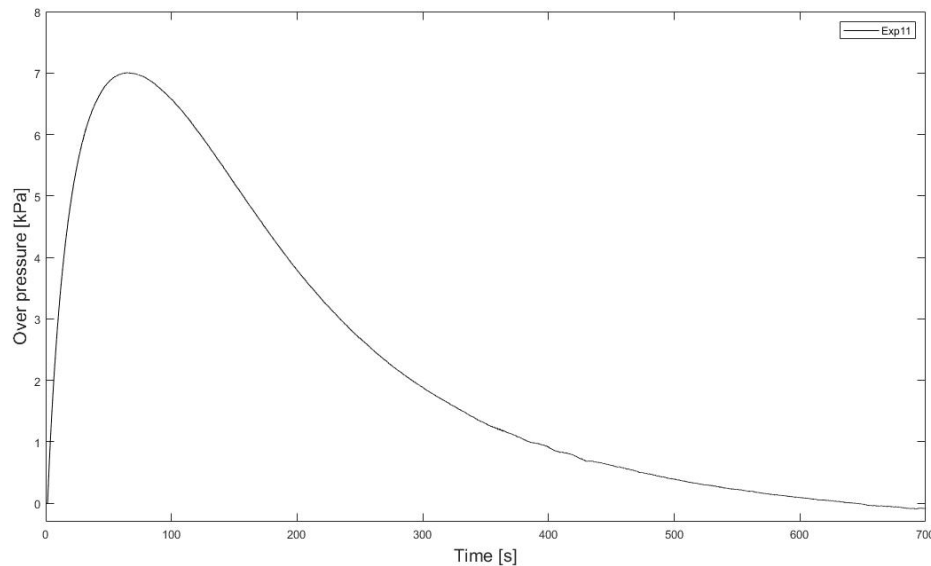


Figure 4-32. Experimental overpressure Exp 11.

#### 4.2.3.4 Hydrogen concentration

A hydrogen sensor was mounted in the center of the front wall for Exp 2-5 and a second sensor was added for Exp 6-11 placed at the top of the back plate. Due to the use of steel plates for mounting sensors, the Wi-Fi connection has been disturbed during experiments. This is the reason for no data storing for Exp 4 and Exp 5. Figure 4-33 to Figure 4-40 present hydrogen concentration for all experiments except Exp 4 and Exp 5. The obtained results show that concentration grows after opening hydrogen release into enclosure. For Exp 9 and Exp 10 the data was restored from both sensors without Wi-Fi disruption. The concentration data for the Exp 9 from both sensors coincide. For Exp 10, data from sensor located at the top showed 0.5% of higher concentration compared to the sensor located in the middle of the front wall. During Exp 11 the PC with the installed software was shutdown. Nevertheless, the data obtained from sensors recorded 122 s of the experiment and was used for further simulations. Maximum

### D2.3. Final report on analytical, numerical and experimental studies on hydrogen dispersion in tunnels, including innovative prevention and mitigation strategies

concentration was obtained during Exp 6, with higher MFR (10.1 g/s) and relatively large vent area  $A_v=0.0014 \text{ m}^2$ . High concentration was obtained also for experiments with  $A_v=0.0006 \text{ m}^2$  with MFR 4.75 g/s and 4.2 g/s (Exp 9 and 10, respectively). For Exp 11, performed in case of blowdown, the concentration reached 34 vol. % at the end of stored data (after 122 s).

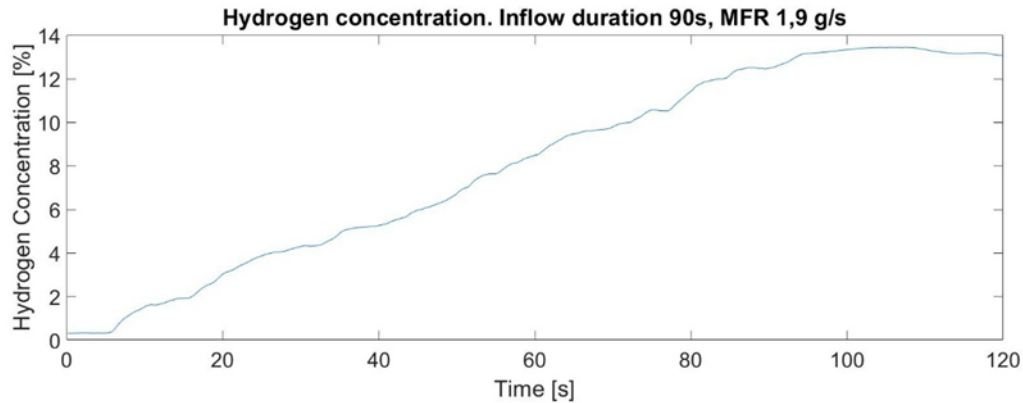


Figure 4-33. Hydrogen volume concentration from experiment 2.

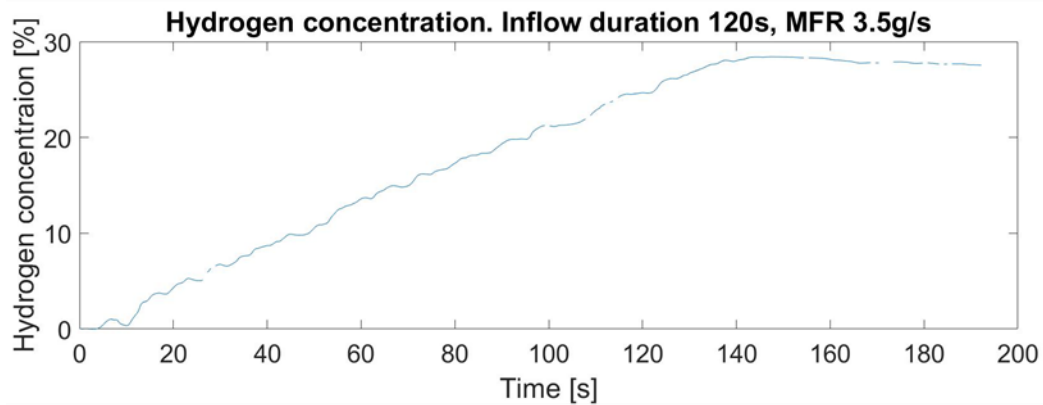


Figure 4-34. Hydrogen volume concentration from experiment 3.

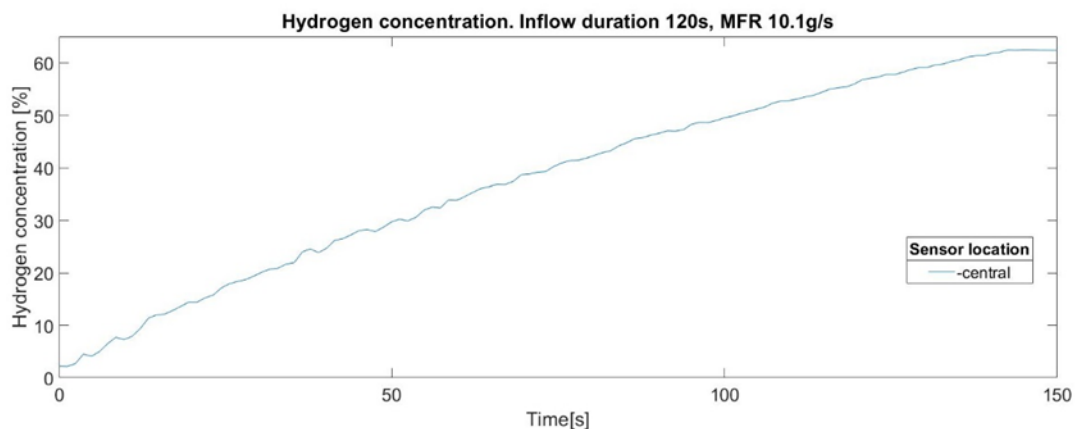


Figure 4-35. Hydrogen volume concentration from experiment 6.

### D2.3. Final report on analytical, numerical and experimental studies on hydrogen dispersion in tunnels, including innovative prevention and mitigation strategies

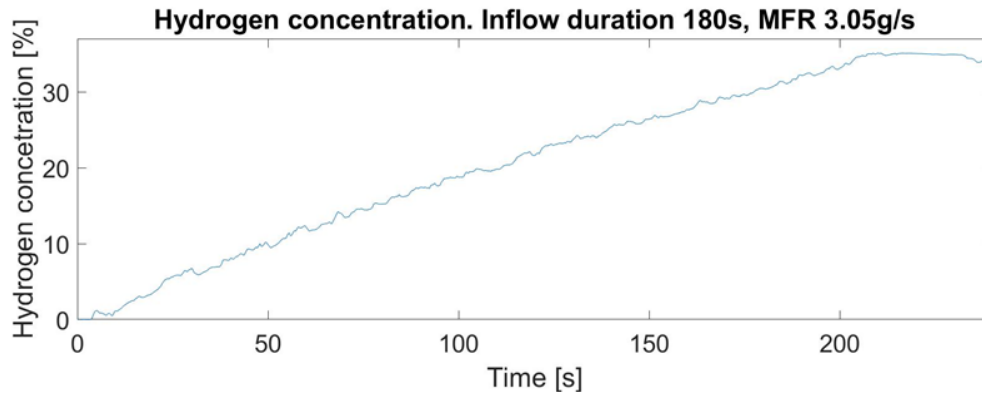


Figure 4-36. Hydrogen volume concentration from experiment 7.

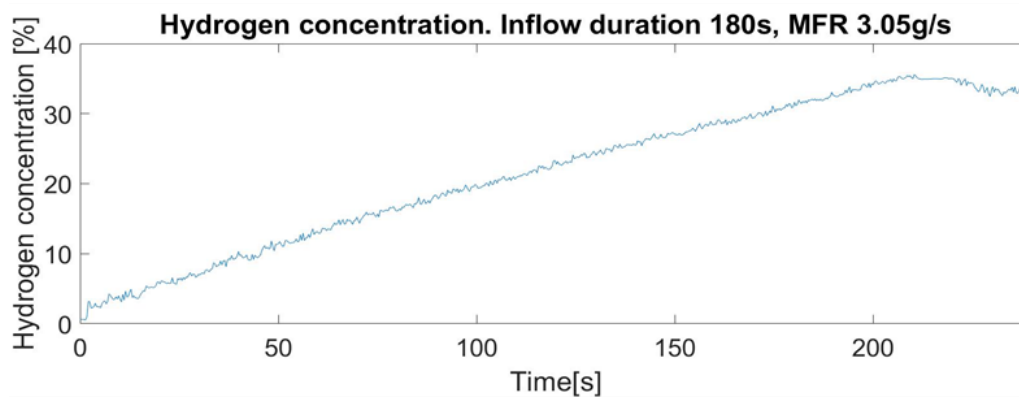


Figure 4-37. Hydrogen volume concentration from experiment 8.

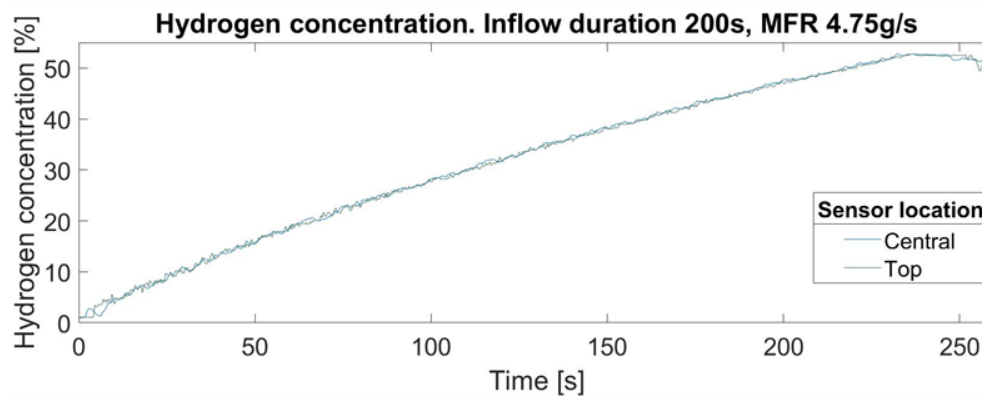


Figure 4-38. Hydrogen volume concentration from experiment 9.

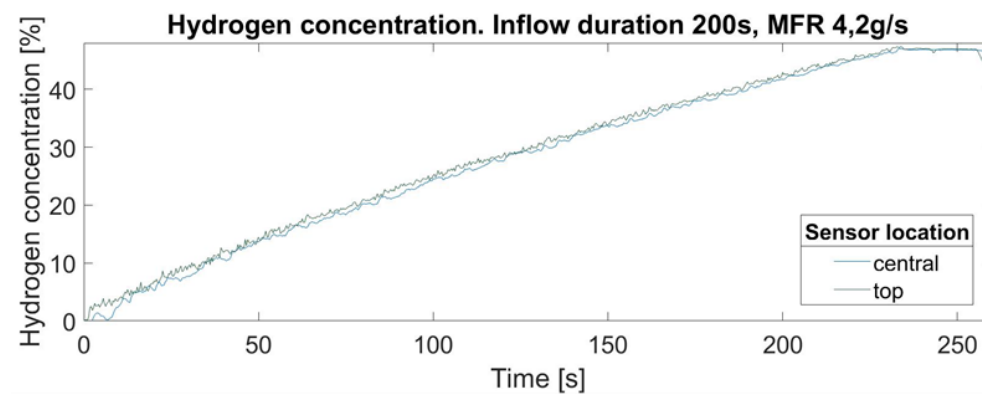


Figure 4-39. Hydrogen volume concentration from experiment 10.

### D2.3. Final report on analytical, numerical and experimental studies on hydrogen dispersion in tunnels, including innovative prevention and mitigation strategies

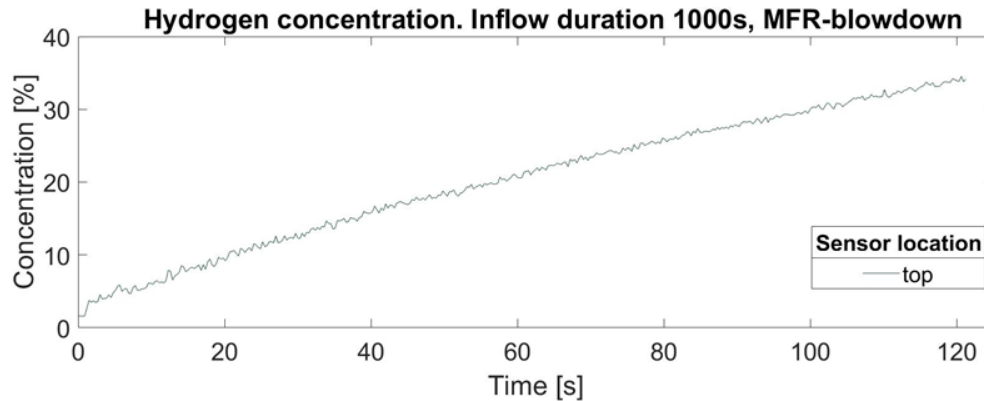


Figure 4-40. Hydrogen volume concentration from experiment 11.

A detailed analysis of the experimental results can be found in the full report (Lach et al., 2020).

#### 4.2.3.5 Experimental data

The experimental data is uploaded on the HyTunnel-CS website members area: see HyTunnel-CS Documents->Work-package documents-> WP2 unign PPP Experiments

### 4.3 Dynamics of H<sub>2</sub> release and dispersion in a tunnel (Sub-task 2.4.3/HSE)

#### 4.3.1 Introduction and objectives

This sub-task aims to investigate the dynamics of hydrogen release and dispersion in a tunnel, including the effect of ventilation. The experiments will aid the determination of hazard distances from unignited releases, i.e. location of flammable hydrogen-air mixtures from releases and their dispersion in realistic scenarios at high storage pressures.

The objectives of the proposed series of experiments are:

- Undertake several scaled hydrogen jet releases representing the blowdown of a vehicle fuel tank following operation of the TPRD.
- Measure the resultant hydrogen concentration profiles downstream of the release point for various ventilation flows.
- Measure the resultant near field hydrogen concentration profiles for three different jet orientations. These will include the effects of obstructions in the tunnel on the near field dispersion in the tunnel.
- Provide experimental data for relevant model developments and their validation.

#### 4.3.2 Detailed specification

The experiments will be performed in the HSE test facility which consists of a circular steel tunnel; it is nominally 3.7 m in diameter and comprises 5 sections totalling 70 m in length. The central section is 8 m long and has a wall thickness of 55 mm. The outer sections have a wall thickness of 25 mm and together are approximately 31 metres in length each side of the central section. The central section can withstand static pressures up to 3 Mpa. The outer sections can withstand static pressures up to 1.4 Mpa. Both the central and outer sections can withstand higher dynamic pressures of at least 3 Mpa resulting from a shock or blast wave travelling along the tunnel. The sections will be aligned with each other and the gaps between sections sealed to prevent any leakage of gas.



### D2.3. Final report on analytical, numerical and experimental studies on hydrogen dispersion in tunnels, including innovative prevention and mitigation strategies

The tunnel will accommodate scaled releases of hydrogen from vessels simulating hydrogen storage in a typical fuel cell powered vehicle, i.e. with the capacity to store an equivalent quantity of hydrogen gas at pressures up to 700 bar. The facility will be equipped with the following ancillary equipment for the purpose of delivering the desired experimental objectives:

- Axial fans.
- Gas booster.
- Hydrogen storage tank.
- Gas release control system.
- Sensors.
- Data acquisition system.

There are two types of releases being undertaken, namely a blowdown release representing the quasi-steady release through a pressure relief device and an instantaneous release representing the catastrophic failure of the gas storage vessel. The amounts to be released and the rates of release will be determined by consideration of full size practical storage situations, scaled to our test tunnel. Two individual test vessels will be used to store the hydrogen at pressures up to 700 bar.

The vessel being used for the blowdown tests comprises three individual carbon fibre cylinders supplied by Luxfer, each with a capacity of 53 litres and connected in parallel. To allow dispersion experiments this blowdown vessel incorporates a suitably sized off-take to which a nozzle representing a TPRD or several TPRD's is attached.

Initial flow rates during a blowdown will approach 0.7 kg/s. The pressure decay within the vessel is measured with a suitable Kulite pressure transducer alongside a type-K thermocouple for temperature measurement, from which the mass flow rates can be derived. The nozzle can be set in different orientations to represent possible release scenarios, namely; vertically upwards, vertically downwards, and inclined at 135 degrees backwards in the direction of the ventilation flow.

Variable-speed axial fans, seven in total, are located at the northern entrance to the tunnel, capable of achieving volumetric flow rates up to  $1.2 \times 10^5 \text{ m}^3/\text{h}$ . This equates to a maximum linear air flow velocity of 3 m/s. The fans drive air through the tunnel from this end. The airflow along the tunnel will be measured and characterised, particularly within the centre section. If necessary, baffle plates and/or flow straighteners will be added near the tunnel entrance to produce a well-developed swirl-free inlet flow.

The whole of the tunnel floor is concreted to provide a flat 'roadway' and provide a secure mounting area for the instantaneous release vessel and for scale models included in some of the tests. A metal plate will also be secured directly under the vertically downwards pointing jet to act as a spreader plate for the jet during these tests, to prevent damage to the floor.

#### *4.3.2.1 Scaling criteria*

It is anticipated that four scaled releases will be undertaken, characterised by the quantity released and the time scale of the releases. These will represent TPRD blowdowns from a

### D2.3. Final report on analytical, numerical and experimental studies on hydrogen dispersion in tunnels, including innovative prevention and mitigation strategies

representative car, bus and two trains as would occur in a typical full-sized tunnel. The actual representations are suggested below.

#### 4.3.2.2 Proposed tests

Based upon the accident scenario analysis carried out in HyTunnel-CS D1.3 (2019), we are undertaking the following test programme for which the following assumptions are considered applicable:

- In the case of normal TPRD operation in a fire, it is assumed that the total inventory is released through the TPRD's. All TPRD's opening at roughly the same time.
- In the case of a spurious TPRD operation it is assumed that at least one tank is involved.
- Only one tank fails catastrophically in a fire due to single TPRD malfunction.
- A tunnel cross-sectional area is represented by a circle of the equivalent area.

The hydrogen inventories carried by the three different types of vehicle, based on HyTunnel-CS D1.3 (2019), are as follows:

- **CAR:** Five makes specified, all operating at 700 bar. Tank capacity varies between 115 and 156 litres, usually made up from two tanks each of similar capacity. Average capacity 135 litres, containing a mass of 5.4 kg hydrogen. Vent lines specified as between 2 – 4 mm diameter, although 4.2 mm diameter seems to be used in some cases. Vent line is downwards from underneath the vehicle at 135 degrees backward. The TPRD diameter is quoted as 2.0 mm, with one TPRD per tank.
- **BUS:** Three makes specified, all operating at 350 bar. They use between four and ten tanks, roof mounted, each with a capacity varying between 74 and 205 litres. More recent designs are using 280 litre tanks. Assume an average of 210 litres per tank on a four-tank pack, each tank containing 4.97 kg of hydrogen, giving a total capacity of about 20 kg. Vent line is upwards from top of vehicle. The TPRD diameter is 3.3 mm and there are two fitted to each cylinder, giving a total of eight. Other buses may have slightly larger capacity tanks with either 11 or 12 TPRD's fitted. Recently Wrightbus have introduced a series of single decker buses with a hydrogen capacity of between 35-50 kg. In view of which we have used a 40 kg capacity (say five tanks) with ten TPRD's fitted as the basis for our modelling.
- **TRAIN:** GE Alstom manufacture a two-carriage unit, each with 96 kg of hydrogen operating at 350 bar. Each unit has 24 cylinders; each with a capacity of 175 litres, containing 4.14 kg of hydrogen. Assume that only one carriage is involved in the fire. Each cylinder has two TPRD's, each with a diameter of 3.3 mm.

A three-carriage unit is also under consideration by GE Alstom for the UK market, known as "Breeze". This will have 417 kg of hydrogen at 350 bar pressure, contained in 72 cylinders; each with a capacity of 245 litres. Each cylinder contains 5.8 kg of hydrogen and there are 36 cylinders in both the lead and trailing carriages. Assume that only one car is involved in the fire, consequently the total inventory per car will be 209 kg. The tanks are arranged in cassettes, comprising nine tanks each. There are four cassettes per car, contained in a unit behind the cab. There are two cassettes on either side of the storage bay, assumed separated by a partition. Each cylinder has two TPRD's, hence each cassette has 18 TPRD's of 3.3 mm diameter. We assume that for

### D2.3. Final report on analytical, numerical and experimental studies on hydrogen dispersion in tunnels, including innovative prevention and mitigation strategies

modelling purposes only two cassettes (one side) would be involved in a fire. The inventory involved in a fire is therefore 105 kg, with 36 TPRD's able to vent the inventory.

**NB:** Information on hydrogen storage capacity, size, and numbers of TPRD's has been obtained through an NDA with a vessel manufacturer.

The cross-sectional areas (area through which vehicles are travelling) of the various types of ROAD tunnels under consideration are as follows:

- Single lane tunnel: 24.1 m<sup>2</sup>. Equivalent diameter D = 5.54 m.
- Double lane tunnel: 39.5 m<sup>2</sup>. Equivalent diameter D = 7.09 m.
- Gotthard tunnel, double lane: 49.35 m<sup>2</sup>. Equivalent diameter D = 7.93 m.
- Rennsteig tunnel, double lane: 72.95 m<sup>2</sup>. Equivalent diameter D = 9.64 m.
- Tyne tunnel (Original), double lane: 48.1 m<sup>2</sup>. Equivalent diameter D = 7.83 m.

The cross-sectional areas (area through which vehicles are travelling) of the various types of RAIL tunnels under consideration are as follows:

- High speed traffic, two rail: 92 m<sup>2</sup>. Equivalent diameter D = 10.82 m.
- Express traffic tunnel, two rail: 79.2 m<sup>2</sup>. Equivalent diameter D = 10.04 m.
- Metro type traffic, single rail: 44.6 m<sup>2</sup>. Equivalent diameter D = 7.54 m.
- Rectangular section urban rail, two rail: 56.3 m<sup>2</sup>. Equivalent diameter D = 8.47 m.
- Severn tunnel, two rail: 60 m<sup>2</sup>. Equivalent diameter 8.74 m.
- Channel tunnel single bore, single rail: 53.5 m<sup>2</sup>. Equivalent diameter D = 8.25 m.

HSE Buxton test tunnel:

- Radius = 1.85 m.
- Depth of ballast = 0.45 m.
- Area of segment containing ballast = 0.745 m<sup>2</sup>.
- Circular area of tunnel (no ballast) = 10.75 m<sup>2</sup>.
- Area through which vehicles travel = 10.0082 m<sup>2</sup>.
- Equivalent diameter D<sub>HSE</sub> = 3.57 m.
- Scaling factor (H) for tunnel diameter is: D/D<sub>HSE</sub>.
- Scaling factor for mass of hydrogen stored is: H<sup>3</sup>.
- Scaling factor for the mass flow rate is: H<sup>5/2</sup>.
- Scaling factor for the discharge time is: H<sup>1/2</sup>.
- Scaling factor for the airflow in the tunnel is: H<sup>1/2</sup>.

Based on the foregoing average scaling factors for the various tunnel types (all tunnels, double bore only) can be obtained, then used to establish the scaled inventories for a car, bus, and train in the relevant tunnels for both continuous and catastrophic releases as shown in Table 4-6.

*Table 4-6. Scaled hydrogen inventories for cars. Buses and trains (Double bore only values in bold are those to be used for the actual modelling exercise).*

		<b>Total inventory (kg)</b>	<b>Single tank inventory (kg)</b>	<b>Average scaling factor</b>	<b>Scaled total inventory (kg)</b>	<b>Scaled inventory single tank</b>

### D2.3. Final report on analytical, numerical and experimental studies on hydrogen dispersion in tunnels, including innovative prevention and mitigation strategies

						(kg)
Car 700 bar	All tunnels	5.4	2.70	2.130	0.56	0.28
<b>Car 700 bar</b>	<b>Double bore only</b>	<b>5.4</b>	<b>2.70</b>	<b>2.275</b>	<b>0.46</b>	<b>0.23</b>
Bus 350 bar	All tunnels	40.0	4.97	2.130	4.14	0.51
<b>Bus 350 bar</b>	<b>Double bore only</b>	<b>40.0</b>	<b>4.97</b>	<b>2.275</b>	<b>3.40</b>	<b>0.42</b>
Train 350 bar	All tunnels	96.0 105.0	4.14 5.80	2.513	6.05 6.62	0.26 0.37
<b>Train 350 bar</b>	<b>Double bore only</b>	<b>96.0 105.0</b>	<b>4.14 5.80</b>	<b>2.665</b>	<b>5.07 5.54</b>	<b>0.22 0.31</b>

Using a commercially available fixed volume off-the-shelf 53 litre tank (MWP 800 bar) or a combination of these, requires the desired inventory to be contained in them but at the relevant pressure. Consequently, the required pressures, scaled vessel inventories, capacities, orifice diameters and initial mass flow rates can be calculated using the suite of programmes given in: <https://elab-prod.iket.kit.edu/>.

We therefore obtain the relevant scaled values for the car, bus and two trains in a double bore tunnel only when using either one or three 53 litre vessels in combination, as shown in Table 4-7. Note that the first four rows show the tank volumes for the actual operating pressures (700 or 350 bar). The final four rows in bold show the pressures required when the volumes are fixed at either 53, 159 litres or 11 litres in the case of a single tank.

*Table 4-7. Proposed hydrogen to actual tank inventories.*

	Total inventory (kg)	Pressure (bar)	Tank volume (litres)	Single tank inventory (kg)	Pressure (bar)	Tank volume (litres)
Car	0.46	700	12	0.23	700	6
Bus	3.40	350	145	0.42	350/700	18/11
Train 1	5.07	350	215	0.22	350/700	10/5
Train 2	5.54	350	251	0.31	350/700	13/8
<b>Car</b>	<b>0.46</b>	<b>118</b>	<b>53</b>	<b>0.23</b>	<b>300</b>	<b>11</b>
<b>Bus</b>	<b>3.40</b>	<b>310</b>	<b>159</b>	<b>0.42</b>	<b>700</b>	<b>11</b>

### D2.3. Final report on analytical, numerical and experimental studies on hydrogen dispersion in tunnels, including innovative prevention and mitigation strategies

<b>Train 1</b>	<b>5.07</b>	<b>510</b>	<b>159</b>	<b>0.22</b>	<b>290</b>	<b>11</b>
<b>Train 2</b>	<b>5.54</b>	<b>580</b>	<b>159</b>	<b>0.31</b>	<b>450</b>	<b>11</b>

Calculation of orifice sizes for the total inventory contained on a car, bus and train, from the literature typical TPRD orifice sizes are 2.0 and 3.3 mm diameter, in addition a car has two tanks, buses; four to twelve (assume five) tanks, and trains; eighteen to twenty-four tanks. In a fire it is assumed that the total inventories are discharged with all TPRD's open at the same time. The equivalent orifice sizes are shown in Table 4-8.

*Table 4-8. Equivalent orifice sizes for full-sized releases.*

<b>Orifice diameter single TPRD (mm)</b>	<b>Car: two TPRD's equivalent diameter (mm)</b>	<b>Bus: 10 TPRD's equivalent diameter (mm)</b>	<b>Train: 48/36 TPRD's equivalent diameter (mm)</b>
2.0	2.83	-	-
3.3	-	10.44	22.86/19.80

Using the above equivalent diameters, the initial mass flow rates and discharge times (to choke point) are obtained for the actual full-size inventories using the actual storage pressures (700 or 350 bar) as shown in Table 4-9.

*Table 4-9. Initial mass flow rates and discharge times for full size and for scaled inventories.*

	<b>^^Total inventory (kg)</b>	<b>Initial mass flow rates (kg/s)</b>	<b>Discharge times (seconds)</b>	<b>^^Scaled total inventory (kg)</b>	<b>Scaled initial mass flow rates (kg/s)</b>	<b>^Scaled discharge times (s)</b>	<b>*Scaled orifice diameters (mm)</b>
Car 700 bar	5.4 (135 l)	0.215	168	0.46 (12 l)	0.0275	120 (111)	1.0
Bus 350 bar	40.0 (1700 l)	1.638	134	3.40 (145 l)	0.2100	86 (89)	3.8
Train 1 350 bar	96.0 (4050 l)	7.850	67	5.07 (215 l)	0.6770	41 (41)	6.7
Train 2 350 bar	105.0 (4450 l)	5.890	97	5.55 (235 l)	0.5080	60 (60)	5.8

### D2.3. Final report on analytical, numerical and experimental studies on hydrogen dispersion in tunnels, including innovative prevention and mitigation strategies

*\*These are the orifice diameters needed to give the correct scaled initial mass flow rates using the actual pressures shown in the first column.*

*^The values in brackets are those obtained from scaling the values shown in column three.*

*^^Numbers in brackets are the volumes in litres required for the inventory at the pressures shown at the start of each row.*

NB: The approach is equally valid for other orifice sizes than those used here.

If using standard 53 litre size cylinders, then we can model the foregoing using different pressures but fixed volumes (multiples of 53 litres) to give the same initial mass flow rates as shown in Table 4-10, giving nozzle diameters appropriate to the different pressures.

As an example, the jet from a car cylinder at 700 bar pressure with an orifice diameter of 1.0 mm is the equivalent of releasing at 118 bar through a 2.2 mm diameter nozzle, given the same initial mass flow rates. This is because the fully expanded jets in both cases have an initial fully expanded diameter of 16.8 mm at atmospheric pressure and thereafter, they both behave in the same manner, namely as a free turbulent jet, for which the decay characteristics are well documented in the literature.

*Table 4-10, Scaled orifice size for experimental releases.*

	<b>Scaled total inventory (kg)</b>	<b>Scaled initial mass flow rates (kg/s)</b>	<b>Discharge times (s)</b>	<b>Scaled orifice diameters used (mm)</b>
Car 118 bar	0.46 (53 l)	0.0275	70	2.2
Bus 310 bar	3.40 (159 l)	0.2100	83	4.0
Train 1 510 bar	5.07 (159 l)	0.6770	46	5.7
Train 2 580 bar	5.55 (159 l)	0.5080	69	4.7

#### 4.3.2.3 Scaling of airflow in HSE tunnel

HyTunnel-CS D1.1 (2019) makes recommendations for maximum required ventilation velocities in actual tunnels. This is deemed to be 3.5 m/s based on physiological and fire-fighting needs. HyTunnel-CS D1.3 (2019) has therefore recommended a range of actual tunnel ventilation velocities for study of 1, 2, 3.5 and 5 m/s. These values correspond to actual full-scale tunnel velocities and, according to the scaling rules which were adopted, should be modified in line with the HSE tunnel being studied. Applying the velocity scaling factor given previously gives the reduced velocities shown in Table 4-11.

*Table 4-11. Scaled ventilation velocities in HSE tunnel*



### D2.3. Final report on analytical, numerical and experimental studies on hydrogen dispersion in tunnels, including innovative prevention and mitigation strategies

<b>Actual tunnel ventilation velocity (m/s)</b>	<b>HSE ventilation velocity (m/s)</b>	
	Scale factor 2.275	Scale factor 2.665
1.0	0.66	0.61
2.0	1.33	1.22
3.5	2.32	2.14
5.0	3.31	3.06

#### 4.3.3 Test programme

Based on the analysis in the previous sections, the test programme will examine combinations taken from scaled orifice sizes for a car, bus and two trains; two ventilation rates and one (either up or down) jet orientation for the four scaled inventories shown. This gives the test matrix of 8 possible combinations. These will be done with and without the model vehicles in the tunnel, thus doubling the test number to 16. This will allow us to establish the differences in dispersion characteristics between the two conditions, without and with models present. The proposed test matrix is shown in Table 4-12. It will be necessary to repeat at least one test, same wind speed, with and without the models present; say one or two of each, giving a further two to four tests. This will give us a feel for how repeatable the tests are. Two further tests should be considered, one in which for the car the nozzle is pointed upwards from the ground, no obstructions present. The second test with the nozzle downwards but angled backwards in the direction of flow at 135 degrees. The former would illustrate the influence of the jet impinging the floor at an angle, the latter illustrating the influence of the vehicle on the dispersion. This gives is a maximum of twenty-two to twenty-four tests. The measurements required are the vessel release conditions, together with the concentration profiles downstream of the release point and the wind speed measurements.

There is also a need to ensure that the tests are aligned with the validation and modelling requirements of KIT, NCSR, UU and CEA, through further discussion with the respective organisations.

*Table 4-12. Proposed matrix of tests*

	<b>Car</b>		<b>Bus</b>		<b>Train 1</b>		<b>Train 2</b>	
<b>Hydrogen quantity (kg)</b>	0.45		3.40		5.07		5.55	
<b>Pressure (bar)</b>	118		310		510		580	
<b>Orifice diameter (mm)</b>	2.2		4.0		5.7		4.7	
<b>Tunnel airflow (m/s)</b>	1.25	2.40	1.25	2.40	1.25	2.40	1.25	2.40
<b>Jet orientation</b>	D	D	U	U	U	U	U	U

## D2.3. Final report on analytical, numerical and experimental studies on hydrogen dispersion in tunnels, including innovative prevention and mitigation strategies

### 4.3.4 Expected results

Due to the COVID-19 outbreak and subsequent restrictions placed on businesses within the UK and hydrogen supply shortage it has not been possible to complete work to the originally planned timescale. A five-month programme extension has therefore been requested and agreed. A detailed report presenting the results and their analysis will be provided following the conclusion of the experimental programme in (HyTunnel-CS-D4.4, 2022).

## 4.4 Efficiency of mechanical ventilation on H<sub>2</sub> dispersion (Sub-task 2.4.4/PS)

### 4.4.1 Introduction – objectives

The objectives of this series of experiments include,

- investigation of hydrogen jet structure and its dispersion in presence of co-, cross- and counter-flow for ventilation;
- experimental determination of hazard distances as a function of the ratio of hydrogen mass flow rate and air flow velocity;
- to provide unique experimental data for related model development and validation; contribution to the recommendations for inherently safer use of hydrogen vehicles in underground transportation systems.

### 4.4.2 Detailed specification

The experiments were performed in the safety vessel V220 (A2), as shown in Figure 4-41. The safety vessel with an inner diameter  $d_i = 6$  m and a height  $h = 8$  m provides a volume of 220 m<sup>3</sup>. It is designed for a static overpressure of 11 bar and temperatures up to 150 °C. The vessel is equipped with numbers of vents and ports and windows for optical access. The largest two flanges with an inner diameter  $d_i = 1890$  mm are parallel and located near the ground. Detailed CAD-drawings of the facility are available (Inventor-files).

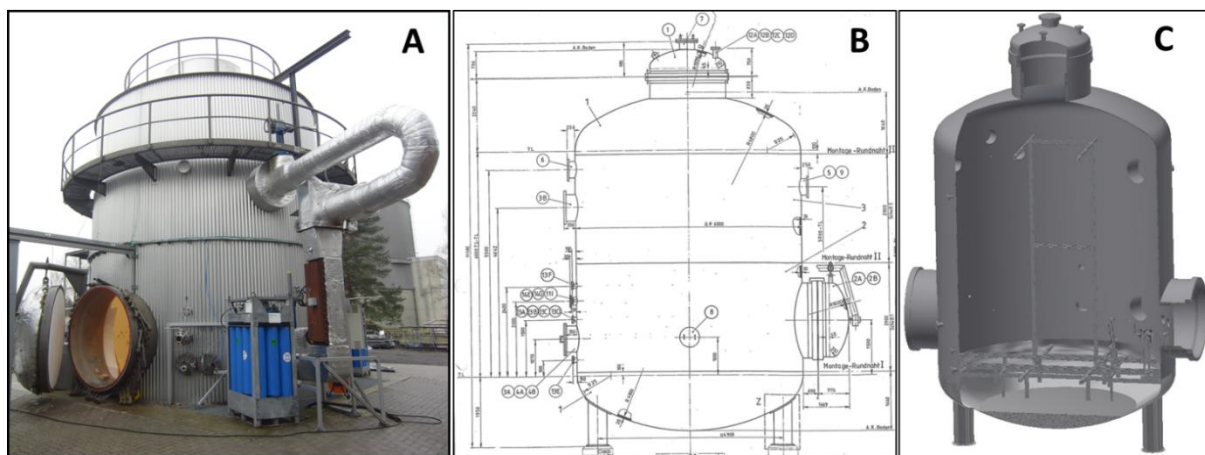


Figure 4-41. A) Safety vessel V220 (A2) of HYKA, B) Technical drawing, C) Example CAD-drawing.

The facility for unignited hydrogen jet dispersion tests, shown in Figure 4-42, is placed inside the safety vessel. The H<sub>2</sub> mass flow rate will be adjusted and controlled by a Coriolis H<sub>2</sub> Flow Meter (0 – 10 g/s) [ELITE – Emerson Process Management]. The H<sub>2</sub> flow first runs through a bypass line which is equipped with the same nozzle as the intended jet release nozzle. After a stable H<sub>2</sub> flow through the bypass line is established, the bypass valve will be closed and the

### D2.3. Final report on analytical, numerical and experimental studies on hydrogen dispersion in tunnels, including innovative prevention and mitigation strategies

jet release valve will be opened simultaneously. The H<sub>2</sub>-Jet is characterized by the nozzle diameter and the measured values of the H<sub>2</sub> Flow rate and the pressure P<sub>2</sub> (Kistler 40058F250) which is measured close to the release nozzle. Additionally, the pressure P<sub>1</sub> (WIKA S 20) between the bypass valve and the release valve will be monitored online and recorded with a sample rate of 2 Hz.

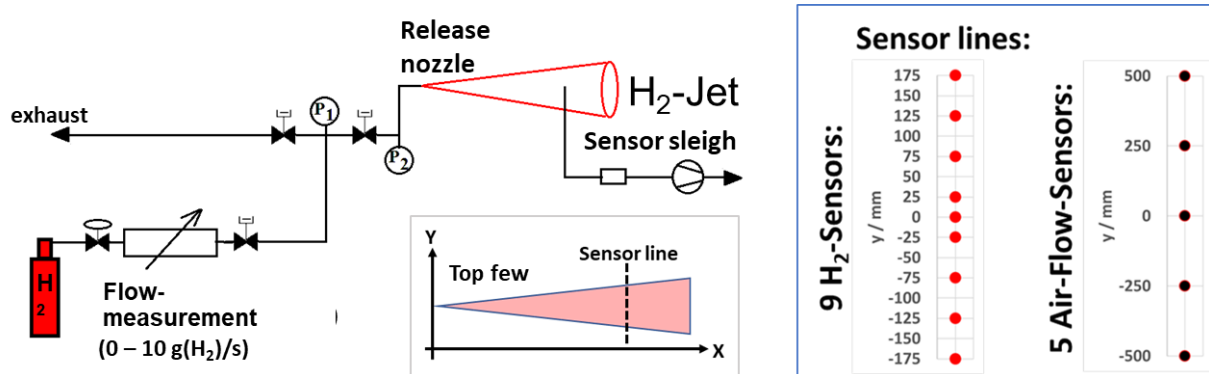


Figure 4-42. Left, schema of the jet-facility. Right, y-positions of the sensor lines for H<sub>2</sub> concentration and airflow velocity.

The release nozzle is located above the release valve to avoid disturbance of the airflow from the ventilation in the co-flow configuration. The centre axis of the jet is placed centred and perpendicular to the two large flanges of the vessel, in the co- and counter-flow configuration, see Figure 4-43. In the cross flow configuration the jet will be adjusted parallel to the flange doors. All experiments are performed with open flange doors.

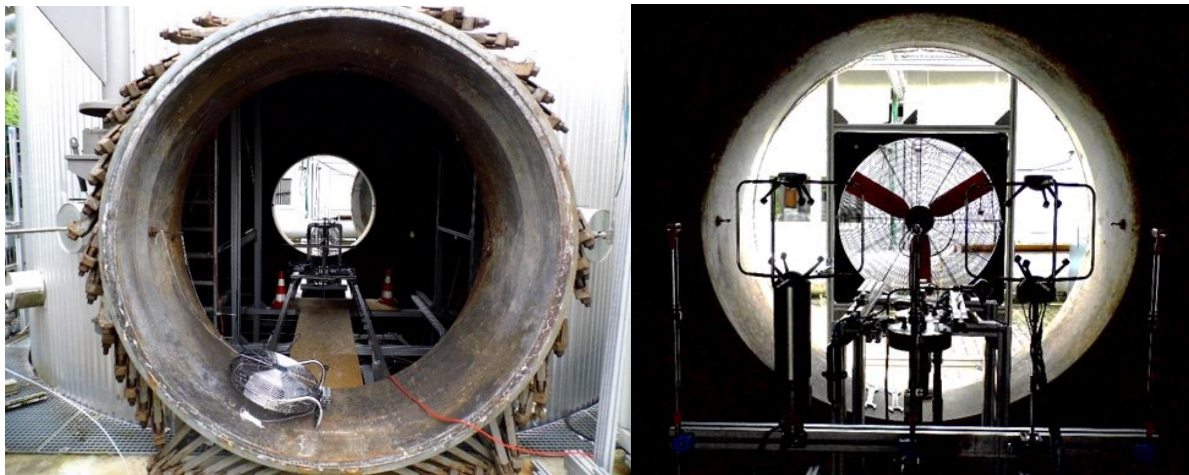


Figure 4-43. Left, jet facility inside the safety vessel V220 (A2). Right, jet facility inside the safety vessel V220 (A2) with wind machine and flow measurement devices in the co-flow configuration.

A wind machine (Trotec) TTW 20000 with a maximum air flow rate of 20000 m<sup>3</sup>/h and a max air flow velocity of 8.8 m/s will be used to simulate a tunnel specific ventilation. Figure 4-43, right shows the wind machine in the co-flow configuration. To observe the unignited H<sub>2</sub> jet flow structure a large-scale shadowgraphy set-up for high-speed (1000 f/s) applications was used in selected configurations.

The designed test cases are summarized in Table 4-13. Two nozzle diameters (1 mm and 4 mm), two H<sub>2</sub> mass flow rates (1 g/s and 5 g/s) and four different airflow velocities (0 m/s, 1.5 m/s, 3.5 m/s and 5 m/s) are the main variables for the three investigated flow directions (co-,

### D2.3. Final report on analytical, numerical and experimental studies on hydrogen dispersion in tunnels, including innovative prevention and mitigation strategies

counter- and cross-flow). Due to the limited widths of the flow-field inside the safety vessel, the initially planed  $H_2$  mass flow rate of 5 g/s in the cross-flow configuration was reduced to 1.5 g/s for the 1 mm nozzle and to 2.5 for the 4 mm nozzle. So, the total number of investigated configurations is 42, see Table 4-13.

Table 4-13. Test matrix of unignited  $H_2$  jets.

H <sub>2</sub> jet nozzle	1 mm				1 mm				4 mm				4 mm			
H <sub>2</sub> mass flow rate, g/s	1				5 (cross-flow: 1.5)				1				5 (cross-flow: 2.5)			
Ventilation flow velocity, m/s	0	1.5	3.5	5	0	1.5	3.5	5	0	1.5	3.5	5	0	1.5	3.5	5
Co-flow	1	2	5	8	11	12	15	18	21	22	25	28	31	32	35	38
Counter-flow		3	6	9		13	16	19		23	26	29		33	36	39
Cross-flow		4	7	10	41	14	17	20		24	27	30	42	34	37	40

The uniformity of the nine different airflow velocity configurations was measured in 2D in the interesting area. Figure 4-44 shows an example of the uniformity of the average airflow velocity for the co-flow configuration with a wind speed of 3.5 m/s.

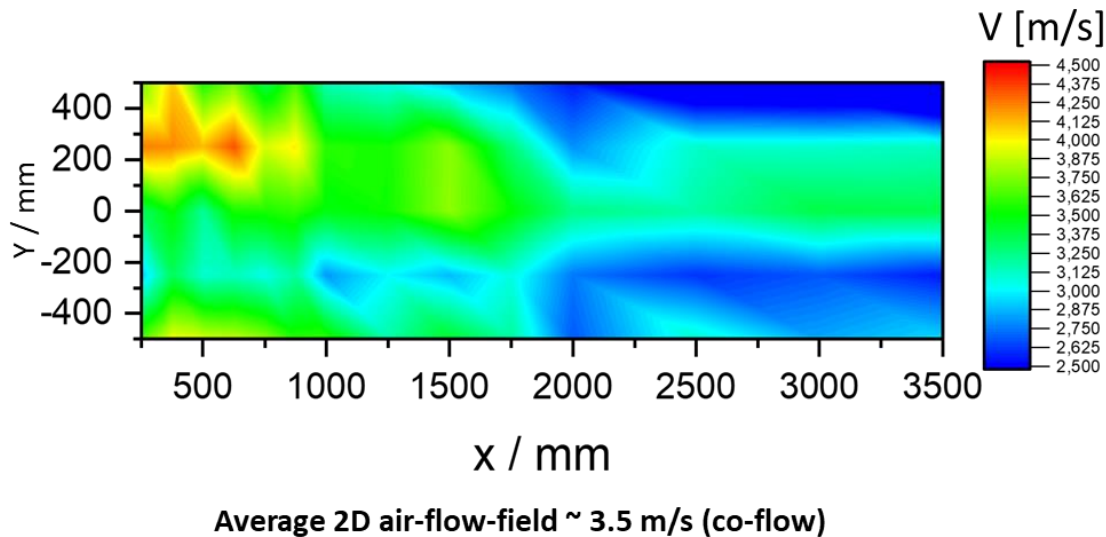


Figure 4-44. Example of measured airflow velocity for the co-flow configuration with a wind speed of 3.5 m/s.

#### 4.4.3 Results

Hydrogen concentration distributions were measured in axial and radial jet direction. All configurations of the jet mass flow rate, the jet nozzle diameter and the ventilation flow velocities for the three, co-, counter- and cross-flow cases corresponding to Table 4-13 were investigated. All scheduled experiments regarding this campaign have been performed. All

### D2.3. Final report on analytical, numerical and experimental studies on hydrogen dispersion in tunnels, including innovative prevention and mitigation strategies

measured values are available and are provided as x-y H<sub>2</sub>-concentration matrix in Excel-files. The Excel files contain also specific experimental properties. An example of the results for 1 mm nozzle and 5 g/s H<sub>2</sub>-jet mass flow rate is shown as H<sub>2</sub>-concentration contour plots in Figure 4-45.

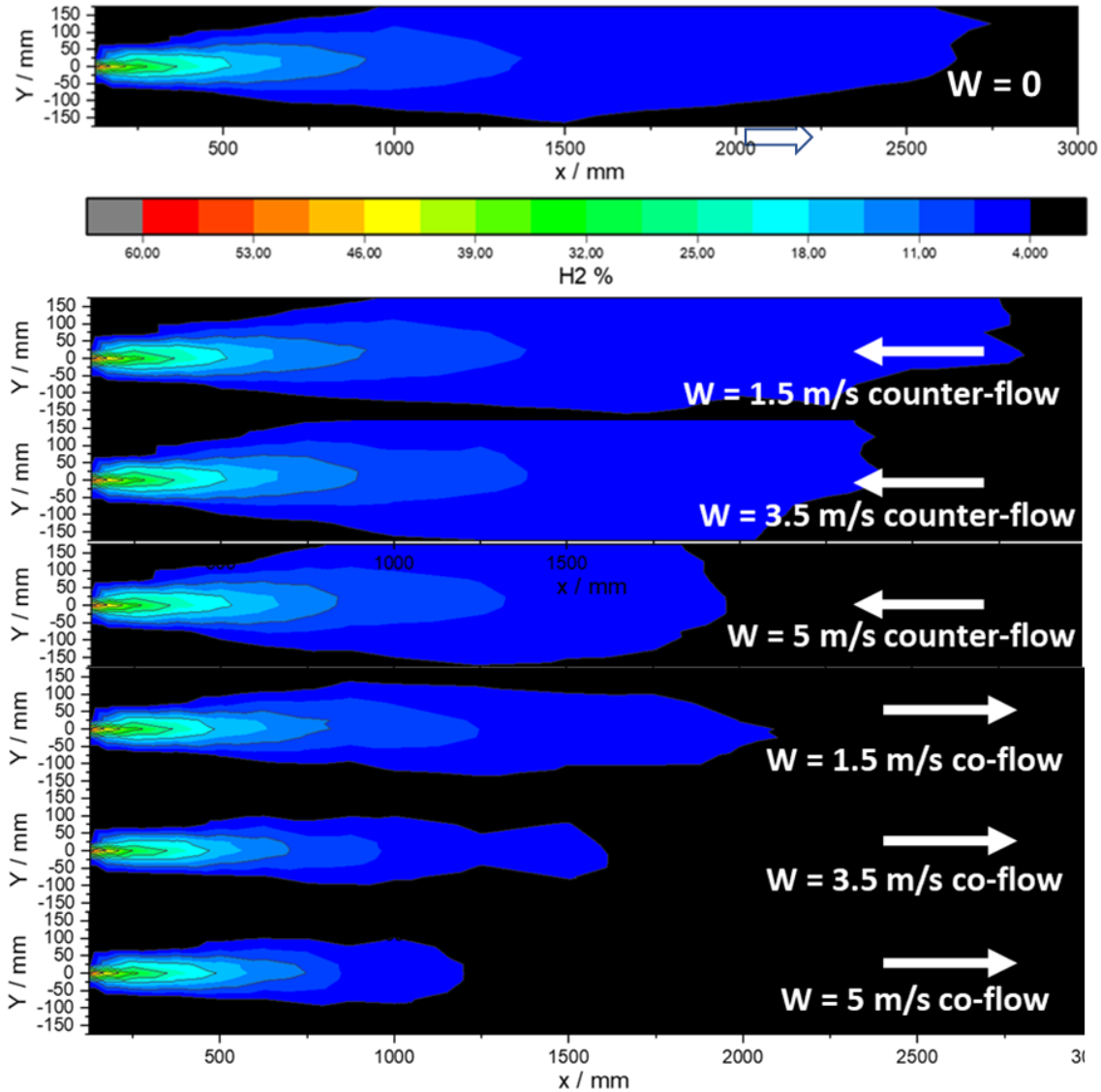


Figure 4-45. Example of H<sub>2</sub>-concentration contour plots for 1 mm nozzle and 5 g/s H<sub>2</sub>-jet mass flow rate.

A detailed data analysis based on the entire experimental campaign was conducted and presented next. Based on linear interpolations to the measured hydrogen volumetric concentrations in the vented H<sub>2</sub> jet experiments, the lengths of the hydrogen jet clouds are obtained in terms of 4 vol. % H<sub>2</sub> and 10 vol. % H<sub>2</sub>, referring to flammability and potential to fast flame, respectively. The parameters are as follows.

- a) jet nozzle diameters: 1 or 4 mm,
- b) hydrogen release rates:
  - 1 or 5 g/s in case of co- or counter-flow ventilation,
  - 1, 1.5 or 2.5 g/s in case of cross-flow ventilation,



## D2.3. Final report on analytical, numerical and experimental studies on hydrogen dispersion in tunnels, including innovative prevention and mitigation strategies

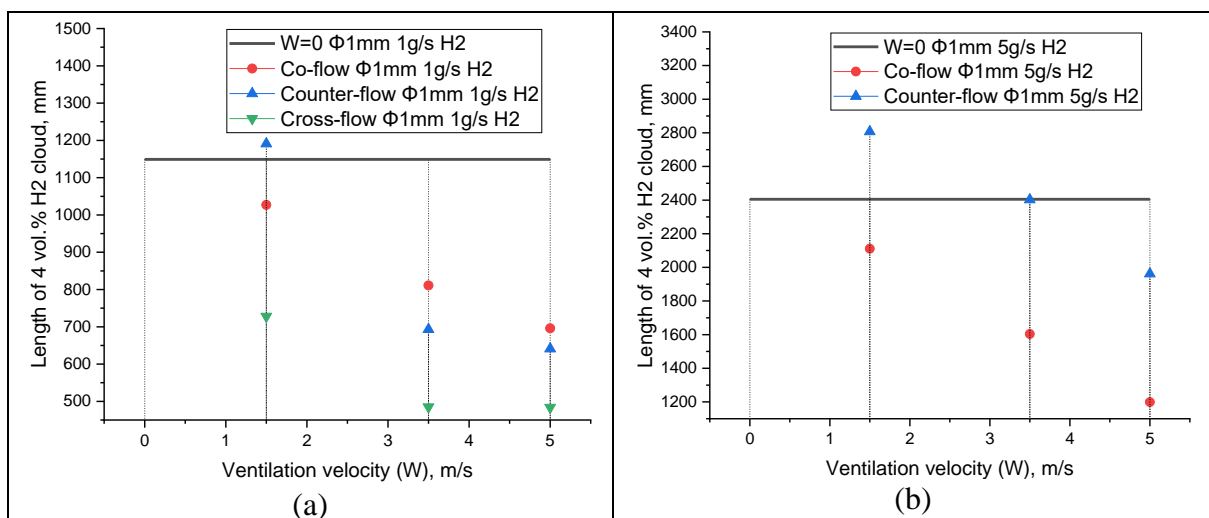
- c) ventilation velocities: 0, 1.5, 3.5 or 5.0 m/s,
- d) ventilation directions: co-, counter- or cross-flow.

### 4.4.3.1 Ventilation efficiency analysis in terms of the length of 4 vol. % H<sub>2</sub> cloud

The length of the 4 vol. % H<sub>2</sub> cloud of the jet is plotted as a function of ventilation velocity for different cases, as shown in Figure 4-46. The data point of the hydrogen cloud length in case of no ventilation ( $W=0$ ) is extended horizontally as a reference line for comparison convenience. In case of cross-flow ventilation, the “length” means the maximal extension of the hydrogen cloud in the direction of the jet nozzle axis, instead of the curved length along the central line of the bent jet flow.

As shown in Figure 4-46, ventilation can reduce the length of the flammable cloud in most cases because the ventilation flow prompts gas mixing and hydrogen diffusion in general. Exception is that the flammable cloud length increases a little in case of counter-flow ventilation with a small velocity of 1.5 m/s in Figure 4-46 (a), (b) and (e). In such circumstances, the counter flow impedes the hydrogen dispersion in the far field along the jet direction, where it is supposed to be filled with low concentration hydrogen e.g., < 4 vol. % in case of no ventilation. However, due to the counter-flow, this part of hydrogen is pushed backwards and concentrated to > 4 vol. %. Finally, the flammable length is increased by the ventilation in opposite direction. When the ventilation velocity is not less than 3.5 m/s, which is the recommended ventilation velocity for traffic tunnels in practice, the ventilation is always effective to reduce the length of flammable cloud, no matter the ventilation direction is a co-flow or counter-flow or a cross-flow, and no matter the H<sub>2</sub> release rate is small (1 g/s) or large (5 g/s).

Figure 4-46 (a), (c) and (f) manifest that the cross-flow ventilation is the most effective way to reduce the flammable length by e.g., more than 50% in some cases of  $W = 3.5$  m/s.





### D2.3. Final report on analytical, numerical and experimental studies on hydrogen dispersion in tunnels, including innovative prevention and mitigation strategies

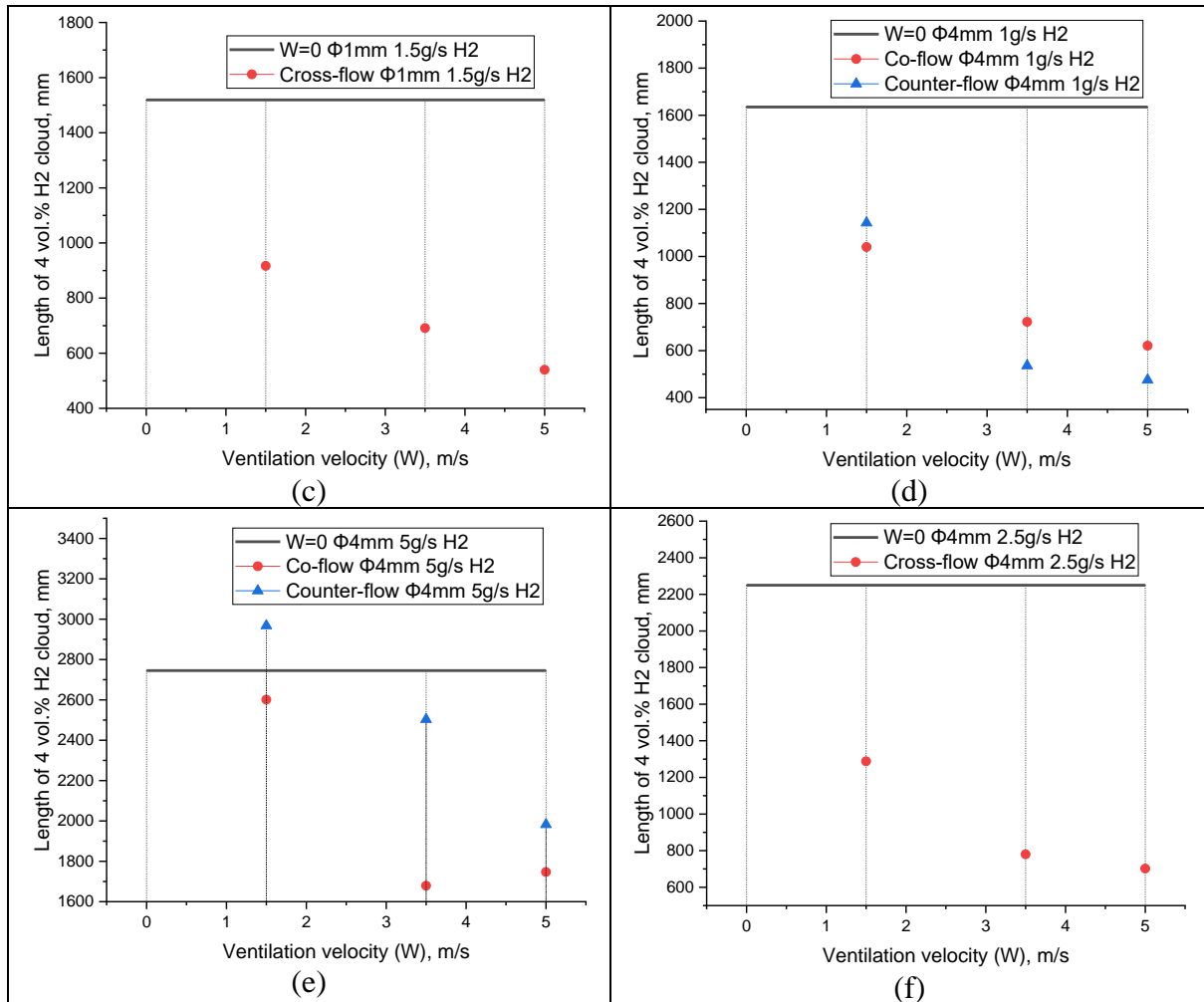


Figure 4-46. Length of 4 vol. % H<sub>2</sub> cloud as a function of ventilation velocity in different cases: (a) nozzle Φ 1 mm and 1 g/s H<sub>2</sub>; (b) Φ 1 mm and 5 g/s H<sub>2</sub>; (c) Φ 1 mm and 1.5 g/s H<sub>2</sub>; (d) Φ 4 mm and 1 g/s H<sub>2</sub>; (e) Φ 4 mm and 5 g/s H<sub>2</sub>; (f) Φ 4 mm and 2.5 g/s H<sub>2</sub>.

#### 4.4.3.2 Ventilation efficiency analysis in terms of the length of 10 vol. % H<sub>2</sub> cloud

The 10 vol. % H<sub>2</sub> cloud in air has potentially larger risk of fast flame. Thus, the influence of ventilation on the dimension of the 10 vol. % H<sub>2</sub> cloud is also analysed based on the data.

Similar conclusions can be made that the ventilation can effectively reduce the length of the 10 vol. % H<sub>2</sub> cloud, certainly due to the dispersing and mixing effects caused by ventilation flow. According to Figure 4-47, the length of the 10 vol. % H<sub>2</sub> cloud decreases as long as the ventilation velocity increases in general cases. It is logic in physics that the dimension of the potentially detonable hydrogen cloud becomes smaller, if the ventilation flow is stronger. In case of the ventilation velocity of 3.5 m/s, e.g., the hydrogen cloud length is decreased by 10% – 38%, averagely by 25%.

### D2.3. Final report on analytical, numerical and experimental studies on hydrogen dispersion in tunnels, including innovative prevention and mitigation strategies

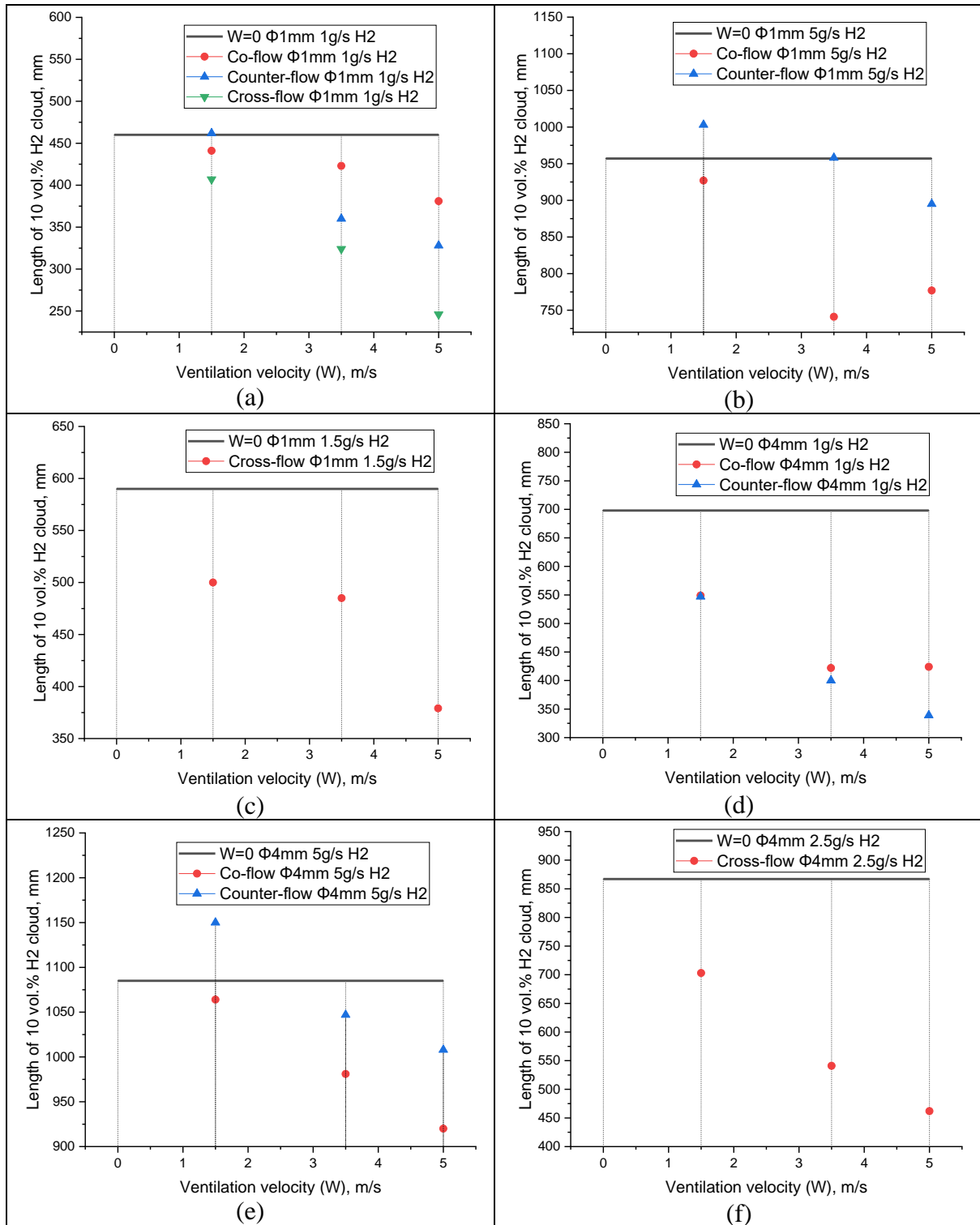


Figure 4-47. Length of 10 vol. % H<sub>2</sub> cloud as a function of ventilation velocity in different cases: (a) nozzle  $\Phi 1\text{ mm}$  and 1 g/s H<sub>2</sub>; (b)  $\Phi 1\text{ mm}$  and 5 g/s H<sub>2</sub>; (c)  $\Phi 1\text{ mm}$  and 1.5 g/s H<sub>2</sub>; (d)  $\Phi 4\text{ mm}$  and 1 g/s H<sub>2</sub>; (e)  $\Phi 4\text{ mm}$  and 5 g/s H<sub>2</sub>; (f)  $\Phi 4\text{ mm}$  and 2.5 g/s H<sub>2</sub>.

#### 4.4.3.3 Conclusive remarks

- Tunnel ventilation is an effective measure to reduce hydrogen risk, by means of decreasing the dimension of the flammable and detonable hydrogen clouds caused by the accidental release.

### D2.3. Final report on analytical, numerical and experimental studies on hydrogen dispersion in tunnels, including innovative prevention and mitigation strategies

- In the case of the nominally recommended ventilation velocity 3.5 m/s for general traffic tunnels, the reported experimental data manifests that the length of flammable hydrogen cloud can be reduced by 30% – 75%, averagely by 45% due to the ventilation measure; and that the length of detonable hydrogen cloud can be reduced by 10% – 38%, averagely by 25% owing to the ventilation flow.
- The conclusion can be instructive to RCS organizations, while defining safety distance and, even the interval distance for hydrogen safety concerns between two hydrogen vehicles operating in a traffic tunnel.

## 4.5 Helium dispersion test results in a full-scale tunnel (CEA)

### 4.5.1 Introduction

Hydrogen Fuel Cell Electric Vehicles (HFC EVs) represent an alternative to replace current internal combustion engine vehicles. The use of these vehicles with storage of compressed gaseous hydrogen (CGH<sub>2</sub>) or cryogenic liquid hydrogen (LH<sub>2</sub>) in confined spaces, such as tunnels, underground car parks, etc., creates new challenges to ensure the protection of people and property and to keep the risk at an acceptable level. Several studies have shown that confinement or congestion can lead to severe accidental consequences compared to accidents in an open atmosphere. It is, therefore, necessary to develop validated hazard and risk assessment tools for the behavior of hydrogen in tunnels. Among the experiments carried out in support of the validation, the CEA is conducting tests on helium dispersion in a full-scale tunnel geometry.

The tests were organized in two phases. The first one in October 2020 in which type II helium cylinders under 200 bar were used. The second in June 2021 in which type IV tanks of 78 liters under 700 bar were used as a source of compressed gas. In these tests, in addition to the effect of the internal pressure, the effect of the diameter of the release and its orientation was studied on the dispersion of the helium in the tunnel.

In the next sections, the geometry of the tunnel used for the test is briefly described. Then, the different phases of the test and the test matrix are detailed. Finally, the results are provided for the behavior of the helium dispersion. Some conclusions and recommendations are also provided.

### 4.5.2 Test geometry

The relevant information regarding the test geometry, the type of sensors as well as their locations are provided in a separate document (Sauzedde et al., 2021). A schematic description of the test arrangement is provided in Figure 4-48. The tests were performed in the tunnel du Mortier (near Autrans village, Isère, France). This disused road tunnel is a horse-shoe type geometry with a total length of about 502 m. The slope is 3.6% and the tunnel is divided in two different sections. The one located on the Autrans side is made of a flat concrete ceiling arch and the second one on the Montaud side is raw limestone rocks. The injection device was installed in this second section for the 2021 tests whereas for the 2020 tests it was located in the concrete section.

The tunnel dimensions vary in the rocky section, an average height is close to 5.9 m, and the diameter is about 8.9 m. Two sidewalks are also present on each side of the road. The chassis representing a real car is parallel to the road. The calibrated orifice representing the thermally

### D2.3. Final report on analytical, numerical and experimental studies on hydrogen dispersion in tunnels, including innovative prevention and mitigation strategies

activated relief device (TPRD) of a real compressed gaseous hydrogen storage is located at the rear of the chassis and it can be oriented upward (UP), downward (DW) with two angles ( $90^\circ$  or  $45^\circ$  to the rear). The angles are counted from the chassis which means that  $90^\circ$  does not correspond to the vertical because of the slope of the tunnel.

The monitoring system can be divided into two parts:

- The one related to the injection tank and the release pipes. Relative pressures and gas temperature were recorded inside the tank ( $P_0$ ,  $T_0$ ), at the outlet of the tank ( $P_1$ ,  $T_1$ ) and upstream the calibrated orifice ( $P_2$ ,  $P_{2bis}$  and  $T_2$ ). These are used to check the mass balance and compute the release flowrate.
- The one related to the tunnel. Ten vertical masts were used to support the measuring devices in the upper part of the tunnel. Additional supporting structures were installed around the chassis on the lower part to monitor the downward releases. These sensors are mainly helium concentration measurement (Xe and He catharometers) and thermocouples (Tk). Oxygen concentration sensors (Ox) were also installed to confirm the helium concentration measurements. Ultrasonic wind sensors monitored the convection flow in the tunnel during the tests.

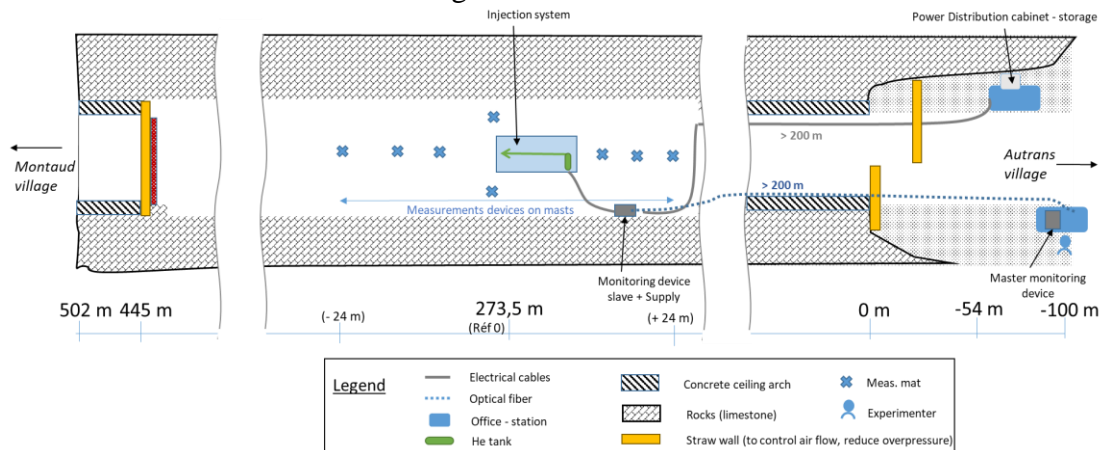


Figure 4-48. General sketch of the 2021 dispersion tests.

#### 4.5.3 Test sequence and test matrix

The test sequence is divided into several steps:

- Step 1: connection of the tank to the injection system, opening of the main tank valve to pressurize the pipe between the tank and the solenoid valve, control a leakage;
- Step 2: opening of the solenoid valve of the tank to release helium;
- Step 3: closure of the solenoid valve and continuation of the measurement phase up to the decrease of the helium concentration inside the tunnel.

Time zero has been set to the beginning of Step 2.

The two tests matrices are given in Table 4-14.

Table 4-14. Helium dispersion test matrix.

Type test	of	Nb of test	Volume (liter)	Pressure (bar)	Configuration	Ø TPRD (mm)	Test number
		10	50 (type II)	200	UP	2	n°3,4

### D2.3. Final report on analytical, numerical and experimental studies on hydrogen dispersion in tunnels, including innovative prevention and mitigation strategies

<b>He dispersion 2020</b>				UP	0.5	n°5
				UP	3	n°6,7
				DW 90°	3	n°9
				DW 90°	2	n°11, 12
				DW 90°	1	n°13
				DW 90°	4	n°14
<b>Type of test</b>	<b>Nb of test</b>	<b>Volume (liter)</b>	<b>Pressure (bar)</b>	<b>Configuration</b>	<b>Ø TPRD (mm)</b>	<b>Test number</b>
<b>He dispersion 2021</b>	4	50 (type II)	200	UP	2	n°01
		78 (type IV)	600 to 700	UP	2	n°02
				DW 45°	2	n°05
				DW 45°	1	n°07

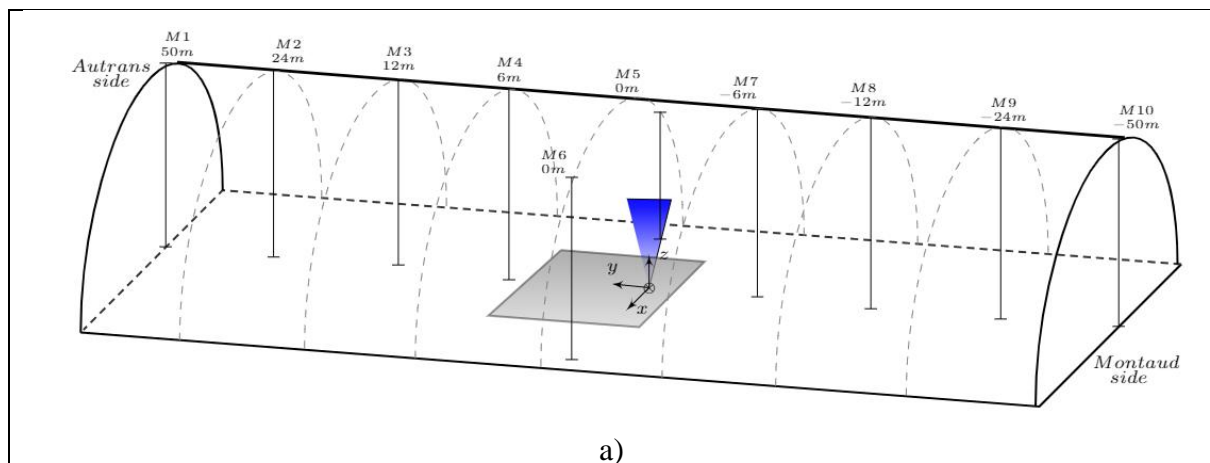
In this document, the results of the 2021 tests are mainly described. References to the 2020 test results are given when necessary. As a reminder, these 2020 tests were performed with a type II tank and pressure limited to 200 bar and a volume of 50 liters. The first test of the 2021 campaign was therefore intended to reproduce a release under the conditions of 2020 but under the rock vault.

Then, the comparison between the results of tests 1 and 2 (2021 series) enables to quantify the effect of the increase in storage pressure and of larger quantities. Comparison between tests 2Z and 5 allows quantifying the effect of release location. For downward release, the effect of orientation (45 or 90°) can only be assessed by comparing the results of test 5 with 2020 tests 11 or 12. However, the driving pressure is not the same. Finally, the effect of release diameter for a downward release of 45° can be assessed by comparing tests 5 and 7.

#### 4.5.4 Test results

##### 4.5.4.1 Reference test (200 bar, 2 mm TPRD, UP)

The reference test (test 01) is performed with a type II cylinder filled with 200 bar of helium. The calibrated orifice used is 2 mm and is oriented vertically upwards. The purpose of this test is to confirm the results obtained in 2020 (test 3 or 4) for similar conditions, except for the location in the tunnel.



### D2.3. Final report on analytical, numerical and experimental studies on hydrogen dispersion in tunnels, including innovative prevention and mitigation strategies

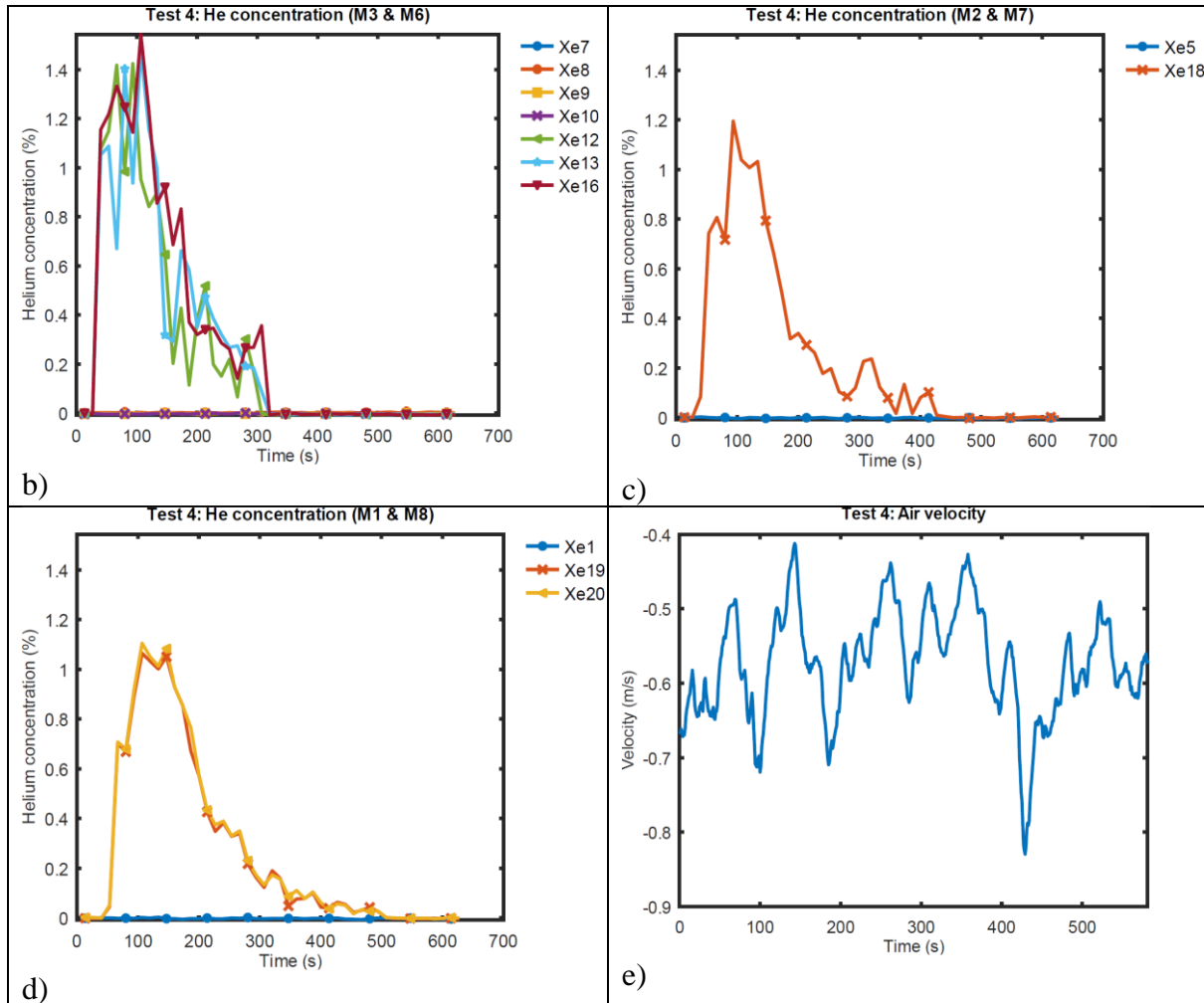


Figure 4-49. Results of 2020 test 4 : a) Experiment setup, b) Helium concentration at M3 and M6, c) Helium concentration at M2 and M7, d) Helium concentration at M1 and M8, e) Wind velocity inside the tunnel (+ refers from Montaud side to Autrans side).

The results of 2020 test 4 (Figure 4-49) showed that, in the upper part of the tunnel, the maximum concentration measured was about 1 vol%. Due to the convective flow in the tunnel (Figure 4-49 e), only the sensors located towards Montaud, i.e. the bottom of the tunnel, measured helium. The dilution over the 18 m (between M6 and M8) was the order of 0.3 vol%. The sensors located near the injection (M4 and M5) did not work.

For the 2021 test (test 01), very similar concentrations around 1 vol% are measured (Figure 4-50). However, for this test the flow of the natural ventilation of the tunnel is in the opposite direction (from Montaud to Autrans) and consequently only the sensors located towards Autrans measure helium. The measured ventilation velocity is slightly higher (Figure 4-51 b) which may explain why the sensors react more quickly for this last test. The distance of 24 m is reached in about twenty seconds, whereas in 2020 it was twice as long.

We also notice that the time during which the sensor located at 24 m measures helium is shorter in 2021 than in 2020, which corroborates the effect of a more intense ventilation in the tunnel.



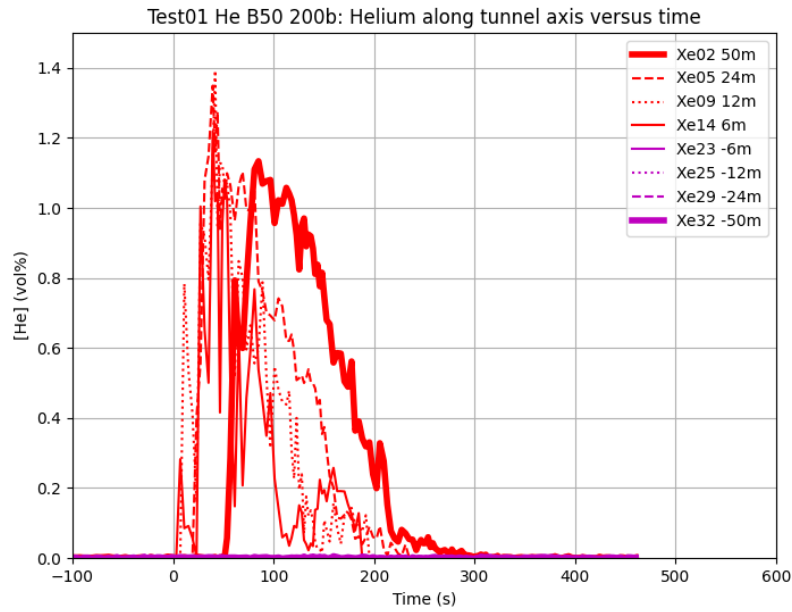


Figure 4-50. 2021 Test 01: Helium concentration close to the ceiling of the tunnel.

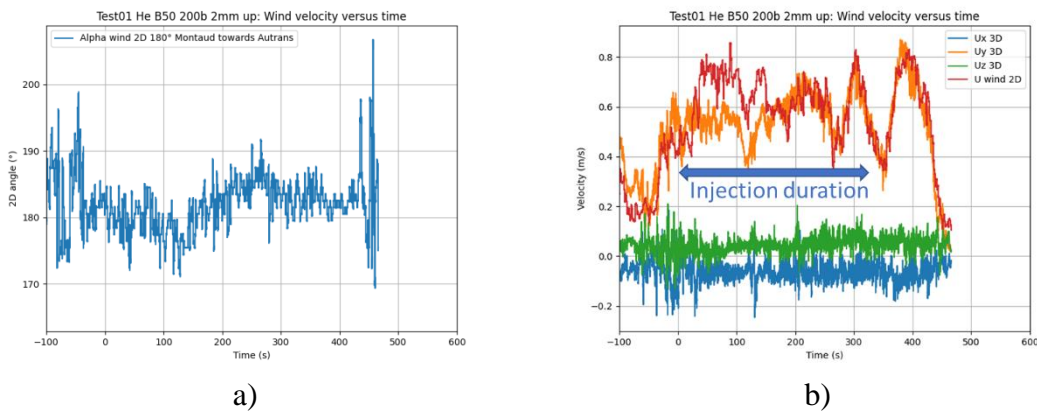
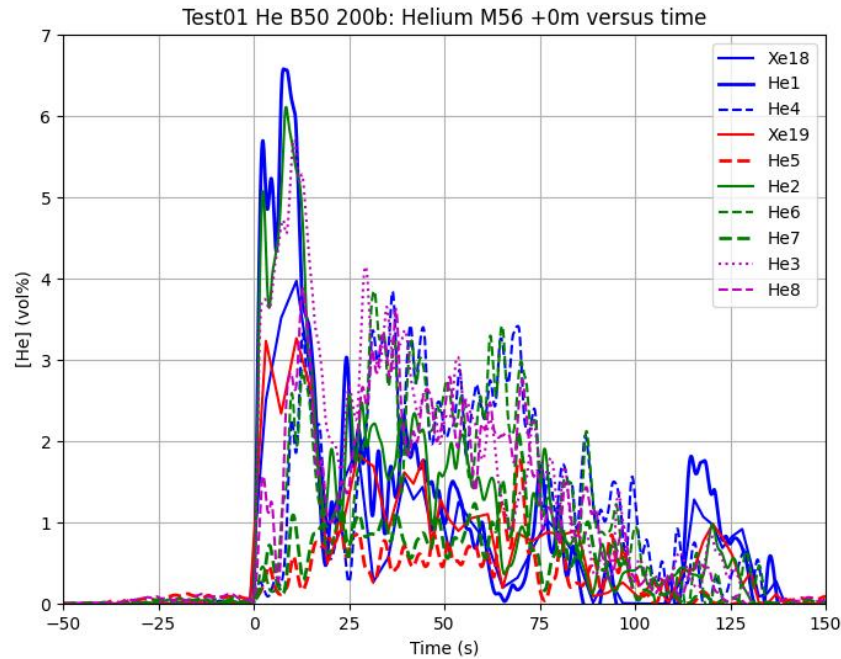


Figure 4-51. 2021 Test 01: Ventilation flow in the tunnel a) Orientation measured by the 2D ultrasonic anemometer, b) Velocities.

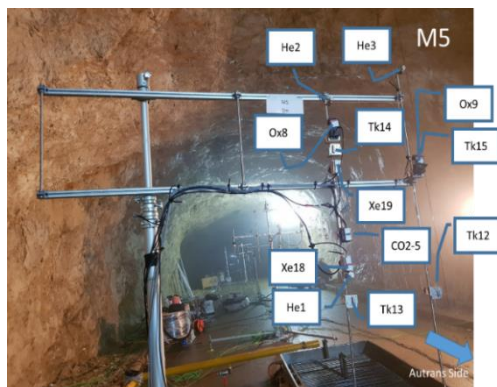
In the 2021 tests, measurements of helium concentration near the injection were available. Notably, the He3 sensor (Figure 4-52 bottom left) was located on the axis of the release about 5 meters above the injection point. Using similarity laws for the on-axis concentration during an under-expanded release (Molkov et al., 2009), it is possible to compare our measurements to theoretical data. This concentration decay is expressed as:

$$Y = 5.4 \sqrt{\frac{\rho_N}{\rho_S}} \frac{D}{z}$$

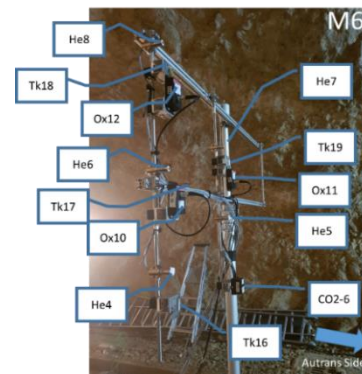
with D the diameter of the release,  $\rho_N$  the density at the release,  $\rho_S$  the density in the external environment, Y the mass fraction of the released gas in the mixture and z the elevation



a)



b)



c)

Figure 4-52. 2021 Test 01: Top - Helium concentration, Bottom - Position of sensors close to the injection (He3 is located on the vertical axis of the injection) b) M5 and c) M6.

Numerical application to the case of test 01 ( $D=2\text{mm}$ ,  $\rho_N=31.1\text{ kg/m}^3$ ,  $\rho_S=1.06\text{ kg/m}^3$ ) gives a concentration at the beginning of the release of 7.9 vol%. However, the measurement gives between 5 and 6 vol%. The non-symmetry of the measurements (He1-He4 or He2-He8) can explain the orientation of the release preferentially towards mast 5 and thus explain the deviation of the measurement of the He3 sensor compared to the theory.

In addition, the Xe18 and He1 sensors are placed next to each other. They should theoretically measure close helium concentrations. However, the Xe18 sensor measures at peak 4 vol% and the He1 sensor 6.5 vol%, the latter seeming to better follow the dynamics of the release. During the static calibration tests, the two values were identical.

Finally, if we assume that the explosive atmosphere corresponds to a concentration range of 4 to 75 vol%, this cloud is mainly contained in the rising section of the release for test 01.

## D2.3. Final report on analytical, numerical and experimental studies on hydrogen dispersion in tunnels, including innovative prevention and mitigation strategies

### 4.5.4.2 Effect of pressure increase for a 2 mm release

Test 02 of the 2021 campaign was conducted with a Type IV tank initially containing 645 bar of helium. Due to an unexpected closure of the solenoid valve at low temperature, the tank was partially emptied. Only 2.5 kg of helium were released out of the 6.5 kg initially in the tank, 2 kg of which were released in about 30 seconds.

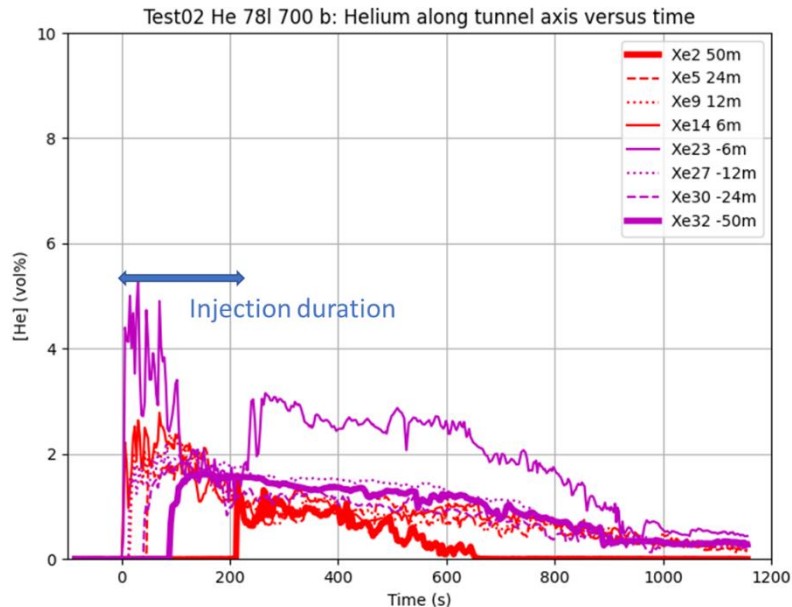


Figure 4-53. 2021 Test 02: Helium concentration close to the ceiling of the tunnel.

Over this short period, the helium concentration measured at -6 m at the ceiling reaches 5 vol% (Figure 4-53). Moreover, it remains close to 4 vol% for about a hundred seconds. We do not observe the same behavior at +6 m. This can be explained by the fact that the discharge being perpendicular to the road, it is slightly inclined with respect to the vertical and thus feeds preferentially the negative side of the Y axis. Moreover, the ventilation measured (Figure 4-54a) during this test shows a flow from Autrans to Montaud which reinforces the feeding towards the negative Y axis. Further into the tunnel, the maximum concentrations measured at the ceiling are of the order of 2 vol%. We also note that the sensors located at +/- 12 and 24 m react at about the same time, which confirms the importance of the inertia of the injection. On the other hand, at +/- 50 m the sensor located towards Montaud sees helium before the one located towards Autrans, which seems to be indicative of the effect of the ventilation in the tunnel.

## D2.3. Final report on analytical, numerical and experimental studies on hydrogen dispersion in tunnels, including innovative prevention and mitigation strategies

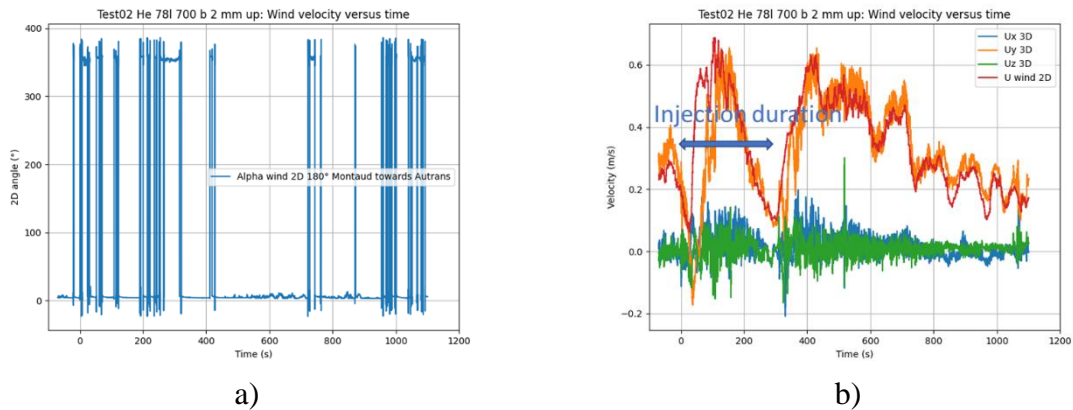


Figure 4-54. 2021 Test 02: Ventilation flow in the tunnel a) Orientation measured by the 2D ultrasonic anemometer, b) Velocities.

Note also that the ventilation in the tunnel decreases at the end of the injection phase to almost zero. Then, it resumes at the end of the injection and slowly decreases. These changes, probably because the tunnel is partially blocked by straw walls on both sides, may have an impact on the dispersion of the gas in the tunnel. Numerical simulations are needed to quantify this effect.

Finally, together with the end of the injection and the recovery of the ventilation in the tunnel, the concentration at -6 m increases from 1.5 to 3 vol%. The injection column and the helium-rich gas in the area around the point of impact on the ceiling are probably responsible for this increase. The dilution by the external flow of the global ventilation then slowly decreases the helium concentration in the tunnel. A larger extension and a larger quantity associated with a smaller ventilation means that the concentration in the tunnel takes longer to disappear until about 1000 seconds in the lower section of the tunnel (Montaud side), whereas for test 01 in 300 seconds everything had disappeared.

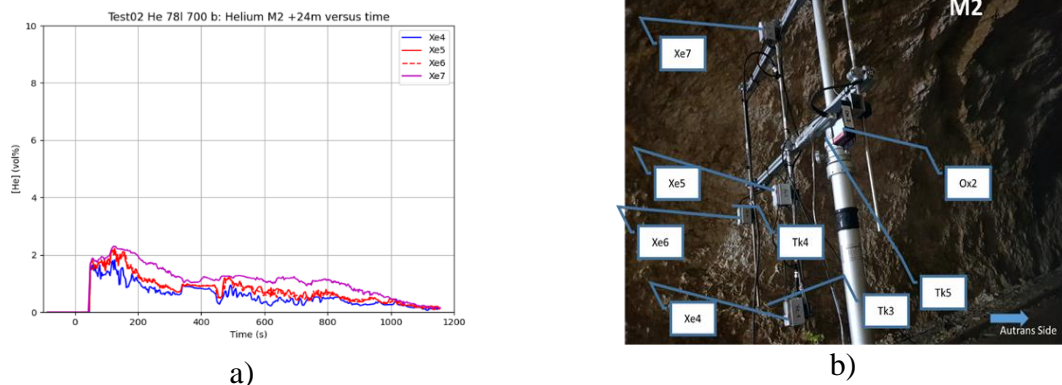


Figure 4-55. 2021 test 02: Helium layer at +24 m a) Helium concentration, b) Sensors location.

Looking at the helium dispersion in a tunnel cross-section (Figure 4-55), the helium-containing layer at the top shows no X-axis gradient (Xe5 and Xe6). The gradient along the Z-axis is small over at least a height of 1.0 m.

In the cross section of the injection (Figure 4-56), the differences are much more pronounced. The He3 sensor measures up to 15 vol% of helium while the theoretical value should only be 12.5 vol%. This discrepancy may be due to a contribution from the injected flow if the sensor is not well parallel to it. The positioning in the tunnel being difficult the paralleling is not always

### D2.3. Final report on analytical, numerical and experimental studies on hydrogen dispersion in tunnels, including innovative prevention and mitigation strategies

guaranteed. The asymmetry is still present because the sensors on the mast 5 side see more helium than those on the mast 6 side. Now, the He3 sensor actually sees a higher concentration of helium than the others do. It should also be mentioned that due to very high humidity, the masts were lowered every evening to protect the sensors during the night. In spite of the care taken to place the masts always in the same place (use of an alignment laser), it is always possible that small differences in positioning are present from one test to another. We can also clearly see the problems of unexpected closing of the solenoid valve with a series of concentration peaks corresponding to the different helium puffs.

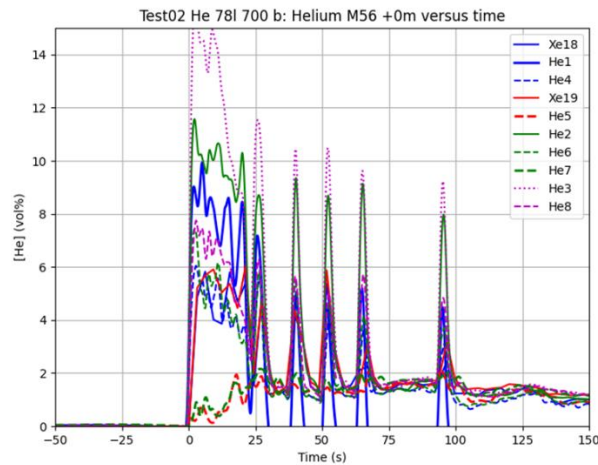
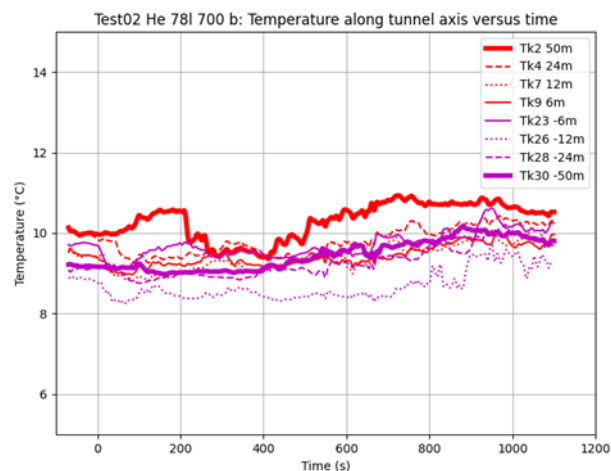


Figure 4-56. 2021 Test 02: Helium concentration near the injection (He3 is located on the vertical axis of the injection).

In Test 02, the temperature variations at the tunnel scale are small and out of the release, the problem can be considered as isothermal (Figure 4-57 - top).

The oxygen concentration measurements confirm the helium concentration measurements at the same location. Adding up to 3 vol% helium corresponds well to a decrease in the molar oxygen concentration of 0.6 vol% (Figure 4-57 - bottom).





## D2.3. Final report on analytical, numerical and experimental studies on hydrogen dispersion in tunnels, including innovative prevention and mitigation strategies

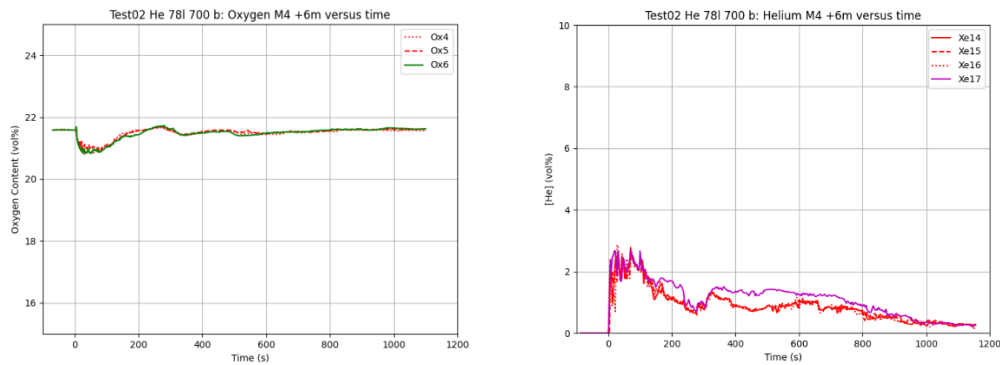


Figure 4-57. 2021 Test 02: Additional results, Top – gas temperature along the tunnel ceiling, Bottom – left Oxygen concentration and right Helium concentration at the same location (Mast 4).

### 4.5.4.3 Injection under the chassis for a 2 mm release

If at the time of the accident the FCHV did not overturn, the release through the TPRD is oriented downward. In the reference situation, we still considered a release through a 2 mm hole oriented at 45° towards the rear of the vehicle (test 05).

In this test, of the 6.5 kilograms of helium initially contained in the tank, four kilograms are released in the first forty seconds and an additional kilogram is then released in the following three minutes. This last kilogram is emitted in the form of puffs due to the unexpected closing of the solenoid valve.

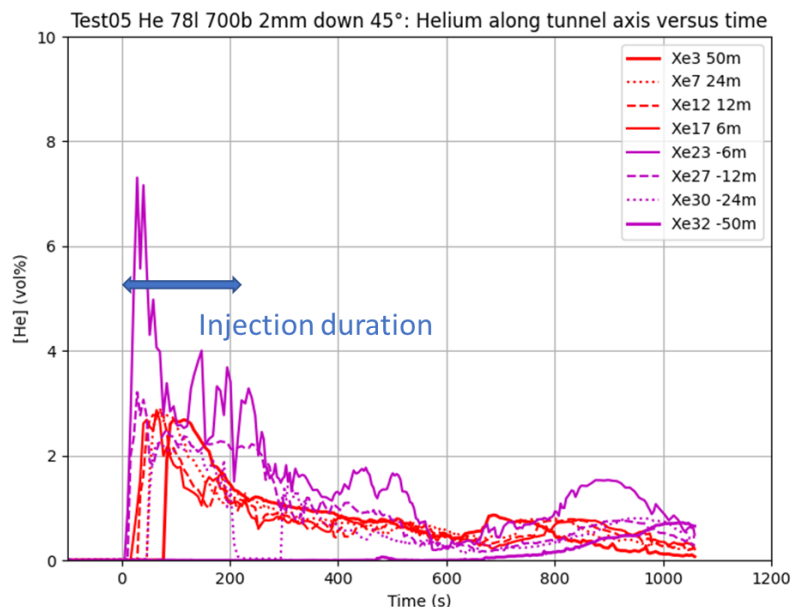


Figure 4-58. 2021 Test 05: Helium concentration close to the ceiling of the tunnel.

Although the discharge takes place downwards, a concentration higher than 4 vol% is measured on the sensor located in the upper part of the tunnel at -6 m from the injection (Figure 4-58). The other sensors located in the upper part of the tunnel have concentrations equal to 3 vol% at the most.



### D2.3. Final report on analytical, numerical and experimental studies on hydrogen dispersion in tunnels, including innovative prevention and mitigation strategies

During injection, the ventilation flow in the tunnel is almost zero (Figure 4-59). Then, a flow of 0.5 m/s is set up from Autrans to Montaud. This ventilation flow can explain the rise in concentration on the sensor located at -24 m (~300 seconds) as well as the very late arrival of helium on the sensor located at -50 m.

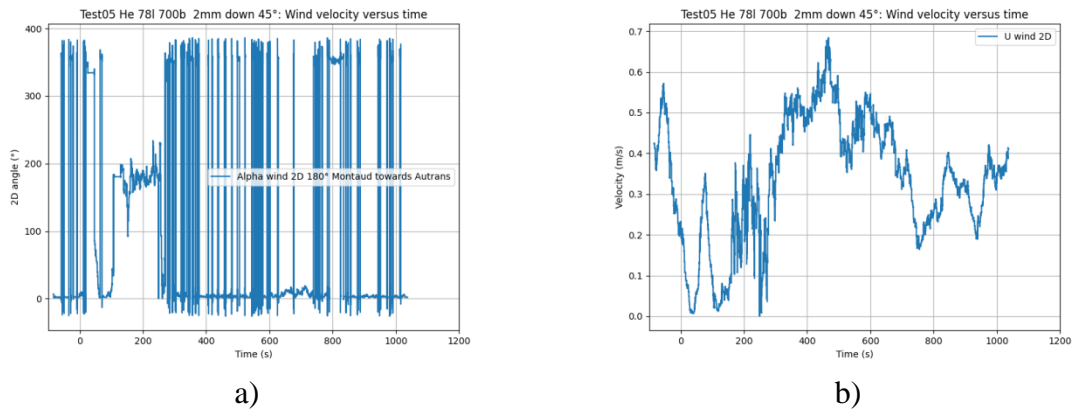


Figure 4-59. 2021 Test 05: Ventilation flow in the tunnel a) Orientation measured by the 2D ultrasonic anemometer, b) Velocity.

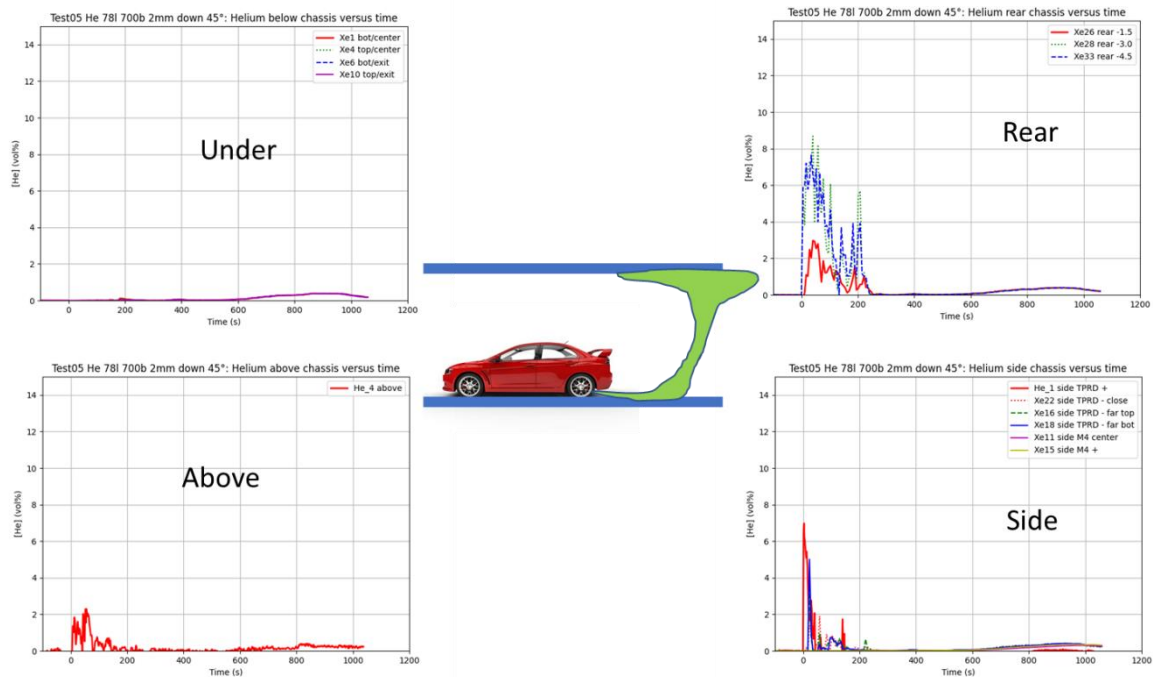


Figure 4-60. 2021 Test 05: Helium concentration close to the chassis.

It is also interesting to examine the helium concentration measured near the chassis (Figure 4-60). First, under the chassis there is no helium accumulation. Then, above, the concentration is close to the concentration measured at different points of the tunnel cross-section at 0 m, i.e. 1 to 2 vol%. Higher concentrations are measured on the sides and at the back of the chassis, i.e. in the area covered by the impinging discharge.

The jet is located very close to the ground (sensor Xe26 closer to the injection shows lower concentration than Xe28 or Xe33) and extends up to 4.5 m behind the chassis. Then, the

### D2.3. Final report on analytical, numerical and experimental studies on hydrogen dispersion in tunnels, including innovative prevention and mitigation strategies

buoyancy transports the helium to the upper part of the tunnel located at -6 m. A schematic representation of the vertical section of this cloud is provided in green in Figure 4-60.

For comparison, in the 2020 tests, discharges under the chassis but oriented perpendicular to the road were performed (Figure 4-61). In these tests, the pressure in the tank was only 200 bar. The helium concentration measurements under the chassis were completely different with very high values up to 20 vol%. Orienting the jet at 45° towards the rear allows to avoid the formation of an explosive atmosphere under the chassis and to localize it at the rear of the vehicle but up to the top of the tunnel at 6 m behind the car (~5m height). This is in line with the CFD observation of Ulster in an underground car park (Shentsov et al., 2021).

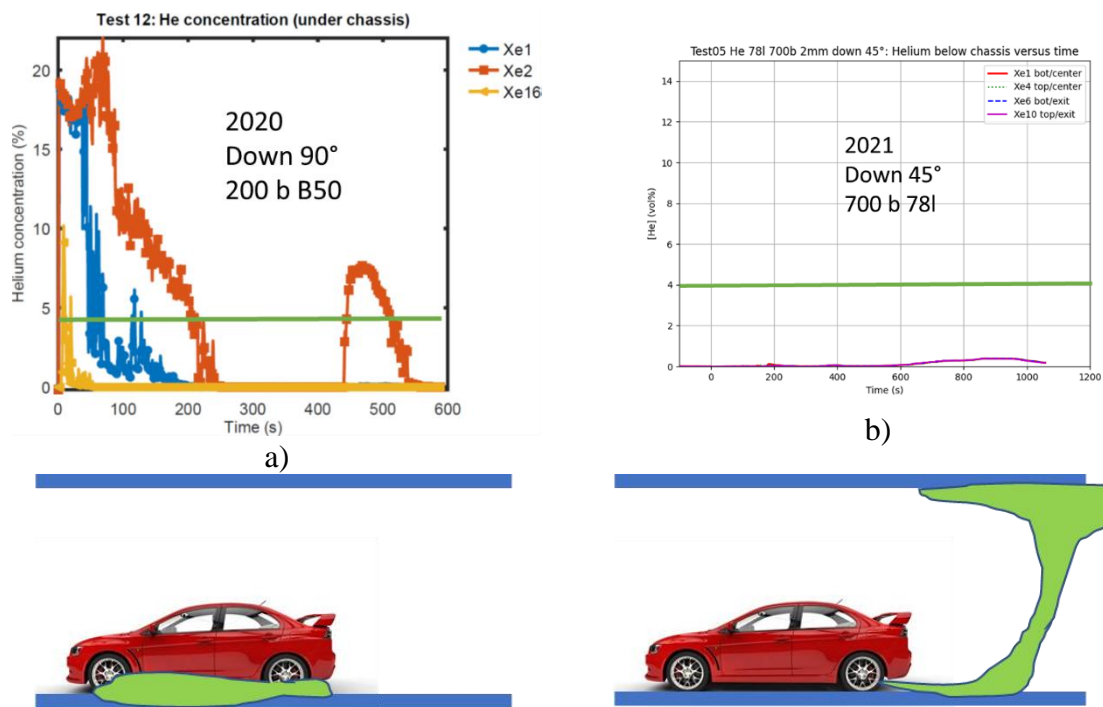


Figure 4-61. 2020 versus 2021 Test results: Helium accumulation in case of 2 mm release downward  
a) 2020 vertical 200 bar 50 liters type II tank, b) 2021 45° to the rear 700 bar 78 liters type IV tank.

#### 4.5.4.4 Effect of release diameter in case of downward 45° releases

To conclude this series of dispersion tests, the effect of the discharge orifice diameter was studied for a 45° orientation towards the rear of the vehicle.

Decreasing the size of the release orifice to 1mm (Test 07-Figure 4-62) prevents a concentration higher to 4 vol% in the upper part of the tunnel at -6 m. Consequently, the explosive atmosphere no longer reaches the upper part of the tunnel at the beginning of the release. However, it still extends to at least 4.5 m at the rear of the chassis and persists for a longer period due to the longer release time.

## D2.3. Final report on analytical, numerical and experimental studies on hydrogen dispersion in tunnels, including innovative prevention and mitigation strategies

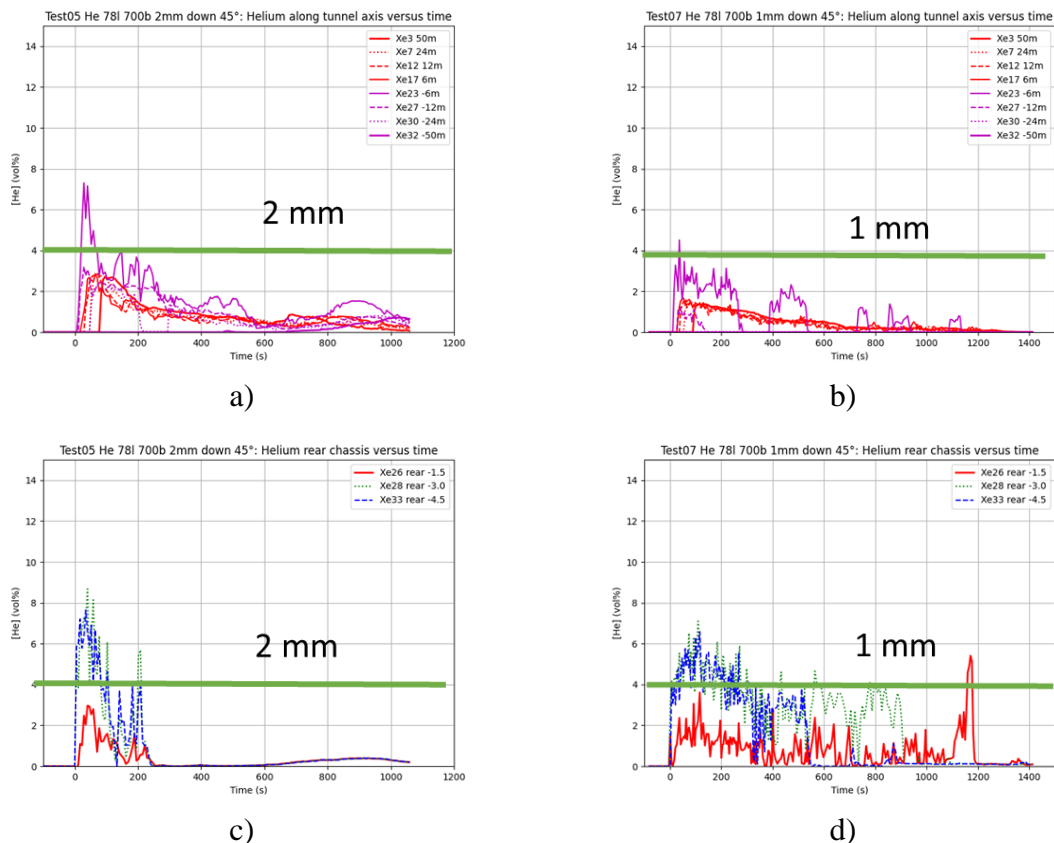


Figure 4-62. Effect of orifice diameter 45° downward: concentration close to the tunnel ceiling a) 2 mm and b) 1 mm, concentration at the rear of the chassis c) 2 mm and d) 1 mm.

### 4.5.5 Conclusions and recommendations

This document details the results obtained during dispersion tests of helium releases under pressure at 700 bar in the Mortier road tunnel. The releases through calibrated orifices occurred downward or upward to simulate the opening of a TPRD with or without the rollover of the damaged car. The main results show that:

- In the case of a downward release, tilting the TPRD 45° backwards will prevent the formation of an explosive atmosphere under the vehicle chassis.
- At the scale of “le tunnel du Mortier” (5.5 m height), a discharge diameter of 2 mm at the bottom up or down leads to the formation of an explosive atmosphere that extends from the bottom to the top of the tunnel but does not extend along the vault. Using a 1 mm diameter greatly restricts this extension but results in a greater persistence of this explosive atmosphere.
- External convection flow due to natural ventilation (< 1 m/s) does not affect the maximum concentration but drives the transport and dilution of the cloud after the release is complete.
- The presence of geometric changes in the shape of the tunnel at the top or a highly variable roughness (rock tunnel) can modify the dispersion by preferentially orienting the release, creating areas of accumulation that are more slowly diluted.

These test results as well as those obtained during the 2020 campaign under 200 bar constitute a unique database for the understanding and validation of dispersion models at the road tunnel scale.

### D2.3. Final report on analytical, numerical and experimental studies on hydrogen dispersion in tunnels, including innovative prevention and mitigation strategies

## 5. Summary and interaction of work tasks

The final analytical, numerical and experimental results of Work Package 2 on unignited leaks in tunnels and confined spaces have been presented in detail. Some experimental activities are delayed due to COVID-19 situation and are planned to be performed during the 5-months extension of the project.

There was a strong interaction between the simulation program and the experimental program at the level of the pre-test simulations, in order for the former to provide critical information about hydrogen dispersion and suggestions for appropriate sensors' positioning. Further interaction took place at the level of the validation simulations, which led to a strong improvement of models, modelling strategies and contributed to the understanding of the relevant physical phenomena. Additional validation simulations will be carried out based on the experimental activities that will be completed within the next months (during the project extension) and will be reported in (HyTunnel-CS D4.4, 2022).

There is also a strong interaction between WP2 and WP4, since dispersion experiments and simulations provided the necessary input for the subsequent combustion phenomena.

The performed research contributed to closing the following knowledge gaps for hydrogen releases in confined areas identified in HyTunnel-CS D1.2 "Report on hydrogen hazards and risks in tunnels and similar confined spaces" (2019):

- Effectiveness of regulated ventilation systems in case of hydrogen release accident;
- Hazard distances of unignited release, i.e. location of flammable hydrogen-air mixture for releases and dispersion in realistic scenarios at storage pressures up to 700 bar;
- The upper limit of hydrogen release rate that will not require change in ventilation system;
- Engineering tool for the assessment and design of ventilation system parameters to prevent and mitigate flammable mixture formation in tunnels.
- Non-adiabatic blowdown of hydrogen storage tank, including scenario of a storage tank behaviour in a fire;
- Tool for analysis of hydrogen release in enclosures and design of mechanical ventilation in underground parks;
- Dynamics of release and dispersion of hydrogen in a tunnel, including tunnels with forced ventilation and tunnels with regulated slope (below 5%);
- The effect of using fans in confined spaces;
- The pressure peaking phenomenon validation for garage-like enclosures for unignited releases;
- Predictive tool for the design of tunnel ventilation systems and corresponding ventilation protocols;
- Impinging hydrogen unignited jets.

The overall safety strategy for an inherently safer use of hydrogen vehicles in underground transportation systems were formulated based on WP2 (together with WP3, WP4 and WP5) outcomes. The strategy is to eliminate the formation of a flammable cloud under the ceiling preventing the potential of cloud ignition and destructive deflagration/DDT/detonation. Finally, the detailed list of recommendations to achieve this strategy for different release scenarios is presented in the project deliverable (HyTunnel-CS D6.9, 2022) and recommendations for RCS - in deliverable (HyTunnel-CS D6.10, 2022), which are the main outputs of WP6.

## 6. References

- Abe, S., Studer, E., Ishigaki, M., Sibamoto, Y. and Yonomoto, T. (2018). Stratification breakup by a diffuse buoyant jet: the MISTRA HM1-1 and 1-1bis experiments and their CFD analysis. *Nucl. Eng. Des.*, vol. 331, pp. 162–175.
- ArcelorMittal, ‘Underground car parks’. [Online]. Available from: <https://projects.arcelormittal.com/repository/Unassigned/Docs/Case%20studies/carparks.pdf>.
- Ballesteros-Tajadura, R., Santolaria-Morros, C. & Blanco-Marigorta, E. (2006). Influence of the slope in the ventilation semi-transversal system of an urban tunnel. *Tunnelling and Underground Space Technology*, 21(1), pp.21–28.
- Birch, A.D., Brown, D.R., Dodson, M.G. & Swaffield, F. (1984). The structure and concentration decay of high pressure jets of natural gas. *Combustion Science and Technology*, 36(5–6), pp.249–261.
- British Standard institution BS 7346-7 (2013). Components for smoke and heat control systems – Part 7: Code of practice on functional recommendations and calculation methods for smoke and heat control systems for covered car parks.
- Dadashzadeh, M., Makarov, D., Kashkarov, S. and Molkov, V. (2019). Non-adiabatic under-expanded jet theory for blowdown and fire resistance rating of hydrogen tank, presented, in: International Conference on Hydrogen Safety, Adelaide, Australia.
- Du, T., Yang, D., Ding, Y. (2018). Driving force for preventing smoke backlayering in downhill tunnel fires using forced longitudinal ventilation, *Tunnelling and Underground Space Technology*, vol. 79, pp. 76–82.
- Ewan, B.C.R., Moodie, K., Structure and velocity measurements in underexpanded jets, *J Combustion Science and Technology*, vol. 45(5-6), pp. 275-288.
- Fan, C.G., Li, X.Y., Mu, Y., Guo, F.Y., Ji, J. (2017). Smoke movement characteristics under stack effect in a mine laneway fire, *Applied Thermal Engineering*, vol. 110, pp. 70–79.
- Gebhart, B, Jaluria, Y, Mahajan, R L, and Sammakia, B. (1988). Buoyancy-induced flows and transport. United States: N. p., Web.
- Giannissi, S.G. et al. (2015). CFD benchmark on hydrogen release and dispersion in confined, naturally ventilated space with one vent, *Int. J. Hydrogen Energy*, vol. 40, no. 5, pp. 2415–2429.
- Gianniss, S.G., Toliass, I.C., Venetsanos, A.G. (2016). Mitigation of buoyant gas releases in single-vented enclosure exposed to wind: Removing the disrupting wind effect, *Int. J. Hydrogen Energy*, vol. 41, no. 6, pp. 4060-4071.
- Giannissi, S.G., Toliass, I.C., Ebne Abbasi, H., Makarov D., Grune J., Sempert K. (2021). Modelling of ventilated hydrogen dispersion in presence of co-flow and counter-flow, in: International Conference on Hydrogen Safety, Edinburgh, UK.
- Guelfi, A. et al., (2017). NEPTUNE: A new software platform for advanced nuclear thermal hydraulics. *Nucl. Eng. Des.*, vol. 156, pp. 281–324.

D2.3. Final report on analytical, numerical and experimental studies on hydrogen dispersion in tunnels, including innovative prevention and mitigation strategies

Haddad, R. K., Maluk, C., Reda, E., & Harun, Z. (2019). Critical Velocity and Backlayering Conditions in Rail Tunnel Fires: State-of-the-Art Review. *Journal of Combustion*, pp. 1-20.

HyTunnel-CS D1.2 (2019). Deliverable D1.2 Report on hydrogen hazards and risks in tunnels and similar confined spaces. Aug. 31, 2019, [Online]. Available: [https://hytunnel.net/wordpress/wp-content/uploads/2019/09/HyTunnel-CS\\_D1.2\\_Risks-and-Hazards.pdf](https://hytunnel.net/wordpress/wp-content/uploads/2019/09/HyTunnel-CS_D1.2_Risks-and-Hazards.pdf).

HyTunnel-CS D1.3 (2019), Deliverable D1.3 Report on selection and prioritisation of scenarios. Nov. 30, 2019, [Online]. Available: [https://hytunnel.net/wordpress/wp-content/uploads/2019/12/HyTunnel-CS\\_D1.3\\_Selection-and-Prioritisation-of-Accident-Scenarios.pdf](https://hytunnel.net/wordpress/wp-content/uploads/2019/12/HyTunnel-CS_D1.3_Selection-and-Prioritisation-of-Accident-Scenarios.pdf).

HyTunnel-CS D2.1 (2019). Deliverable D2.1 Detailed research programme on unignited leaks in tunnels and confined space. Nov. 30, 2019, [Online]. Available: [https://hytunnel.net/wordpress/wp-content/uploads/2019/12/HyTunnel-CS\\_D2.1\\_Detailed-research-programme-on-unignited-leaks-in-tunnels-and-confined-space-.pdf](https://hytunnel.net/wordpress/wp-content/uploads/2019/12/HyTunnel-CS_D2.1_Detailed-research-programme-on-unignited-leaks-in-tunnels-and-confined-space-.pdf).

HyTunnel-CS D4.3 (2022). Deliverable D4.3 Final report on analytical, numerical and experimental studies on explosions, including innovative prevention and mitigation strategies, February 2022.

HyTunnel-CS D4.4 (2022). Deliverable D4.4 Results of the deferred experimental programme and associated activities, July 2022.

HyTunnel-CS D6.9 (2022). Deliverable D6.9 Recommendations for inherently safer use of hydrogen vehicles in underground traffic systems, April 2022.

HyTunnel-CS D6.10 (2022). Deliverable D6.10 Recommendations for RCS, January 2022.

HyTunnel-CS M2.3 (2021). Milestone M2.3 Results of experimental, analytical and numerical studies for final report, November 2021.

Ingason, H., Li, Y. Z. (2010). Model scale tunnel fire tests with longitudinal ventilation. *Fire Safety Journal*, pp. 371-384.

Ji, J., Wan, H., Li, K., Han, J., Sun, J. (2015). A numerical study on upstream maximum temperature in inclined urban road tunnel fires. *International Journal of Heat and Mass Transfer*, vol. 88, pp. 516–526.

Ji, J., Wang, Z., Ding, L., Yu, L., Gao, Z., & Wan, H. (2019). Effects of ambient pressure on smoke movement and temperature. *International Journal of Thermal Sciences*, vol. 145.

Jiang, L., Creyssels, M., Hunt, G. R., Salizzoni, P. (2019). Control of light gas releases in ventilated tunnels. *J. Fluid Mech.*, pp. 515-531.

Koutsourakis, N., Tolas, I.C., Giannissi, S.G., Venetsanos, A.G. (2021). Numerical study of the effects of tunnel inclination and ventilation on the dispersion of hydrogen released from a car, in: the International Conference on Hydrogen Safety, Edinburgh, UK.

Krarti, M., Ayari, A. (2001). Ventilation for enclosed parking garages. *ASHRAE J*, vol. 43, pp. 52-57.



D2.3. Final report on analytical, numerical and experimental studies on hydrogen dispersion in tunnels, including innovative prevention and mitigation strategies

Lach, A.W, Gaathaug, A.V. (2020) Mechanical ventilation systems- unignited releases, USN, Porsgrunn, Norway.

Lach, A. W., Gaathaug, A.V. (2021). Effect of Mechanical Ventilation on Accidental Hydrogen Releases—Large-Scale Experiments. *Energies*, vol. 14, iss. 11.

Lach A.W., Gaathaug A.V., Vaagsaether K. (2020). Pressure peaking phenomena: Unignited hydrogen releases in confined spaces – Large-scale experiments, *International Journal of Hydrogen Energy*, vol. 45, iss. 56, Pages 32702-32712, ISSN 0360-3199, <https://doi.org/10.1016/j.ijhydene.2020.08.221>.

Le Clanche, J., Salizzoni, P., Creyssels, M., Mehaddi, R., Candelier, F., Vauquelin, O. (2014). Aerodynamics of buoyant releases within a longitudinally ventilated. *Experimental Thermal and Fluid Science*, pp. 121-127.

Mimouni, S. et al., (2017). Dispersed Two-Phase Flow Modeling for Nuclear Safety with NEPTUNE\_CFD Code.. *Hindawi Sci. Technol. Nucl. Install.*, vol. 2017, no. 3238545, p. 41.

Mimouni, S., Foissac, F. and Lavieville, J. (2011). CFD modelling of wall steam condensation by a two-phase flow approach. *Nucl. Eng. Des.*, vol. 241, pp. 4445–4455.

Molkov, V., Makarov, D., Bragin, M. (2009). Physics and modelling of underexpanded jets and hydrogen dispersion in atmosphere, in *Physics of Extreme States of Matter-2009*, Russian Academy of Sciences, p. 146-149.

Molkov V. (2012). *Introduction to Hydrogen Safety Engineering*. BookBoon, ISBN: 978-87-403-0226-4.

Molkov V., Shentsov, V. (2014). Numerical and physical requirements to simulation of gas release and dispersion in an enclosure with one vent, *Int. J. Hydrog. Energy*, vol. 39, no. 25, pp. 13328–13345.

Molkov, V., Shentsov, V., Quintiere, J. (2014). Passive ventilation of a sustained gaseous release in an enclosure with one vent, *Int. J. Hydrog. Energy*, vol. 39, no. 15, pp. 8158–8168.

Molkov, V., Dadashzadeh, M., Kashkarov, S., Makarov, D. (2021). Performance of hydrogen storage tank with TPRD in an engulfing fire. *Int. J. Hydrog. Energy*, vol.46, iss. 73, pp. 36581-36597. Available from: <https://doi.org/10.1016/j.ijhydene.2021.08.128> [Accessed 27-02-2022].

Morton, B. (1959). Forced plumes. *Int. J. Fluid Mechanics*, pp.151-163.

Mukai, S., Suzuki, J., Mitsuishi, H., Oyakawa, K. & Watanabe, S. (2005). CFD simulation of diffusion of hydrogen leakage caused by fuel cell vehicle accident in tunnel, underground parking lot and multi-story parking garage. In *19th Int. Technical Conf. on the Enhanced Safety of Vehicles (ESV)*, Washington D.C., 6–9 June, 2005.

Musto, M., Rotondo, G. (2014), Numerical comparison of performance between traditional and alternative jet fans in tiled tunnel in emergency ventilation, *Tunnelling and Underground Space Technology*, vol. 42, pp. 52–58.

Sauzedde, F., Martin, m., Forero, D., Studer, E. (2021). Experimental devices of 2021 CEA tests, HyTunnel-CS, 2021.

D2.3. Final report on analytical, numerical and experimental studies on hydrogen dispersion in tunnels, including innovative prevention and mitigation strategies

Seike, M., Kawabata, N., Hasegawa, M. & Tanaka, H. (2019). Heat release rate and thermal fume behavior estimation of fuel cell vehicles in tunnel fires. *International Journal of Hydrogen Energy*, 44(48), pp.26597–26608.

Shentsov, V., Makarov, D., Molkov, V. (2021). Effect of TPRD diameter and direction of release on hydrogen dispersion and fire in underground parking, in: *International Conference on Hydrogen Safety*, Edinburgh, UK, 21-24 September, 2021.

Studer, E. et al., (2018). Stratification break-up by a diffuse buoyant jet: a CFD benchmark exercise. Qingdao, China, October 14-18, 2018.

Tuovinen, H., Holmstedt, G., Bengtson, S. (1996). Sensitivity Calculations of Tunnel Fires using CFD, *Fire Technology*, vol. 32, iss. 2, pp. 99-119.

Van den Bremer, T., Hunt, G. (2010). Universal solutions for Boussinesq and non-Boussinesq plumes. *JFM*, pp. 165-192.

Vauquelin, O. (2008). Experimental simulations of fire-induced smoke control in tunnels. *Tunnelling and Underground Space Technology*, pp. 171-179.

Venetsanos, A.G., Giannissi, S.G., Tolias, I.C., Friedrich, A., & Kuznetsov, M. (2021a). Cryogenic and ambient gaseous hydrogen blowdown with discharge line effects, in: *International Conference on Hydrogen Safety*, Edinburgh, UK, 21-24 September, 2021.

Venetsanos, A.G., Ustolin, F., Tolias, I.C., Giannissi, S.G., Momferatos, G., Coldrick, S., Atkinson, G., Lyons, K., Jallais, S. (2021b). Discharge modeling of large scale LH2 experiments with an engineering tool, in: *International Conference on Hydrogen Safety*, Edinburgh, UK, 21-24 September, 2021.

Weng, M.-c., Lu, X.-l., Liu, F., Shi, X.-p., & Yu, L.-x. (2015). Prediction of backlayering length and critical velocity in metro tunnel. *Tunnelling and Underground Space Technology*, pp. 64-72.

Woodburn, P.J., Britter, R.E. (1996). CFD Simulations of a Tunnel Fire - Part II, *Fire Safety Journal*, vol. 26, pp. 63-90.

Zhao, S., Li, Y.Z., Kumm, M., Ingason, H. & Liu, F. (2019). Re-direction of smoke flow in inclined tunnel fires. *Tunnelling and Underground Space Technology*, vol. 86, pp.113–127.

## D2.3. Final report on analytical, numerical and experimental studies on hydrogen dispersion in tunnels, including innovative prevention and mitigation strategies

### Appendix A Tables and Figures for HSE pre-tests

*Table A-1. The sensors' coordinates. The tunnel center is located at  $(x,y)=(35,0)$ . The  $z$  coordinate is in respect to the bottom plane (not the tunnel floor, i.e.  $z=2$  m means actually 1.55 m above the floor to account for the ballast height)*

No	X(m)	Y(m)	Z(m)	No	X(m)	Y(m)	Z(m)	No	X(m)	Y(m)	Z(m)
1	20.00	-1.72	2.05	135	27.50	-0.20	1.20	269	55.00	0.37	2.20
2	25.00	-1.72	2.05	136	30.00	-0.20	1.20	270	60.00	0.37	2.20
3	27.50	-1.72	2.05	137	32.50	-0.20	1.20	271	20.00	0.40	0.65
4	30.00	-1.72	2.05	138	34.00	-0.20	1.20	272	25.00	0.40	0.65
5	32.50	-1.72	2.05	139	36.00	-0.20	1.20	273	27.50	0.40	0.65
6	34.00	-1.72	2.05	140	37.50	-0.20	1.20	274	30.00	0.40	0.65
7	36.00	-1.72	2.05	141	40.00	-0.20	1.20	275	32.50	0.40	0.65
8	37.50	-1.72	2.05	142	42.50	-0.20	1.20	276	34.00	0.40	0.65
9	40.00	-1.72	2.05	143	45.00	-0.20	1.20	277	36.00	0.40	0.65
10	42.50	-1.72	2.05	144	55.00	-0.20	1.20	278	37.50	0.40	0.65
11	45.00	-1.72	2.05	145	60.00	-0.20	1.20	279	45.00	0.40	0.65
12	50.00	-1.72	2.05	146	20.00	0.00	1.75	280	55.00	0.40	0.65
13	55.00	-1.72	2.05	147	25.00	0.00	1.75	281	60.00	0.40	0.65
14	60.00	-1.72	2.05	148	27.50	0.00	1.75	282	20.00	0.51	1.46
15	20.00	-1.52	0.88	149	30.00	0.00	1.75	283	25.00	0.51	1.46
16	25.00	-1.52	0.88	150	32.50	0.00	1.75	284	27.50	0.51	1.46
17	27.50	-1.52	0.88	151	34.00	0.00	1.75	285	30.00	0.51	1.46
18	30.00	-1.52	0.88	152	36.00	0.00	1.75	286	32.50	0.51	1.46
19	32.50	-1.52	0.88	153	37.50	0.00	1.75	287	34.00	0.51	1.46
20	34.00	-1.52	0.88	154	40.00	0.00	1.75	288	36.00	0.51	1.46
21	36.00	-1.52	0.88	155	42.50	0.00	1.75	289	37.50	0.51	1.46
22	37.50	-1.52	0.88	156	45.00	0.00	1.75	290	40.00	0.51	1.46
23	40.00	-1.52	0.88	157	50.00	0.00	1.75	291	45.00	0.51	1.46
24	42.50	-1.52	0.88	158	55.00	0.00	1.75	292	50.00	0.51	1.46
25	45.00	-1.52	0.88	159	60.00	0.00	1.75	293	55.00	0.51	1.46
26	50.00	-1.52	0.88	160	20.00	0.00	2.33	294	60.00	0.51	1.46
27	55.00	-1.52	0.88	161	25.00	0.00	2.33	295	20.00	0.57	1.85
28	60.00	-1.52	0.88	162	27.50	0.00	2.33	296	25.00	0.57	1.85
29	20.00	-1.15	1.95	163	30.00	0.00	2.33	297	27.50	0.57	1.85
30	25.00	-1.15	1.95	164	32.50	0.00	2.33	298	30.00	0.57	1.85
31	27.50	-1.15	1.95	165	34.00	0.00	2.33	299	32.50	0.57	1.85
32	30.00	-1.15	1.95	166	36.00	0.00	2.33	300	34.00	0.57	1.85
33	32.50	-1.15	1.95	167	37.50	0.00	2.33	301	36.00	0.57	1.85
34	34.00	-1.15	1.95	168	40.00	0.00	2.33	302	37.50	0.57	1.85
35	36.00	-1.15	1.95	169	42.50	0.00	2.33	303	40.00	0.57	1.85
36	37.50	-1.15	1.95	170	45.00	0.00	2.33	304	42.50	0.57	1.85
37	40.00	-1.15	1.95	171	50.00	0.00	2.33	305	45.00	0.57	1.85

### D2.3. Final report on analytical, numerical and experimental studies on hydrogen dispersion in tunnels, including innovative prevention and mitigation strategies

38	42.50	-1.15	1.95	172	55.00	0.00	2.33	306	50.00	0.57	1.85
39	45.00	-1.15	1.95	173	60.00	0.00	2.33	307	55.00	0.57	1.85
40	50.00	-1.15	1.95	174	20.00	0.00	2.33	308	60.00	0.57	1.85
41	55.00	-1.15	1.95	175	25.00	0.00	2.33	309	20.00	0.75	2.64
42	60.00	-1.15	1.95	176	27.50	0.00	2.33	310	25.00	0.75	2.64
43	20.00	-1.12	3.09	177	30.00	0.00	2.33	311	27.50	0.75	2.64
44	25.00	-1.12	3.09	178	32.50	0.00	2.33	312	30.00	0.75	2.64
45	27.50	-1.12	3.09	179	34.00	0.00	2.33	313	32.50	0.75	2.64
46	30.00	-1.12	3.09	180	36.00	0.00	2.33	314	34.00	0.75	2.64
47	32.50	-1.12	3.09	181	37.50	0.00	2.33	315	36.00	0.75	2.64
48	34.00	-1.12	3.09	182	40.00	0.00	2.33	316	37.50	0.75	2.64
49	36.00	-1.12	3.09	183	42.50	0.00	2.33	317	40.00	0.75	2.64
50	37.50	-1.12	3.09	184	45.00	0.00	2.33	318	42.50	0.75	2.64
51	40.00	-1.12	3.09	185	50.00	0.00	2.33	319	45.00	0.75	2.64
52	42.50	-1.12	3.09	186	55.00	0.00	2.33	320	50.00	0.75	2.64
53	45.00	-1.12	3.09	187	60.00	0.00	2.33	321	55.00	0.75	2.64
54	50.00	-1.12	3.09	188	20.00	0.00	2.92	322	60.00	0.75	2.64
55	55.00	-1.12	3.09	189	25.00	0.00	2.92	323	20.00	1.01	1.17
56	60.00	-1.12	3.09	190	27.50	0.00	2.92	324	25.00	1.01	1.17
57	20.00	-1.01	1.17	191	30.00	0.00	2.92	325	27.50	1.01	1.17
58	25.00	-1.01	1.17	192	32.50	0.00	2.92	326	30.00	1.01	1.17
59	27.50	-1.01	1.17	193	34.00	0.00	2.92	327	32.50	1.01	1.17
60	30.00	-1.01	1.17	194	36.00	0.00	2.92	328	34.00	1.01	1.17
61	32.50	-1.01	1.17	195	37.50	0.00	2.92	329	36.00	1.01	1.17
62	34.00	-1.01	1.17	196	40.00	0.00	2.92	330	37.50	1.01	1.17
63	36.00	-1.01	1.17	197	42.50	0.00	2.92	331	40.00	1.01	1.17
64	37.50	-1.01	1.17	198	45.00	0.00	2.92	332	45.00	1.01	1.17
65	40.00	-1.01	1.17	199	50.00	0.00	2.92	333	50.00	1.01	1.17
66	42.50	-1.01	1.17	200	55.00	0.00	2.92	334	55.00	1.01	1.17
67	45.00	-1.01	1.17	201	60.00	0.00	2.92	335	60.00	1.01	1.17
68	55.00	-1.01	1.17	202	20.00	0.00	2.92	336	20.00	1.12	3.09
69	60.00	-1.01	1.17	203	25.00	0.00	2.92	337	25.00	1.12	3.09
70	25.00	-0.75	2.64	204	27.50	0.00	2.92	338	27.50	1.12	3.09
71	27.50	-0.75	2.64	205	30.00	0.00	2.92	339	30.00	1.12	3.09
72	30.00	-0.75	2.64	206	32.50	0.00	2.92	340	32.50	1.12	3.09
73	32.50	-0.75	2.64	207	34.00	0.00	2.92	341	34.00	1.12	3.09
74	34.00	-0.75	2.64	208	36.00	0.00	2.92	342	36.00	1.12	3.09
75	36.00	-0.75	2.64	209	37.50	0.00	2.92	343	37.50	1.12	3.09
76	37.50	-0.75	2.64	210	40.00	0.00	2.92	344	40.00	1.12	3.09
77	40.00	-0.75	2.64	211	42.50	0.00	2.92	345	42.50	1.12	3.09
78	42.50	-0.75	2.64	212	45.00	0.00	2.92	346	45.00	1.12	3.09
79	45.00	-0.75	2.64	213	50.00	0.00	2.92	347	50.00	1.12	3.09

### D2.3. Final report on analytical, numerical and experimental studies on hydrogen dispersion in tunnels, including innovative prevention and mitigation strategies

<b>80</b>	50.00	-0.75	2.64	<b>214</b>	55.00	0.00	2.92	<b>348</b>	55.00	1.12	3.09
<b>81</b>	55.00	-0.75	2.64	<b>215</b>	60.00	0.00	2.92	<b>349</b>	60.00	1.12	3.09
<b>82</b>	60.00	-0.75	2.64	<b>216</b>	20.00	0.00	3.50	<b>350</b>	20.00	1.15	1.95
<b>83</b>	20.00	-0.57	1.85	<b>217</b>	25.00	0.00	3.50	<b>351</b>	25.00	1.15	1.95
<b>84</b>	25.00	-0.57	1.85	<b>218</b>	27.50	0.00	3.50	<b>352</b>	27.50	1.15	1.95
<b>85</b>	27.50	-0.57	1.85	<b>219</b>	30.00	0.00	3.50	<b>353</b>	30.00	1.15	1.95
<b>86</b>	30.00	-0.57	1.85	<b>220</b>	32.50	0.00	3.50	<b>354</b>	32.50	1.15	1.95
<b>87</b>	32.50	-0.57	1.85	<b>221</b>	34.00	0.00	3.50	<b>355</b>	34.00	1.15	1.95
<b>88</b>	34.00	-0.57	1.85	<b>222</b>	36.00	0.00	3.50	<b>356</b>	36.00	1.15	1.95
<b>89</b>	36.00	-0.57	1.85	<b>223</b>	37.50	0.00	3.50	<b>357</b>	37.50	1.15	1.95
<b>90</b>	37.50	-0.57	1.85	<b>224</b>	40.00	0.00	3.50	<b>358</b>	40.00	1.15	1.95
<b>91</b>	40.00	-0.57	1.85	<b>225</b>	42.50	0.00	3.50	<b>359</b>	42.50	1.15	1.95
<b>92</b>	42.50	-0.57	1.85	<b>226</b>	45.00	0.00	3.50	<b>360</b>	45.00	1.15	1.95
<b>93</b>	45.00	-0.57	1.85	<b>227</b>	50.00	0.00	3.50	<b>361</b>	50.00	1.15	1.95
<b>94</b>	55.00	-0.57	1.85	<b>228</b>	55.00	0.00	3.50	<b>362</b>	55.00	1.15	1.95
<b>95</b>	60.00	-0.57	1.85	<b>229</b>	60.00	0.00	3.50	<b>363</b>	60.00	1.15	1.95
<b>96</b>	20.00	-0.51	1.46	<b>230</b>	20.00	0.00	3.50	<b>364</b>	20.00	1.52	0.88
<b>97</b>	25.00	-0.51	1.46	<b>231</b>	25.00	0.00	3.50	<b>365</b>	25.00	1.52	0.88
<b>98</b>	27.50	-0.51	1.46	<b>232</b>	27.50	0.00	3.50	<b>366</b>	27.50	1.52	0.88
<b>99</b>	30.00	-0.51	1.46	<b>233</b>	30.00	0.00	3.50	<b>367</b>	30.00	1.52	0.88
<b>100</b>	32.50	-0.51	1.46	<b>234</b>	32.50	0.00	3.50	<b>368</b>	32.50	1.52	0.88
<b>101</b>	34.00	-0.51	1.46	<b>235</b>	34.00	0.00	3.50	<b>369</b>	34.00	1.52	0.88
<b>102</b>	36.00	-0.51	1.46	<b>236</b>	36.00	0.00	3.50	<b>370</b>	36.00	1.52	0.88
<b>103</b>	37.50	-0.51	1.46	<b>237</b>	37.50	0.00	3.50	<b>371</b>	37.50	1.52	0.88
<b>104</b>	40.00	-0.51	1.46	<b>238</b>	40.00	0.00	3.50	<b>372</b>	40.00	1.52	0.88
<b>105</b>	42.50	-0.51	1.46	<b>239</b>	42.50	0.00	3.50	<b>373</b>	42.50	1.52	0.88
<b>106</b>	45.00	-0.51	1.46	<b>240</b>	45.00	0.00	3.50	<b>374</b>	45.00	1.52	0.88
<b>107</b>	55.00	-0.51	1.46	<b>241</b>	50.00	0.00	3.50	<b>375</b>	50.00	1.52	0.88
<b>108</b>	60.00	-0.51	1.46	<b>242</b>	55.00	0.00	3.50	<b>376</b>	55.00	1.52	0.88
<b>109</b>	20.00	-0.40	0.65	<b>243</b>	60.00	0.00	3.50	<b>377</b>	60.00	1.52	0.88
<b>110</b>	25.00	-0.40	0.65	<b>244</b>	20.00	0.20	1.20	<b>378</b>	20.00	1.72	2.05
<b>111</b>	27.50	-0.40	0.65	<b>245</b>	25.00	0.20	1.20	<b>379</b>	25.00	1.72	2.05
<b>112</b>	30.00	-0.40	0.65	<b>246</b>	27.50	0.20	1.20	<b>380</b>	27.50	1.72	2.05
<b>113</b>	32.50	-0.40	0.65	<b>247</b>	30.00	0.20	1.20	<b>381</b>	30.00	1.72	2.05
<b>114</b>	34.00	-0.40	0.65	<b>248</b>	32.50	0.20	1.20	<b>382</b>	32.50	1.72	2.05
<b>115</b>	36.00	-0.40	0.65	<b>249</b>	34.00	0.20	1.20	<b>383</b>	34.00	1.72	2.05
<b>116</b>	37.50	-0.40	0.65	<b>250</b>	36.00	0.20	1.20	<b>384</b>	36.00	1.72	2.05
<b>117</b>	55.00	-0.40	0.65	<b>251</b>	37.50	0.20	1.20	<b>385</b>	37.50	1.72	2.05
<b>118</b>	60.00	-0.40	0.65	<b>252</b>	40.00	0.20	1.20	<b>386</b>	40.00	1.72	2.05
<b>119</b>	20.00	-0.37	2.20	<b>253</b>	45.00	0.20	1.20	<b>387</b>	42.50	1.72	2.05
<b>120</b>	25.00	-0.37	2.20	<b>254</b>	50.00	0.20	1.20	<b>388</b>	45.00	1.72	2.05
<b>121</b>	27.50	-0.37	2.20	<b>255</b>	55.00	0.20	1.20	<b>389</b>	50.00	1.72	2.05

### D2.3. Final report on analytical, numerical and experimental studies on hydrogen dispersion in tunnels, including innovative prevention and mitigation strategies

<b>122</b>	30.00	-0.37	2.20	<b>256</b>	60.00	0.20	1.20	<b>390</b>	55.00	1.72	2.05
<b>123</b>	32.50	-0.37	2.20	<b>257</b>	20.00	0.37	2.20	<b>391</b>	60.00	1.72	2.05
<b>124</b>	34.00	-0.37	2.20	<b>258</b>	25.00	0.37	2.20	<b>392</b>	34.00	0.61	0.59
<b>125</b>	36.00	-0.37	2.20	<b>259</b>	27.50	0.37	2.20	<b>393</b>	35.00	0.61	0.59
<b>126</b>	37.50	-0.37	2.20	<b>260</b>	30.00	0.37	2.20	<b>394</b>	36.00	0.61	0.59
<b>127</b>	40.00	-0.37	2.20	<b>261</b>	32.50	0.37	2.20	<b>395</b>	34.00	0.61	1.00
<b>128</b>	42.50	-0.37	2.20	<b>262</b>	34.00	0.37	2.20	<b>396</b>	35.00	0.61	1.00
<b>129</b>	45.00	-0.37	2.20	<b>263</b>	36.00	0.37	2.20	<b>397</b>	36.00	0.61	1.00
<b>130</b>	50.00	-0.37	2.20	<b>264</b>	37.50	0.37	2.20	<b>398</b>	34.00	0.61	2.00
<b>131</b>	55.00	-0.37	2.20	<b>265</b>	40.00	0.37	2.20	<b>399</b>	35.00	0.61	2.00
<b>132</b>	60.00	-0.37	2.20	<b>266</b>	42.50	0.37	2.20	<b>400</b>	36.00	0.61	2.00
<b>133</b>	20.00	-0.20	1.20	<b>267</b>	45.00	0.37	2.20				
<b>134</b>	25.00	-0.20	1.20	<b>268</b>	50.00	0.37	2.20				

### Car scenario with vehicles – $d=2.2$ mm – $u_{vent}=1.25$ m/s

Table A-2. The sensors that detected hydrogen concentration above LFL for the car scenario.

No Sensor		
21	127	266
22	128	276
23	129	278
36	139	316
37	140	317
52	154	329
53	168	330
54	169	343
63	182	344
64	183	356
65	197	357
77	198	369
78	211	370
90	212	371
91	224	372
92	225	373
102	226	384
103	227	385
104	238	392
114	239	393
115	240	
116	241	



### D2.3. Final report on analytical, numerical and experimental studies on hydrogen dispersion in tunnels, including innovative prevention and mitigation strategies

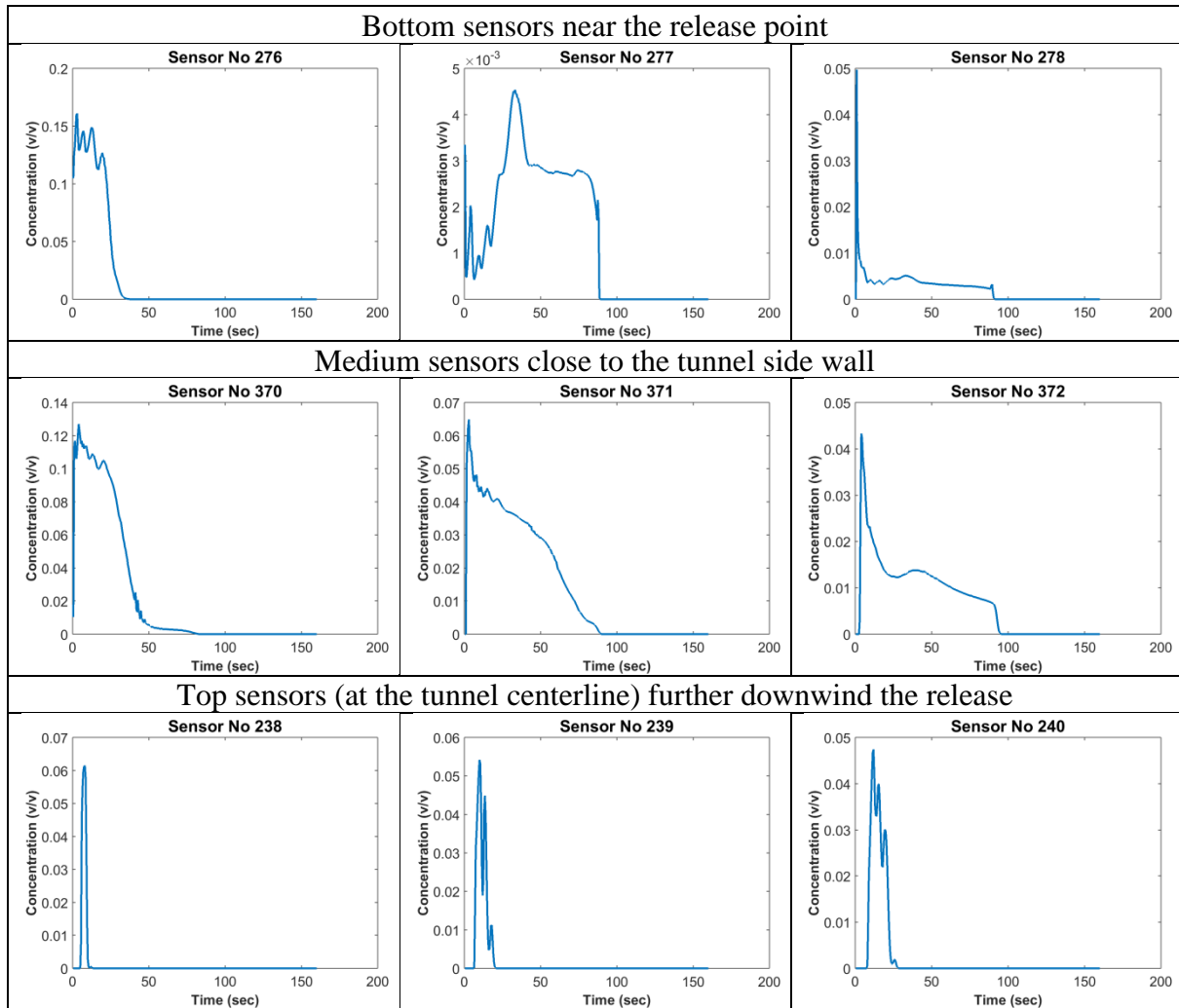
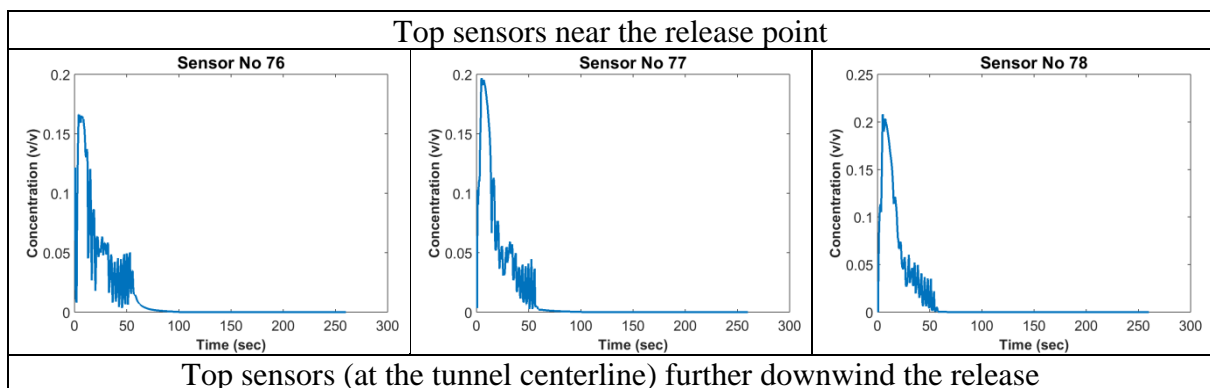


Figure A-1. Hydrogen concentration (volume fraction) time series for several sensors for the car scenario.

**Train scenario with vehicles–  $d=5.7$  mm –  $u_{vent}=1.25$  m/s**



### D2.3. Final report on analytical, numerical and experimental studies on hydrogen dispersion in tunnels, including innovative prevention and mitigation strategies

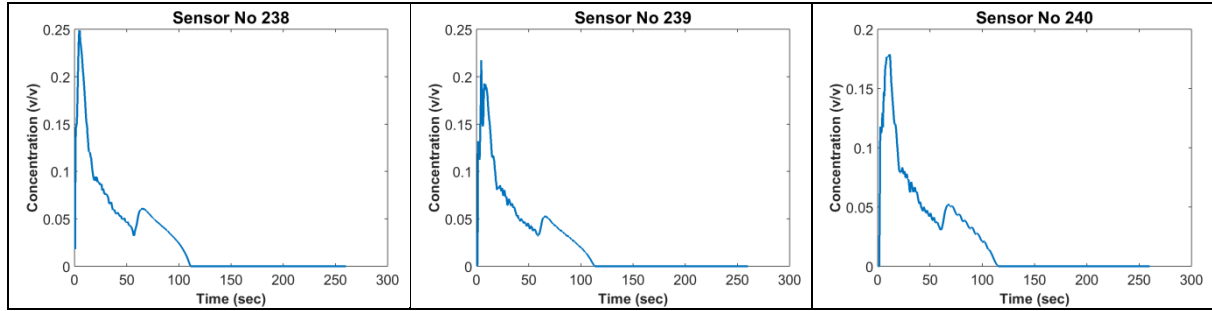


Figure A-2. Hydrogen concentration (volume fraction) time series for several sensors for the train scenario with vehicles.

## Appendix B Scaling criteria

The objective of a steady state scaled experiment is to match the concentration of hydrogen in the downstream flow and the proportion of the tunnel over which the flow is distributed. The defined variables are described in Figure B-1.

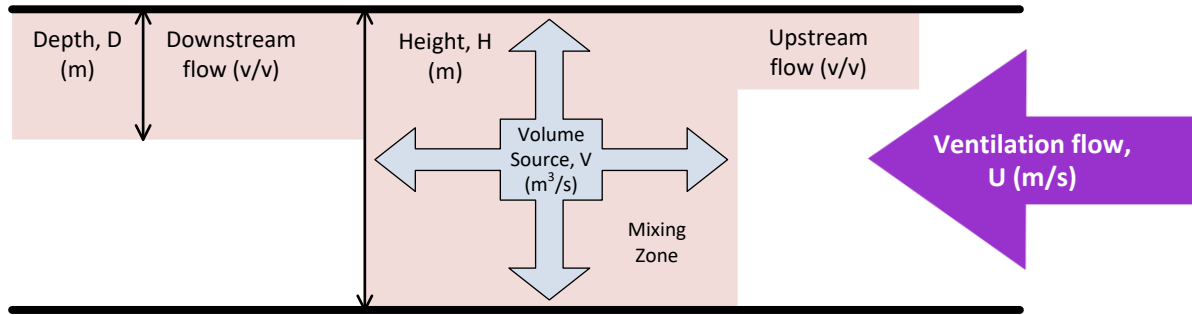


Figure B-1. Schematic diagram showing modelling of jet and tunnel ventilation interactions.

$$C_{model} = C_{fullscale} \quad (1)$$

$$\frac{D_{model}}{H_{model}} = \frac{D_{fullscale}}{H_{fullscale}} \quad (2)$$

Assume there is a mixing zone of limited size around the source where the flow is dominated by source momentum. Outside this zone the flow is controlled by the interaction between the buoyant gas and the tunnel flow.

If the downstream flow occupies the same proportion of the model as in the full scale tunnel area then mass conservation gives:

$$C \propto \frac{\dot{V}}{UH^2} \quad (3)$$

Since hydrogen is very light the density difference associated with the downstream flow is:

$$\frac{\Delta\rho}{\rho_0} \sim C \quad (4)$$

If  $\Delta P_{buoyancy}$  is the buoyancy head associated with the flow:

$$\Delta P_{buoyancy} \propto Hg\rho_0 C \quad (5)$$

### D2.3. Final report on analytical, numerical and experimental studies on hydrogen dispersion in tunnels, including innovative prevention and mitigation strategies

The dynamic head associated with the tunnel flow is:

$$\Delta P_{\text{tunnel flow}} \propto \rho_0 U^2 . \quad (6)$$

If these are in the same proportion then the tendency for back flow and the stability of the downstream layer will be matched for the model and full-scale flow when:

$$\rho_0 U^2 \propto H g \rho_0 C \quad (7)$$

$$\text{Or} \quad C \propto \frac{U^2}{H} . \quad (8)$$

This equation implies that the tunnel flow speed should be scaled as  $\sqrt{H}$ .

$$U \propto \sqrt{H} . \quad (9)$$

Combining this with (3) gives

$$\dot{V} \propto H^{5/2} . \quad (10)$$

#### Matching the mixing zone by choice of source momentum

The velocities associated with a jet source with a momentum flux,  $M$ , vary with scale as

$$M \propto H^2 U_{\text{source}}^2 . \quad (11)$$

The edge of the mixing zone corresponds to locations where  $U_{\text{source}} \sim U_{\text{tunnel}}$

The mixing zones will have similar shapes at different scales if

$$M U_{\text{source}} \propto \frac{\sqrt{M}}{H} \propto U_{\text{tunnel}} \quad (12)$$

$$\text{Since} \quad U_{\text{tunnel}} \propto \sqrt{H} . \quad (13)$$

This means that the mixing zones will be similar if

$$M \propto H^3 . \quad (14)$$

In summary, the appropriate scaling relationships between the tunnel flow,  $U$ , the hydrogen volume flow,  $\dot{V}$ , and the tunnel diameter,  $H$ , for a *steady* release experiment in a model tunnel is

$$U \propto H^{\frac{1}{2}} \quad (15)$$

$$\dot{V} \propto H^{\frac{5}{2}} . \quad (16)$$

If  $U$  and  $\dot{V}$  are chosen in this way then the concentration in the flow developing around the source will be the same and the relationship between the buoyancy head associated with the release and the dynamic head of the flow will be the same. This means there will be a similar tendency for the gas to be blown down stream or flow backwards at high level.